Characterizing the pathophysiological mechanisms of early disease in amyotrophic lateral sclerosis using multimodal neuroimaging

by

Avyarthana Dey

A thesis submitted in partial fulfillment of the requirements for the degree of

Doctor of Philosophy

Neuroscience

University of Alberta

Abstract

Amyotrophic lateral sclerosis (ALS) is a, neurodegenerative disorder which is characterized by progressive impairment of the upper motor neurons in the brain and lower motor neurons in the brainstem and spinal cord. The disease is ultimately fatal with death eventually resulting from aspiration pneumonia. The motor neuronal impairment results in clinical signs such as muscle weakness, increased muscle tone and reflexes, and muscular atrophy and fasciculations. Cognitive impairment, recognized as a correlate of frontotemporal lobar degeneration, may occur concurrently with the disease process in ALS. Despite the recognition of corticospinal tract and corpus callosal degeneration as hallmarks of white matter microstructural impairment, the functional connectivity alterations of the default mode and sensorimotor cerebral networks as hallmarks of gray matter impairments, and alterations in concentrations of excitatory and inhibitory neurochemicals as well as neurochemical markers of neuronal health, there is an inadequate understanding of the relationship between these independent observations across various measurement modalities as well as an inadequate understanding of the pathophysiological mechanisms underlying such disease characteristics. This makes accurate stratification of patients based on disease pathophysiology challenging, and hinders the study of targeted therapeutic interventions or inclusion in clincial trials. In addition, due to the stringency of inclusion criteria for clinical drug trials, some patients are deemed ineligible for inclusion based on a decline in their clinical measures.

Therefore, this thesis aimed to characterize markers of early disease using an approach that stratifies patients based on interindividual similarities in disease pathophysiology using neuroimaging instead of clinical measures. In order to assess the performance of such neuroimaging-based measures against clinically-defined methods, a comparison of clinical and functional neuroimaging measures is performed in Chapter 2. This study provides evidence of better sensitivity of the imaging-derived method of patient stratification over the clinically-defined method. The next step is to perform an evaluation of network-based evolution of disease

pathophysiology in clinically-defined and imaging-derived patient subgroups. These evaluations were performed in Chapters 3 and 4. Chapter 3 was able to demonstrate that longitudinal network connectivity alterations were present in both motor and extra-motor networks in the comprehensive ALS cohort as well as in the clinically-defined patient subgroups. Additionally, an assessment of cerebral function in this chapter revealed that brain regions participating in motor encoding have altered longitudinal functional connectivities in the motor imagery network in early disease and in the action observation network in advanced disease. In chapter 4, distinct disease evolution patterns were identified in imaging-derived patient subgroups. While one subgroup had a more severe (advanced pathophysiological) disease with a predominantly motor phenotype, the other subgroup had a less severe (early pathophysiological) disease with a motor-frontotemporal phenotype. Clinical features of the disease in both patient subgroups correlated with their network characteristics. The longitudinal patterns of network functional alterations in patients stratified by both clinically-defined and imaging-derived criteria are suggestive of the role of the motor network in the disease process. Therefore, identifying the neuroanatomical basis of motor network impairment might help provide clues to the biological mechanisms underlying functional impairment of the upper motor neurons. Chapter 5 performed an assessment of the neuroanatomical features of white matter microstructure and neurochemical concentrations within the foot region of the primary motor cortex homunculus. As expected, a correlation was observed between reduced neurochemical concentrations of N-acetyl aspartate (a marker of neuronal health) and reduced foot tapping scores in ALS. Furthermore, these clinically-relevant neurochemical concentrations demonstrated both positive and negative associations with reduced motor cortex functional connectivity.

In sum, the evidence presented in this thesis highlights that the connectivity of the motor network plays a vital role in ALS disease pathophysiology, thereby corroborating the extensive evidence in the literature. Specifically, the evidence in this thesis suggests that the pathophysiological disease mechanisms manifest differently in ALS patients, and these differences are apparent when distinct patient stratification criteria are used. However, this thesis also highlights the lack of congruence between the various criteria used in this thesis to stratify patients. This is indicative of a gap in

biological-phenotypic coherence of pathophysiological disease characterization, which remains a major player in the lack of identification of an effective biomarker for disease monitoring in the clinical setting.

Preface

This thesis is an original work of Avyarthana Dey.

Chapter 5 of this thesis has been published as

Motor cortex functional connectivity is associated with underlying neurochemistry in ALS

Avyarthana Dey, Collin C. Luk, Abdullah Ishaque, Daniel Ta, Ojas Srivastava, Dennell Krebs, Peter Seres, Chris Hanstock, Christian Beaulieu, Lawrence Korngut, Richard Frayne, Lorne Zinman, Simon Graham, Angela Genge, Hannah Briemberg, and Sanjay Kalra for the Canadian ALS Neuroimaging Consortium (CALSNIC)

AD* analyzed and interpreted data and drafted the manuscript for intellectual content. CL acquired data and revised the manuscript for intellectual content. AI, DT, and OS analyzed data and revised the manuscript for intellectual content. DK acquired data and revised the manuscript for intellectual content. PS contributed to MRI acquisition and revised the manuscript for intellectual content. CH contributed to the design of the MRS protocol, analyzed data, and revised the manuscript for intellectual content. CB contributed to the study design and revised the manuscript for intellectual content. LK, RF, LZ, SG, AG, and HB acquired data and revised the manuscript for intellectual content. SK contributed to the design and conceptualization of the study, acquired, analyzed and interpreted the data, and revised the manuscript for intellectual content.

Chapter 2 of this thesis is formatted for submission to the Annals of Neurology and will be submitted to the journal for review by the time of the thesis defense as

Cerebral networks reveal patient subtypes with distinct endophenotypes in amyotrophic lateral sclerosis

Avyarthana Dey, Tobias Robert Baumeister, Michael Benatar, Shana Rae Black, Hannah Briemberg, Annie Dionne, Karleyton Evans, Richard Frayne, Angela Genge, Simon Graham, Vincent Koppelmans, Lawrence Korngut, Grant Liu, Collin Luk, Donald McLaren, Pedram Parnianpour, Peter Seres, Robert Cary Welsh, Lorne Zinman, Sanjay Kalra

AD* analyzed and interpreted data and drafted the manuscript for intellectual content. TRB and GL analyzed and interpreted data and revised the manuscript for intellectual content. MB, HB, AD, RF, AG, SG, LK, and LZ acquired data and revised the manuscript for intellectual content. SRB, VK, RCW, PP, and SK were involved in experimental design and revised the manuscript for intellectual content. KE and DM contributed to the ideation of the study, were involved in experimental design, and revised the manuscript for intellectual content. CL acquired data and revised the manuscript for intellectual content. PS contributed to MRI acquisition and revised the manuscript for intellectual content. SK contributed to the design and conceptualization of the study, acquired, analyzed and interpreted the data, and revised the manuscript for intellectual content.

Due to the paper-based nature of this thesis, the supplementary material for Chapter 5 is presented as published and for Chapter 2 is presented as planned for submission to the journal.

Following is a list of ethics applications (approved) put in place at the University of Alberta for the research projects I was involved in throughout the duration of my PhD program:

1. MRI Biomarkers in ALS (Pro00036028)
2. Hudson Imaging Study (Pro00061945)
3. Multimodal Imaging of MND (Pro00011079)
4. Phase 4 – MRI Biomarkers in ALS (Pro00042912)
5. Post-mortem Evaluation of ALS and MND (Pro00090736)

Dedication

I dedicate this thesis to my parents, for always giving me a loving environment to spread my wings and dream.

“The cosmos is within us. We are made of star-stuff. We are a way for the universe to know itself.”

- Carl Sagan

Acknowledgements

I have been incredibly lucky to have Dr. Sanjay Kalra as my PhD supervisor and mentor. Words fall short to describe the impact he has had in my life. His kindness and steadfastness throughout my PhD, in the good times and the bad, have made me a better researcher and human being. Shadowing him in the ALS clinic has been an invaluable experience for me as I have experienced first-hand his exceptional commitment to bettering the lives of his patients and to educating his students and residents. I can only hope to be a mentor like you someday. Thank you for an amazing academic experience, this one is for the books.

Thank you to Dr. Sumit Das for teaching me cool brain things under the microscope, and being a great friend, mentor, and supervisory committee member throughout the years. Thank you for your patience and kindness when I didn't know my lateral from medial geniculate nuclei.

Thank you to Dr. Trevor Steve for your thought-provoking questions and incredible support in your capacity as a member of my supervisory committee.

Thank you to Dr. Wendy Johnston, co-director of the ALS Clinic with Dr. Kalra, for inspiring me with her commitment and leadership in advocating for her patients and for providing me with guidance and opportunities along the way.

A special thank you to Dr. David Taylor, VP Research at the ALS Society of Canada, for being a wonderful human being, for relaying the intricacies of everyone's research so eloquently, and for the kindness you have shown me through the years. Your unwavering belief in my abilities, the opportunities you have given me, and your words of encouragement have meant the world to me – and will continue to do so.

Dr. Collin Luk – my lab best friend (and confidant) and fantastic former lab clinical research fellow. It has been an absolute honour to share our 'corner' office, depend on each other for work

and life during the pandemic, and have scientific/philosophical discussions about everything. Couldn't have asked for a better lab/office mate!

Dr. Robert Baumeister, thank you for being a great friend and lab postdoc! I will cherish our fun back-and-forths where we never seemed to agree on research things.

Dennell Krebs and Dr. Abdullah Ishaque – it wouldn't have been a fun first year without the two of you, thank you for all the laughs and the ridiculous sticky notes.

Matthew Harrison, my study partner and sounding board in the last year and a half of my PhD – thank you for being you! Thank you to all the past and present lab members who I couldn't name (because of space constraints)! Katherine and Kelsey, honourary lab members, thank you for your incredible friendship over the years – I couldn't have survived my PhD without you both.

I would also like to thank the Macdonalds and the Elliotts for accepting me into the family, and never letting me miss home. A very big thank you to the pets in my life – Orly, Willis, Tache, and Georgie – for your endless love, croons, and undivided attention (no treats included) when I practiced my talks, studied for the candidacy exam, or wrote my thesis.

It wouldn't be a true acknowledgement section without acknowledging the massive contribution of all patients with ALS and their caregivers/next-of-kin. Your selfless commitment and willingness to improve the lives of future generations of patients with ALS are inspirational and granted me a perspective into the disease through your lens, and for your grace I am forever grateful. Your legacy will live on through your contributions to research, my thesis being a very small drop in that ocean.

It really does take a village!

Table of contents

List of tables

Chapter 1

Chapter 2

Table 2. Group differences in voxel-wise intra- and inter-network FC across different RSNs in all patients with ALS compared to HCs. ALS = amyotrophic lateral sclerosis, HC = healthy controls, R = right, L = left, B = bilateral.

Table 3. Intra-network FC in study cohorts. Means for intra-network FC values, corrected for the effects of age, sex, and education level, are displayed. The standard errors for intra-network FCs for all RSNs across all study cohorts were ≤0.01. Asterisk (*) represents significant differences ($p<0.05$) in intra-network FC in ALS patients (and ALS subgroups) when compared to HCs.

Table 4. Differences in voxel-wise FC across imaging-derived and clinically-defined ALS subgroups. ALS = amyotrophic lateral sclerosis, HC = healthy controls, R = right, L = left, B = bilateral.

Supplementary. Group differences in voxel-wise intra- and inter-network FC across different RSNs in imaging-derived patient subgroups compared to HCs. ALS = amyotrophic lateral sclerosis, HC = healthy controls, R = right, L = left, B = bilateral.

Chapter 3

Table 1. Baseline demographic and clinical characteristics of the study population. Single asterisk (*) denotes $p < 0.05$ and double asterisk (**) denotes $p < 0.001$.

Table 2. Voxel-wise alterations in longitudinal FC between ALS and HC. RSN = resting-state network, MNI = Montreal Neurological Institute, ALS = amyotrophic lateral sclerosis, HC = healthy controls, BA = Brodmann area, R = right, L = left, B = bilateral

Table 3. Voxel-wise alterations in longitudinal FC between E-ALS and A-ALS. RSN = resting-state network, MNI = Montreal Neurological Institute, ALS = amyotrophic lateral sclerosis, HC = healthy controls, BA = Brodmann area, R = right, L = left

Table 4. Voxel-wise alterations in longitudinal FC between ALS subgroups (E-ALS and A-ALS) and HCs. RSN = resting-state network, MNI = Montreal Neurological Institute, ALS = amyotrophic lateral sclerosis, HC = healthy controls, BA = Brodmann area, R = right, L = left, B = bilateral

Supplementary. Visit-wise functional activations of distinct resting-state networks

Chapter 4

Table 1. Baseline and longitudinal demographic and clinical characteristics of the study cohort. Means (SD) are displayed for the assessed characteristics. Single asterisk (*) denotes $p < 0.05$ and double asterisk (**) denotes $p < 0.001$. n.s. denotes no significant differences.

Table 2. Longitudinal evolution of RSN activation values of the study groups

Table 3. Voxel-wise differences in longitudinal functional connectivity between ALS subgroups (S1 and S2) and HCs. RSN = resting-state network, MNI = Montreal Neurological Institute, BA = Brodmann area, R = right, L = left, B = bilateral

Supplementary. S1. Patterns of longitudinal change from visit 1 to visit 3 in clinical measures

Supplementary. S2. Patterns of longitudinal change from visit 1 to visit 3 in functional activation measures

Chapter 5

Table 1. Participant demographics and clinical characteristics

Table 2. Differences in resting-state FC. T-values and coordinates in MNI standard space are reported (T; x,y,z). R = right, B = bilateral, BA = Brodmann area, MNI = Montreal Neurological Institute.

Table 3. Summary of structural and neurochemical measures in the PMC. FA = fractional anisotropy, MD = mean diffusivity, RD = radial diffusivity, AD = axial diffusivity, tNAA = total NAA moieties, Cr = creatine, Cho = choline, SE = standard error. MD, RD, AD are x 10^{-3} mm^2/s

Table 4. Regional associations of reduced functional connectivity with PMC neurochemistry and FA. T-values and coordinates in MNI standard space are reported (T; x, y, z). L = left, R = right, B = bilateral.

Supplementary. S1. Demographic and clinical characteristics

Supplementary. Table S2. Differences in resting-state FC between Bulbar-onset ALS and HC. T-values and coordinates in MNI standard space are reported (T; x,y,z). R = right, L = left, BA = Brodmann area, MNI = Montreal Neurological Institute.

Supplementary. S3. Group differences in diffusion and neurochemical measures in the primary motor cortex in Bulbar-onset ALS

Supplementary. S4. Relationship of diffusion and neurochemical measurements with UMN function in Bulbar-onset ALS

Supplementary. Table S5. Regional associations of reduced functional connectivity with PMC neurochemistry in Bulbar-onset ALS compared to HC. T-values and coordinates in MNI standard space are reported (T; x, y, z). L = left, R = right.

Supplementary. S6. Demographics and clinical characteristics

Supplementary. Table S7. Differences in resting-state FC between Limb-onset ALS and HC. T-values and coordinates in MNI standard space are reported (T; x,y,z). R = right, L = left, BA = Brodmann area, MNI = Montreal Neurological Institute.

Supplementary. S8. Group differences in diffusion and neurochemical measures in the primary motor cortex in Limb-onset ALS

Supplementary. S9. Relationship of diffusion and neurochemical measurements with UMN function in Limb-onset ALS

List of figures

Chapter 1

Figure 4. A schematic of the steps involved in the generation of in-vitro models for the study of neurodegenerative disorders. In panel (a), the schematic pathway for neuronal differentiation from human-induced pluripotent stem cells involves (1) reprogramming human primary fibroblasts or other somatic primary cells back into the fetal state by introducing defined transcription factors, (2) inducing neural fate through the inhibition of an dual intercellular signalling pathway (also known as the SMAD pathway), resulting in the formation of neural stem cells, and (3) differentiating neurons with the help of neurotrophic factors. Panel (b) shows a schematic of a pathway for the direct conversion of fibroblasts to neurons in which the same starting fibroblasts can be directly converted into induced neurons by the introduction of neuron-specific transcription factors and other small molecules that include SMAD pathway inhibitors and cell cycle blockers. Source: D'Souza et al., 2021.

Figure 5. Sites of motor neuronal involvement in ALS. Upper motor neurons are localized to the primary motor cortex and shown in blue. Bulbar and spinal lower motor neurons are shown in red. These two groups of motor neurons are preferentially affected in ALS. Extra-motor neuronal involvement includes the neurons of the frontal and temporal cortices, shown in orange. There is rare involvement of the oculomotor and vesicorectal motor neurons, shown in green and yellow respectively; although it is thought that these motor neurons can be affected in the later stages of longstanding disease. Source: Swinnen et al., 2014

Figure 6. Hierarchical levels of assessment. Level I is the lowest level of complexity and can be adapted to a clinical setting. The implementation of levels II and III require formal neuropsychological and speech and language expertise, expertise with higher statistical complexity, and include tests that may require further validation in the ALS population. Source: Strong et al., 2015

Figure 7. On the left, protons are misaligned as there is no external aligning magnetic field. On the right, on the application of an external magnetic field, the protons align themselves parallel and anti-parallel to the magnetic field. The number of protons aligned in the direction of the applied magnetic field is greater than the number of protons aligned in the direction opposite to the applied magnetic field. Adapted from (Azhar and Chong 2023).

Figure 8. On application of a 90° radiofrequency (RF) pulse, the net magnetization vector undergoes displacement into the transverse plane (Azhar and Chong 2023)

Figure 9. Representative images from the CALSNIC dataset of image contrast when different lengths of TR and TE are applied at the time of image acquisition.

Figure 10. Random (Gaussian) and restricted (non-Gaussian) diffusion of water molecules in unrestricted and restricted environments (Mahmood and Hansen 2017).

Figure 11. Spherical and elliptical orientations of water molecules in unrestricted and restricted motion, respectively (Karlsgodt et al. 2008).

Figure 12. Ellipsoid or diffusion tensor model corresponding to water diffusion in neural tissue (Kashefi and Winston 2020). In unrestricted (isotropic) diffusion, the tensor attains a spherical orientation and in restricted (anisotropic) diffusion, the tensor attains an elliptical orientation. The greater the $\lambda 1$ magnitude, the greater the fractional anisotropy.

Chapter 2

Chapter 3

Chapter 4

Chapter 5

Figure 3. Correlations between foot tapping frequency and a) white matter fractional anisotropy and b) tNAA/Cr metabolite ratios.

Figure 4. Regional associations of reduced functional connectivity with PMC neurochemistry. L = left, R = right, A = anterior, P = posterior.

Supplementary. Figure S1. FC of the PMC in Bulbar-onset ALS. The colour bars represent the SPM(T) statistic for increased and reduced FC. Colour bars represent the SPM(T) statistic for each map across the whole brain ranging from lowest (blue) to the highest (red). See Table S2 for details on the cluster extents and locations. L = left, R = right, A = anterior, P = posterior.

Supplementary. Figure S2. Positive regional associations of reduced functional connectivity with PMC neurochemistry and WM diffusion. Colour bars represent the positive SPM(T) statistic for each map (red to yellow). See Table S5 for details on the cluster extents and locations.

Supplementary. Figure S3. FC of the PMC in Limb-onset ALS. The colour bar represents the SPM(T) statistic for reduced FC. Colour bars represent the SPM(T) statistic for each map across the whole brain ranging from lowest (blue). See Table S7 for details on the cluster extents and locations. L = left, R = right, A = anterior, P = posterior.

Supplementary. S11. Assessment of whether correlations in Table 4 in the main document are driven by either ALS subgroup (Limb-onset ALS or Bulbar-onset ALS)

List of abbreviations

ALS	amyotrophic lateral sclerosis
UMN	upper motor neuron
LMN	lower motor neuron
TARDBP	tar DNA binding protein
SOD1	superoxide dismutase 1
C9orf72	chromosome 9 open reading factor 72
FUS	fused in sarcoma
AMPA	α-amino-3-hydroxy-5-isoxazole propionate
EAAT	excitatory amino acid transporter
ROS	reactive oxygen species
FTD	frontotemporal dementia
iPSC	induced pluripotent stem cell
iNSC	induced neural stem cell
iN	induced neurons
FTLD	frontotemporal lobar degeneration
ALSci	ALS cognitive impairment
ALSbi	ALS behavioural impairment
ECAS	Edinburgh Cognitive and Behavioral ALS Screen

MoCA	Montreal Cognitive Assessment
2SD-NAC	2 standard deviations – North American cutoff
PLS	primary lateral sclerosis
PMA	progressive muscular atrophy
bvFTD	behavioural variant of FTD
MRI	magnetic resonance imaging
PET	positron emission tomography
EEG	electroencephalography
TMS	transcranial magnetic stimulation
MEG	magnetoencephalography
NMR	nuclear magnetic resonance
RF	radiofrequency
TR	repetition time
TE	echo time
DWI	diffusion weighted imaging
FA	fractional anisotropy
MD	mean diffusivity
AD	axial diffusivity
RD	radial diffusivity

DTI	diffusion tensor imaging
fMRI	functional MRI
BOLD	blood-oxygenation-level-dependent
RSN	resting-state network
DMN	default mode network
MRS	magnetic resonance spectroscopy
ROI	region-of-interest
VBA	voxel-based analysis
TBSS	tract-based spatial statistics
FC	functional connectivity
ICA	independent component analysis
TBR	template-based rotation
CST	corticospinal tract
SBC	seed-based connectivity
CALSNIC	Canadian ALS Neuroimaging Consortium
ComBat	Combating batch effects when combining batches

Chapter 1: General Introduction

1.1. General overview of ALS

Amyotrophic lateral sclerosis (ALS) is a complex adult-onset neurodegenerative disorder. The incidence of ALS is 2/100,000 per year (Marin et al. 2017) with a mean age of onset of 55 years. It is considered to be the most frequently occurring motor neuron disorder (Braak et al. 2013) and is characterized by the degeneration of cortical or upper motor neurons (UMNs) and spinal or lower motor neurons (LMNs). The complexity of ALS is a result of its genotypic and phenotypic heterogeneity. Over 50 genes contribute to the genotypic heterogeneity of ALS (Taylor, Brown, and Cleveland 2016). The occurrence of ALS has been linked to genetic or familial factors in about 5-10% of all cases, with the remaining majority of cases having an unknown or sporadic etiology. Phenotypic variability in ALS is contributed by factors such as genetics, region of onset, type of motor neuron involvement, the extent of extra-motor involvement, and the duration of symptoms (Swinnen and Robberecht 2014) – providing evidence of the multisystem nature of the disease. Depending on a combination of variables contributing to disease in an individual, the presentation of the symptoms of ALS can be heterogenous. Classically, ALS can present as painless progressive muscle weakness (paresis) (Goutman 2017) which can result in a decreasing ability to perform activities such as walking, running, swallowing food, and ultimately respiration. A recent review has suggested that after the onset of symptoms, patients wait for about 3-6 months before contacting a primary care provider (Richards, Morren, and Pioro 2020). Coupled with other factors such as delays from referrals to specialists, misdiagnosis, age and region of onset, or the presence of comorbidities, the diagnostic delay for a patient with ALS can range from 10 to 16 months (Richards, Morren, and Pioro 2020). Following diagnosis, the survival of an ALS patient ranges from 3-5 years (Taylor, Brown, and Cleveland 2016).

The most common presentation of ALS involves onset in a distal limb with contiguous spread rostrocaudally and contralaterally to other limbs (Goutman 2017). This type of onset is generally

classified as limb-onset ALS. Some patients may present with difficulties in swallowing (dysphagia) and speech (dysarthria), which is classified as bulbar-onset ALS and occurs in approximately 20-30% of all ALS cases (Swinnen and Robberecht 2014). A small percentage of cases can present with breathing difficulties and/or cognitive and behavioural impairment (Goutman 2017). ALS can also coexist with other disease pathologies and present with extrapyramidal involvement (impairment of the dopaminergic neurons in the nigrostriatal pathway), cerebellar ataxia (impairment of the cerebellar circuits), as well as sensory involvement (Swinnen and Robberecht 2014). Therefore, given the heterogeneity of presentation, it is important to stratify the patients into well-established clinical phenotypic subtypes (based on genetic information, and diverse motor and psychological features) to provide an accurate diagnosis, treatment plan, and aid their inclusion in clinical trials (Swinnen and Robberecht 2014).

1.2. Pathophysiology of ALS

Identification of the biological mechanisms that contribute to the presentation of these clinical features is important to understanding the pathophysiology of ALS. These pathophysiological mechanisms include the interplay of a variety of factors such as environmental and lifestyle factors, genetics, neuronal and glial dysfunction, impaired protein homeostasis, aberrant RNA metabolism, mitochondrial dysfunction, excitotoxicity, and metabolic dysregulation (Figure 1) which are discussed in the following sections.

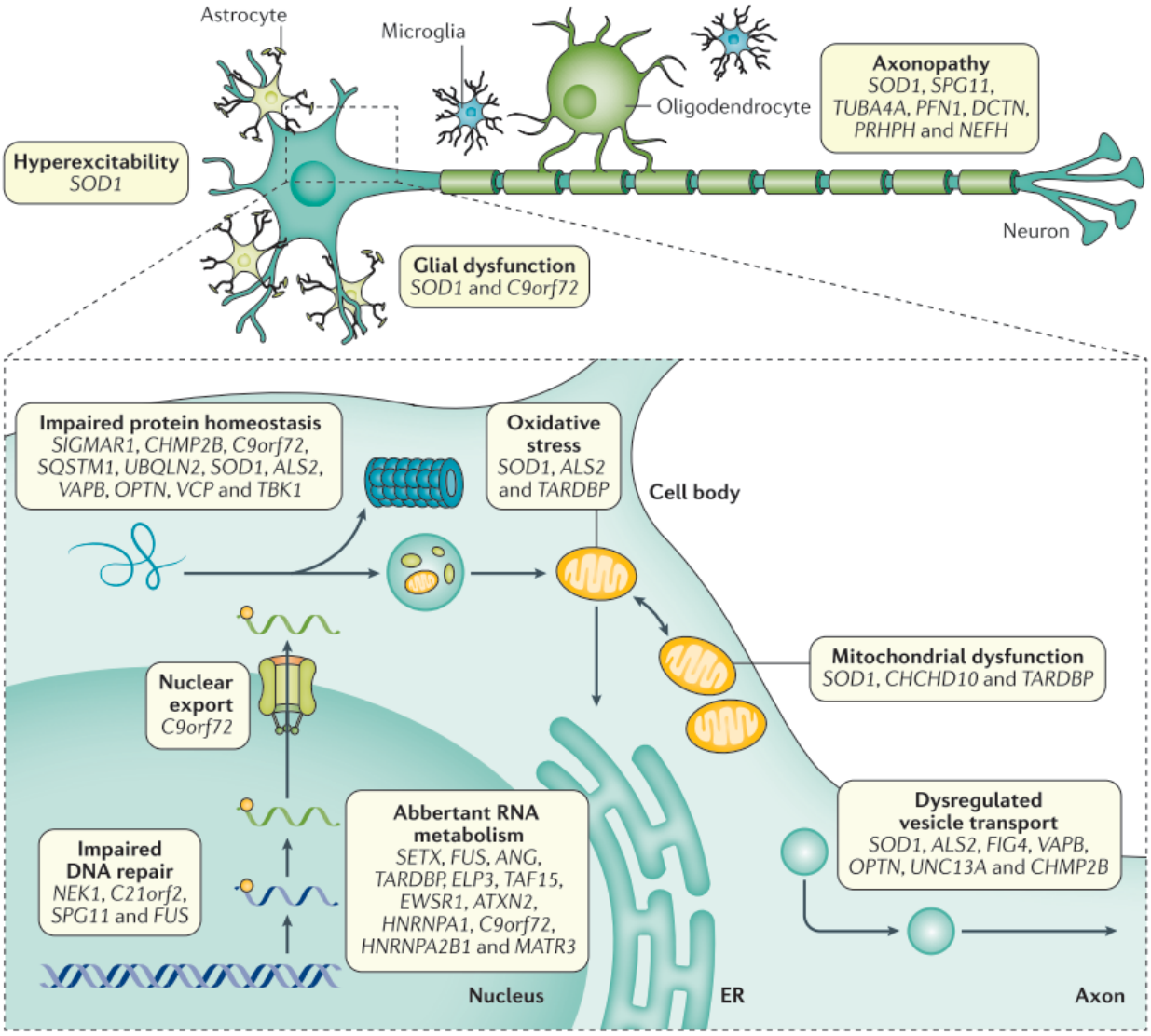

Figure 1. Mechanisms contributing to the pathophysiology of ALS. These mechanisms have been implicated to be direct consequences of several gene mutations in ALS and have been thought to be interlinked. SOD1 is a gene that has been studied extensively and has been associated with, in combination with other genes, the occurrence of a large number of pathophysiological mechanisms such as hyperexcitability, glial dysfunction, mitochondrial dysfunction, and oxidative stress. C9orf72 has been linked to mechanisms such as aberrant RNA metabolism, impaired DNA repair, impaired nuclear transport, and impaired protein homeostasis. Other mechanisms such as impaired nuclear export, impaired DNA repair and dysregulated vesicle transport can directly alter neuronal function. Source: Hardiman et al., 2017

1.2.1. Environmental and lifestyle factors

Environmental exposure to neurotoxins is assumed to be a weak factor in the causation of the disease. For example, exposure to water containing cyanobacteria blooms, or exposure to the neurotoxin β-methylamino-l-alanine have been suggested to be possible environmental triggers in susceptible populations (Hardiman et al. 2017). An epidemiological study has suggested that environmental triggers could be active for years before the clinical onset of disease (Factor-Litvak et al. 2013). These environmental factors could include excessive smoking, exposure to pollutants, dietary patterns, occupation, excessive physical activity, and changes to the body's immune response (Eisen et al. 2014).

1.2.2.Genetics

ALS is a neurodegenerative disorder that has a complex Mendelian inheritance pattern (Hardiman et al. 2017). Variations in over 50 genes have already been associated with ALS (Taylor, Brown, and Cleveland 2016). Of the 5-10% cases of *genetically linked (familial)* ALS, a majority of cases (30%) can result from a hexanucleotide repeat expansion in the chromosome 9 open reading factor (C9orf72), 20% result from a mutation in the superoxide dismutase 1 (SOD1) gene, and 4-5% of the cases have been linked to mutations in the transactive response DNA binding protein (TARDBP) and fused in sarcoma (FUS) genes (S. Chen et al. 2013). The remainder (45%) of the familial cases have been linked to mutations in other genes such as the vesicle associated membrane protein associated protein B (VAPB), angiogenin (ANG), ataxin 2 (ATXN2), factor induced gene 4 (FIG 4), optineurin (OPTN), and other genes that are still undiscovered (S. Chen et al. 2013).

However, the discovery of genes contributing to *sporadic forms of ALS* (90-95% of all cases) has been largely unsuccessful with only about 10% of the cases having an identified genetic basis (Boylan 2015). Genome wide association studies in sporadic ALS suggest that the genetic variants

that render the patients 'high-risk' might be specific to their family ancestry (van Rheenen et al. 2016). Heritability studies estimate that 60% of the risk for ALS is determined genetically and the remaining 40% is contributed by environmental factors (Al-Chalabi et al. 2010). The interactions between mutations in the genes for familial ALS and cellular, neuronal, and glial functions have been shown to result in the degeneration of motor neurons via biological mechanisms which contribute to ALS pathophysiology. These genetically linked pathophysiological mechanisms include protein aggregation, aberrant RNA processing, oxidative stress, mitochondrial disruption, apoptosis or programmed cell death, microglial activation, metabolic dysregulation, and axonal dysfunction (Figure 2) (S. Chen et al. 2013).

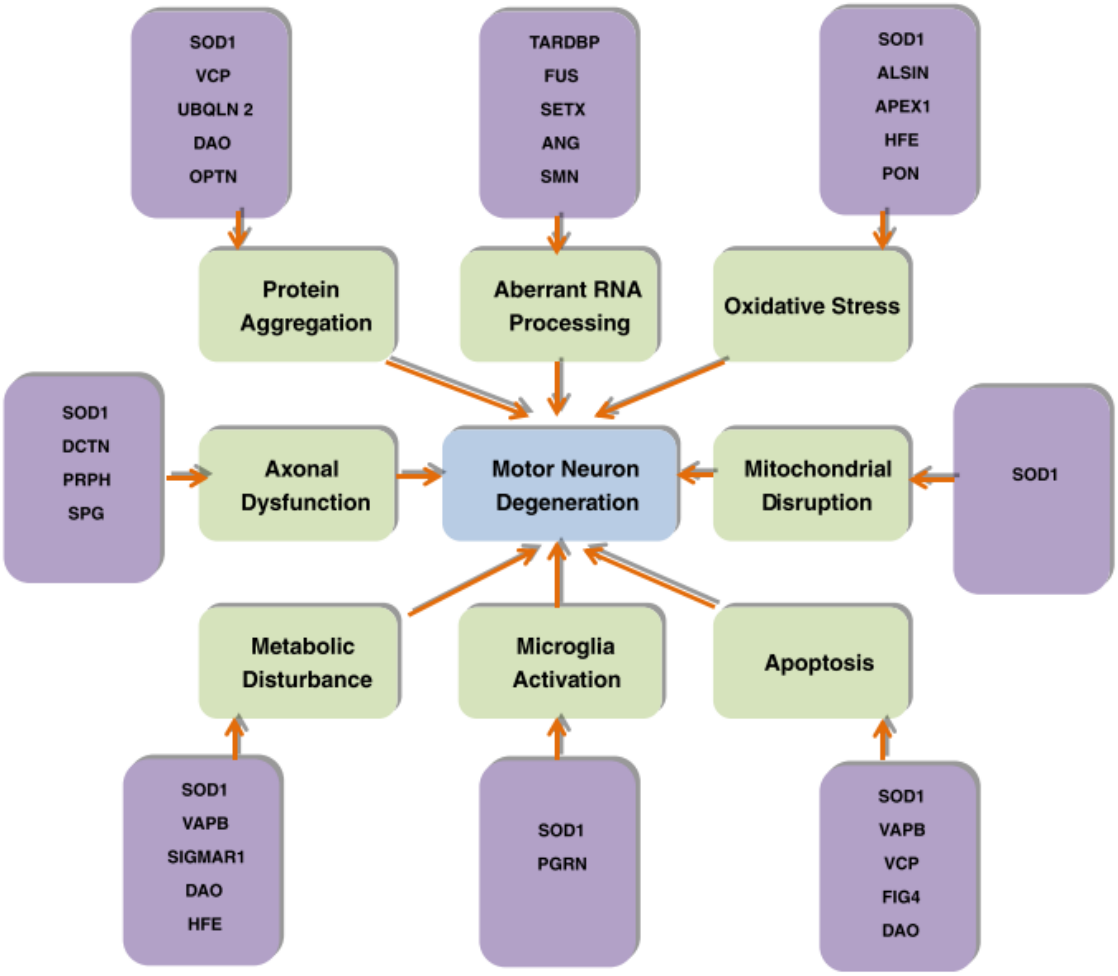

Figure 2. Interactions of ALS-specific genes with cellular, neuronal, and glial processes contributing to the degeneration of motor neurons in familial ALS. Boxes on the outside in purple list the genes associated with the different pathophysiological processes (boxes on the inside in green). Source: Chen et al., 2013.

1.2.3.Impaired protein homeostasis

Protein homeostasis involves the translation of a gene to a protein, protein folding, and clearance. During the translation process of a gene into a protein, the presence of mutations in a gene can result in the generation of misfolded proteins. The accumulation of these misfolded proteins can contribute to various neurodegenerative diseases and is central to ALS pathophysiology. The disruption of the two main pathways for excessive protein clearance – autophagy and the ubiquitin-proteasome system – are considered to be key players in the pathogenesis of ALS (Mejzini et al. 2019). The proteinopathies of ALS-linked genes (e.g., SOD1, TDP-43, and C9orf72) contributing to impaired protein-related ALS pathogenesis are discussed in the following sections.

a) TDP-43 is a DNA/RNA binding protein consisting of 414 amino acids which is localized to the nucleus and is encoded by the TARDBP gene (Mejzini et al. 2019). TDP-43 acts as a regulator of gene expression and plays an important role in different steps of RNA processing including RNA splicing, mRNA transport, regulation of mRNA stability, and the regulation of non-coding RNAs (Mejzini et al. 2019). TDP-43 also functions as a transporter protein molecule that can easily cross the nuclear membrane into the extra-nuclear cytoplasm of the cell and shuttle back and forth (Ayala et al. 2008).

   Mutations in the TARDBP gene resulting in abnormal function of TDP-43 were first identified in 2008 as a cause of neurodegeneration in ALS (Mejzini et al. 2019). Familial cases of ALS with C9orf72 hexanucleotide repeat expansions and sporadic cases of ALS not containing any pathogenic variants in the TARDBP gene were shown in histopathological studies to contain ubiquitin-positive cytoplasmic aggregates of TDP-43 protein (Takeuchi et al. 2016), suggesting a dysfunction of the ubiquitin-proteasome system and mislocalization of the protein

from the nucleus to the cytoplasm in the brain and spinal cord (Hardiman et al. 2017) (Figure 2) – this is now considered to be a pathological hallmark of ALS.

The discovery of mislocalization of TDP-43 from the nucleus to the cytoplasm has been instrumental in proposing different mechanisms of the disease which involve a loss of normal TDP-43 function in the nucleus, a gain of toxic TDP-43 function, or a combination of both (Mejzini et al. 2019). The various animal models used to study the loss/gain of TDP-43 function are discussed in a later section.

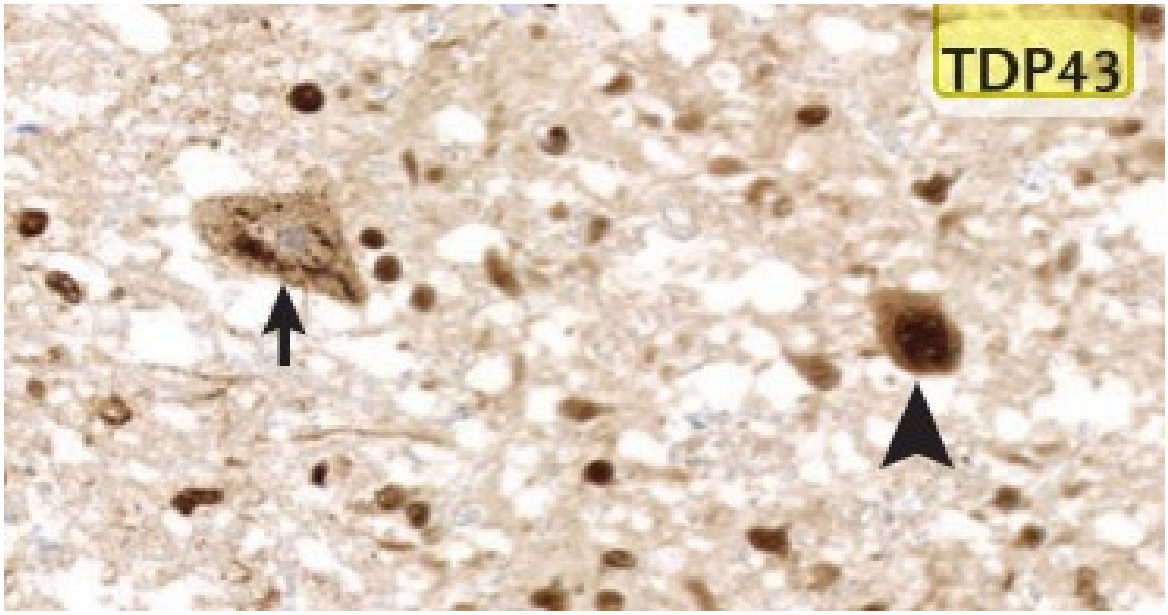

Figure 3. Normal and aberrant localization of TDP-43 in the neuronal cell. The arrow on the left depicts a neuron showing abnormal localization of TDP-43 in the cytoplasm of the neuron, whereas the arrowhead on the right depicts a neuron showing normal localization of TDP-43 in the nucleus of the neuron. Figure sourced and modified from Hardiman et al., 2017.

The depletion of TDP-43 in the nucleus has been thought to result in the upregulation of TDP-43 synthesis continually and the increase of TDP-43 in the cytoplasm has been linked to the formation of protein aggregates resulting in cellular dysfunction alongside the dysregulation of mRNA metabolism in the nucleus (Mejzini et al. 2019).

b) SOD1 is a protein that maps to the chromosome 21q22.1 (S. Chen et al. 2013), encodes a metalloenzyme consisting of 153 amino acids, binds one molecule each of copper and zinc (S. Chen et al. 2013) generating an extremely stable homodimer (Mejzini et al. 2019). SOD1 protein dimers are present in the cytosol and intermembrane space of the mitochondria and provide an important antioxidant defence mechanism against reactive oxygen species produced as a product of normal cellular respiration (Mejzini et al. 2019). The pathogenic variants of SOD1 have been shown to occur in approximately 15-30% of the familial cases of ALS (Zou et al. 2017) and about 1-4% of the sporadic cases of ALS (S. Chen et al. 2013).

   Mutations in the SOD1 gene have been studied extensively and related to disease phenotype, duration, and severity. Approximately 185 mutations have been located in the SOD1 gene; patients with mutations recognized as the G85R and G93A variants, among others, have been observed to have a rapid progression of the disease and shorter survival, and those with G93C, D90A, and H46R variants have been associated with longer life expectancies (Mejzini et al. 2019). The exact mechanisms by which SOD1 mutations contribute to the pathophysiology of ALS are unknown; however, mechanisms such as misfolded protein aggregation, oxidative stress, mitochondrial dysfunction, glutamatergic excitotoxicity, inflammation, and mitochondrial dysfunction have been postulated to contribute to gain of toxic SOD1 function in ALS (S. Chen et al. 2013).

c) A hexanucleotide repeat expansion in the non-coding region of the C9orf72 gene was discovered in 2011 as the cause for a majority of the cases for familial ALS (Renton et al. 2011) and has been shown to occur in 34% of familial and 5% of sporadic cases of ALS in the European populations but not in the Asian populations (Zou et al. 2017). People without ALS typically have about 5-10 copies but patients with ALS may have thousands of copies of this hexanucleotide repeat expansion (Mejzini et al. 2019).

   The mechanisms of action of the C9orf72 gene in ALS are still unknown. The C9orf72 gene might contribute to ubiquitin-positive, p62-positive, and TDP-43 negative inclusions in the

extra-motor brain regions and result in a loss of function in autophagy initiation, contributing to the toxic accumulation of misfolded proteins (Hardiman et al. 2017). However, a reduction in the levels of C9orf72 mRNA and proteins in patients with ALS formed the basis for a hypothesis that states that a loss of the protein might be associated with the disease (Xiao et al. 2015). The models for loss and gain of function for C9orf72 are discussed in a later section.

1.2.4.Aberrant RNA metabolism

RNA metabolism includes various processes such as RNA splicing, transcription, transport, translation, and storage in free granules. These processes are mediated by RNA-binding proteins. In ALS, disease causing variations have been associated with the RNA-binding proteins such as TARDBP, C9orf72, and FUS (Mejzini et al. 2019), among others. ALS-linked RNA-binding proteins contain many prion-like domains that result in the development of stress granules that sequester specific mRNAs and inhibit the mRNA translation process (Mejzini et al. 2019).

1.2.5.Glial dysfunction

Microglia are the innate immune cells of the central nervous system and are employed in all forms of ALS (Taylor, Brown, and Cleveland 2016). The GTPase namely RAC1 in microglial cells are responsible for the reduction of oxidative stress by limiting the activation of the enzyme NADPH oxidase that generates intracellular superoxidase; however, in SOD1 ALS, misfolded mutant SOD1 can interfere with this process and drive microglia to generate excess amounts of extracellular superoxidase (Taylor, Brown, and Cleveland 2016). Therefore, the microglial synthesis of mutant SOD1 is considered to be an important determining factor of rapid disease progression. A number of experiments have been performed to study this including the silencing of mutant SOD1 in microglia, using cell grafts to replace mutant SOD1 microglia with normal microglia, and inhibition of the transcription factor NF-κB to suppress the neuroinflammation resulting from the toxic functions of activated microglia (Taylor, Brown, and Cleveland 2016). In a C9orf72-linked ALS mouse model, the inactivation of a potential guanine exchange factor for

one or more G-proteins has been shown to result in abnormal microglia and age-related neuroinflammation, providing evidence of non-cell-autonomous inflammatory processes in ALS (Taylor, Brown, and Cleveland 2016).

Oligodendrocytes are myelinating cells of central nervous system processes such as axons of the UMNs and the initial axonal segments of the LMNs. These cells are replaced by the proliferation of oligodendrocyte precursor cells which are abundantly present throughout the central nervous system. However, in ALS, the differentiation process of the precursor cells fails at the final stages, contributing to motor neuronal axonopathy (Hardiman et al. 2017). In SOD1 ALS, a delay in the onset of disease has been associated with a suppression of mutant SOD1 protein expression in the early stages of oligodendrocyte maturation (Taylor, Brown, and Cleveland 2016). The levels of the energy metabolite lactate protein, namely the monocarboxylate transporter 1, supplied by the oligodendrocytes to support the functioning of motor neurons, have been shown to be reduced in the motor cortices of mice models as well as ALS patients (Mejzini et al. 2019; Taylor, Brown, and Cleveland 2016).

Astrocytes are glial cells that are involved in providing motor neurons with nutrients, ion buffering and recycling of the neurotransmitter glutamate, as well as interacting with microglial cells (Taylor, Brown, and Cleveland 2016). The association between astrocytic impairment and excitotoxicity is discussed in the next section.

1.2.6. Excitotoxicity – metabolic dysregulation and astrocytic dysfunction

Hyperexcitability is a characteristic of cortical or upper motor neurons which can occur because of increased intrinsic excitation, decreased inhibition, or a combination of both. An increase in cortical excitability can occur due to increased concentrations and reduced uptake of extracellular

glutamate. Glutamatergic excitotoxicity can result in the impaired uptake of excess glutamate by the GluR2 subunit of the α-amino-3-hydroxy-5-isoxazole propionate (AMPA) receptor system of the neuronal cell membrane and the excitatory amino acid transporter (EAAT)-2 receptor subunit localized to the neuronal and glial cell membranes (Blasco et al. 2014; Van Den Bosch et al. 2006). The dysregulation of both of these synaptic glutamate uptake pathways have been linked to mutations in the SOD1 gene in familial ALS; mutant SOD1 sensitizes the GluR2 subunit to glutamatergic excitation and inactivates the EAAT2 receptor in the presence of ROS (Blasco et al. 2014). Sensitization of the GluR2 AMPA receptor subunit results in an increase in the levels of extracellular glutamate in the neuronal environment which results in increased influx of calcium ions into the neurons (Bear 2016). Decreased calcium buffering capability of the cell, in addition to impaired glutamate clearance, results in a constant state of depolarization for the neuronal membrane – thereby reducing the threshold for depolarization of the neuronal membrane (hyperexcitability). Increased calcium concentrations in the neuronal cell activates apoptotic enzymes such as phospholipases, proteases, and endonucleases that can damage the components of the cytoskeleton, cell membrane, mitochondria, and genetic material, and lead to neuronal cell death (Bear 2016; Blasco et al. 2014). Reduced glutamate clearance from the synapses and the extracellular neuronal environment also occurs due to the dysfunction of the astrocytic EAAT2 transporter protein. Reduced expression of the EAAT2 transporter protein channels as well as mutations in the EAAT2 gene have been reported in SOD1 mice models of ALS (Van Den Bosch et al. 2006); however, these findings have not been confirmed in humans. In addition, excitotoxicity in ALS occurs because of other factors including the selective vulnerability of motor neurons, high concentrations of calcium permeable AMPA receptors on the neuronal cell membrane, chloride influx related AMPA receptor mediated excitotoxicity (Van Den Bosch et al. 2006).

1.2.7.Mitochondrial dysfunction and oxidative stress

Mitochondrial dysfunction is an event that can occur early on in various neurodegenerative diseases (Reddy 2008) and serve as a precursor to various neurodegenerative processes. An imbalance in mitochondrial fission/fusion reactions is postulated to cause mitochondrial

fragmentation in the presymptomatic/early stages of ALS (Eisen et al. 2014). As a result of being a very active process, mitochondrial renewal can cause mutations in the mitochondrial DNA, thereby accelerating the accumulation of disease pathology (Chinnery et al. 2012). Mitochondrial dysfunction related pathogenic mechanisms occur due to the abnormal aggregation products of ALS related genes, impaired autophagic clearance of damaged mitochondria, and mitochondrial damage due to aberrant RNA processing (Mejzini et al. 2019). The majority of reactive oxygen species (ROS), molecules that contribute to oxidative stress are produced in large concentrations by mitochondria, with large amounts of superoxide radicals generated as a by-product of cellular respiration (Mejzini et al. 2019).

Oxidative stress is a process that occurs as a result of the excessive production of reactive oxygen species (ROS), over and above the rate at which these can be removed from the cell by antioxidants. When antioxidants are unable to neutralize ROS, these can result in catastrophic outcomes for the cell, such as lipid peroxidation and protein glycoxidation that have been shown to occur in the spinal cords of sporadic ALS patients (Mejzini et al. 2019). However, in a progressive neurodegenerative process, the capacity of the cells to balance the reduction-oxidation reactions decreases (X. Chen, Guo, and Kong 2012). ROS toxicity can cause damage to the mitochondrial DNA leading to a disruption of the respiratory chain, thereby further increasing ROS levels and facilitating cellular damage – resulting in the formation of a self-amplifying cycle of ROS toxicity (X. Chen, Guo, and Kong 2012).

Mitochondrial dysfunction is also associated with the specificity of the ALS-related genetic mutation. Normal SOD1 acts as a cytosolic antioxidant. However, in ALS, mutant SOD1 does not assume a loss of antioxidant function; it is associated with the increased production of ROS by interacting with mitochondria and other proteins (Mejzini et al. 2019). Mutation of the TAR DNA binding protein (TARDBP) results in increased localization of the TDP-43 protein molecules in the mitochondria (Hardiman et al. 2017) where they bind to and disassemble the respiratory chain complex 1 subunits encoded by micro ribonucleic acids (mRNAs) (W. Wang et al. 2016). A

CHCHD10 mutation can impair mitochondrial genome maintenance, promote the loss of mitochondrial cristae junctions, and interfere with apoptosis by preventing the release of cytochrome c (Genin et al. 2016).

1.3. Models for the study of ALS pathophysiology

1.3.1. General overview of the models for the study of neurodegenerative disorders

Neurodegenerative disorders, in general, are characterized by the uncontrolled, age-related loss of neurons, leading to an impairment of brain function and are associated with a wide range of clinical presentations (phenotypes) including impaired motor function, cognition, and behaviour (Slanzi et al. 2020). As such, the determination of the genotype of an individual with a neurodegenerative disorder is important to obtaining an understanding of the disease phenotype. This genotypic-phenotypic correlation is more feasible if the individual has family members previously diagnosed with a neurodegenerative disorder or if the genotype of the individual resembles previously discovered genetic abnormalities. As the majority of patients have an unknown disease etiology, the information obtained from genetic forms of the disease is unable to completely characterize sporadic forms of the disease. However, such information can provide surrogates to study the physiological mechanisms underlying the disease and for the development of targeted disease-modifying therapies (Dawson, Golde, and Lagier-Tourenne 2018).

1.3.2. Models for the study of ALS

ALS is a neurodegenerative disorder that shares pathogenic pathways with frontotemporal dementia (FTD) (Swinnen and Robberecht 2014). The strongest connecting link between the two disease entities is a hexanucleotide repeat expansion in the C9orf72 gene (Renton et al. 2011). Other genetic links between the two diseases include the mutations and/or mislocalizations of

previously discussed genes such as TDP-43, FUS, ataxin 2 (Dawson, Golde, and Lagier-Tourenne 2018) – to name a few. ALS is therefore considered to be a multisystem disorder, affecting motor, cognitive, and behavioural systems. While ALS and FTD are clinically distinct disorders, motor neuron deficits and cognitive impairment can coexist in familial forms of both disease entities, with substantial clinical, genetic, and pathological overlap (Dawson, Golde, and Lagier-Tourenne 2018).

Therefore, the generation of a controlled system (referred to as modelling) is important to obtain a better understanding of the biological pathways that underlie clinical presentation of the disease. In a model, the complex interactions between cells and cell-specific circulating hormones and factors are important to the characterization of the physiological mechanisms and systemic interactions between different organ systems. Such models are largely generated from animal species, generally other mammals, before applying the findings to human species. This is because humans and other mammals are considered to be complex organisms that develop distinct physiological mechanisms in a highly regulated and integrated manner (Barré-Sinoussi and Montagutelli 2015) in a similar fashion. For example, models generated by inducing a mutation in the SOD1 gene (ALS) or MAPT gene (FTD) have been helpful in the identification of disease mechanisms and in the generation of preclinical models to study the impact of potential therapeutics (Dawson, Golde, and Lagier-Tourenne 2018). However, species-specific differences in genome, brain anatomy, differences in normal aging processes – to name a few – between humans and laboratory regulated mammals can pose challenges to a direct comparison of pathophysiological mechanisms or drug effects (D'Souza et al. 2021). Therefore, there was a need to generate disease models that more closely resembled disease in humans in terms of specific genes, protein and molecular pathways. This was accomplished by the utilization of in-vitro cell culture models such as human-induced pluripotent stem cells (iPSCs), induced neural stem cells (iNSCs), and induced neurons (iNs) (D'Souza et al. 2021). The starting point for each of these in vitro cell cultures are fibroblast cells obtained from humans that are converted using different processes (Figure 4) into human iPSCs and iNs. Human iPSC neurons are versatile cells – they can be differentiated into microglia – and can help characterize a patient's unique genome in a dish

and can help in the identification of factors contributing to the neurodegenerative disease processes, especially those that are genetically determined (D'Souza et al. 2021). Cells that undergo a direct conversion to iNs do not undergo the conversion to the pluripotent fetal state. This may allow the cells to retain more of the epigenetic signature of the starting fibroblast cells, rendering them more likely to represent phenotypes which may occur with normal cellular aging.

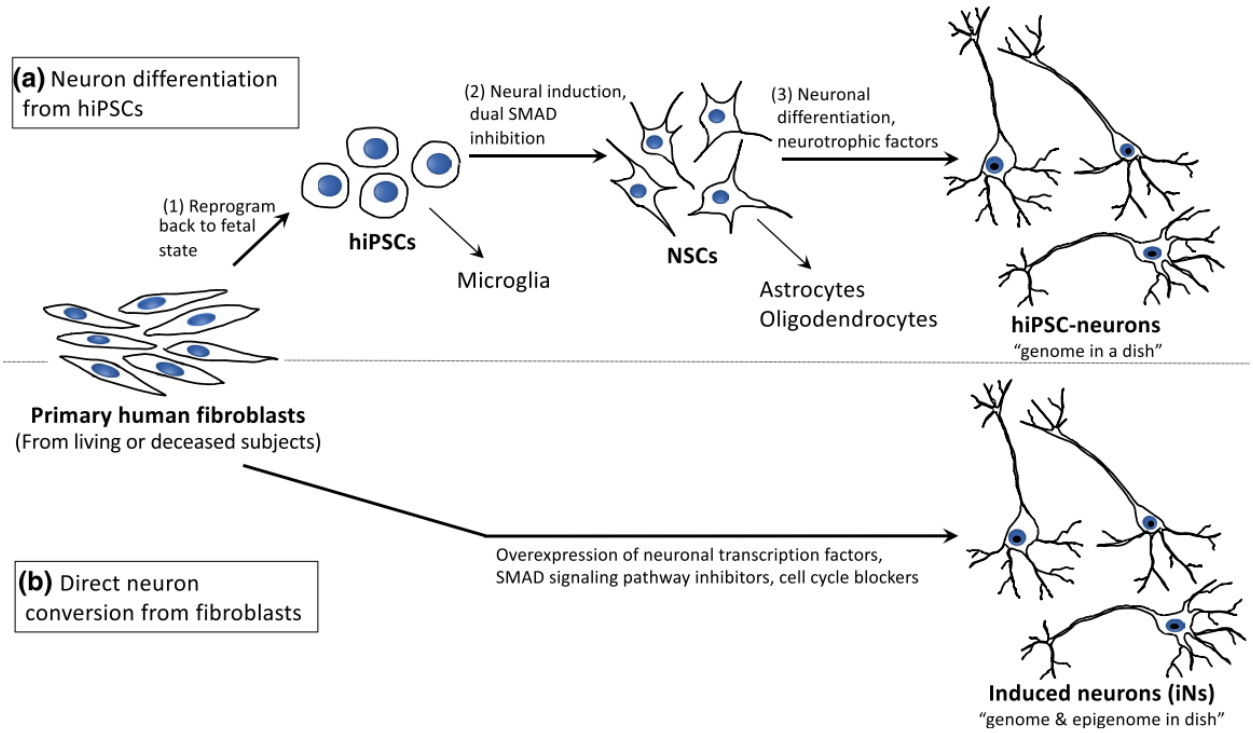

Figure 4. A schematic of the steps involved in the generation of in-vitro models for the study of neurodegenerative disorders. In panel (a), the schematic pathway for neuronal differentiation from human-induced pluripotent stem cells involves (1) reprogramming human primary fibroblasts or other somatic primary cells back into the fetal state by introducing defined transcription factors, (2) inducing neural fate through the inhibition of an dual intercellular signalling pathway (also known as the SMAD pathway), resulting in the formation of neural stem cells, and (3) differentiating neurons with the help of neurotrophic factors. Panel (b) shows a schematic of a pathway for the direct conversion of fibroblasts to neurons in which the same starting fibroblasts can be directly converted into induced neurons by the introduction of neuron-specific transcription

factors and other small molecules that include SMAD pathway inhibitors and cell cycle blockers. Source: D'Souza et al., 2021.

Technological advancements have been instrumental in progressively improving the elegance of models used to study ALS. Models can be classified on the basis of their physical representations which include cell lines and primary cell cultures, various small animal and rodent models, in vitro biochemical models, and patient-derived cellular models. Another method of model classification is dependent on the pathophysiological mechanism being studied including proteinopathies of ALS-linked genes, the role of iNs in the understanding of genetic mutations and cell survival. The following sections briefly outline various models employed to understand ALS pathophysiology.

1.3.2.1. Proteinopathy models

Proteinopathies refer to the misfolding and/or mislocalization of various proteins that are linked to diseases such as ALS. As discussed in earlier sections, TDP-43 and SOD1 are key players towards the understanding of ALS pathophysiology.

In SOD1 rodent (mice, rats) models of ALS, the degeneration of upper and lower motor neurons, denervation of the neuromuscular junction, progressive limb weakness resulting in paralysis, and reduced lifespan (Dawson, Golde, and Lagier-Tourenne 2018) are features that have been observed when the models were made to overexpress the missense, mutant, or truncated human forms of the SOD1 gene (Mejzini et al. 2019); interestingly, the deletion of the SOD1 gene was not associated with an impairment of motor neurons (Dawson, Golde, and Lagier-Tourenne 2018). However, a major limitation of SOD1 rodent models is the inability to characterize sporadic forms of the disease which are associated with the accumulation of mutant and/or misfolded TDP-43.

The physiological mechanisms surrounding the role of TDP-43 in ALS have been postulated to be categorized into two classes – the loss of normal TDP-43 function, and the gain of toxic TDP-43 function. Several mice models have been used to test the loss of TDP-43 function hypothesis in ALS. As TDP-43 is important to embryonic development, homozygous mice models not containing TDP-43 have been shown to not be viable; the same study showed the presence of motor deficits without the degeneration of motor neurons and reduction in TDP-43 protein levels in heterozygous mice with a TARDBP deletion (Kraemer et al. 2010). Other mice models were generated to overexpress TDP-43 in order to study the gain of function hypothesis. The overexpression of the wildtype and mutant forms of TDP-43 resulted in neuronal degeneration, and the overexpression of normal human TDP-43 has been shown to result in protein fragmentation into 25kDa and 35kDa fragments that are typically observed in human ALS (Mejzini et al. 2019).

1.3.2.2. Human induced pleuripotent stem cell models

In ALS, motor neurons derived from iPSCs have been used to study genetic variants in SOD1, TARDBP, C9ORF72, FUS and in models of sporadic disease (Mejzini et al. 2019). SOD1 variant iPSC models of ALS have been successful in reflecting the pathological features observed in patients such as the aggregation of the SOD1 protein (Mejzini et al. 2019). In a TARDBP (M337V) iPSC model, motor neurons derived from iPSCs of patients expressing the TARDBP genetic variant have been reported to show increased levels of soluble and detergent-resistant cytoplasmic TDP-43 inclusions as well as reduced survival, whereas other studies did not report these observations despite the use of the same variant of TARDBP (Mejzini et al. 2019) – demonstrating the heterogeneity in observations from the same pathophysiological model. iPSCs derived motor neurons from patients having the C9orf72 variant of ALS express disease-associated characteristics such as mRNA aggregation, alterations in gene expression, nucleocytoplasmic transport defects, and excitotoxic susceptibility (Mejzini et al. 2019).

1.3.2.3. Induced neuronal models

The introduction of neuron-specific transcription factors to human fibroblasts can result in the generation of motor neurons that display disease-specific degeneration. This process is also referred to as the direct reprogramming of motor neurons. These neurons are able to preserve aging hallmarks such as the loss of heterochromatin, damage to DNA, and nuclear organization (Mejzini et al. 2019). Although, research on directly reprogrammed motor neurons is in the initial phases, it is speculated that this model may be more suitable in the study of late-onset neurodegenerative processes compared to human iPSCs (Mejzini et al. 2019).

1.4. General clinical overview of ALS

1.4.1. Clinical features of ALS

A method commonly used in clinic to diagnose and stratify ALS patients is the administration of a physical or neurological examination of upper and lower motor neuronal impairment. The diagnostic criteria commonly used is the revised El Escorial criteria. In accordance with the revised El Escorial criteria, a diagnosis of ALS requires the presence of UMN degeneration on clinical examination and LMN degeneration on clinical, electrophysiological, or neuropathological examination, a progressive spread of UMN and LMN signs within a single region or other contiguous regions, and the absence of other disease processes that might explain the observed degeneration on electrophysiological, neuroimaging, or neuropathological examination (Brooks et al. 2000). Signs of UMN degeneration include increased muscle tone (spasticity) and increased muscular reflexes (hyperreflexia) on physical exam (Hal Blumenfeld 2010), and signs of LMN degeneration include the presence of irregular muscle twitches (fasciculations) and reduction in muscle size (atrophy) (Hal Blumenfeld 2010) (Table 1). Muscle weakness is an observation on physical exam that can occur as a result of the impairment of both UMN and LMN (Hal

Blumenfeld 2010). Figure 5 provides a visual representation of groups of motor neurons impaired in ALS and the grouping of related clinical signs into upper vs lower motor neuronal signs.

Table 1. Summary of observations on neurological examination in the presence of lesions in the lower and upper motor neurons. In the presence of a LMN lesion, the observed signs are muscle weakness, reduction in muscle bulk (atrophy), increased involuntary muscle twitches (fasciculations), decreased muscle tone, and decreased reflexes. In the presence of an UMN lesion, the signs observed are muscle weakness, increased muscle tone and weakness. Changes to muscle bulk and involuntary muscle twitches are not observed in the presence of an UMN lesion.

Sign	**LMN lesion**	**UMN lesion**
Weakness	Yes	Yes
Atrophy	Yes	No
Fasciculations	Yes	No
Tone	Decreased	Increased
Reflexes	Decreased	Increased

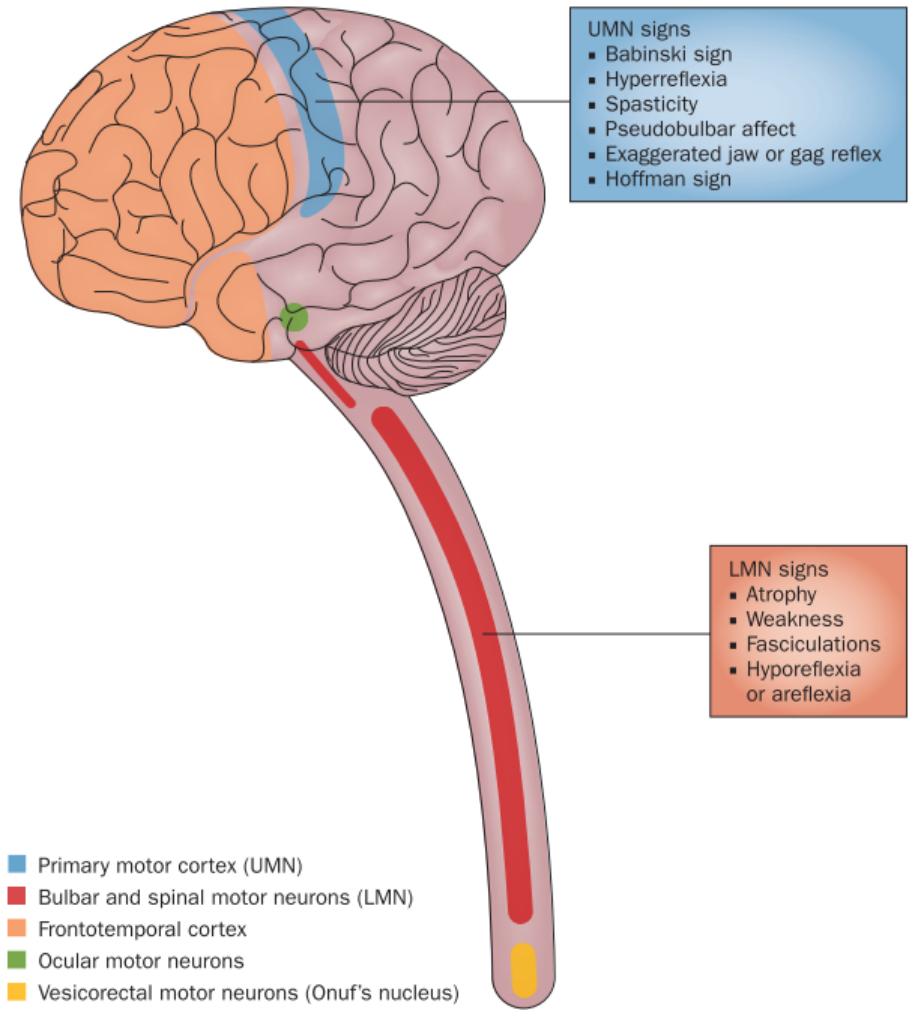

Figure 5. Sites of motor neuronal involvement in ALS. Upper motor neurons are localized to the primary motor cortex and shown in blue. Bulbar and spinal lower motor neurons are shown in red. These two groups of motor neurons are preferentially affected in ALS. Extra-motor neuronal involvement includes the neurons of the frontal and temporal cortices, shown in orange. There is rare involvement of the oculomotor and vesicorectal motor neurons, shown in green and yellow respectively; although it is thought that these motor neurons can be affected in the later stages of longstanding disease. Source: Swinnen et al., 2014

In addition to UMN and LMN degeneration, ALS can also present with non-motor symptoms such as impaired cognition. In a typical multidisciplinary clinic, the incidence of ALS patients with

cognitive impairment is approximately 50% (Woolley and Jonathan 2008). Up to 25% of patients with ALS meet clinical criteria for the clinical manifestation of frontotemporal lobar degeneration, specifically the behavioural variant of frontotemporal dementia (Swinnen and Robberecht 2014). In addition to the impairments of the motor and cognitive systems, small percentages of patients with ALS can also present with extrapyramidal involvement, cerebellar ataxia, deafness, ophthalmoplegia, and the involvement of the sensory, urinary, and autonomic nervous systems – thereby confirming the multisystem nature of the disorder (Swinnen and Robberecht 2014).

1.4.2.Neurological examination for a diagnosis of ALS

The purpose of administering a neurological examination is to diagnose and manage the symptoms that a person might be presenting with. It follows a conventional format which examines mental status, cranial nerves, motor function, reflexes, coordination and gait, and sensory function. The *examination of mental status* is administered to test the function of the frontal and parietal association cortices in the brain (Hal Blumenfeld 2010). The *examination of cranial nerve function* can provide important information that can help pinpoint disorders in the nervous system, rather than a systemic disorder. The examination of *motor function* involves various components such as observation, inspection, palpation, muscle tone testing, functional testing, and muscle strength testing. Examination of *deep tendon reflexes* and plantar response is performed in all patients. These two sections are discussed in the following sections. Examination of *coordination and gait* are performed to identify the presence of any cerebellar dysfunction and a *sensory examination* is performed to check the intactness of sensory responses (Hal Blumenfeld 2010).

1.4.2.1. The examination of motor function

The five components of a motor exam include observation, inspection, palpation, muscle tone testing, functional testing, and muscle strength testing. *Observation* during the motor exam is performed to detect any muscle twitches, tremors, involuntary muscle movements, or any unusual

paucity of movements (Hal Blumenfeld 2010). The *inspection* component involves visually looking at the muscle groups in the hand/arm, shoulder girdle, and leg/thigh to identify muscle wasting or decreases in size (atrophy), increases in muscle size (hypertrophy), and the presence of fasciculations. Typically, in ALS, atrophy of the abductor pollicis brevis and first dorsal interosseous with relative sparing of the abductor digit minimi muscles (split hand syndrome (Z. L. Wang et al. 2019)) and fasciculations are observed (Goutman 2017) which point to the presence of a LMN lesion (Hal Blumenfeld 2010). *Palpation* is performed to check for tenderness in any muscle groups. *Muscle tone testing* is performed to identify any rigidity or resistance when the muscle is in a relaxed state. Typically, in ALS, increased muscle tone (spasticity) is observed (Goutman 2017) which point to the presence of an UMN lesion (Hal Blumenfeld 2010). The modified Ashworth scale is a gradation scale that is used to test muscle tonicity. The scoring ranges from 0 to 4, where 0 corresponds to no increase in muscle tone and 4 corresponds to rigidity in flexion or extension of the affected region (Bohannon and Smith 1987). Following this, *functional testing* of muscles is performed to identify if there are any subtle abnormalities before conducting an examination of muscle strength. This component involves testing for drift and fine motor movements. Next, muscle *strength testing* is performed to identify patterns of weakness that can help localize the presence of a lesion in a cortical or white matter region, spinal cord, nerve root, or peripheral muscle. Muscle strength is often graded on a scale from 0 to 5, where 0 signifies no muscular contraction and 5 signifies normal strength (Hal Blumenfeld 2010).

1.4.2.2. The examination of reflexes

Reflexes can be categorized into deep tendon reflexes and plantar responses. A description of *deep tendon or monosynaptic stretch reflexes* has been provided in a previous section. Increased muscle tone is often accompanied by the increase in reflexes (brisk reflexes or hyperreflexia). With brisk reflexes, a repetitive vibratory contraction of muscle occurring in response to muscle and tendon stretch can be observed (Hal Blumenfeld 2010). This is known as clonus. Deep tendon reflexes are graded according to a scale ranging from 0 to 4+, where 0 corresponds to absent reflex, 1+ corresponds to trace reflexes or reflexes only seen with reinforcement, 2+ corresponds to normal,

3+ corresponds to brisk reflexes, and 4+ corresponds to brisk reflexes with clonus. A normal plantar response is a downward contraction of the toes. However, in ALS, the response is characterized by upward motion of the big toe and the fanning out of the other toes, also known as Babinski sign (Hal Blumenfeld 2010). Other signs of hyperreflexia include the spreading of reflexes to other muscles not being directly tested, crossed adductor reflex of the contralateral leg when the medial aspect of a knee is tapped, and Hoffman's sign indicating brisk reflexes when the fingernail of the middle finger is loosely flicked downward (Hal Blumenfeld 2010). These reflexes can typically be observed in a patient with ALS on neurological examination. Muscle tone and reflexes are usually tested at the same time. In ALS, spasticity and hyperreflexia are thought to occur as a result of the degeneration of pathways that travel in close association with the CST, not as a result of direct damage to the CST itself (Hal Blumenfeld 2010).

Lesions in the frontal lobe can cause the re-emergence of certain primitive reflexes that are present in infants but disappear with increasing age. However, if such responses are observed in adults, they are associated with frontal lobe pathology and are known as frontal release signs. Albeit the controversial nature of such testing, it is of interest in a clinical neurological examination in ALS due to the relative lack of bulbar UMN signs (Tremolizzo et al. 2014). Some examples of frontal release signs observed in ALS are the grasp, snout, and palmomental reflexes (Hal Blumenfeld 2010; Tremolizzo et al. 2014).

1.4.3.Assessment of cognitive and behavioural impairment in ALS

Some patients with ALS can also present with psychological impairments, specifically in cognition and behaviour. These impairments can occur because of the degeneration of brain regions that control various aspects of cognition and behaviour – the temporal and prefrontal cortices (Bear 2016) – known as frontotemporal lobar degeneration (FTLD) (Strong et al. 2009, 2017). The original Strong criteria(Strong et al. 2009) (discussed later) recognized that ALS can coexist with frontotemporal dementia (FTD), a manifestation of FTLD . The criteria recognized the presence

of behavioural and/or cognitive features in ALS that were not sufficient to meet criteria for a diagnosis of dementia but were sufficient to be detected and/or give rise to impairment. These subtypes of ALS were known as ALS-frontotemporal dementia (ALS-FTD), ALS behavioural impairment (ALSbi), and ALS cognitive impairment (ALSci). The criteria was revised in 2015 to include hierarchical axes which would allow the systematic characterization of impairments in social cognition, language, memory, and the presence of neuropsychiatric symptoms (Strong et al. 2017).

A diagnosis of ALSci requires evidence for the impairment of either executive functioning or language or a combination of both (Strong et al. 2017). Some instruments that have been reported in the literature that can be used to screen for impaired cognition or behaviour are the Addenbrooke's Cognitive Examination – revised (ACE-R), the ALS-Brief Cognitive Assessment (ALS-BCA), the ALS-Cognitive Behavioral Screen (ALS-CBS), the Edinburgh Cognitive and Behavioral ALS Screen (ECAS), the Frontal Assessment Battery (FAB), the Mini-Mental State Examination (MMSE), the Montreal Cognitive Assessment (MoCA), the Penn State Screening examination of Frontal and Temporal dysfunction Syndromes (PSSFTS), and the University of California San Francisco – Screening Battery (UCSF-SB) (Gosselt, Nijboer, and Van Es 2020). The majority of these cognitive tests do not perform an in-depth assessment of cognitive function, test only specific cognitive domains, or are non-specific to ALS. While tests such as the MoCA and MMSE are short screening batteries that can provide a starting point for cognitive assessment a wider battery of tests would need to be administered to perform an in-depth examination of cognitive function. A detailed assessment of multiple cognitive domains, tests such as the ECAS also correct for motor impairment that constitutes the clinical presentation of ALS patients. The ECAS assesses cognition in ALS under five domains namely language, verbal fluency, executive function, memory, and visuospatial. Multiple tests are administered, and cutoffs defined within each ECAS domain, to be able to identify cognitively-intact from cognitively-impaired ALS patients. In the current thesis, the total score across all five ECAS domains are used to assess cognition in both ALS patients and healthy controls. Additionally, the 2SD-NAC cutoff (McMillan

et al. 2022) was employed in this thesis as an inclusion criteria for cognitively intact healthy controls.

A diagnosis of ALSbi is dependent on the clinical observation of alterations in behaviour that can not be accounted for by the disease related symptoms, psychological response to the ALS diagnosis, a premorbid personality disorder, a comorbid psychiatric disorder, or pseudobulbar affects (Strong et al. 2017). Instruments that can be used to assess behaviour are the Amyotrophic Lateral Sclerosis-Frontotemporal Dementia-Questionnaire (ALS-FTD-Q), the Apathy Evaluation Scale (AES), the Beaumont Behavioral Inventory (BBI), the Dimensional Apathy Scale (DAS), the Frontal Behavioral Inventory (FBI), the Frontal Systems Behavior scale (FrSBe), Motor Neuron Disease Behavior scale (MiND-B), and the Neuropsychiatric Inventory (NPI) (Gosselt, Nijboer, and Van Es 2020). For behavioural screening instruments, the ALS-FTD-Q, the BBI, and the behavioural subdomain of the ECAS assess all behavioural domains that are affected in ALS patients (Gosselt, Nijboer, and Van Es 2020).

1.5. Diagnostic criteria for ALS

1.5.1. Revised El Escorial criteria

The revised El Escorial criteria is a framework for the diagnosis and stratification of patients with ALS. In accordance with these criteria, a diagnosis of ALS requires the presence of the evidence of LMN degeneration by clinical, electrophysiological, or neuropathological examination, the evidence of UMN degeneration by clinical examination, and the progressive spread of signs within a region or to other regions (Brooks 1994). In addition to these, the criteria also require the absence of electrophysiological evidence of other disease processes that might explain LMN and/or UMN degeneration signs, and neuroimaging evidence of other disease processes that could explain the observed clinical and electrophysiological signs (Brooks 1994). These criteria also provide a detailed categorization of LMN and UMN signs based on region of onset and spinal cord segment.

Table 2 provides a summary of LMN and UMN signs observed in ALS as per the El Escorial criteria.

	Bulbar	Cervical	Thoracic	Lumbosacral
Lower motor neuron signs weakness, atrophy, fasciculations	jaw, face, palate, tongue, larynx	neck, arm, hand, diaphragm	back, abdomen	back, abdomen, leg, foot
Upper motor neuron signs pathologic spread of reflexes, clonus, etc.	clonic jaw, gag reflex, exaggerated snout reflex, pseudobulbar features, forced yawning pathologic DTRs spastic tone	clonic DTRs, Hoffmann response, pathologic DTRs, spastic tone	loss of superficial abdominal reflexes, pathologic DTRs, spastic tone	clonic DTRs, extensor plantar response, pathologic DTRs, spastic tone

Table 2. LMN and UMN signs in four regions. Source: Brooks, 1994.

According to the definition of ALS diagnosis by these criteria, a patient can be diagnosed as having *clinically possible ALS* when both LMN and UMN signs are present only in one region, only UMN signs are present in two or more regions, or LMN signs are rostral to UMN signs (Brooks 1994; Brooks et al. 2000). A diagnosis of *clinically probable ALS* is provided when both LMN and UMN signs are present in two or more regions and some UMN signs must be rostral to LMN signs (Brooks 1994; Brooks et al. 2000). A diagnosis of *clinically definite ALS* is provided when both LMN and UMN signs are present either in the bulbar region and at least two spinal regions, or in three spinal regions (Brooks 1994; Brooks et al. 2000). An additional level, namely, "Clinically Probable ALS – Laboratory-supported" was included to provide an intermediate level between "clinically possible ALS" and "clinically probable ALS". This diagnosis can be provided when clinical LMN and UMN degeneration is present in one region, or when only UMN signs alone are present in one region, and LMN signs defined by EMG criteria are present in at least two regions, with proper application of neuroimaging and clinical laboratory protocols to exclude other causes (Brooks et al. 2000). The various diagnostic levels include "clinically" in their descriptions to indicate that a clinical diagnosis of ALS, without pathological confirmation, may be categorized into various levels by clinical assessment alone, based on the presence of both UMN and LMN

signs in the same anatomical region (Brooks et al. 2000). The revised El Escorial criteria is widely used to stratify patients for their inclusion in research studies and clinical drug trials.

1.5.2.Awaji criteria

With the revised El Escorial criteria, clinical neurophysiologists noted that fibrillation-sharp wave potentials, defined as an obligatory LMN sign, were often absent in otherwise affected muscles (Shefner et al. 2020). To address this concern, the Awaji criteria were defined as a modification of the revised El Escorial criteria. The Awaji criteria was proposed to further integrate electrophysiological criteria with clinical examination findings, and to include the presence of fasciculations as a LMN sign that could replace positive sharp waves of fibrillation potentials in muscles with neurogenic changes (de Carvalho et al. 2008). Furthermore, the Awaji criteria removed the diagnostic level of clinically probable ALS – lab supported, that was added in the revised El Escorial criteria (Shefner et al. 2020). Despite the initial heterogeneity observed in various studies, a recent multicenter study has shown increased diagnostic sensitivity when using the Awaji criteria (Shefner et al. 2020).

Despite efforts in refining the criteria for the diagnosis of ALS, both the revised El Escorial and the Awaji criteria had some limitations. Firstly, the definition of these criteria was ascribed to a high degree of certainty that patients would be diagnosed with ALS. Secondly, there was no clear indication that patients with possible ALS will evolve through the categories of probable and definite disease (Shefner et al. 2020). Thirdly, these criteria provide a diagnosis of possible ALS when UMN signs are present in at least two body regions without the presence of any LMN signs. Such patients could ultimately receive a diagnosis of primary lateral sclerosis based on progressive UMN degeneration and the absence of any LMN degeneration for at least four years from disease onset (M. Turner et al. 2020). Fourthly, these criteria did not account for the cognitive and behavioural impairment occurring in ALS.

1.5.3.Strong criteria

The Strong criteria recognized the biological importance of the presence of cognitive and behavioural impairment, as a manifestation of frontotemporal lobar degeneration (FTLD), as it raised the possibility of an overlap syndrome in which ALS and FTLD existed within a continuum (Strong et al. 2009). Therefore, it was important to consider the presence of FTLD when making a diagnosis of ALS. These criteria recommended that the approach to the clinical characterization of the frontotemporal syndromes in ALS or related MNDs would be based on four 'diagnostic axes', including the following: Axis I to define the MND variant, Axis II to define cognitive and behavioural dysfunction, Axis III to identify additional non-motor disease manifestations, and Axis IV to identify the presence of disease modifiers.

a) Axis I: Bases on this diagnostic axis, disease phenotypes can include ALS, primary lateral sclerosis (PLS), progressive muscular atrophy (PMA), spinal muscular atrophy (SMA), spinal bulbar muscular atrophy (Kennedy's disease), progressive bulbar palsy, bibrachial amyotrophy, and monomelic amyotrophy. Given that the most common presentation of adult-onset MNDs is ALS, the focus was towards the identification of a frontotemporal syndrome in the context of ALS.

b) Axis II: This axis recognized the manifestation of FTD in three clinically distinct phenotypes namely behavioural variant FTD (bvFTD), progressive non-fluent spontaneous speech with agrammatism (PNFA), and semantic dementia (SD) – grouped together as ALS-FTD. As neuropsychological impairments in ALS are often subtle, the need was to define a minimum set of criteria that were both sensitive and specific to these syndromes. The most common deficits are observed in the following domains: problem solving, attention/mental control, word generation, and frontally mediated aspects of memory (verbal learning, source memory, free recall). It was recommended that neuropsychological assessments should include tests geared towards assessing executive functioning that includes a verbal fluency measure. In addition, a recommendation was made to perform a caregiver interview to measure emotional and behavioural functioning. This was thought to be an important step towards assessing the full spectrum of frontotemporal impairments. It was also thought to be important to use tests that minimized the impact of speech and motor dysfunction on performance, particularly when

conducting a longitudinal analysis. Aside from the definition of the category of ALS-FTD, other categories that were defined included ALS behavioural impairment (ALSbi), ALS cognitive impairment (ALSci), and ALS comorbid dementia.

c) Axis III: This recognized the coexistence of additional disease manifestations including extrapyramidal signs (bradykinesia, cogwheel rigidity, tremor), cerebellar degeneration, autonomic dysfunction (abnormal cardiovascular reflexes, bowel, or bladder dysfunction), sensory impairment (decreased vibration, blunting of temperature discrimination), or ocular movement abnormalities with ALS.

d) Axis IV: This axis recognizes the presence of several disease modifiers that can have an impact on survival, in addition to specific disease phenotypes.

The Strong criteria was revised in 2015 to include three levels of complexity or depths of assessment. These hierarchical levels include criteria which can be applied in everyday clinical practice (Level I), utilized for prognostic stratification in clinical trials (Level II), and considered as research intensive to better define the nature and extent of FTD in ALS (Level III) (Figure 6).

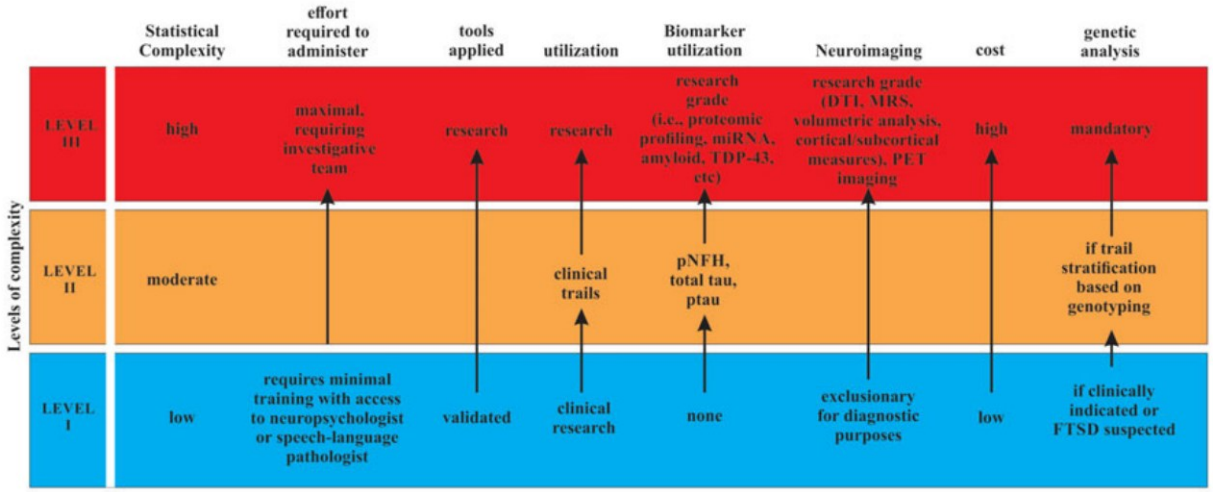

Figure 6. Hierarchical levels of assessment. Level I is the lowest level of complexity and can be adapted to a clinical setting. The implementation of levels II and III require formal neuropsychological and speech and language expertise, expertise with higher statistical

complexity, and include tests that may require further validation in the ALS population. Source: Strong et al., 2015

1.5.4.Gold Coast

The Gold Coast criteria (Shefner et al. 2020) for the diagnosis of ALS were proposed in 2020. In accordance with these criteria, a diagnosis of ALS can be provided if progressive motor impairment preceded by normal motor function is documented in a patient's medical history (including through repeated clinical assessment), if UMN or LMN dysfunction is observed in at least one body region or LMN dysfunction is observed in at least two body regions, and if clinical investigations can exclude other diagnoses. If symptoms are present in only one body region, there needs to be a presence of both UMN and LMN dysfunction within that body region.

The definition of UMN dysfunction entails

1. The presence of increased deep tendon reflexes, including the presence of a reflex in a clinically weak and atrophied muscle, or spread to adjacent muscles,
2. The presence of pathological reflexes, including Hoffman and Babinski signs, crossed adductor reflex, or snout reflex,
3. An increase in velocity-dependent tone (spasticity), and
4. Slowed, poorly coordinated voluntary movement, not attributable to LMN weakness or Parkinsonian features

The definition of LMN dysfunction entails

1. Clinical examination evidence of muscle weakness and atrophy or
2. EMG abnormalities that must include both

a. Evidence of chronic neurogenic change, defined by large motor unit potentials of increased duration and/or increased amplitude, with polyphasia and motor unit instability regarded as supportive but not obligatory evidence, and
b. Evidence of ongoing denervation including Fibrillation potentials or positive sharp waves, or fasciculation potentials

1.6. Disease staging in ALS

Staging systems are criteria that can be used to define clinical milestones during the disease course that reflect severity, prognosis, and treatment options. The two proposed staging systems for ALS are the King's College staging system and the Milano-Torino staging system.

1.6.1.King's College staging

This system (Roche et al. 2012) proposes disease stages based on the number of involved regions, diagnosis, and the need for invasive or non-invasive interventions. This staging system assumed that clinical milestones occur at predictable times during the natural progression of ALS. Stage 1 indicates the involvement of one region, stage 2 indicates the involvement of a second region, stage 3 indicates the involvement of a third region, stage 4A indicates nutritional failure , and stage 4B indicates respiratory failure. It does not follow the revised El Escorial criteria as it does not require the presence of both LMN and UMN involvement but only requires the evidence of neurological weakness. This staging system also allows a progression through the different stages based on the progression of the disease and can also take into account factors such as the rate of early symptom progression and diagnostic delay (Roche et al. 2012).

1.6.2.Milano-Torino staging

In this staging system (Chiò et al. 2015), critical milestones in ALS progression were defined by the loss of independent function in four key domains that are included in both the ALSFRS and ALSFRS-R questionnaires. These four domains are: walking/self-care, swallowing, communicating, and breathing. For each of the subitems within each domain, scored from 0-4, 0 corresponds to complete impairment and 4 corresponds to no impairment. As per the staging system, based on the scores obtained on the various subitems, a stage score of 0 or 1 is provided. These stage scores correspond to a threshold value that recognizes an important transition point in functional status of any anatomical region. Values of 0 (below threshold) or 1 (above threshold) are assigned, and the stages are determined as the sum of threshold values across the four ALSFRS domains. For domains consisting of two ALSFRS subitems, a staging score was provided based on either of both items as indicated. The sum of the threshold scores were used to stage patients as per the following stages as shown in Table 3.

ALS-MITOS	Stage	Functional domains lost
	0	None
	1	1 domain
	2	2 domains
	3	3 domains
	4	4 domains
	5	Death

Table 3. The Milano-Torino stages and the corresponding number of ALSFRS domains associated with functional loss. Sourced and adapted from Chio et al., 2015

The sections above describe the pathophysiological mechanisms underlying the core biological features and clinical presentations of ALS. The following sections describe the basic neuroimaging principles that can be applied to the study of ALS.

1.7. Study of the pathophysiological mechanisms of ALS using neuroimaging

Neuroimaging is a branch of science which allows the non-invasive study of brain structure and function. Good spatial and temporal resolution is necessary in order for neuroimaging to be relevant for use in a clinical or research setting. Spatial resolution pertains to the mapping of the structure of brain tissue and can help identify the occurrence of any alterations to normal brain tissue as a result of any apparent or non-apparent pathological events such as brain trauma or cellular mechanisms causing neuronal loss and related processes. In the case of the latter, these pathological events occur at a micro-scale level which can only be studied *ex vivo* or with the use of invasive techniques. By the time these localized pathological changes of brain tissue assume spatial importance at a macro- or meso-scale level, they can result in the impairment of neuronal function and related behavioural outcomes such as cognition, information processing, motor execution – to name a few.

Pathological processes in neurodegenerative disorders such as ALS can be studied using neuroimaging tools such as magnetic resonance imaging (MRI), positron emission tomography (PET), or techniques that directly probe underlying physiological processes such as electroencephalography (EEG), transcranial magnetic stimulation (TMS), and magnetoencephalography (MEG). As functional MRI has good spatial and temporal resolution and can be used non-invasively to probe neuronal function, it has evolved to be the most widely used neuroimaging technique to map brain function. This thesis aims to study the pathophysiology of ALS using functional MRI in conjunction with other advanced neuroimaging approaches including diffusion weighted imaging, which is applied to assess brain microstructure, and magnetic resonance spectroscopy, which is applied to assess the concentration of neurochemicals. These sequences are based on the property of nuclear magnetic resonance, which is defined in the next section.

1.7.1.Nuclear magnetic resonance

The acquisition of magnetic resonance images is dependent on properties of subatomic particles of the nuclei that constitute the matter within biological tissue. Nuclear magnetic resonance (NMR) is dependent on a property of constituent atomic nuclei known as 'spin'. Only nuclei with an odd number of neutrons or protons can exhibit a spin. Large amounts of free fluid exists in biological tissue in the form of cytoplasmic and extra-cellular water, fat, and bulk fluids (Mansfield 1978). Water exists in abundance in all biological tissue and has the highest concentration in human tissue (Plewes and Kucharczyk 2012). In addition, each water molecule consists of two protons, therefore effectively doubling the number of spins per molecule that can be subjected to an external magnetic field. The majority of NMR imaging thus utilizes water as their molecule-of-interest in the study of biological tissue. The spin of a proton is a fractional value ½ and is a measure of its angular momentum (Plewes and Kucharczyk 2012), a property wherein a rotating object (here, proton) maintains its state of rotational motion unless it is resisted by force (here, external magnetic field).

In the absence of an external magnetic field, protons are distributed equally between high and low energy states, creating a sum zero magnetic effect. When an external magnetic field (B_0) is applied to tissue containing protons, the spins align either parallel or anti-parallel to the magnetic field. However, the number of spins that align parallel are higher than those that align anti-parallel to the magnetic field (Plewes and Kucharczyk 2012). Figure 7 is a diagrammatic representation of the behaviour of protons in the absence of and when exposed to an external magnetic field.

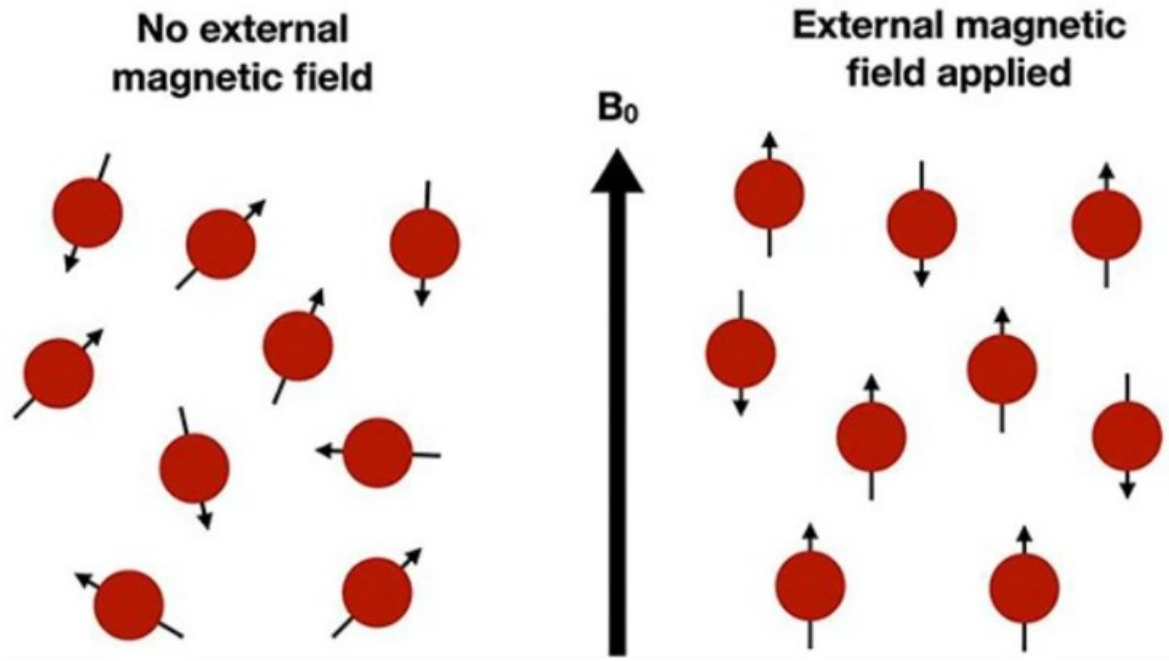

Figure 7. On the left, protons are misaligned as there is no external aligning magnetic field. On the right, on the application of an external magnetic field, the protons align themselves parallel and anti-parallel to the magnetic field. The number of protons aligned in the direction of the applied magnetic field is greater than the number of protons aligned in the direction opposite to the applied magnetic field. Adapted from (Azhar and Chong 2023).

The number of protons experiencing an equal and opposite magnetic field produce a net zero magnetic field. The remaining protons that are aligned parallel to the external magnetic field can thus be represented as a magnetic field vector and constitute the net magnetization that can be used to generate an MR image (Azhar and Chong 2023). It is difficult to directly measure this net magnetization as it has a small magnitude and is in the same direction as the strong, external magnetic field. This small net magnetization can be indirectly measured when a radiofrequency pulse is applied to perturb the magnetic field vector such that it undergoes displacement (Figure 8) into a transverse plane that is perpendicular to the external magnetic field (Azhar and Chong 2023).

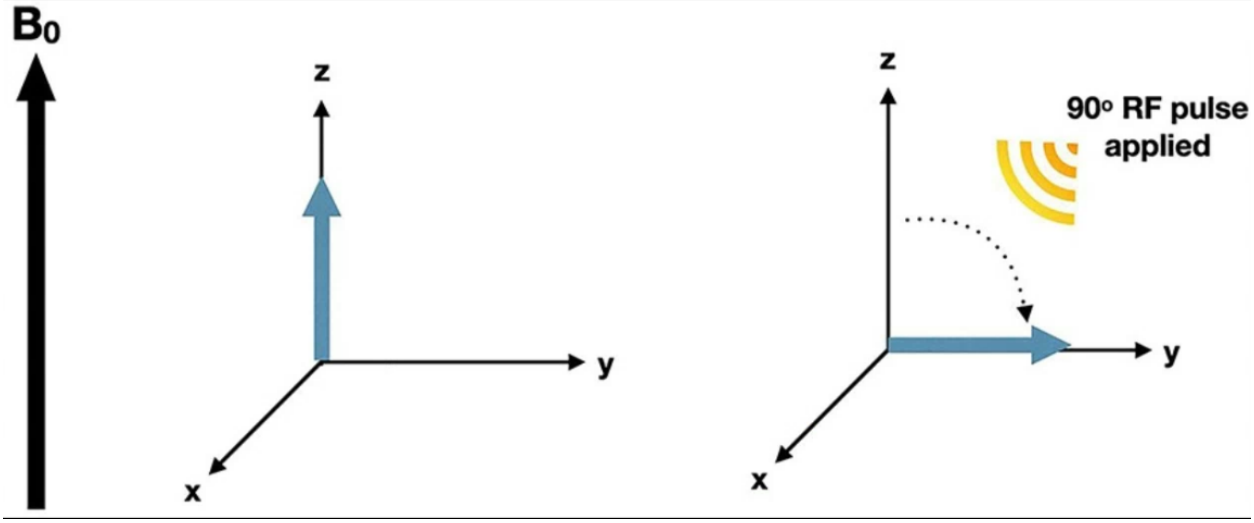

Figure 8. On application of a 90° radiofrequency (RF) pulse, the net magnetization vector undergoes displacement into the transverse plane (Azhar and Chong 2023)

The interaction between the net magnetization and the excitatory radiofrequency pulse generates two properties, namely longitudinal and transverse relaxations, which are fundamental to the generation of contrast in an MR image. The following sections define these properties and the MRI sequences that can be derived from them.

1.7.2.Magnetization relaxation in the study of brain structure

1.7.2.1. Longitudinal relaxation

Longitudinal relaxation refers to the recovery of the net magnetization after the protons are displaced in the perpendicular plane by an excitatory radiofrequency (RF) pulse. As soon as the RF pulse is removed, the protons start to lose the energy received from the RF pulse into the surrounding environment. This results in the exponential regrowth of the longitudinal magnetization along the direction of the externally applied magnetic field B_0 with a time constant

known as the longitudinal or T1 relaxation time. More specifically, T1 is the time taken by the net longitudinal magnetization to recover 63% of its original value (Azhar and Chong 2023).

1.7.2.2. Transverse relaxation

Transverse relaxation refers to the property by which energy is transferred between neighbouring protons that exhibit slight differences in transverse magnetization, in a process known as dephasing. The protons dephase in the transverse plane after receiving energy from the RF pulse and result in a decrease in the net transverse magnetization. This process causes differences in precession of individual protons relative to the precession of the adjacent protons, therefore causing them to lose phase with each other. This in turn results in decay of the net transverse magnetization over time with a time constant known as the transverse or T2 relaxation time. More specifically, T2 is the time taken by the net transverse magnetization to decay to approximately 37% of its original value (Azhar and Chong 2023).

While T2 relaxation represents the exponential decay of transverse magnetization in an ideal homogeneous B_0 field, such decay might occur faster due to the presence of inhomogeneities in the B_0 field in a practical setting. Rapid proton-proton dephasing can occur due to the variations in the B_0 field (Azhar and Chong 2023). Therefore, the combined effects of tissue-specific T2 relaxation and the additional dephasing from B_0 inhomogeneities can be expressed as T2* relaxation.

Both the T1 and T2 relaxation times are properties that are independent of each other and are inherently specific to different tissue types for a given magnitude of B_0. These relaxation times are used to define the two numerical properties which are crucial to MRI acquisition: repetition time (TR) and echo time (TE). TR is the time interval between two excitation RF pulses and is used to determine the time interval for T1 relaxation. TE is the time interval between the excitation RF

pulse and the received echo, and is used to determine the time interval for T2 relaxation (Azhar and Chong 2023). Depending on the property-of-interest of the specific tissue, the TR and TE can be modified to generate adequate contrast in the MR images.

For example, a short TR is used to achieve maximal differences in longitudinal magnetization and thus maximizes contrast between different tissue types and a short TE minimizes the effect of T2 decay on image contrast as it decreases differences in transverse magnetization between tissues (Azhar and Chong 2023). Therefore, a T1-weighted image is acquired with a short TR and short TE for ease of assessment of different tissue types. In a T1-weighted image of the brain, the white matter is hyperintense (bright), the CSF, air, and bone are hypointense (dark), and gray matter is of intermediate brightness. T1-weighted imaging is therefore performed as part of routine clinical tests to assess neuroanatomical details.

A long TR is used to minimize T1 effects on image contrast by reducing longitudinal magnetization and thus minimizes contrast between different tissue types and a long TE maximizes the transverse magnetization between tissue types (Azhar and Chong 2023). In T2-weighted imaging, image contrast is achieved by differing the T2 times between tissue types. Therefore, in a T2-weighted image of the brain, the CSF and tumours are hyperintense, gray matter is hypointense, and white matter is of intermediate brightness. T2-weighted imaging is used in clinical settings to assess for the presence of edema from various pathologies such as trauma, infection, or inflammation. Figure 9 shows examples of T1-weighted and T2-weighted MRI.

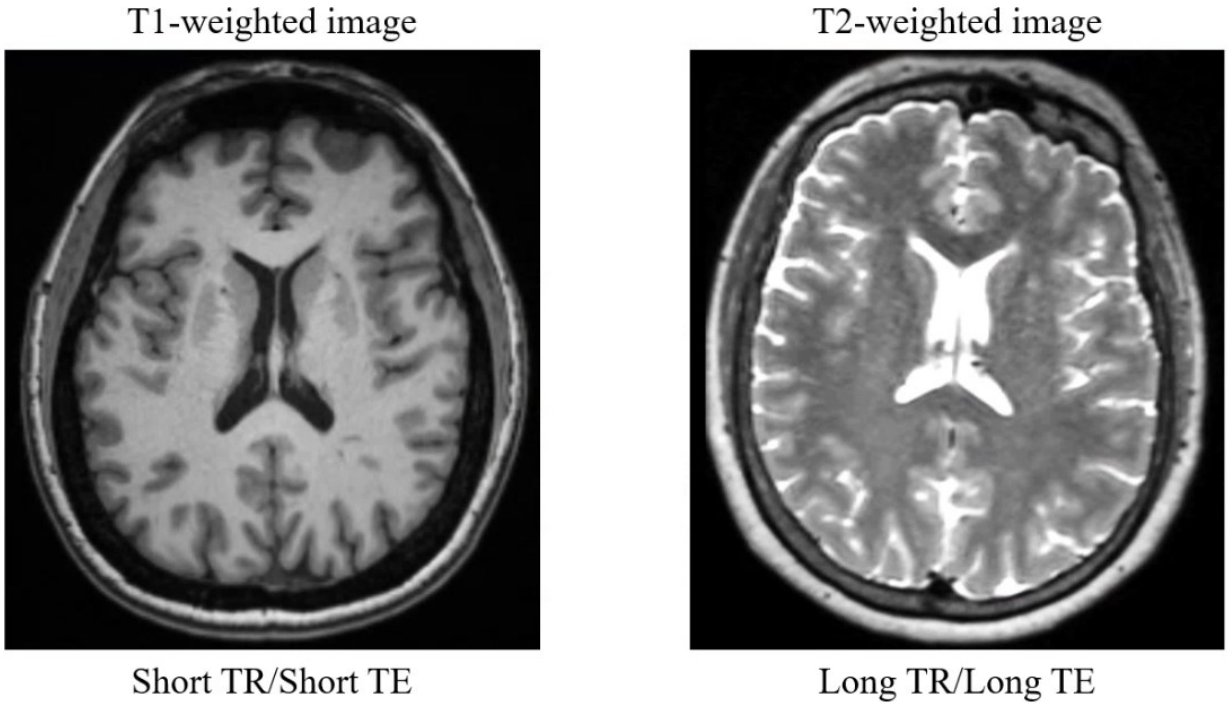

Figure 9. Representative images from the CALSNIC dataset of image contrast when different lengths of TR and TE are applied at the time of image acquisition.

In addition to these conventional MRI sequences, advanced neuroimaging sequences such as diffusion-weighted imaging, functional MRI, and magnetic resonance spectroscopy are used to study the properties of brain tissue in health and disease. These sequences are defined in the following sections.

1.7.3.Advanced neuroimaging

1.7.3.1. Diffusion-weighted imaging

Sequences such as diffusion-weighted imaging (DWI) quantify information based on the displacement of water molecules in myelinated axons (white matter). In an unrestricted

environment, water molecules can move in all directions without encountering any impedance from permeable or semi-permeable axonal membranes (Figure 7). This random motion of water molecules is termed Brownian, Gaussian, or isotropic diffusion. However, in biological tissue, the displacement or diffusion of water molecules is restricted by cells and extracellular compartments such as cellular membranes and axons. The introduction of such boundaries place restrictions on Gaussian diffusion in terms of the distance of diffusion and the number of collisions experienced by the water molecules within the bounding membranes. This causes the diffusion of water molecules to assume a non-Gaussian or anisotropic property (Figure 7). In an unrestricted diffusion environment, water molecules retain their spherical orientation whereas in a restricted environment such as in axons, the water molecules assume an elliptical orientation (Figure 8).

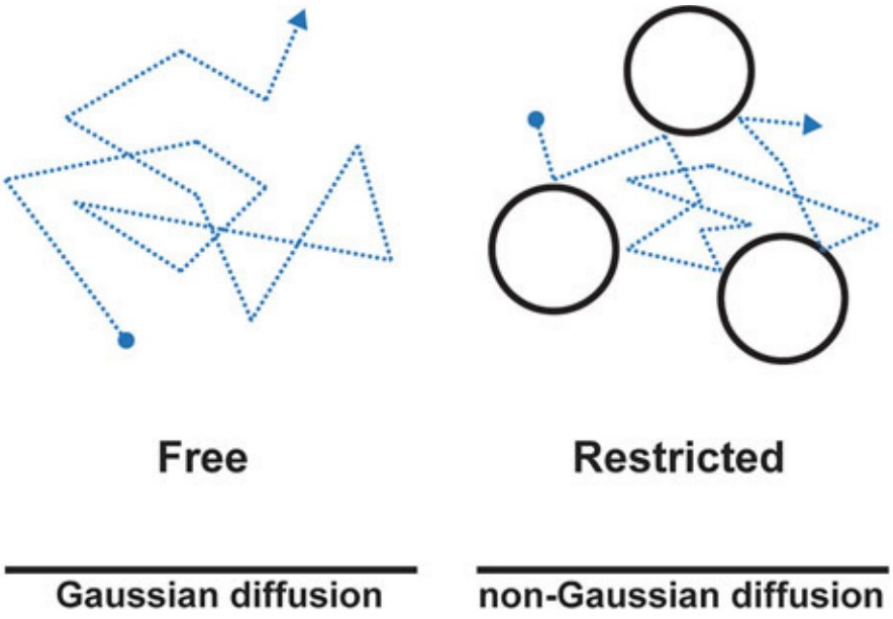

Figure 10. Random (Gaussian) and restricted (non-Gaussian) diffusion of water molecules in unrestricted and restricted environments (Mahmood and Hansen 2017).

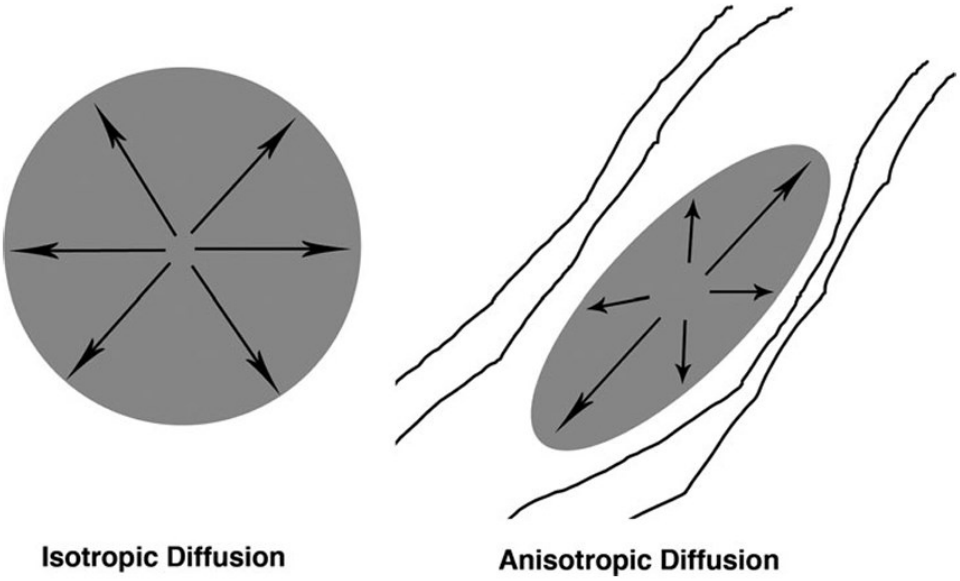

Figure 11. Spherical and elliptical orientations of water molecules in unrestricted and restricted motion, respectively (Karlsgodt et al. 2008).

Mathematical modelling of the diffusion of water has been performed extensively in a model known as the diffusion tensor model. The tensor that describes the diffusion of water in neural tissue is represented by an ellipsoid with three axes that correspond to their respective eigenvalues (λ1, λ2, and λ3) and are determined by their corresponding eigenvectors (Figure 9). λ1 represents the long axis of the ellipsoid (Tae et al. 2018) which corresponds to the predominant direction of water diffusion in each voxel of a DW image. λ2 and λ3 respectively represent the width and depth of the ellipsoid (Tae et al. 2018) and correspond to the diffusion of water along or perpendicular to the long axis of the ellipsoid or tensor within a voxel. The greater the magnitude of the eigenvalue λ1, the greater is the property of fractional anisotropy (FA) – a measure that is most extensively used to quantify anisotropic diffusion of water and is representative of the degree of directionality of water diffusion within a voxel (Kashefi and Winston 2020). It therefore provides a sensitive marker of cerebral white matter microstructural integrity, based on the assumption that the shape of the ellipsoid changes due to degeneration (Tae et al. 2018).

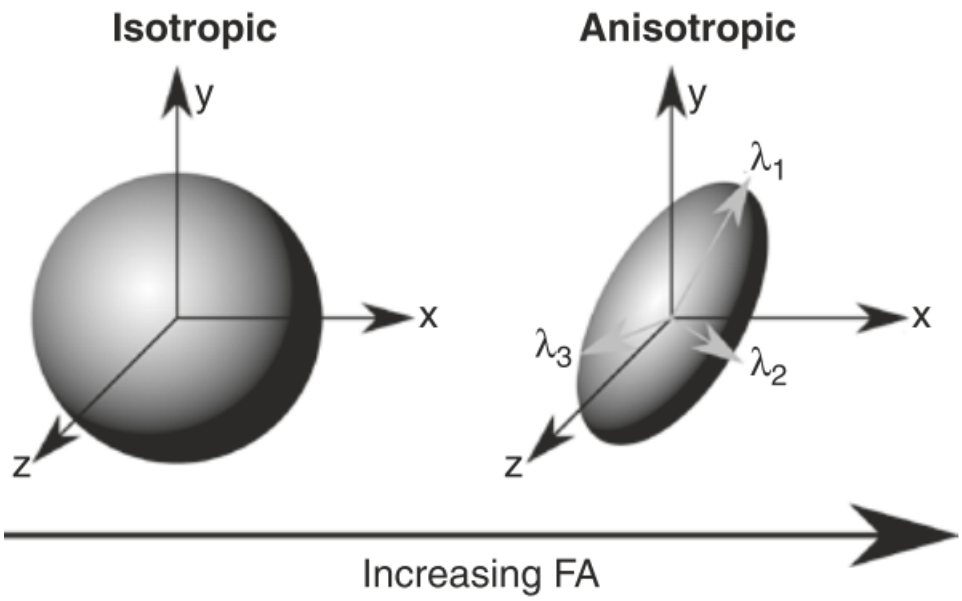

Figure 12. Ellipsoid or diffusion tensor model corresponding to water diffusion in neural tissue (Kashefi and Winston 2020). In unrestricted (isotropic) diffusion, the tensor attains a spherical orientation and in restricted (anisotropic) diffusion, the tensor attains an elliptical orientation. The greater the λ1 magnitude, the greater the fractional anisotropy.

Although FA provides a measure of tensor directionality within a voxel based on λ1, it can be mathematically expressed in terms of all three eigenvalues as

$$FA = \sqrt{\frac{1}{2}} \cdot \sqrt{\frac{(\lambda 1 - \lambda 2)^2 + (\lambda 2 - \lambda 3)^2 + (\lambda 3 - \lambda 1)^2}{(\lambda 1)^2 + (\lambda 2)^2 + (\lambda 3)^2}}$$

Mean diffusivity (MD) is a measure that evaluates microstructural alterations in white matter as a function of the average of all three eigenvalues, effectively quantifying the average distance of the displacement of water molecules without placing any restrictions on the directionality of motion. It can be mathematically expressed as

$$MD = \frac{\lambda 1 + \lambda 2 + \lambda 3}{3}$$

MD can be further decomposed into its constituent diffusivity measures – axial diffusivity (AD) and radial diffusivity (RD). AD quantifies the displacement of water molecules **along** or parallel to the predominant direction (λ1) of water displacement within the axon, and can be mathematically expressed as

$$AD = \lambda 1$$

RD quantifies the displacement of water molecules **perpendicular** to λ1, which represents the predominant direction of water displacement within the axon, and can be mathematically expressed as

$$RD = \frac{\lambda 2 + \lambda 3}{2}$$

DWI is sensitive to the presence of artifacts such as motion, field inhomogeneities, and distortions due to eddy currents. Motion in DWI can have multiple sources. Phase shifts induced by diffusion-driven displacements of water molecules (microscopically), and head motion, cardiac pulsation, and breathing (macroscopically) can contribute to motion artifacts in DWI (Soares et al. 2013). Field inhomogeneities refer to spatial and intensity distortions that are induced by magnetic susceptibility variations due to field inhomogeneity in the static magnetic field (B_0) (Arsenault et al. 2021). All DWIs suffer from field inhomogeneity distortions which intensify with increasing field strength and along the phase encoding direction (Arsenault et al. 2021). Distortions due to eddy currents occur due to rapidly changing diffusion gradients and can be induced in the scanner or the subject being scanned; this warps the image and can result in time-varying gradients and

shifts in the static magnetic field (Arsenault et al. 2021). Assessment of and correction for such artifacts constitute important steps for quality control and preprocessing of DWI data.

Once the DWI data is quality controlled and preprocessed, the next step of processing involves the estimation of the diffusion tensor. Estimation of the diffusion tensor entails the availability of diffusion-encoding gradients in at least six non-collinear directions as well as the application of one of three methods for tensor estimation (ordinary least squares, weighted linear least squares, and non-linear least squares) (Soares et al. 2013). This is used to generate the diffusion tensor which is a symmetric 3x3 matrix defined by its eigenvalues and corresponding eigenvectors, which can then be utilized to generate scalar indices and tractography measures.

The diffusion tensor matrix can be expressed as

$$D = \begin{bmatrix} D_{xx} & D_{xy} & D_{xz} \\ D_{yx} & D_{yy} & D_{yz} \\ D_{zx} & D_{zy} & D_{zz} \end{bmatrix}$$

where D_{xx}, D_{yy}, and D_{zz} represent diffusion coefficients measured along the principal axes and D_{xy}, D_{xz}, D_{yx}, D_{yz}, D_{zx}, and D_{zy} represent the pairwise correlation in random motion between principal axes or directions. The following pictographic demonstrates the diffusion trajectory, shape of the diffusion ellipsoid, and the diffusion tensor matrix for various diffusion conditions of water

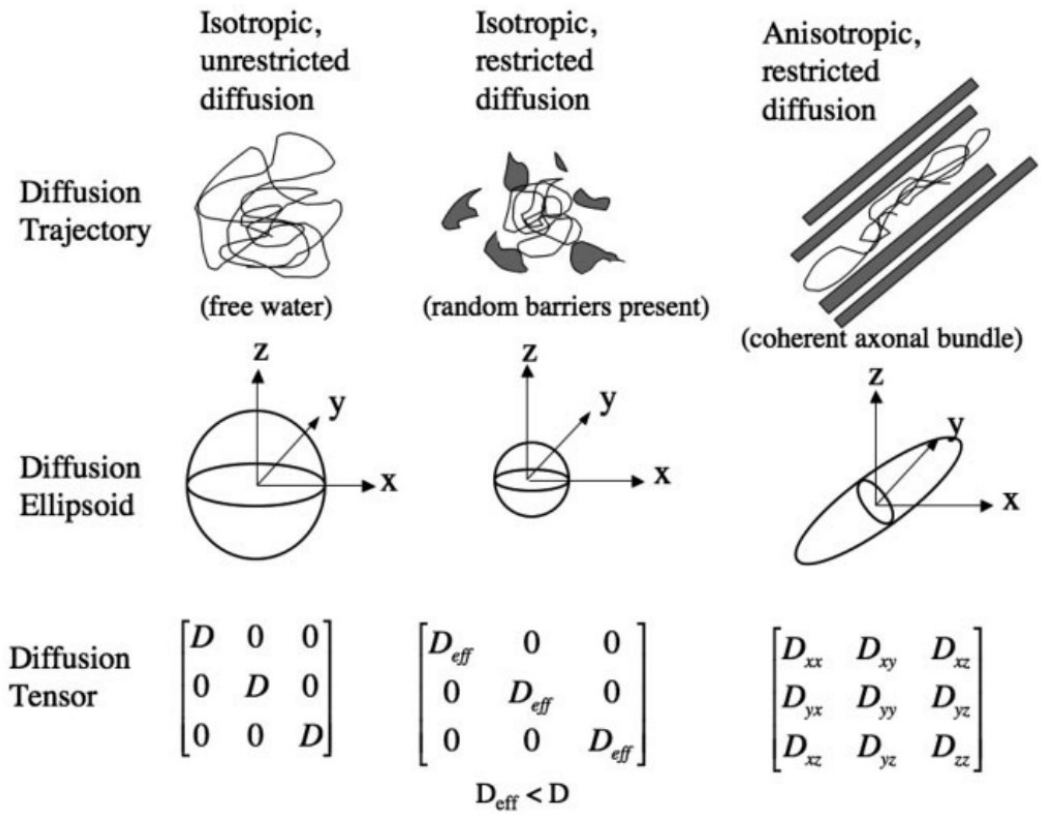

Figure 13. Trajectory, shape of ellipsoid, and tensor matrix for various diffusion conditions (Mukherjee et al. 2008)

DTI is sensitive to microstructural properties of brain tissue and is therefore very useful in a research or clinical setting to examine white matter anatomy. DTI has been successfully used to study brain structure in conditions such as acute stroke or brain tumors, neurodegenerative and neuropsychiatric disorders, developmental disorders, and movement disorders – to name a few. Measures of brain microstructure obtained from DTI, including fractional anisotropy, radial diffusivity, axial diffusivity etc., usually relate to alterations in structure occurring as a result of disease and can uncover microscale impairments such as the loss of myelin or axonal injury (Soares et al. 2013).

1.7.3.2. Functional MRI

Functional MRI (fMRI) is a non-invasive neuroimaging technique that is sensitive to neuronal activity-related changes in local blood flow. When neurons are actively engaged in the performance of a task, they utilize oxygen from blood in the surrounding blood vessels. This oxygen is provided to the neurons from the blood via a molecule known as hemoglobin which is an oxygen transporter. Hemoglobin contains iron and its properties changes depending on its oxygenation. Oxygenated hemoglobin is diamagnetic in nature and deoxygenated hemoglobin is paramagnetic in nature.

When a neuron is activated, oxygen from the surrounding blood is used up. This results in deoxygenation of local hemoglobin, making it paramagnetic. Within a magnetic field, the increase in concentration of deoxygenated blood causes a loss of signal on a T2*-weighted MRI because of the generation of a local magnetic field by the deoxygenated hemoglobin. When the quantities of deoxygenated hemoglobin increase in the local neuronal environment, blood flow to the region increases to replenish the supply of oxygenated hemoglobin. As oxygenated hemoglobin is diamagnetic in nature, it does not produce a local magnetic field, therefore causing no loss of T2* signal. As neuronal activation continues until the task is completed, the hemoglobin in the surrounding blood cycles through its properties of oxygenation and deoxygenation. The differences in magnetic properties of oxygenated and deoxygenated hemoglobin provide the basis for the blood-oxygenation-level-dependent (or, BOLD) contrast utilized in fMRI.

This interdependence between transient neural activity and cerebral blood flow is known as neurovascular coupling. Despite being tightly linked, the increase in blood flow to replenish the amounts of oxygenated hemoglobin in the immediate neuronal environment occur later than the initial neuronal activation, creating a delay between the two phenomena. If these independent, but highly-linked, phenomena are plotted against time, two waveforms can be identified (Figure 14).

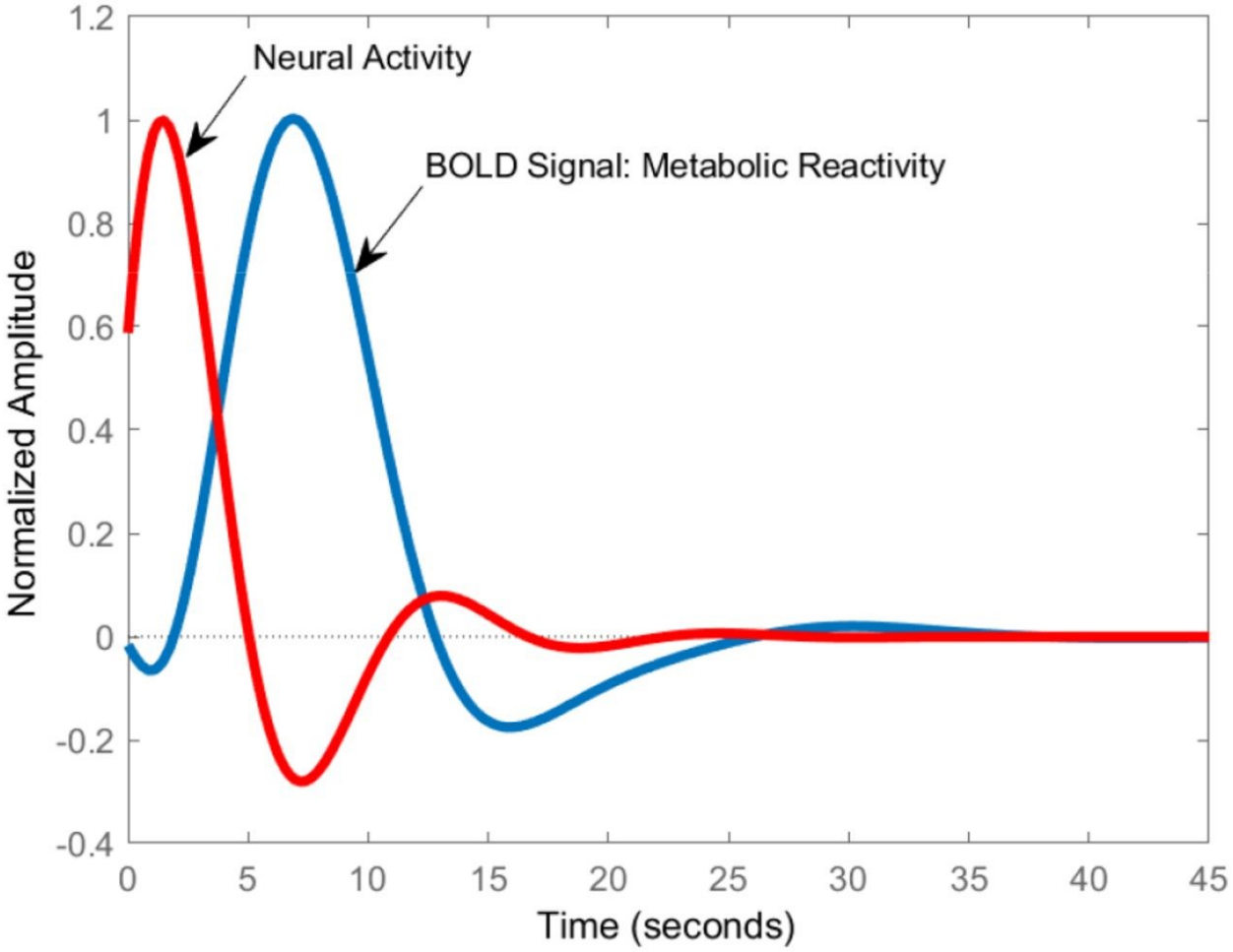

Figure 14. Graphical representation of the neuronal activation and cerebral blood flow signals over time (Schaper 2019).

As the direct study of neuronal function can be challenging without the use of invasive methods such as electrophysiological recordings, a non-invasive characterization of the T2* contrast can be useful as a proxy measure for neuronal function. As the T2* contrast in MRI is sensitive to local magnetic fields, the oxygenation-deoxygenation (i.e., the paramagnetic-diamagnetic) cycling of hemoglobin in the local neuronal environment can act as a proxy to neuronal function. In task-based fMRI studies, this property can be used to identify the cerebral areas that are activated when performing a task. However, the brain is active even when not performing an explicit task i.e., when the brain is in a state of rest. These resting-state activations occur to maintain normal

functioning of the human brain and illustrate slow, synchronous, spontaneous fluctuations of spatially-organized neuronal activity (Pizoli et al. 2011). The network of neurons that are active at rest are known as resting-state networks (RSNs). These RSNs represent physiological processes that are important to developmental process and towards the maintenance of the brain's functional integrity. Two theories existed regarding the organization of functional activity in the resting brain. One suggested the presence of two anticorrelated functional systems whereas the other suggested the presence of local, modular functional systems (Doucet et al. 2011). Findings from the investigations of these two theoretical viewpoints were successful in the identification of two sets of brain regions (Seitzman et al. 2019): one with highly correlated, spontaneous activity that is involved in goal-directed response to external stimuli as well as the default mode network (DMN) (Raichle 2015) which is not activated during goal-directed activity (Figure 15). These sets of brain networks constitute the functional organization of the human brain and undergo activation in different states.

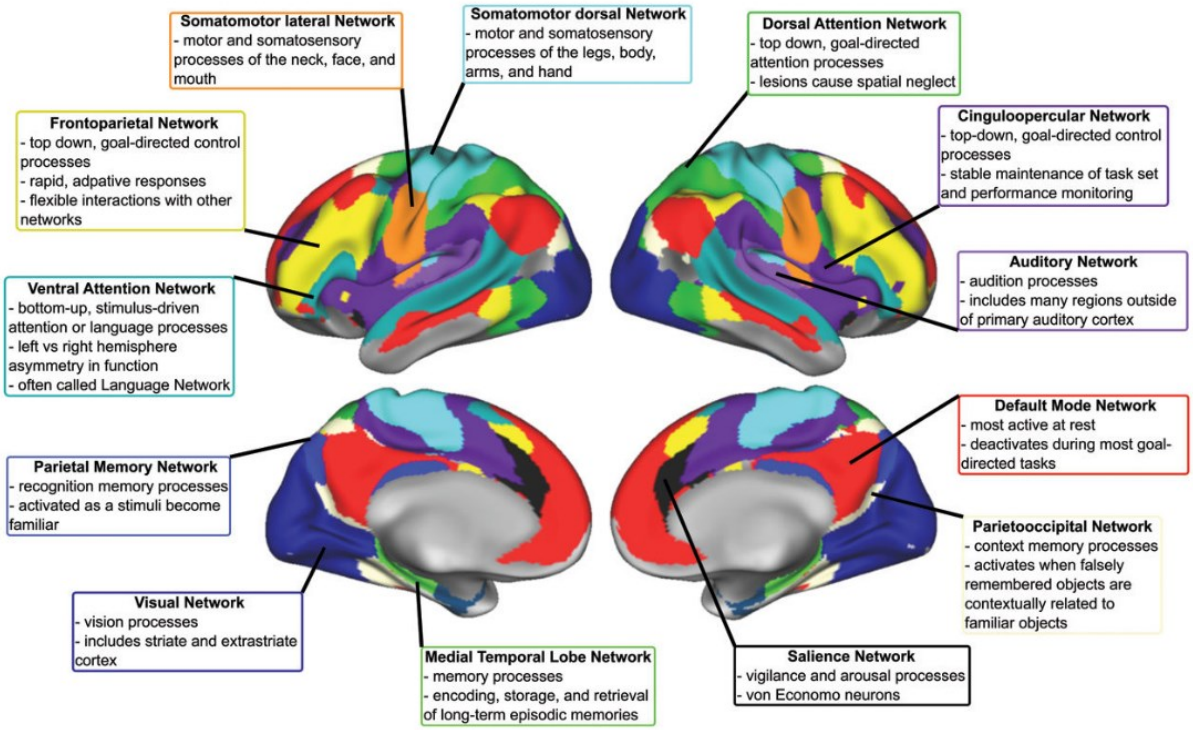

Figure 15. Resting-state networks of the human brain and their associated functions (Seitzman et al. 2019)

Brain networks are organized hierarchically (Doucet et al. 2011). The highest level of hierarchy is comprised of task-positive networks and the DMN that is active when no task is being performed. At lower levels of hierarchy, task-positive networks can be further delineated based on their response to a behavioural task condition. Unsupervised learning methods such as hierarchical clustering or independent component analyses have been successful in identifying the task-positive networks that are involved in the performance of specific tasks. These techniques have been discussed in detail in section 1.8.2.

1.7.3.3. Magnetic resonance spectroscopy

Magnetic resonance spectroscopy (MRS) is a non-invasive neuroimaging technique that refers to the utilization of the phenomenon of magnetic resonance to determine the relative concentrations of neurochemicals within specific regions-of-interest within the cerebral cortex. Spectroscopic evaluation of brain tissue provides a graphical representation of the MR signal from specific nuclei as a function of their temporal frequencies (Buonocore and Maddock 2015). Some of the most extensively studied neurochemicals in health and disease are N-acetyl aspartate, creatine, choline, myoinositol, lactate, glutamate, and γ-aminobutyric acid. Their spectral signatures are specific to the spins of the nuclei that constitute the neurochemical molecules. In the absence of an external magnetic field, the nucleus of a neurochemical molecule has a non-zero intrinsic magnetic moment which is dependent on the unique intrinsic spin of the nucleus. The spin of the nucleus is a function of the quantum mechanical intrinsic spin of the individual protons and neutrons that comprise the nucleus. In the presence of an external applied magnetic field, the nuclei within the respective neurochemical nuclei precess around the static magnetic field at a frequency known as the Larmor frequency. The Larmor frequency is a temporal frequency that is a product of the unique

gyromagnetic ratio (which is a function of the intrinsic nuclear magnetic moment) and the strength of the experienced magnetic field (Buonocore and Maddock 2015).

However, the acquisition of the spectral signature of a single neurochemical does not occur at a single Larmor frequency. This can be due to a multitude of factors such as a combination of constituent nuclei within a neurochemical molecule, the inherent T2 relaxation of transverse magnetization, and the range of magnetic field values and inhomogeneities within the MRS region-of-interest (or, MRS voxel). This causes spreading of the spectral signature from the MRS voxel over a narrow range of frequencies which is characterized by a property known as linewidth of the MRS chemical peak (Buonocore and Maddock 2015) (Figure 16).

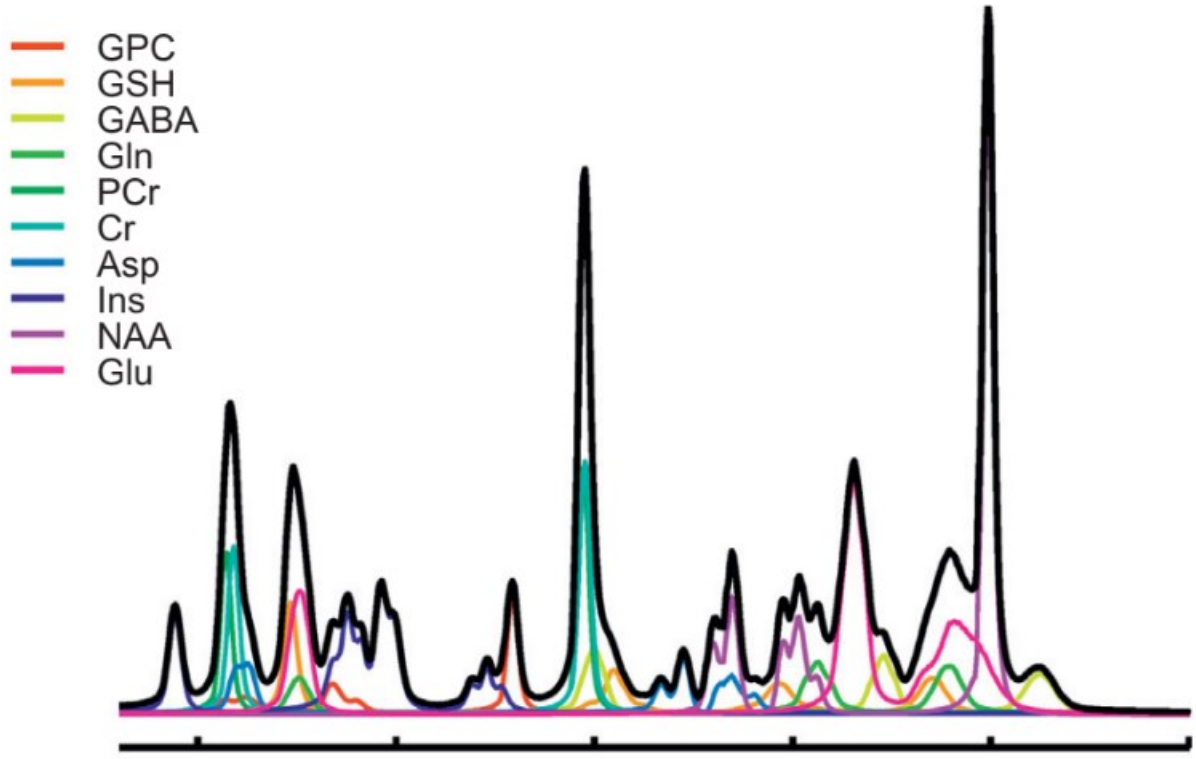

Figure 16. Representative linewidth of the MRS spectrum (Juchem and Rothman 2013)

Another nuclear property that defines the MRS spectra is known as chemical shift. The physical basis of chemical shift is due to the presence of electrons around the nuclei of the constituent neurochemical molecules. These electrons generate local magnetic fields which alter the applied magnetic field experienced by the nuclei in the neurochemical molecule. Each nucleus in the neurochemical molecule thus experiences a unique magnetic field based on their immediate microenvironment, therefore exhibiting a Larmor frequency that is slightly different from the Larmor frequencies of the other constituent nuclei within the same molecule or across different molecular species (Buonocore and Maddock 2015). Because different molecules (and subsequently, nuclei) have different Larmor frequencies, a molecule with zero magnetic moment (tetramethylsilane) is designated as the reference molecule. Based on this reference, chemical shift of the constituent neurochemical nuclei is defined as the difference between the Larmor frequency of the molecule-of-interest and the reference molecule (Buonocore and Maddock 2015).

Multiple methods can be employed to acquire MRS data from a cerebral region-of-interest. These methods include single-voxel MRS, 2D and 3D chemical shift imaging, and proton echo planar spectroscopic imaging (Buonocore and Maddock 2015). Single-voxel MRS provides a robust method for the acquisition of a large signal from a relatively large cerebral region-of-interest, typically spanning one anatomical region. 2D and 3D chemical shift imaging is used to cover larger brain regions, typically spanning multiple anatomical regions, and provides spatially-resolved MRS spectra throughout the selected brain region. The spatial resolution of spectra obtained from 2D and 3D chemical shift imaging provides higher resolution than single-voxel spectroscopic imaging. The proton echo planar spectroscopic imaging replaces one direction of phase encoding performed in 2D/3D chemical shift imaging with frequency encoding, therefore interleaving the spectral estimation echo acquisition with spatial encoding (Buonocore and Maddock 2015). The development of the PEPSI MRS sequence therefore allowed frequency encoding in the same time frame as the time between sampling points for spectroscopy (Buonocore and Maddock 2015).

Once conventional or advanced neuroimaging sequences are acquired, they need to undergo processing in order to obtain important information for the study of the neurological disorder (in this thesis, ALS). The following sections define the different processing steps that can be employed to identify specific characteristics of brain tissue types which can act as biomarkers for the diagnosis or to rule out the presence of other disorders.

1.8. Processing of conventional and advanced MRI

Some of the common approaches used to extract information from conventional and advanced MR images include region-of-interest-based, whole-brain-based, or graph theoretical analyses. Depending on the specificity of the MR sequence used, additional preprocessing steps are employed to correct for artifactual signals arising from normal physiological functions of the body or due to MRI hardware. The following sections briefly describe the approaches that are used to extract information from different MRI sequences

1.8.1.Region-of-interest-based approaches

Regions-of-interest (ROIs) can be defined either based on a pre-existing atlas (for analyses not proposing *a priori* hypotheses) or an area that has been previously identified in the literature as a salient region (for analyses requiring the proposition of an *a priori* hypothesis). In studies with no *a priori* hypotheses regarding affected brain regions, examples of some atlases used for the definition of ROIs are the Desikan-Killiany atlas (Desikan et al. 2006), Harvard-Oxford cortical and subcortical atlases (https://www.nmr.mgh.harvard.edu/~nikos/Public/CMA/CMA-Segmentation-Manual.pdf), Julich-Brain Cytoarchitectonic Atlas (Amunts et al. 2020). In hypothesis-driven studies with regard to the brain regions affected, ROIs can be defined using manual, semi-automatic, or completely automatic segmentation methods. Such ROI-based approaches can be applied to the analysis of volumes of different brain regions, cortical thickness measurements, measurements of brain microstructure from diffusion tensor images, or the

measurement of physiological measures relating to neuronal function such as the amplitude of low frequency fluctuations or regional homogeneity measures obtained from functional MRI. ROI-based approaches are quite versatile in that they can be used to extract information from derived maps (for example, graph theory, discussed in section 1.8.3.) of brain structure and function.

1.8.2. Whole-brain-based approaches

Such approaches can be employed to obtain information about multiple regions at the same time, either to examine the congruence in their activation or deactivation or to ascertain the sequence of neural events that link the detected regions. Such approaches are important to the study of brain function in task-based fMRI studies but can also be employed for conventional and advanced neuroimaging sequences. This approach can also be used as a precursor to the extraction of information using ROI-based approaches when no *a priori* hypothesis is present.

1.8.3. Graph theory-based approaches

Graph theory is a branch of mathematics that is being increasingly applied to study the brain and its networks. The term "network theory" in the context of the brain refers to the collection of brain regions that are connected in terms of their structure and/or functional coherence. However, the principle underlying network-based studies of the brain suggests that brain function does not rely only on the presence of brain regions or their connections, but on the idea that functioning of the brain is governed by the topology of this network as a whole (van den Heuvel and Sporns 2011). The comprehensive brain network, taken as a whole, is termed connectome. The brain regions constituting the connectome are referred to as nodes and the connections between them are referred to as edges. Some brain regions or nodes play an integral role in facilitating and maintaining communication between remote brain regions i.e., in the overall organization of the brain network. These brain regions are designated as "hubs"; the hubs that are closely linked to each other constitute the "rich-club" organization of the human brain connectome. (van den Heuvel and

Sporns 2011). The presence of the "rich-club" brain regions is indicative of the need for the system of brain regions to maintain stability and distribute the processing of behaviourally-intensive processes so as to not overload the connectome, analogous to that in a highly connected power grid; subsequently, the non-inclusion of certain brain nodes into the "rich-club" suggests that these regions are highly functionally specialized (van den Heuvel and Sporns 2011). Graph metrics that are extensively used to study structural and functional brain networks in health and disease include degree, degree centrality, betweenness centrality, path length, clustering coefficient, global efficiency, modularity – among others. These metrics point to specific properties of the connectome and can be used independently or in conjunction to assess health or disease in the brain. For example, for the same magnitude of "attack" on global efficiency, impairment of the "rich-club" hubs is 3x more severe than less connected nodes (van den Heuvel and Sporns 2011). Graph metrics can be estimated for the whole-brain or within an ROI, therefore being versatile in the study of the connectome.

The sections above discussed the various approaches that can be employed to estimate measures of brain structure and function. These steps can only be applied to structural (T1- and T2-weighted, DW images) and functional MRI, but not to MRS. The following sections describe the specifics of preprocessing steps that are applied to DWI, fMRI, and MRS.

1.8.4.Preprocessing of diffusion-weighted images

Information regarding the microstructural properties of different brain tissue types can be obtained using the diffusion tensor model that is estimated on DW images. An overview of the tensor estimation has already been provided in section 1.7.3.1. The eigenvector corresponding to the primary direction of water diffusion can be utilized to obtain 3D representations of cerebral white matter tracts, in a method known as tractography. The estimation of 3D tracts between brain regions using DTI can be performed in three steps: seeding, propagation, and termination (Soares et al. 2013). *Seeding* entails the definition of regions- or voxels-of-interest between which the

white matter tracts would be estimated. *Propagation* entails the generation of tracts between seeds and can be performed with different algorithms. The methods for the estimation or generation of tracts can be categorized into two classes: deterministic and probabilistic tractography. Deterministic tractography is used to generate one tract from one seed. Probabilistic tractography is used to estimate the likelihood of a voxel constituting a white matter tract, thus providing multiple possible tract orientations at a single seed. *Termination* aims to avoid the propagation of tracts in voxels where the vectorial field is not assured. The common termination criteria are minimum FA thresholds (0.1-0.3 in adult brain and 0.1 in infant) and turning angle threshold (typically 40°-70°, depending on the white matter tract-of-interest) (Soares et al. 2013).

DWI data can also be processed to identify differences across study populations and to identify associations between diffusion measures and covariates of interest. Two major methods that approach such questions are the voxel-based analysis (VBA) and tract-based spatial statistics (TBSS). VBA entails the automated estimation of maps of diffusion measures-of-interest which are then transformed into a standard space so as to achieve congruence across subjects in terms of the location of anatomical structures. TBSS is another automated method wherein group-level voxel-wise changes are detected in the whole brain based on a skeleton defined using group-level registered FA maps. TBSS is the most widely used method of estimating group differences in diffusion measures as it eliminates the need to perform spatial smoothing and increases statistical power by reducing the total number of voxels tested (Soares et al. 2013). However, TBSS can be subject to inaccuracies due to image artifacts such as large anatomical shifts, white matter lesions, or registration errors that might be challenging to detect visually. In addition, back projection to native space is also prone to errors as the skeletonization process aligns local maxima which may not necessarily correspond to the same anatomical location across subjects (Soares et al. 2013).

1.8.5.Processing of resting-state functional MRI

In resting-state fMRI studies, brain networks are studied using different methods such as seed-based connectivity analysis, independent component analysis/dual regression, or template-based rotation in order to establish patterns of functional connectivities of the brain regions in health and disease. These methods are defined in the following sections.

1.8.5.1. Seed-based functional connectivity

Seed-based functional connectivity (FC) can be quantified using a technique known as seed-based correlational analysis. This technique was first described by (Biswal et al. 1995) and is the most commonly used FC analysis technique in both task-based and resting-state fMRI studies. In this technique, the time series of a 'seed' region (or simply, a region-of-interest (ROI)) undergoes a Pearson's correlation with the time series of voxels in other brain regions. The strength of correlation between the pair of time series defines the connectivity between the two regions. Seed-based FC analysis is very versatile as it allows the definition of multiple ROIs and subsequently the assessment of the strength of connections between them. However, as this method requires user input in the definition of ROIs, it can be cumbersome to assess all the distinct brain networks. In addition, each of the brain networks consists of numerous hub regions which have connectivities with brain regions in other networks, therefore making the definition of seeds a complex process. Consequently, testing the same seed region as part of different brain networks can result in a problem of multiple comparisons which might render meaningful study findings statistically insignificant after corrections.

1.8.5.2. Independent component analysis/Dual regression

Independent component analysis (ICA) is a statistical technique that is used to identify and separate features from a set of observations that are assumed to be a linear mixture of independent

features. The ICA algorithm performs higher-order statistical manipulations of these observations to achieve features that are maximally independent of each other.

In fMRI, it is typically considered that the different brain networks are spatially and temporal independent or non-overlapping. In such, ICA in fMRI can be split into two components: spatial ICA and temporal ICA. Spatial ICA is used to identify network components that are spatially-distinct while retaining the temporal coherence across them. Most studies use spatial ICA to study brain networks as it is difficult to study the temporal coherence properties of brain networks using fMRI without an adequate understanding of the brain-activation model (Calhoun and Adali 2006). The purpose of ICA is to decompose an fMRI data matrix (number of time points x number of voxels) into a set of time courses that each correspond to a set of spatial patterns. ICA can be used at a single-subject as well as a group-level. Although single-subject level ICA analyses can help identify unique spatial components at the level of a single individual, this information cannot be used to draw inferences at a group or population level, as different individuals within the group will have different time series information in their fMRI data matrix. After obtaining a group-level delineation of spatial components that are spatially distinct but temporally coherent, these spatial components can be back projected to obtain spatial components for every individual within the group.

The most commonly used back projection method for group ICA is the dual regression method. It estimates voxel-level FC maps at an individual subject level from group ICA components generated on the same dataset. In dual regression, spatial components are regressed onto all functional volumes of an individual's fMRI. Here each functional volume is estimated as a linearly weighted sum of ICs. The corresponding beta weights from the regression are then considered as time courses and mapped onto the temporal signal at each voxel, producing maps of FC at an individual subject level (Schultz et al. 2014). However, such back projection maps can only be computed when the assumption of maximal independence of the ICs is true. When there is overlap between two or more components, the parameter estimates of the beta weights become relatively

unstable. Therefore, the orthogonality assumptions of dual regression can be beneficial when there is minimal overlap between ICs as it can accurately isolate neuronal signal and remove any sources of non-neuronal signal (noise). However, this can be a disadvantage when there is considerable overlap between the ICs as it can result in the removal of shared neuronal information across components in order to maintain maximal spatial independence.

1.8.5.3. Template based rotation

This is a technique that improves upon the back projection method used by dual regression wherein it removes the spatial and temporal orthogonality assumptions of the dual regression method and additionally allows for the utilization of an external template set for the estimation of FC maps. The core difference between the two methods is in the directionality of FC estimation. While FC maps are estimated within each functional volume as a linear combination of group-specific ICs in dual regression, the template-based rotation (TBR) method predicts components or templates as a linear combination of functional volumes. This inversion of directionality enables the estimation of each network independently and also retains any shared variance between networks. Figure 17 shows a schematic of the directionalities of voxel-wise FC estimations by the dual regression and TBR methods. The TBR method also estimates signal from white matter, cerebrospinal fluid, and noise or artifactual sources within each functional volume, therefore providing a method to remove unwanted sources of signal.

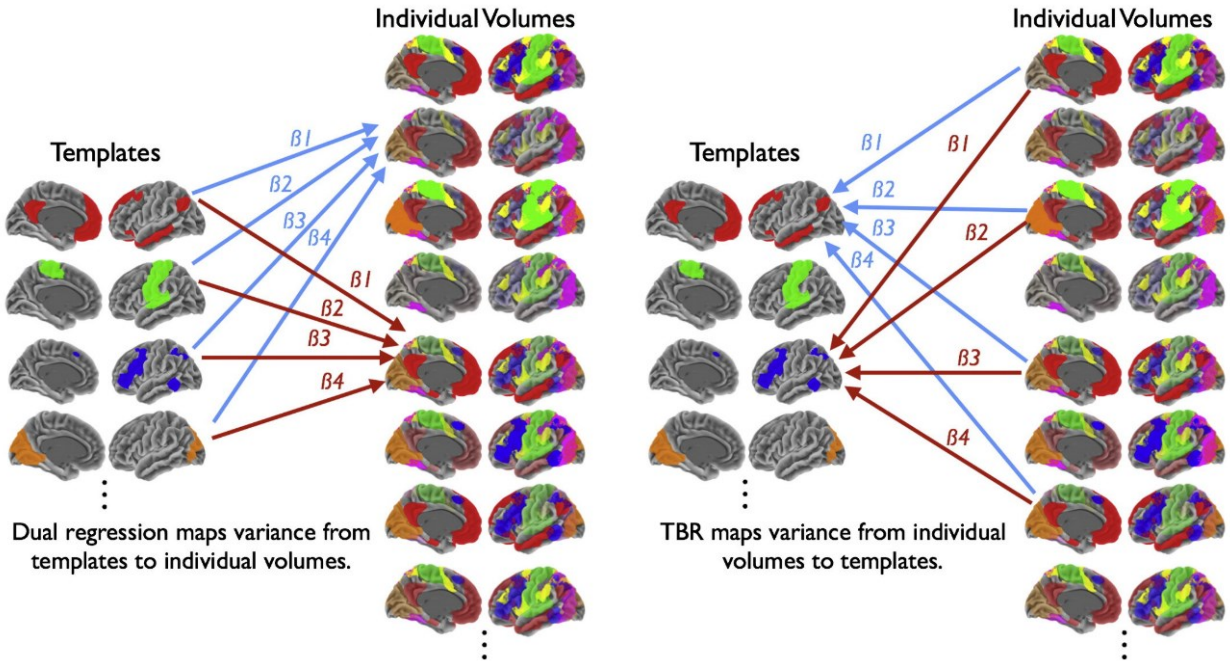

Figure 17. Schematic representation of the dual regression (left) and template-based rotation (right) methods.

1.8.5.4. Magnetic resonance spectroscopy

The area under the linewidth in an MR spectrum represents the concentration of the metabolites that constitute the spectrum. Approaches that have commonly been used to quantify these areas are peak integration and fitting. Peak *integration* entails the definition of a frequency range containing the peak-of-interest followed by summing the values across that frequency range and subtracting an estimate of the baseline above which the peak rises, providing the area under the curve (Buonocore and Maddock 2015). Peak *fitting* can provide more accurate quantification of the metabolite signal intensity compared to peak integration. In peak fitting, each peak-of-interest is fit to a mathematically-defined model peak shape for which the fitted peak has a predetermined area under the curve. This is followed by iterative calculation of peak integral values for the entire set of peaks. This method is most useful when prior knowledge of peak characteristics such as frequency relationships, amplitude ratios, scalar coupling is available (Buonocore and Maddock

2015). Prior knowledge of peak characteristics can be obtained from simulated or empirical metabolite basis sets. Such approaches are available with the linear combination model (LCModel) software and with the Quantitation Based on Quantum Estimation (QUEST) program. The use of these methods requires the in vitro simulation of the specific spectroscopic response of every anticipated metabolite (phantoms) to the exact scanning parameters to be used (Buonocore and Maddock 2015).

1.9. Neural correlates of disease in ALS

Neuroimaging studies have been successful in uncovering biomarkers that can be employed in the diagnosis, stratification, monitoring of disease progression, and in the identification of drug targets for patients with ALS. The following sections outline the most consistent findings of the neural correlates of ALS across various MRI modalities.

1.9.1. Diffusion-weighted MRI

Brain microstructure in ALS has been studied extensively using DTI. The majority of studies have consistently been able to identify microstructural alterations of white matter in the corticospinal tract and the corpus callosum, as well as in tracts connecting the frontotemporal regions of the brain in patients experiencing cognitive impairments (Agosta, Spinelli, and Filippi 2018). Despite the consistently observed alterations in CST FA, a meta-analytic study was unable to identify a good discrimination property of this measure when differentiating between ALS patients and healthy controls (Bradley R. Foerster et al. 2012). Greater upper motor neuronal impairment was observed to be associated with significant FA decreases in the CST with increases in AD, MD, and RD co-localized to areas showing FA decreases in the CST, superior longitudinal fasciculi, and corpus callosum (Agosta et al. 2014; Ricarda A. L. Menke et al. 2014). While a direct correlation was observed between TBSS-derived CST FA and disease progression rate (Ricarda A.L. Menke et al. 2012), an inverse correlation was observed between CST MD and the lower limb subscore

on the ALSFRS (Ricarda A. L. Menke et al. 2014). Longitudinally, progressive impairment of white matter microstructure in the corticospinal tract has been linked to worsening clinical function (Kalra, Müller, et al. 2020; Ricarda A L Menke et al. 2016).

1.9.2.Functional MRI

The literature on resting-state FC alterations of the sensorimotor network is quite heterogeneous in ALS (Agosta, Spinelli, and Filippi 2018). In addition to increased activation of the cortical motor areas during the performance of a motor task (Mohammadi et al. 2011), connectivity impairments of the motor network and extra-motor networks such as the DMN and frontoparietal networks have been identified and associated with impairments in cognitive and behavioural processing (Agosta et al. 2013a; Chenji et al. 2016; Luo et al. 2012; Ricarda A L Menke et al. 2016). In the past decade, there has been a paradigm shift in the number of resting-state networks studied and the definition of statistical significance in resting-state fMRI studies assessing FC at the voxel level. Previous studies (Agosta et al. 2013b; Chenji et al. 2016; Mohammadi et al. 2009; Tedeschi et al. 2012; Welsh, Jelsone-Swain, and Foerster 2013) have assessed a maximum of five RSNs (default mode, salience, sensorimotor, executive, frontoparietal). It is also important to note that previous studies using SBC or ICA techniques (Agosta et al. 2013b; Chenji et al. 2016; Mohammadi et al. 2009; Tedeschi et al. 2012) have used very liberal statistical thresholds. In the recent years, the study by (Bharti et al. 2022) has examined all known RSNs and identified clinically-relevant alterations in FC in a multicenter sample of ALS patients. In addition to cerebral networks, alterations of cerebellar functional connectivity have been identified in ALS patients (Bharti et al. 2020), specifically in symptomatic sporadic patients and asymptomatic carriers of mutations in ALS-relevant genes (Schmidt et al. 2014). Methodological differences across task-based and resting-state fMRI studies as well as the clinical and cognitive heterogeneity of the patient samples examined in the respective studies have contributed to inconsistencies in observations of brain network function in ALS.

1.9.3.Neurochemical concentrations

Despite a limited number of studies examining neurochemical concentrations in ALS, the finding of reductions in the concentrations of the neurometabolite N-acetyl aspartate (NAA) has been consistently reported. As NAA is the most abundant neurometabolite in the human brain (Barker et al. 2010), reductions in its concentrations have been identified in cortical and subcortical gray matter regions as well as along the length of the corticospinal tract (Agosta, Spinelli, and Filippi 2018; Ricarda A L Menke et al. 2016). In terms of other metabolites, reduced concentrations of the inhibitory neurotransmitter γ-aminobutyric acid and increased concentrations of the excitatory neurotransmitter glutamate have been identified in the motor cortex in ALS patients (Agosta, Spinelli, and Filippi 2018; B. R. Foerster et al. 2012; Ricarda A L Menke et al. 2016). However, longitudinal alterations in neurometabolite concentrations were very inconsistent across studies. Treatment with Riluzole has previously been shown to reduce the concentrations of glutamate (Bradley R. Foerster et al. 2013) and increase the concentrations of NAA (Kalra et al. 2006; Sanjay Kalra, Neil R. Cashman 1998). Levels of total NAA moieties have been shown to be associated with reduced foot tapping, a measure of upper motor neuron impairment, and with reduced functional connectivity of the primary motor cortex with other brain regions (Dey et al. 2022), therefore providing a potential biomarker of importance to the objective examination of ALS.

The heterogeneity in observations of cerebral alterations across these modalities at cross-sectional and longitudinal evaluations might occur due to differences in study populations including differences in sample sizes, inadequate sampling of disease phenotypes, longitudinal sampling intervals, the ability of patients to complete an adequate number of longitudinal visits, differences in disease stages across patients based on clinical phenotype and underlying pathophysiology, and the extent/severity of cerebral pathology at baseline. Other factors that are thought to contribute to these inconsistencies include the use of magnets with different hardware and software as well as the pharmacodynamic effects of drugs approved by regulatory health organizations for use in the treatment of ALS. Therefore, future studies could conduct a prospective evaluation of the effects of Riluzole on neurochemical concentrations to distinguish disease effects from drug effects.

1.10. Multicenter analysis of cerebral changes in ALS

In order to partially address the limitations within the ALS literature i.e., small sample sizes, inadequate sampling of disease phenotypes, inconsistencies across MRI acquisition protocols, and sampling of different ALS populations, the respective studies within this thesis utilized data from the Canadian ALS Neuroimaging Consortium (CALSNIC) (Kalra, Khan, et al. 2020). While conducting an evaluation of cerebral changes across multiple centers can help overcome these limitations, it comes with its own set of challenges. Despite the use of an MRI acquisition protocol that is preharmonized across multiple centers participating in the consortium, the acquired data can suffer from the additive and multiplicative effects of scanner variances arising due to the differences in manufacturers, hardware, or software. To minimize these systemic effects, thesis chapters 2-4 utilized an empirical Bayesian method known as ComBat for baseline (Fortin et al. 2017) and longitudinal (Beer et al. 2020) data. The term ComBat stands for ‘‘combating batch effects when combining batches”.

1.11. Thesis rationale and overarching objective

Despite consistently reported evidence of cerebral alterations in ALS in terms of cerebral function, microstructure, and the concentrations of neurochemicals, some gaps in the literature still persist. These gaps contribute to the rationale for the current thesis:

1. There is no adequate understanding of the biological mechanisms underlying ALS pathophysiology,
2. The long clinical prodrome of ALS impedes the identification of the specific disease processes that contribute to the different clinical manifestations of ALS. This makes it challenging to accurately stratify patients for disease diagnosis and management including their enrollment in clinical trials,

3. The differences in the chronological order of manifestation of disease features across ALS patients makes it challenging to perform a qualitative or quantitative assessment of patient disease stage, and
4. There is a lack of effective biomarkers for the determination of disease stage and in monitoring the pharmacodynamic effect of drugs on disease characteristics.

The overarching objective of the experimental chapters in this thesis is to uncover the biological mechanisms that underlie cerebral function, and how they relate to clinical observations, in ALS. As early disease characterization is important to defining a timeline for effective therapeutic intervention, the focus of this thesis is to first examine whether existing patient stratification criteria based on clinical features are sensitive to the identification of cerebral network patterns. This is followed by a clinically-blinded method of patient stratification wherein a data-driven approach utilizes neuroimaging variables to stratify patients, followed by an assessment of their cerebral function and clinical features. Chapters 2-4 present a comparison of clinically-defined and data-driven patient subgrouping methods in the characterization of cerebral function. Cortical functioning depends on factors such as the microstructure and biochemistry of the underlying neurons. Chapter 5 presents an examination of the neuroanatomical features that underlie cerebral function in ALS. The specific aims within the respective chapters and the corresponding findings are presented in the next sections.

1.12. Thesis organization – experimental chapters

1.12.1. Chapter 2

This study had three aims:

a) To identify cerebral connectivity alterations in ALS at baseline,
b) To utilize a data-driven method to characterize early and advanced pathophysiological disease in ALS using baseline cerebral connectivity measures, and

c) To perform a comparison of baseline demographic, clinical, and cerebral function features between the imaging-derived patient subgroups and those identified by clinically-defined criteria.

The salient findings of the study were:

a) Two biologically-distinct patient subgroups were identified based on the connectivities of different cerebral networks at baseline,
b) A combination of clinical and connectivity measures for these subgroups were indicative of the differences in group-specific disease severity albeit relative to each other, and
c) The spatial extents of cerebral connectivities of different resting-state networks in by imaging-derived patient subgroups was observed to be greater than that in clinically-defined patient subgroups.

Next steps: To identify longitudinal patterns of cerebral function differences between clinically-defined (Chapter 3) and imaging-derived (Chapter 4) patient subgroups.

1.12.2. Chapter 3

This study aimed to examine the longitudinal properties of cerebral networks in ALS patients and clinically-defined patient subgroups.

The salient findings of the study were:

a) Network connectivity alterations were exhibited by both motor and extra-motor networks in the comprehensive ALS cohort as well as in the clinically-defined patient subgroups.

b) Assessments of cerebral function in clinically-defined patient subgroups revealed that brain regions participating in motor encoding have altered longitudinal functional connectivities. Specifically, the connectivity of the motor imagery network is altered in early disease and that of the action observation network is altered in advanced disease.

1.12.3. Chapter 4

This study aimed to examine the longitudinal properties of cerebral networks in imaging-derived patient subgroups.

The salient findings of the study were:

a) Disease evolution patterns were distinct across the two identified patient subgroups. While one subgroup had a more severe (advanced pathophysiological) disease with a predominantly motor phenotype, the other subgroup had a less severe (early pathophysiological) disease with a motor-frontotemporal phenotype.
b) Clinical features of the disease in both patient subgroups corroborated their network characteristics. Specifically, the subgroup with the predominantly motor phenotype had reduced foot tapping scores at visit 1 and the subgroup with the motor-frontotemporal phenotype had lower cognitive function scores at visit 3.

Next steps: Owing to the selective specificity of the motor network (encompassing the primary motor cortex) towards disease severity in ALS, the thesis findings thus far suggest that the motor network undergoes progressive changes in connectivity across various pathophysiological disease stages of ALS. Combined with pathological evidence of a corticofugal axonal spread of TDP-43 proteinopathy originating at the motor cortex, a characterization of motor connectivity in terms of the neuroanatomical substrates of this region could enable the identification of an objective marker of upper MN function in ALS.

1.12.4. Chapter 5

This study had two aims:

a) To examine alterations in resting-state functional connectivity of the primary motor cortex with other brain regions
b) To identify the neuroanatomical features that were associated with these alterations

The salient findings of the study were:

a) The FC of the primary motor cortex with other brain regions was reduced
b) Although both neurochemical and structural measures were associated with clinical impairment, alterations in primary motor cortex FC were associated only with corresponding reductions in neurochemical concentrations within the primary motor cortex. This suggests that neurochemical alterations of the motor cortex might occur in earlier stages of disease pathophysiology and be more relevant to cerebral connectivity alterations.

In conclusion, the thesis findings characterize connectivities of the motor and extra-motor neuronal systems in ALS both at baseline and longitudinally from both clinical and neuroimaging standpoints. As expected, imaging-derived criteria are better able to characterize distinct patterns of disease spread compared to clinical criteria. This is suggestive of the need to include imaging-derived early disease characterization in addition to clinical measures when monitoring disease and also in the assessment of drug effectiveness in clinical trials. This could be beneficial towards encouraging the stratification of patients based on both their upper and lower MN function, assessing the pharmacodynamic effects of existing and upcoming drugs in clinical trials, and suggesting targets for potential drugs. This could not only help improve clinical outcomes but also the overall quality of life. In addition, routine monitoring of brain function, not only in people with a familial/genetic predisposition to ALS but also in people with no prior family history of

neurological or neuropsychiatric illnesses, might offer helpful clues for early diagnosis, prognosis, and relevant therapeutic intervention.

Chapter 2: Cerebral networks reveal patient subtypes with distinct endophenotypes in amyotrophic lateral sclerosis

Avyarthana Dey[1], Tobias Robert Baumeister[2], Michael Benatar[3], Shana Rae Black[4], Hannah Briemberg[5], Annie Dionne[6], Karleyton Evans[7], Richard Frayne[8], Angela Genge[2], Simon Graham[9], Vincent Koppelmans[4], Lawrence Korngut[8], Grant Liu[1], Collin Luk[1], Donald McLaren[7], Pedram Parnianpour[1], Peter Seres[10], Robert Cary Welsh[4], Lorne Zinman[9], Sanjay Kalra[1]

Author affiliations

1. Division of Neurology, Faculty of Medicine and Dentistry, University of Alberta, Edmonton AB, Canada
2. The Neuro, Montreal Neurological Institute and Hospital, McGill University, Montreal QC, Canada
3. Department of Neurology, University of Miami, Miami, Florida, United States
4. University of Utah, Salt Lake City UT, United States
5. Division of Neurology, Department of Medicine, University of British Columbia, Vancouver, British Columbia, Canada
6. CHU de Québec, Université Laval, Québec City QC, Canada
7. Biogen Pharmaceuticals, Cambridge MA, United States
8. Hotchkiss Brain Institute, University of Calgary, Calgary AB, Canada
9. Sunnybrook Research Institute, University of Toronto, Toronto ON, Canada
10. Department of Biomedical Engineering, University of Alberta, Edmonton AB, Canada

Corresponding author: Sanjay Kalra, kalra@ualberta.ca

2.1. Abstract

2.1.1. Introduction

Characterization of early disease in ALS is important for understanding pathophysiology and identifying patients who are more likely to respond to therapy in clinic or in clinical drug trials. However, identification of early disease based on observable clinical features may be subjective and not necessarily related directly to disease state. This study hypothesized that biologically distinct patient subgroups exist based on brain functional connectivity (FC).

2.1.2. Methods

174 ALS patients and 165 healthy participants from seven university centers in Canada and the United States were included from the Canadian ALS Neuroimaging Consortium (CALSNIC). A template-based rotation analysis technique was utilized to obtain maps of FC across 11 resting-state networks (RSNs) which were used in a hierarchical clustering algorithm to identify imaging-derived patient subgroups with similar characteristics of brain function. Early and advanced disease stages were characterized for imaging-derived patient subgroups based on their clinical and neuroimaging measures. Clinical staging was performed using stratification criteria adapted from 2 clinical drug trials (Criteria 1 and 2) and by disease progression rate (Criteria 3). Derived patient subgroups were compared with respect to clinical and FC characteristics.

2.1.3. Results

Two patient subgroups were identified using connectivity characteristics of RSNs. These imaging-derived patient subgroups demonstrated FC differences ($pFWE<0.05$) for all RSNs, and had significantly different symptom durations, disease progression rates, and foot tapping scores ($p<0.05$). Patient subgroups defined using clinical Criteria 1 demonstrated FC differences for the salience, right control, and primary visual RSNs ($pFWE<0.05$) and had significantly different

symptom duration, disease progression rate, forced vital capacity (FVC), ALSFRS-R total score, and foot tapping score ($p<0.05$). Patient subgroups defined using Criteria 2 demonstrated FC differences for the dorsal attention and subcortical RSNs and had significantly different symptom duration, disease progression rate, and FVC ($p<0.05$). While no differences in RSN FC were observed, Criteria 3 subgroups had significantly different education level, symptom duration, and ALSFRS-R, neurological examination, and cognitive scores ($p<0.05$).

2.1.4. Discussion

Individual-level imaging-derived patient stratification criteria are able to better distinguish ALS patients in terms of degree of cerebral degeneration than clinically-defined criteria of early versus late-stage disease. Resting-state brain FC requires further study as a potential biomarker for patient stratification, including for patient selection, and predicting and monitoring therapeutic response in clinical trials.

2.2. Introduction

Amyotrophic lateral sclerosis (ALS) is a neurodegenerative disease characterized by the impairment of motor neurons (MNs) in the cerebral cortex, brainstem, and spinal cord. This manifests as a combination of clinical features including spasticity, hyperreflexia, atrophy, fasciculations, and weakness. The clinical syndrome of ALS can be explained, in part, by the 'neural network disruption hypothesis' which assesses the impact of disease (neurodegeneration) on healthy interconnected neuronal populations (functional networks) (Strong and Swash 2022). The complexity of the ALS disease process is also reflected by the region and laterality of disease onset, the rate of functional decline, and is accentuated by the subjectiveness of diagnosis due to a limited window of observation during clinical visits, goals-of-care, or quality-of-life. Therefore, it is essential to disentangle the individual and interaction effects of such variables on core disease features in order to determine disease phenotypes that are biologically intuitive.

From a phenotypic perspective, it is important to subtype patients based on their clinical observations to allow for an objective examination of their disease characteristics. Such clinical observations can help define standardized criteria that are useful in observational studies or in the design of endpoints for clinical trials. From a biological perspective, an assessment of vulnerable neuron pools (van den Heuvel and Sporns 2011) can help uncover the core unifying features of disease in ALS, notwithstanding observable clinical phenotypes. This can help provide insights into a (structural or functional) network-specific spread of neurodegeneration (Strong and Swash 2022) common to all disease phenotypes. Recent studies in ALS (Bede et al. 2022a; Tan et al. 2022; Thome et al. 2022) have attempted to identify phenotypic patient subtypes, or classify ALS patients from healthy controls (HCs), based on structural measurements including brain volume, cortical thickness, and white matter fractional anisotropy. In terms of functional brain measures, static and dynamic resting-state functional connectivity (FC) measures have been used to classify study participants as ALS patients or HCs with a classification accuracy of ~62 percent (Bede et al. 2022a). Comparable classification accuracies (Bede et al. 2022a) across structural and functional studies, in addition to the neural network disruption hypothesis (Strong and Swash 2022), suggest that brain function might be a more intuitive measure of disease pathophysiology and could provide biological-phenotypic clues to address the heterogeneity problem in ALS.

Therefore, this study had two hypotheses: a) biologically distinct patient subtypes are identifiable based on imaging features of resting brain function, and b) these imaging-derived patient subtypes are phenotypically distinct. The current study had three aims which included 1) the identification of group differences in voxel-wise FC between ALS patients and HCs, 2) the identification of biologically-distinct patient subgroups based on intra-network FC of individual patients, and 3) a comparison of demographic, clinical, and imaging (FC) features between imaging and phenotypic ALS subtypes.

2.3. Methods

2.3.1. Study design

The Canadian ALS Neuroimaging Consortium (CALSNIC) (Kalra, Khan, et al. 2020) is a prospective multicenter study conducted at participating hospitals affiliated with seven university centers across Canada and the United States. These centers included the University of Alberta (Edmonton), University of Calgary (Calgary), University of Miami (Miami), McGill University (Montreal), Université Laval (Quebec City), University of Toronto (Toronto), and University of British Columbia (Vancouver).

2.3.2.Participant inclusion and exclusion

Participants enrolled in CALSNIC until October 2022 were considered for inclusion in the current study. Inclusion criteria for patients required the completion of a resting-state functional MRI scan, presence of both upper and lower MN signs on neurological examination, a diagnosis of clinically possible, probable, or definite ALS based on the El Escorial diagnostic criteria (Brooks et al. 2000), and a symptom duration not greater than 5 years. Inclusion criteria for HCs required them to obtain a minimum ECAS total score of 95 to be classified as cognitively intact as per the 2SD-NAC recommendation (McMillan et al. 2022). Patients were excluded from the study if they presented

with co-morbid frontotemporal dementia or other neurological conditions (e.g., traumatic brain injury requiring hospitalization). HCs were excluded from the study if they had previously experienced traumatic brain injury requiring hospitalization or received a diagnosis of/therapeutic intervention for depression. The final study sample consisted of 174 patients and 165 HCs. The demographics and clinical characteristics of the study sample are shown in Table 1.

2.3.3.Imaging acquisition

A multicenter harmonized MRI protocol was employed(Kalra, Khan, et al. 2020). Whole brain 3D T2*-weighted rs-fMRI data was acquired axially using an echo-planar imaging pulse sequence (repetition time = 2200 ms, echo time = 30 ms, flip angle = 70 degrees, field of view = 224 mm x 224 mm) with 3.5 mm^3 isotropic voxels. Patients were instructed to keep their eyes closed for the duration of the scan. The rs-fMRI acquisition times for CALSNIC 1 and 2 were respectively ~7 min and ~10 min (Kalra, Khan, et al. 2020). 3D T1-weighted structural MRI data was acquired for anatomical localization and normalization with 1 mm^3 isotropic voxels, 176 slices, and 256 mm x 256 mm field of view (Kalra, Khan, et al. 2020).

2.3.4.Imaging analysis and corrections for multicenter data

2.3.4.1. Preprocessing for rs-fMRI

The CONN toolbox (https://web.conn-toolbox.org/) was used to preprocess the rs-fMRI images. The first four functional volumes were removed for every participant to allow for the stabilization of signal intensity. Functional data were corrected for differences in slice acquisition times and realigned for head motion and orientation using a six-parameter rigid body transformation algorithm. The mean functional image was co-registered to the T1-weighted structural image, and the resulting transformation was applied to all functional images within each session. Following this, all functional images underwent normalization to the MNI space and smoothing with a

Gaussian kernel of 8 mm full-width-at-half-maximum. The white matter and cerebrospinal fluid signals as well as motion estimates were removed from the data and further denoising was performed using a bandpass filter of 0.008-0.09 Hz. The filtered and denoised images were used in further analyses using the template-based rotation (TBR) method (section 2.3.4.2).

2.3.4.2. Template based rotation

Maps of FC were generated by applying TBR to preprocessed rs-fMRI data. TBR allows for the utilization of the spatial stability of brain functional organization, thereby incorporating the strengths of seed-based-connectivity (SBC) analysis, independent component analysis (ICA), and dual regression analysis for the estimation of RSNs. This technique predicts RSN components at an individual level as a linear combination of time courses that correspond to spatial patterns of an *a priori* out-of-sample template set, thus removing the spatial and temporal orthogonality assumptions of distributed functional networks (at a group level) (Schultz et al. 2014). Of the 20 targets estimated for each participant by the TBR method, we preselected 11 RSN components (cerebellar, default mode, salience, dorsal attention, frontal, left and right control, motor, primary visual, subcortical, and temporal language networks) for assessment. The remaining nine components corresponding to white matter and artifactual signals (cerebellar white, extrastriate visual, eyes, frontal artifact, global signal, lateral artifact, nasal artifact, sagittal sinus, white matter) were excluded from assessment owing to their non-relevance to gray matter function. Individual RSN components underwent FisherZ transformation to allow for variance normalization. These FischerZ-transformed TBR maps were then entered into the Combat harmonization algorithm to correct for site- and scanner-specific effects.

2.3.4.3. Adjustment for site effects using ComBat Harmonization

ComBat is a tool based on an Empirical Bayesian algorithm which can be used to eliminate unwanted technical variability in biological data (Fortin et al. 2017). This technical variability can

occur because of differences in scanner hardware at the respective sites for data acquisition, software, or imaging acquisition protocols. ComBat can help dissect and remove this technical variability from biological variability by correcting for additive and multiplicative scanner effects, thereby improving statistical power (Fortin et al. 2017). In CALSNIC, technical variability was addressed at the point of acquisition by pre-harmonizing imaging protocols across scanners and in part across both phases of the CALSNIC study (Kalra, Khan, et al. 2020). However, the data can still retain some technical variability due to additive and multiplicative effects from scanner hardware and software. Therefore, in the current study, the ComBat harmonization method for baseline data (Fortin et al. 2017) was employed on the FisherZ-transformed TBR maps to correct for the remaining technical variability. For this, the 3D maps for each participant were grouped into a 4D image using the 'fslmerge' function. These 4D images for individual subjects were subsequently entered into the ComBat harmonization algorithm, allowing us to account for the covariance across different RSNs. The ComBat-harmonized FisherZ-transformed 3D TBR maps were entered into further analyses in the study.

2.3.4.4. Differences in RSN functional connectivity in ALS

Individual FisherZ-transformed TBR maps were included in a two-sample t-test generalized linear model (GLM) in SPM12 (https://www.fil.ion.ucl.ac.uk/spm/software/spm12/) to examine group differences in within- and between-network FC between the ALS and HC group. Age, sex, and education levels were included as regressors in the statistical model. Monte Carlo simulations were performed to correct for multiple comparisons over 11 RSNs. Simulations were performed over 10,000 iterations with global and local p-values of 0.05 and 0.001 to set the significance threshold at 27 voxels per cluster.

2.3.4.5. Patient subgrouping based on RSN connectivity

The TBR templates for individual RSNs were used as regions-of-interest to calculate RSN FC values from TBR maps for an individual subject at a voxel-level. The voxel-wise FC values were averaged to obtain a single measure of intra-network connectivity for each RSN. These FC averages underwent adjustments for demographic variables (age, sex, and education level) using a multiple regression model. Adjusted FCs for the ALS group were transformed into z-scores based on the HC average. These z-transformed time courses for the ALS group were used as inputs in a hierarchical clustering analysis to identify patient subgroups with distinct biological characteristics. Eleven continuous variables (z-scored FC for 11 RSNs) were entered into the clustering model as inputs, the Ward's method was used for estimating the clusters, and a squared-Euclidean distance function was used as a measure of dissimilarity to identify patient subgroups. The number of solutions were not defined *a priori*. The solution clusters (patient subgroups) were assessed for differences in clinical, demographic, and mean FC measures using SPSS28. Statistical significance was set at $p < 0.05$ for all clinical/demographic and intra-network FC comparisons.

2.3.4.6. Group differences in RSN functional connectivity in imaging-derived subgroups

A two-sample t-test GLM was used in SPM12 to examine group differences in voxel-wise FC between patient subgroups identified in section 2.6. As age, sex, and education levels were matched across the subgroups, these variables were not included as regressors to allow for an increase in the degrees of freedom. Statistical significance for voxel-level differences between subgroups was set at a family wise error corrected p-value < 0.05.

2.3.4.7. Phenotypic patient subtyping

The ALS patients in the study were also subtyped based on disease stage and progression. In this study, disease staging was defined based on clinical drug trial inclusion criteria for two drugs

approved by Health Canada for the treatment of sporadic and familial ALS – riluzole (Criteria 1) and edaravone (Criteria 2). These drugs have been previously shown to increase survival (Bensimon, Lacomblez, and Meininger 1994) and slow the accrual of disability (Abe et al. 2017) when administered to patients who are deemed to be in early disease stages based on their respective clinical trial criteria. *Criteria 1*, extrapolated from the riluzole criteria (Sanofi-Aventis 2010), identified patients as being in early disease stages if they had experienced symptoms for less than 2 years and had an FVC greater than or equal to 60%. *Criteria 2*, formulated on the edaravone criteria, identified patients as being in early disease stages if they had experienced symptoms for less than 2 years, had an FVC greater than or equal to 80%, and a minimum total ALSFRS-R score of 24/48 (minimum of 2 points per scale item)(Abe et al. 2017). Only patients meeting all conditions of the disease staging criteria were categorized as experiencing early disease ("Early-ALS" [E-ALS]). Patients not meeting one or more conditions were categorized as experiencing advanced disease ("Advanced-ALS" [A-ALS]). An additional subtyping method (*Criteria 3*) was employed that used estimated disease progression rate to subtype patients into slow progressors (SP-ALS) and fast progressors (FP-ALS).

Independent sample t-tests were performed to identify differences in three demographic and twelve clinical features between the E-ALS and A-ALS as well as SP-ALS and FP-ALS subgroups. The demographic features assessed included age, sex, education level and the clinical features assessed included symptom duration, general functional status (ALSFRS-R), disease progression rates, forced vital capacity, finger and foot tapping rates, and neurological (upper and lower MN) examination scores. Significance for all comparisons was set at $p < 0.05$. A two-sample t-test statistical GLM was used in SPM12 to identify differences in voxel-wise FC between the clinically-defined E-ALS and A-ALS patient subgroups. Statistical significance for voxel-level differences between subgroups was set at a family wise error corrected p-value < 0.05.

2.4. Results

2.4.1.Demographic and clinical characteristics of the study groups

A total of 339 participants (174 ALS, 165 HC) were included in this study. The demographic and clinical characteristics of all study groups are given in Table 1.

Table 1. Demographic and clinical characteristics of the study cohort. Single asterisk (*) represents significant group differences at $p < 0.05$ and double asterisk (**) represents group differences at $p < 0.001$. Group differences in all continuous variables were assessed using an independent samples t-test. Differences in sex distributions were assessed using chi-square test. HC = healthy controls, ALS = amyotrophic lateral sclerosis, E-ALS = Early ALS, A-ALS = Advanced ALS, Sig. = Significance of group differences, M = males, F = females, ALSFRS-R = ALS Functional Rating Scale (Revised), UMN = upper MN, LMN = lower MN, n.s. = not significant.

Characteristic	HC	ALS	Sig.	Imaging-derived subgroups			Clinically-defined subgroups								
							Criteria 1			Criteria 2			Criteria 3		
				Subtype 1	Subtype 2	Sig.	E-ALS	A-ALS	Sig.	E-ALS	A-ALS	Sig.	SP-ALS	FP-ALS	Sig.
Number of participants	165	174	-	109	62	-	100	59	-	78	81	-	85	89	-
Age (years)	55.4 (10.1)	59.9 (10.5)	**	60.1 (10.6)	59.8 (9.8)	n.s.	59.5 (10.8)	60.7 (9.3)	n.s.	59.5 (11.1)	60.4 (9.5)	n.s.	59.8 (10.4)	59.7 (10.8)	n.s.
Sex: M/F	74/91	108/66	*	66/43	41/21	n.s.	63/37	37/22	n.s.	48/30	52/29	n.s.	58/27	50/39	n.s.
Education level (years)	16.5 (3.0)	15.2 (3.5)	**	15.1 (3.4)	15.4 (3.6)	n.s.	14.9 (3.4)	15.4 (3.4)	n.s.	15.2 (3.6)	15.0 (3.2)	n.s.	15.7 (3.4)	14.6 (3.4)	*
Symptom duration	-	1.7 (1.1)	-	1.6 (0.9)	1.9 (1.2)	*	1.1 (0.4)	2.7 (1.1)	**	1.1 (0.5)	2.3 (1.2)	**	2.2 (1.1)	1.2 (0.7)	**
Functional status (ALSFRS-R total)	-	37.9 (6.2)	-	37.7 (5.9)	38.8 (6.2)	n.s.	38.7 (5.1)	36.5 (7.3)	*	38.6 (4.8)	37.2 (7.1)	n.s.	41.2 (4.4)	34.7 (6.1)	**
Disease progression rate	-	0.7 (0.6)	-	0.8 (0.7)	0.5 (0.3)	*	0.8 (0.6)	0.5 (0.5)	**	0.9 (0.7)	0.6 (0.6)	*	0.3 (0.1)	1.1 (0.6)	**
Forced vital capacity (%)	-	89.0 (19.8)	-	89.7 (18.8)	88.3 (21.7)	n.s.	93.8 (16.5)	81.2 (22.3)	**	98.8 (13.5)	79.8 (20.5)	**	90.9 (22.2)	87.4 (17.1)	n.s.
Left UMN exam score	-	2.5 (1.5)	-	2.6 (1.5)	2.4 (1.5)	n.s.	2.6 (1.5)	2.6 (1.6)	n.s.	2.7 (1.5)	2.5 (1.5)	n.s.	2.2 (1.3)	2.8 (1.6)	*
Right UMN exam score	-	2.4 (1.6)	-	2.5 (1.6)	2.4 (1.5)	n.s.	2.5 (1.5)	2.6 (1.6)	n.s.	2.6 (1.5)	2.4 (1.6)	n.s.	2.2 (1.4)	2.7 (1.6)	*

Left LMN exam score	-	2.4 (1.2)	-	2.6 (1.2)	2.3 (1.4)	n.s.	2.5 (1.1)	2.4 (1.3)	n.s.	2.4 (1.2)	2.5 (1.2)	n.s.	2.2 (1.2)	2.7 (1.2)	*
Right LMN exam score	-	2.5 (1.3)	-	2.6 (1.2)	2.3 (1.3)	n.s.	2.5 (1.2)	2.3 (1.4)	n.s.	2.4 (1.2)	2.5 (1.3)	n.s.	2.2 (1.3)	2.7 (1.2)	*
Left finger tapping score	53 (13)	38 (16)	**	38 (16)	38 (16)	n.s.	38 (18)	36 (14)	n.s.	38 (18)	37 (15)	n.s.	40 (13)	36 (18)	n.s.
Right finger tapping score	59 (14)	43 (17)	**	43 (17)	42 (18)	n.s.	42 (20)	41 (13)	n.s.	42 (20)	42 (16)	n.s.	44 (16)	41 (19)	n.s.
Left foot tapping score	40 (10)	23 (15)	**	22 (15)	26 (15)	n.s.	25 (15)	19 (14)	*	25 (15)	21 (15)	n.s.	25 (14)	21 (15)	n.s.
Right foot tapping score	43 (10)	25 (15)	**	23 (15)	29 (15)	*	26 (15)	21 (15)	*	26 (15)	22 (15)	n.s.	27 (16)	24 (15)	n.s.
ECAS total (/136)	114 (8)	103 (21)	**	103 (23)	103 (19)	n.s.	100 (25)	106 (16)	n.s.	100 (27)	104 (16)	n.s.	107 (15)	100 (25)	*

2.4.2.Differences in RSN functional connectivity in ALS

Comparing all ALS patients with healthy controls, the motor, temporal language, and right control networks had both increased and decreased FC with other brain regions. The frontal, dorsal attention, and primary visual networks had decreased FC, and the salience and subcortical networks had increased FC, with other brain regions (Figure 1, Table 2).

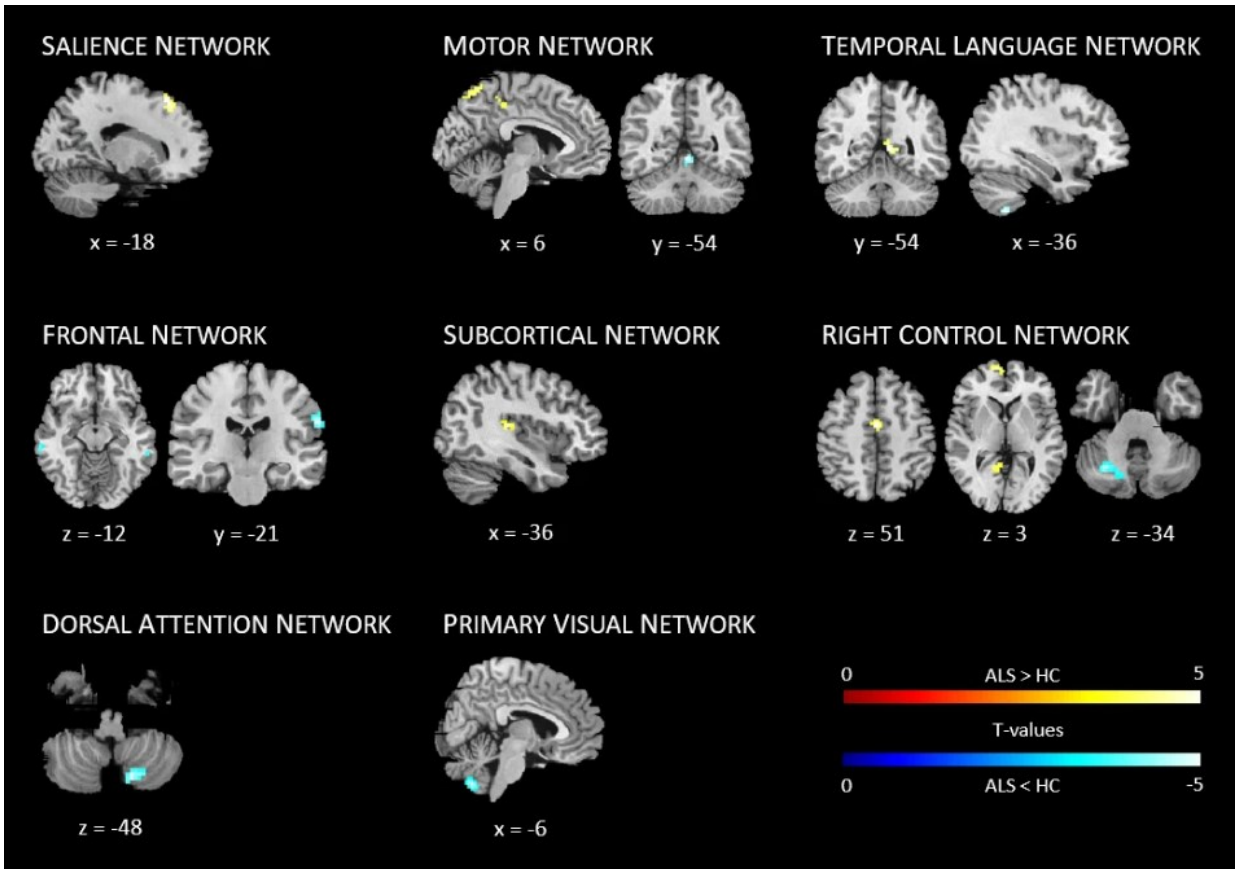

Figure 1. Group differences in voxel-wise intra- and inter-network FC in all patients with ALS compared to HC. HC=healthy controls.

Table 2. Group differences in voxel-wise intra- and inter-network FC across different RSNs in all patients with ALS compared to HCs. ALS = amyotrophic lateral sclerosis, HC = healthy controls, R = right, L = left, B = bilateral.

Resting-state network	Contrast	Brain region	Cluster size	Cluster coordinates (x,y,z)	T-value
Salience	ALS > HC	L frontal eye fields	29	-18, 27, 54	3.93
Motor	ALS > HC	B visuomotor area	48	-3, -72, 57	4.18
		B dorsal posterior cingulate cortex	32	-3, -39, 48	3.98

	ALS < HC	R anterior cerebellum	33	3, -54, -6	3.94
Temporal Language	ALS > HC	R posterior cingulate cortex	44	6, -51, 9	4.01
	ALS < HC	L posterior cerebellum	29	-36, -54, -57	4.08
Frontal	ALS < HC	B medial temporal cortex	27	-66, -33, -15	4.42
		R supramarginal gyrus	73	63, -21, 27	4.31
Subcortical	ALS > HC	L primary auditory cortex	47	-36, -27, 12	4.16
Right Control	ALS > HC	L anterior cingulate gyrus	29	0, -9, 51	4.26
		L anterior prefrontal cortex	71	-12, 63, 3	3.95
		L ventral posterior cingulate gyrus	78	-6, -57, 9	3.93
	ALS < HC	L posterior cerebellum	58	-30, -63, -36	4.29
Dorsal Attention	ALS < HC	R posterior cerebellum	57	15, -69, -48	4.05
Primary Visual	ALS < HC	L posterior cerebellum	102	-6, -63, -48	4.87

2.4.3.Clustering based on intra-network RSN connectivity values

The hierarchical clustering algorithm revealed two ALS subgroups (Subtype 1: n = 109, Subtype 2: n = 62) based on network-specific FC. An assessment of the intra-network FC (Table 3) revealed that FCs were lower in Subtype 1 compared to Subtype 2, except in the subcortical RSN which showed no significant difference between subgroups. *Post hoc* pairwise comparisons with HCs showed that the cumulative ALS cohort had increased intra-network FCs in all RSNs, except in the cerebellar network for which the FC was decreased, and the subcortical network for which the FC did not differ in comparison to HCs. Intra-network FCs were significantly different for nine RSNs in Subtype 1 and ten RSNs in Subtype 2 compared to HCs.

Table 3. Intra-network FC in study cohorts. Means for intra-network FC values, corrected for the effects of age, sex, and education level, are displayed. The standard errors for intra-network FCs for all RSNs across all study cohorts were ≤0.01. Asterisk (*) represents significant differences ($p<0.05$) in intra-network FC in ALS patients (and ALS subgroups) when compared to HCs.

Resting-state network	HC	ALS	Imaging-derived ALS subgroups	
			Subtype 1	Subtype 2
Default Mode Network	0.20	0.26*	0.23*	0.30*
Motor Network	0.23	0.29*	0.27*	0.32*
Frontal Network	0.37	0.40*	0.38	0.42*
Temporal Language Network	0.25	0.31*	0.29*	0.35*
Salience Network	0.23	0.25*	0.24*	0.28*
Dorsal Attention Network	0.22	0.27*	0.25*	0.30*
Left Control Network	0.23	0.27*	0.24*	0.31*
Right Control Network	0.22	0.25*	0.23*	0.28*
Subcortical Network	0.30	0.30	0.30	0.31
Cerebellar Network	0.31	0.22*	0.21*	0.24*
Primary Visual Network	0.33	0.39*	0.37*	0.41*

2.4.4. Demographic and clinical features of imaging and phenotypic subgroups

The demographic and clinical features of patient subgroups are summarized in Table 1.

Patient subgroups were matched for demographics (age, sex, and education levels), except for Criteria 3 subgroups (SP-ALS and FP-ALS) that were different in terms of their education.

In terms of clinical features, imaging-derived subgroups had significantly different symptom durations (Subtype 2 > Subtype 1), disease progression rate (Subtype 1 > Subtype 2), and right foot tapping scores (Subtype 2 > Subtype 1). Criteria 1 subgroups had significantly different

symptom durations (A-ALS > E-ALS), ALSFRS-R total scores (E-ALS > A-ALS), disease progression rates (E-ALS > A-ALS), FVC% (E-ALS > A-ALS), right and left foot tapping scores (E-ALS > A-ALS). Criteria 2 subgroups had significantly different symptom durations (A-ALS > E-ALS), disease progression rates (E-ALS > A-ALS), FVC% (E-ALS > A-ALS). Criteria 3 subgroups had significantly different symptom durations (SP-ALS > FP-ALS), ALSFRS-R total scores (SP-ALS > FP-ALS), disease progression rates (FP-ALS > SP-ALS), upper and lower MN function scores (FP-ALS > SP-ALS), and ECAS total scores (SP-ALS > FP-ALS). On correcting for multiple comparisons, subgroup differences for upper and lower MN function scores (Criteria 3) and foot tapping scores (imaging-derived subgrouping and Criteria 1) did not retain their significance.

2.4.5. Intra- and inter-network FC alterations in imaging-derived and clinically-defined subgroups

See figures 2, 3 and table 4 for details on FC differences in imaging- and clinically-defined ALS subgroups. *Post hoc* t-tests were performed pairwise to compare voxel-wise FCs of imaging-derived and clinically-defined subgroups with HCs (supplementary).

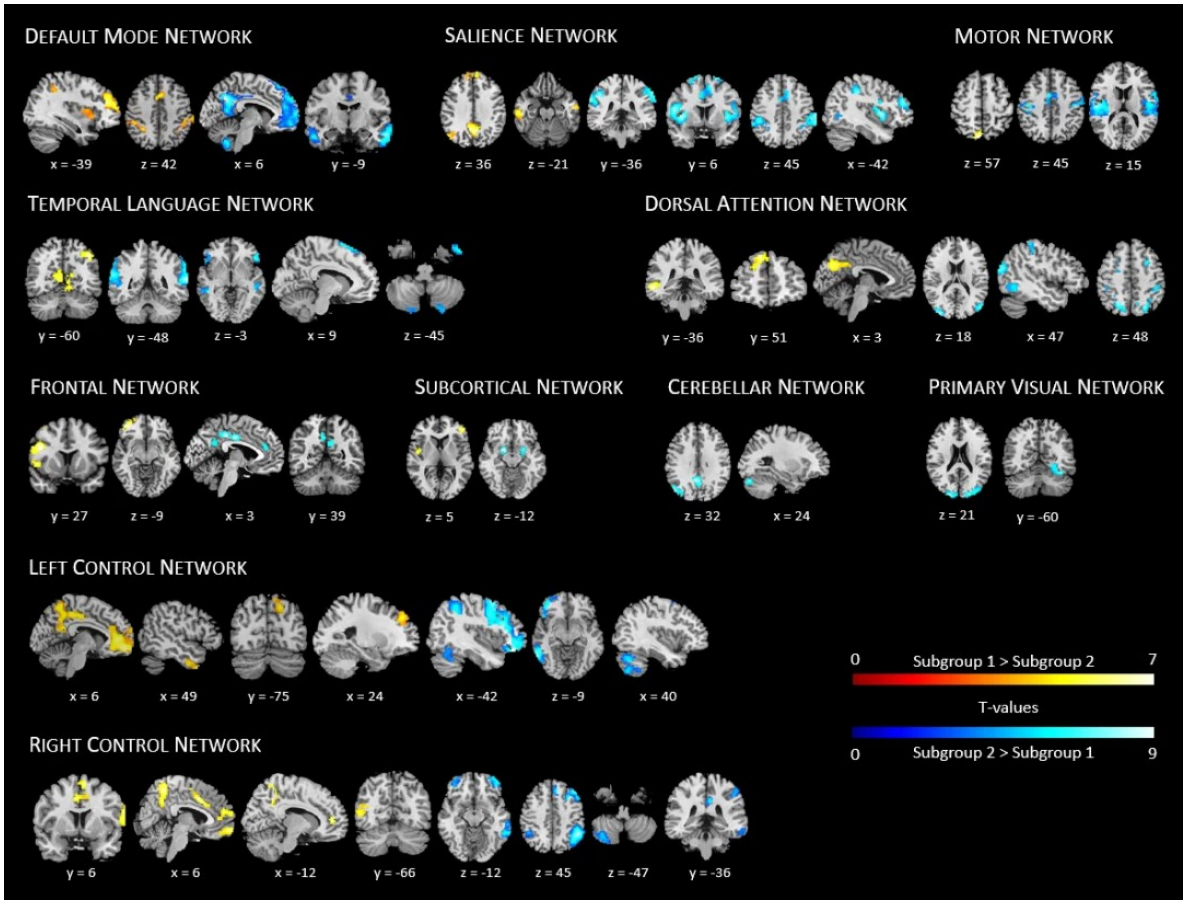

Figure 2. Differences in voxel-wise FC across imaging-derived ALS subgroups

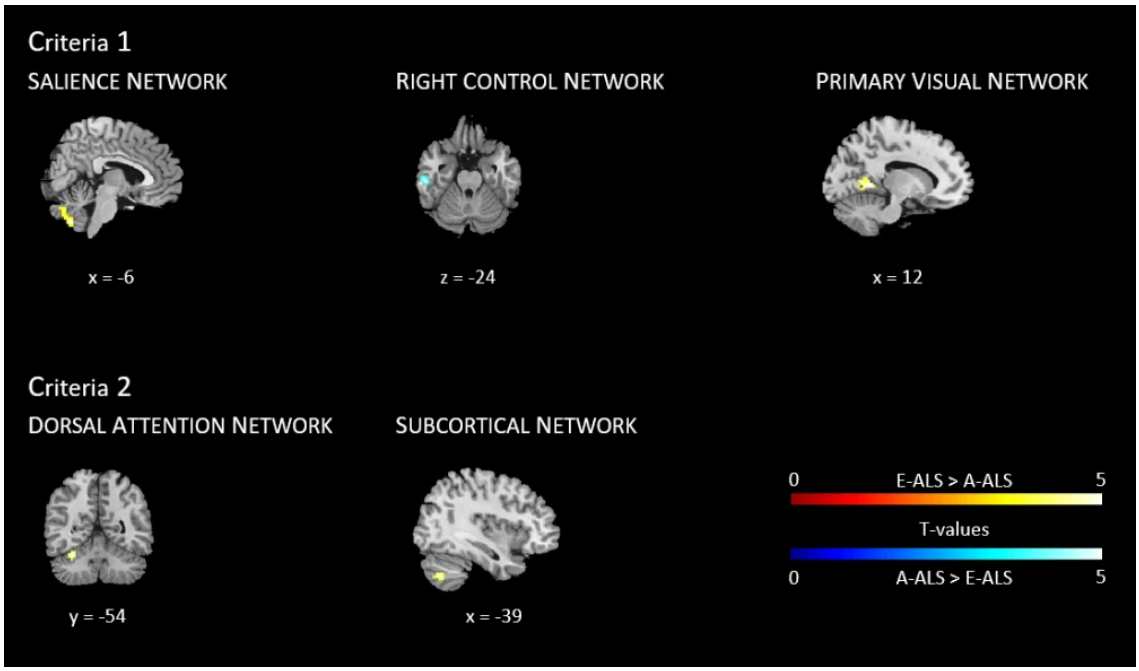

Figure 3. Differences in voxel-wise FC across clinically-defined ALS subgroups

Table 4. Differences in voxel-wise FC across imaging-derived and clinically-defined ALS subgroups. ALS = amyotrophic lateral sclerosis, HC = healthy controls, R = right, L = left, B = bilateral.

Contrast	Brain region	Cluster size	Coordinates (x,y,z)	T-value
Default Mode Network				
Subgroup 1 > Subgroup 2	L anterior prefrontal cortex	202	-39, 42, 21	6.4
	B insula	269	-45, 9, -3	4.9
	R dorsal dorsolateral prefrontal cortex	90	33, 51, 30	4.8
	L inferior parietal lobule	92	-33, -45, 39	4.6
	L premotor and supplementary motor areas	71	-21, -3, 54	4.5
	R postcentral gyrus	149	66, -27, 42	4.5

Subgroup 2 > Subgroup 1	R dorsal posterior cingulate cortex	789	6, -60, 36	8.2
	L dorsal dorsolateral prefrontal cortex	2171	-6, 45, 45	7.8
	B medial temporal gyrus	557	60, -9, -21	7.7
	R angular gyrus	287	-42, -60, 33	6.8
	B posterior cerebellum	191	9, -54, -45	6.3
Motor Network				
Subgroup 1 > Subgroup 2	L visuomotor cortex	212	-6, -75, 57	5.2
Subgroup 2 > Subgroup 1	L supramarginal gyrus	879	-54, -18, 15	7.2
	L premotor and supplementary motor areas	1423	-6, 3, 45	6.1
Frontal Network				
Subgroup 1 > Subgroup 2	L Broca's area (opercularis)	318	-45, 12, 27	5.2
	L anterior prefrontal cortex	171	-39, 48, -9	5.1
Subgroup 2 > Subgroup 1	R ventral posterior cingulate cortex	131	3, -15, 36	5.1
	L ventral anterior cingulate cortex	131	-6, 39, 9	4.8
	L dorsal posterior cingulate cortex	77	-9, -54, 39	4.3
Temporal Language Network				
Subgroup 1 > Subgroup 2	R angular gyrus	130	42, -60, 45	4.8
	B ventral posterior cingulate cortex	175	15, -54, 12	4.6
Subgroup 2 < Subgroup 1	R angular gyrus	418	63, -48, 15	7.1
	L angular gyrus	456	-60, -51, 21	6.0
	R pars orbitalis	194	51, 27, -3	5.7
	R premotor and supplementary motor areas	374	9, 15, 66	5.3
	L Broca's area (triangularis)	441	-51, 21, 6	5.2
	R inferior temporal gyrus	68	48, 3, -45	5.2
	B posterior cerebellum	85	24, -78, -39	4.3
Salience Network				
Subgroup 1 > Subgroup 2	R dorsal posterior cingulate cortex	334	3, -60, 36	6.0
	L medial temporal gyrus	116	-57, -21, -21	5.0

	R inferior temporal gyrus	107	57, -3, -33	4.8
	L angular gyrus	65	-48, -75, 36	4.8
	R superior frontal gyrus	532	3, 54, 36	4.7
Subgroup 2 > Subgroup 1	L inferior parietal lobule	382	-66, -36, 30	6.5
	B insula	364	-42, 6, 3	6.3
	R supramarginal gyrus	426	63, -24, 45	6.0
	B premotor and supplementary motor areas (superior)	150	-12, -3, 72	5.9
	B anterior prefrontal cortex	168	-42, 42, 24	5.5
	R premotor and supplementary motor areas (midline)	203	9, 6, 54	5.3
	B fusiform gyrus	112	-60, -63, -12	4.6
E-ALS > A-ALS (Criteria 1)	L posterior cerebellum	66	-6, -66, -45	4.8
Dorsal Attention Network				
Subgroup 1 > Subgroup 2	L medial temporal gyrus	105	-57, -36, -6	5.3
	L dorsal dorsolateral prefrontal cortex	80	-12, 51, 39	4.8
Subgroup 2 > Subgroup 1	L premotor and supplementary motor areas	150	-27, -3, 66	6.3
	L visual association area	141	-36, -90, 18	6.1
	L superior parietal lobule	279	-24, -60, 51	5.8
	R fusiform gyrus	162	57, -60, -9	5.1
	R supramarginal gyrus	98	36, -39, 45	4.8
	R frontal eye fields	99	27, 9, 48	4.6
E-ALS > A-ALS (Criteria 2)	L posterior cerebellum	68	-33, -54, -24	4.2
Left Control Network				
Subgroup 1 > Subgroup 2	R anterior prefrontal cortex	636	6, 57, -9	6.1
	L sensory association area	611	-12, -30, 48	5.2
	R medial temporal gyrus	151	57, -3, -30	5.1
	R visuomotor cortex	78	15, -75, 42	4.5
	R dorsal dorsolateral prefrontal cortex	94	24, 42, 39	4.5
Subgroup 2 > Subgroup 1	L pars orbitalis	1197	-42, 39, -15	7.9

	L fusiform gyrus	454	-63, -54, -9	7.0
	L frontal eye fields	123	-3, 27, 45	6.6
	R middle frontal gyrus	189	51, 30, 33	6.5
	L supramarginal gyrus	473	-51, -48, 51	6.4
	R posterior cerebellum	516	33, -69, -51	6.2
Right Control Network				
Subgroup 1 > Subgroup 2	R premotor and supplementary motor areas (midline)	315	3, 0, 63	5.2
	R premotor and supplementary motor areas (lateral)	112	63, 6, 21	4.8
	L visuomotor area	148	-6, -51, 54	4.9
	L orbitofrontal cortex	59	-6, 60, -15	4.8
	L dorsal anterior cingulate cortex	120	-12, 45, 6	4.8
	L visual association area	61	-51, -66, 3	4.2
Subgroup 2 > Subgroup 1	B anterior prefrontal cortex	944	33, 54, 0	8.4
	R supramarginal gyrus	506	51, -48, 54	8.1
	R ventral posterior cingulate cortex	57	6, -36, 36	5.8
	R frontal eye fields	85	6, 30, 45	5.7
	R fusiform gyrus	182	57, -48, -12	5.3
	L angular gyrus	66	-51, -51, 51	4.9
	L posterior cerebellum	136	-36, -69, -48	4.9
A-ALS > E-ALS (Criteria 1)	L inferior temporal gyrus	61	-57, -24, -24	4.4
Subcortical Network				
Subgroup 1 > Subgroup 2	R anterior prefrontal cortex	71	42, 45, 18	4.4
	L superior temporal gyrus	64	-51, 3, -9	4.1
Subgroup 2 > Subgroup 1	L globus pallidus	89	-18, 0, -12	5.8
	R putamen	77	24, 3, -12	5.0
E-ALS > A-ALS (Criteria 2)	L posterior cerebellum	57	-39, -66, -45	4.4
Cerebellar Gray Network				
Subgroup 2 > Subgroup 1	L dorsal posterior cingulate cortex	197	-3, -60, 39	5.5

	L angular gyrus	109	-48, -72, 30	4.8
	R posterior cerebellum	178	27, -78, -27	4.8
Primary Visual Network				
Subgroup 2 > Subgroup 1	L secondary visual cortex	261	-21, -96, 21	5.9
	R visual association area	371	12, -87, 42	5.5
	R fusiform gyrus	181	36, -60, -18	5.2
E-ALS > A-ALS (Criteria 1)	R secondary visual cortex	75	12, -51, 3	4.3

2.5. Discussion

The current study aimed to assess FC alterations in ALS, stratify patients using imaging-derived measures of cerebral FC as a proxy for biological state, and perform a comparison of clinical and imaging features across imaging-derived and clinically-defined subgrouping methods. In line with the study hypotheses, two patient subgroups were identified based on RSN FC. These patient subgroups were distinct in terms of both their clinical phenotypes and FC-based network alterations. Although the combination of patient clinical features in imaging-derived subgroups were comparable to those of the clinically-defined subgroups, patterns of FC were vastly different. While clinically-defined subgrouping revealed single (Criteria 1 and 2) or no (Criteria 3) clusters of altered FC in a few subsets of RSNs, imaging-derived subgrouping revealed large-scale FC alterations for all RSNs. Therefore, RSN-derived stratification is more sensitive than clinical stratification in identifying groups with distinct states of cerebral degeneration in ALS patients. Interpretations of study findings corresponding to the specific aims of the study are discussed in the following sections.

2.5.1.Functional connectivity alterations in ALS vs HC

An assessment of RSNs in the current study suggests the occurrence of a dissociation of corticocerebellar connectivity in ALS. Specifically, there was decreased intra-network FC of the cerebellar network compared to increased intra-network FC of other networks (Table 3), indicating

a reduction in cerebellar self-connectivity. Decreased connectivity between the cerebellum and other networks (motor, temporal, dorsal attention, primary visual, and right control) indicates reduced corticocerebellar FC. In contrast, increased connectivity between cortical networks suggests that corticocortical circuits are preferentially utilized over corticocerebellar circuits in ALS. This leads to a speculation that stronger corticocortical connectivity occurs to counteract the loss of corticocerebellar connectivity as a compensatory response towards the maintenance of cerebral homeostasis. This can be partially addressed by a phenomenon known as 'cerebellar diaschisis' (Fornito, Zalesky, and Breakspear 2015) where there is reduced involvement of a remote anatomical region (cerebellum) following reduced excitatory signalling from the source of the 'anatomical lesion' (cortical functional impairment). Cerebellar dysfunction has been widely implicated in ALS (Bharti et al. 2020; R. Chipika et al. 2022). While increased corticocerebellar FC is considered a compensatory mechanism in ALS literature, a decrease in such connectivity (as in the current study) suggests a disengagement between the cerebellar and cortical functional networks. In a previous study in which patients were grouped based on simulated neuronal excitation-inhibition signatures, improved clustering performance was observed when corticocerebellar networks were considered in the clustering algorithm in addition to cortical networks (Monteverdi et al. 2022). This improvement was observed specifically in ALS rather than in Alzheimer's disease or FTD (Monteverdi et al. 2022). Therefore, corticocerebellar connectivity alterations seem to be a feature with some specificity to neurodegeneration in ALS.

In contrast to other RSNs in the current study, the frontal network had reduced connectivity with other cortical regions, specifically with the middle temporal cortex (Table 2). Reduced frontotemporal connectivity, in addition to increased intra-network FC (Table 3) of the frontal network, is suggestive of a breakdown in functional integration between the frontal and non-frontal cortical networks – impaired frontal networks dissociate from the rest of the cortex and become more self-connected. These independent processes likely occur in a progressive and complementary fashion resulting in progressive impairment of the frontal network, which could contribute to the evolution of cognitive dysfunction with advancing disease in ALS(Crockford et al. 2018). Impairments of frontotemporal structural and (resting-state) functional connections have

been respectively observed in the C9orf72-linked (cognitive) ALS subtype (van Veenhuijzen et al. 2022) and in ALS patients not carrying the C9orf72 mutation (Bharti et al. 2022; Govaarts et al. 2022; Proudfoot, Bede, and Turner 2018). In accordance with reduced FC in the frontal network, ALS patients had significantly lower ECAS total scores compared to HCs (Table 1).

FC impairments of the right control, primary visual, and dorsal attention networks occur with regions subserving the processing of semantic (Ogura et al. 2019; Pinto-Grau et al. 2021) and sensory (R. H. Chipika et al. 2022b) information in ALS. The subcortical network has increased FC with the primary auditory cortex, a brain region shown to be impaired in bulbar-onset ALS (Shellikeri et al. 2019) and to have reduced cortical thickness (R. H. Chipika et al. 2022b; Consonni et al. 2018). The salience network has increased FC with the frontal eye fields (FEFs), brain regions that have been anatomically localized to the precentral sulcus in both human and animal (primate) studies, are responsible for eye movements, and are heavily interconnected with the temporal, parietal, and occipital cortices, brainstem, and cerebellum (Vernet et al. 2014). Alterations in volume (Yunusova et al. 2019) and function (Witiuk et al. 2014) of the FEFs have been linked to the performance of anti-saccade tasks in ALS.

2.5.2. Identification of patient subgroups based on individual-level intra-network FC

To our best knowledge, this is the first study that utilized the biological characteristics of brain networks (FC) at an individual level to subtype ALS patients. The findings of the current study suggest that, in terms of their clinical characteristics, Subtype 1 patients might be in more advanced disease stages as they have a faster disease progression rate, shorter symptom duration, and worse voluntary motor function than Subtype 2 patients.

In terms of cerebral FC, Subtype 1 patients have lower generalized FC compared to Subtype 2 patients. Despite the understanding that the lack of longitudinal assessments, as in the current study, might pose an impediment towards characterizing disease evolution, the Scaffolding Theory of Aging and Cognition (STAC) (D. C. Park and Reuter-Lorenz 2009; Reuter-Lorenz and Park 2014) might provide clues as to the severity of the disease process in the imaging-derived subgroups even at baseline. STAC suggests that, as part of a normal adaptive response of the brain towards healthy aging, additional brain networks are recruited (resulting in increased network activation) to compensate for alterations in goal-oriented functioning of relevant brain networks. When healthy aging is interrupted by a pathological event, STAC suggests that normal adaptive processes to the pathological stressor are still maintained to preserve normal function. However, with increasing intensity of the pathological process, the rate of network activation impairment surpasses that of restorative adaptation, eventually reaching a critical point in the disease course and resulting in a decline in compensatory mechanisms (increased network activation) for the preservation of brain function (Gregory et al. 2017). However, as there currently exists no quantification of the critical threshold in ALS, it is difficult to infer from such baseline assessments whether the critical point has been reached or surpassed for either of the subgroups. Therefore, three scenarios are likely –

a) Both patient subgroups are experiencing an increase in functional activation to counteract the pathological event before the critical threshold is reached. In this case, patients in Subtype 2 are experiencing advanced disease.

b) Both patient subgroups have reached the critical threshold at the time of assessment. This would indicate that patients in Subtype 1 are experiencing advanced disease as their decline in network activation is greater than that of Subtype 2.

c) Only one patient subgroup has reached the critical threshold and is experiencing a decline in network activation, indicating that patients in Subtype 1 are experiencing advanced disease. In this case, Subtype 2 is approaching critical threshold.

Based on the plausibility of these independent scenarios, the responses in network activation for the two subgroups suggest that patients in Subtype 1 are more likely to be experiencing advanced disease. In sum, both the clinical and FC observations independently suggest that the disease is more advanced in patients belonging to Subtype 1. However, a characterization of the critical point is necessary to confidently arrive at such inferences from imaging features alone and to identify targets for disease management or modification.

Persistent low-level excitation of inhibitory interneurons has been hypothesized to induce compensatory restructuring of sensorimotor functional pathways, disinhibiting sensorimotor connectivity and resulting in sustained hyperexcitability of the primary motor cortex (Rosenthal et al. 2020). Cortical hyperexcitability, a correlate of impaired inhibitory interneuronal (GABAergic) activity and/or calcium-mediated excitotoxicity resulting in reduced synaptic transport and elevated glutamate concentrations (M. R. Turner and Kiernan 2012; Vucic et al. 2021), is postulated to occur in early pathophysiological disease stages before the clinical onset of ALS as evidenced by transcranial magnetic stimulation studies (M. R. Turner and Kiernan 2012). Riluzole, a drug commonly used to treat ALS, is believed to regulate cortical glutamate concentrations by preventing its release from the presynaptic terminal to the extra-neuronal space (Sanofi-Aventis 2010), and is shown to be beneficial when administered early in the disease (Thakore et al. 2022). Therefore, one of the aims of the current study was to characterize the features of early disease in ALS based on the clinical drug trial criteria for Riluzole with the additional criteria of symptom duration under 2 years.

2.5.3. Choice of pathophysiological disease staging criteria and recommendations for targeted therapeutics

Assessing disease staging across clinically-defined and imaging-derived criteria, it seems apparent that the two stratification methods subgroup patients based on different characteristics of the disease. While clinical criteria focus on early disease characterization (likely driven by how ‘soon

after' the first onset of symptoms the patient presents at an ALS clinic), the imaging-derived criteria focus on characterizing disease stage based on pathophysiology (cerebral network properties). Intuitively, this suggests that there could be a possible discordance in the properties of the two stratification methods in segregating distinct patient clusters, as patients with minimal extents of network alteration (and longer duration of symptoms) would be considered to be in the early stages of disease as per the imaging-derived criteria and patients with shorter duration of symptoms (presumably with extensive network alterations) are identified early as per the clinical trial criteria. However, patients with shorter symptom durations had a faster rate of disease progression according to both imaging-derived and clinically-defined criteria – being suggestive of similarities in disease staging shared by the two methods. An assessment of similarities in disease staging revealed a concordance of imaging-derived subgrouping with Criteria 1 for 66/174 patients (E-ALS, n = 32; A-ALS, n = 34) as well as with Criteria 2 for 76/174 patients (E-ALS, n = 26; A-ALS, n = 50). Therefore, only 38% (Criteria 1) and 44% (Criteria 2) of patients in the ALS cohort were accurately characterized to be in their respective disease stages according to both clinically-defined and imaging-derived stratification criteria.

Contrary to expectations and despite observed FC differences, neurological examination or cognitive scores were not different between patient subgroups identified using imaging-derived or clinically-defined (1 and 2) criteria. Additionally, although no FC differences were observed, patient subgroups identified using Criteria 3 differed in terms of their neurological examination and cognitive scores. While imaging-derived and clinically-defined criteria (Criteria 1) differentiated between patients experiencing early and advanced disease in terms of voluntary motor function, there were no differences in voluntary motor function in Criteria 2 and 3 subgroups. This suggests that, in the context of imaging-derived characterization, the clinically-defined stratification criteria were able to characterize patients only partially in terms of their phenotypic and biological characteristics. This provides objective evidence of a lack of biological-phenotypic correlation in ALS.

As evidenced by findings from the current study, contemporary clinical criteria for clinical drug trials inaccurately designate disease stage for more than 50% of the patient sample, further supporting a proposed need for the modification of clinical trial design to accurately widen the scope of patient enrollment (van Eijk et al. 2021). Accurate identification of disease stage would have implications for clinical management and drug trials. For example, the ATLAS clinical trial aims to identify phenoconversion in presymptomatic ALS SOD1 carriers as inferred by an increase in plasma neurofilament light chains (NfL) (Benatar et al. 2018; Benatar, Turner, and Wuu 2019); such patients are then randomized to receive active treatment (tofersen) or placebo. FC itself may also play a role as a biomarker of therapeutic efficacy. For example, in mild cognitive impairment, repetitive transcranial magnetic stimulation of the dorsolateral prefrontal cortex resulted in a significant long-term increase in FC in the frontoparietal RSN at baseline and longitudinal time points (Esposito et al. 2022). In Parkinson's disease (PD), treatment with levodopa has been shown to improve the functioning of the default mode network (Spetsieris et al. 2015). Future research is required to further examine the potential of FC in patient selection and stratification, and as a biomarker of efficacy in clinical trials.

2.5.4. Implications of the methodology of the current study in comparison with contemporary practice

To our best knowledge, this is the first neuroimaging study in ALS that utilizes two novel methods to respectively assess voxel-wise FC (TBR) and adjust for site and scanner effects (ComBat harmonization). It is therefore prudent for the authors to acknowledge the reasons for a dissonance in findings between the current and a previous CALSNIC study (Bharti et al. 2022) assessing FC in approximately similar study cohorts. Firstly, the preprocessing steps for rsfMRI data in the two studies were different. Differences in fMRI preprocessing strategies have been suggested to yield heterogeneous findings and reduce data reproducibility (B. Y. Park, Byeon, and Park 2019). Additionally, RSN maps were generated in the standard MNI space in the current study, but in the 'native' space in the previous study (Bharti et al. 2022). Secondly, FC analysis techniques employed in the two studies were different in terms of two inherent properties: sample size

requirements and assumptions of spatial and temporal orthogonality (for a review, see Schultz et al. (Schultz et al. 2014)). Thirdly, the two studies used different statistical thresholds for the identification of distinct clusters in group comparisons. The threshold used in the current study (minimum cluster size = 27 voxels) was more stringent compared to that used in the previous study. When the cluster threshold of the current study was applied to the Bharti et al. study, a consensus was achieved with regards to network-specific FC alterations in ALS compared to HCs. Notably, there are a number of factors that can contribute to heterogeneity in findings across neuroimaging studies, including differences in patient cohorts, number of ICs assessed, differences in statistical methods used to correct for site or scanner effects in multicenter studies. To our knowledge, this is the second study (following the Bharti et al. study) to have assessed all known RSNs within the human connectome. Previous studies (Agosta et al. 2013b; Chenji et al. 2016; Mohammadi et al. 2009; Tedeschi et al. 2012; Welsh, Jelsone-Swain, and Foerster 2013) have assessed a maximum of five RSNs (default mode, salience, sensorimotor, executive control, frontoparietal networks). It is also important to note that this study has used more stringent statistical threshold compared to prior studies using SBC or ICA techniques (Agosta et al. 2013b; Chenji et al. 2016; Mohammadi et al. 2009; Tedeschi et al. 2012). Given the significant variations in the approaches employed, it is a challenging direct comparison across studies – possibly resulting in their heterogeneity. However, it does speak to the importance of the appropriate selection of analysis method to the given objective, and more broadly to the need for standardization in neuroimaging acquisition and processing practices. TBR, as used this study, may be more suited to the identification of brain function in ALS at an individual level.

2.5.5.Limitations in the current study

A limitation of the current study was that patient subgrouping was restricted to elements of clinical and neuroimaging measures available in the CALSNIC dataset. Additional phenotyping based on clinical and biological features such as genotype, region/laterality of disease onset, serum or cerebrospinal fluid NfL might provide a more comprehensive understanding of the complex pathophysiology at hand.

2.6. Conclusion

In contrast to clinical measures, neuroimaging measures of resting brain function are better able to stratify patient subgroups in terms of their clinical and neuroimaging characteristics. This may serve as a biomarker for participant enrichment in clinical trials. This requires further research along with such strategies with other potential imaging and biofluid measures. Another future direction to further understand the underlying biology of the MND spectrum could be the assessment of presymptomatic ALS gene carriers and patients with a pure upper (primary lateral sclerosis) or lower (primary muscular atrophy) MN clinical presentation.

2.7. Supplementary

Group differences in voxel-wise intra- and inter-network FC across different RSNs in imaging-derived patient subgroups compared to HCs. ALS = amyotrophic lateral sclerosis, HC = healthy controls, R = right, L = left, B = bilateral.

Resting-state network	Contrast	Brain region	Brodmann area	Cluster size	Cluster coordinates (x,y,z)	T-value
Cerebellar Gray	Subgroup 2 < HC	R anterior cerebellum	-	36	18, -24, -21	4.76
		R ventral posterior cingulate cortex	BA 23	27	12, -48, 30	4.08
Dorsal attention	Subgroup 1 < HC	L lingual gyrus	BA 18	72	-3, -75, -9	4.23
Frontal	Subgroup 1 < HC	R anterior cerebellum	-	91	33, -45, -36	4.50
	Subgroup 2 > HC	L frontal eye fields	BA 8	40	-3, 36, 48	4.57
	Subgroup 2 < HC	R ventral anterior cingulate cortex	BA 24	61	0, -12, 39	4.67

Left control	Subgroup 1 > HC	R anterior prefrontal cortex	BA 10	29	21, 60, -9	4.06
		R fusiform gyrus	BA 37	29	51, -66, -3	3.81
	Subgroup 2 > HC	R anterior prefrontal cortex	BA 10	39	6, 63, 9	3.98
		L visual association cortex	BA 19	29	-24, -87, 15	3.77
Motor	Subgroup 1 < HC	B secondary visual cortex	BA 18	54	-9, -81, -9	4.23
		R visual association cortex	BA 19	35	42, -72, -9	3.83
	Subgroup 2 > HC	R dorsal posterior cingulate cortex	BA 31	66	0, -33, 48	4.52
	Subgroup 2 < HC	B visual association cortex	BA 19	580	21, -54, -9	4.51
Primary Visual	Subgroup 1 > HC	L angular gyrus	BA 39	98	-57, -63, 27	4.44
		R supramarginal gyrus	BA 40	52	60, -57, 36	4.26
		L putamen	-	38	-24, 3, -6	4.13
	Subgroup 1 < HC	L primary motor cortex	BA 4	114	-48, -15, 42	4.64
		R precentral gyrus	BA 6	38	57, -3, 21	4.50
		L paracentral lobule	BA 5	40	-3, -42, 69	4.25
		L posterior cerebellum	-	49	-12, -63, -51	4.16
	Subgroup 2 > HC	L anterior prefrontal cortex	BA 10	66	-39, 54, 0	4.82
		R angular gyrus	BA 39	51	57, -51, 45	4.15
	Subgroup 2 < HC	R primary sensory cortex	BA 1	216	3, -42, 63	5.50
		R precentral gyrus	BA 4	110	42, -15, 51	4.63
Right Control	Subgroup 1 > HC	L dorsal posterior cingulate cortex	BA 31	119	-12, -48, 39	4.75
		R fusiform gyrus	BA 37	59	51, -72, -6	4.31

	Subgroup 2 > HC	L anterior prefrontal cortex	BA 10	39	-3, 57, -6	4.12
		L secondary visual cortex	BA 18	39	-27, -90, 0	3.73
	Subgroup 2 < HC	L frontal eye fields	BA 8	28	-3, 39, 42	4.42
		R thalamus	-	39	3, 0, 6	4.05
		L supramarginal gyrus	BA 40	46	-60, -39, 27	3.56
Salience	Subgroup 1 < HC	R anterior cerebellum	-	99	6, -60, -27	4.33
	Subgroup 2 < HC	L frontal eye fields	BA 8	40	-3, 15, 48	4.02
Subcortical	Subgroup 1 < HC	R posterior cerebellum	-	86	18, -84, -36	4.82
	Subgroup 2 > HC	L insula	BA 13	57	-42, 6, 0	4.40
		L anterior cerebellum	-	50	-3, -54, -12	4.16
	Subgroup 2 < HC	L fusiform gyrus	BA 37	40	-54, -63, -12	4.22
		R dorsal dorsolateral prefrontal cortex	BA 9	45	15, 51, 42	4.12
Temporal Language	Subgroup 1 > HC	R angular gyrus	BA 21	27	30, -75, 21	3.96
	Subgroup 1 < HC	L premotor + supplementary motor area	BA 6	38	-6, 12, 66	3.81
	Subgroup 2 > HC	R medial temporal gyrus	BA 21	99	57, -36, 3	4.18
	Subgroup 2 < HC	L anterior cerebellum	-	52	-18, -45, -27	4.70
		R dorsal dorsolateral prefrontal cortex	BA 9	28	39, 36, 33	3.89

Chapter 3: Clinically-defined subgrouping criteria are able to identify motor encoding impairments in amyotrophic lateral sclerosis

Avyarthana Dey[1], Tobias Robert Baumeister[2], Michael Benatar[3], Shana Rae Black[4], Hannah Briemberg[5], Annie Dionne[6], Karleyton Evans[7], Richard Frayne[8], Angela Genge[2], Simon Graham[9], Vincent Koppelmans[4], Lawrence Korngut[8], Collin Luk[1], Donald McLaren[7], Peter Seres[10], Robert Cary Welsh[4], Lorne Zinman[9], Sanjay Kalra[1]

Author affiliations:

1. Division of Neurology, Faculty of Medicine and Dentistry, University of Alberta, Edmonton AB, Canada
2. The Neuro, Montreal Neurological Institute and Hospital, McGill University, Montreal QC, Canada
3. Department of Neurology, University of Miami, Miami, Florida, United States
4. University of Utah, Salt Lake City UT, United States
5. Division of Neurology, Department of Medicine, University of British Columbia, Vancouver, British Columbia, Canada
6. CHU de Québec, Université Laval, Québec City QC, Canada
7. Biogen Pharmaceuticals, Cambridge MA, United States
8. Hotchkiss Brain Institute, University of Calgary, Calgary AB, Canada
9. Sunnybrook Research Institute, University of Toronto, Toronto ON, Canada
10. Department of Biomedical Engineering, University of Alberta, Edmonton AB, Canada

3.1. Abstract

3.1.1.Introduction

Amyotrophic lateral sclerosis (ALS) is a neurodegenerative disorder that affects the ability of patients to perform activities of daily living. Therapeutics for the treatment of ALS are commonly prescribed to patients early in their disease course, identified based on a combination of clinical features in contemporary clinical trials. While such trials have shown moderate improvements in clinical function in patients meeting these stratification criteria, there is a lack of understanding of the pharmacodynamic effects of these drugs on their cerebral function. Additionally, objective disease monitoring in only a subpopulation of patients is counterintuitive towards an understanding of the biological mechanisms associated with clinically-defined disease severity. This study sought to identify if the pattern of evolution of cerebral network function is distinct in patients stratified using clinically-defined criteria.

3.1.2.Methods

One hundred and seventy-four ALS patients and 165 healthy controls (HCs) participated in the prospective, longitudinal, multicentre CALSNIC study. Each of these participants underwent a resting-state functional MRI (rs-fMRI) and was assigned to a patient subgroup based on a characterization of their disease features using clinically-defined stratification criteria. A template-based rotation analysis method was utilized to obtain maps of functional connectivity (FC) from the rs-fMRI data. The longitudinal ComBat harmonization pipeline was utilized to remove variance effects of multicenter data. A sandwich estimator model was used to identify longitudinal alterations in FC in ALS patients and subgroups. Clinical criteria 1 and 2 (based on clinical trial criteria) subgrouped patients into early (E-ALS) and advanced (A-ALS) disease, and Criteria 3 subgrouped patients based on their disease progression rate into slow (SP-ALS) and fast (FP-ALS) progressors.

3.1.3.Results

In ALS compared to HCs, FCs of the motor, cerebellar gray, and temporal language networks were observed to be altered longitudinally. E-ALS patients (Criteria 1) demonstrated reduced FC of the cerebellar gray network and the precentral gyrus and increased FC of the motor network and the visual association area. In A-ALS patients (Criteria 1), the FC of the frontal network was reduced with the middle temporal gyrus and FC of the salience network was reduced with the caudate. E-ALS patients (Criteria 1) had increases in FC of the left control network and the agranular retrolimbic cortex and reductions in FC of the temporal language network and the visual association cortex when compared to A-ALS patients. In E-ALS patients (Criteria 2), FC was increased between the motor network and the visual association area. In A-ALS patients (Criteria 2), FC of the motor network was reduced with the sensory association area and FC of the temporal language network was increased with the posterior cerebellum. E-ALS patients (Criteria 2) had increased FC of the motor network and the left visual association cortex and reduced FC of the motor network and the sensory association cortex when compared to A-ALS patients. In SP-ALS, FC of the dorsal attention network was reduced with the primary visual cortex, FC of the frontal network was reduced with the angular gyrus, FC of the salience network was reduced with the caudate, and FC of the cerebellar gray network was reduced with the visuomotor area, premotor/supplementary motor area (premotor/SMA), and the ventral posterior cingulate cortex. In FP-ALS, FC of the left control network and premotor/SMA was reduced, FC of the motor network and secondary visual cortex was increased, and FC of the subcortical network and the posterior cerebellum was increased. No differences in voxel-wise longitudinal FC were observed between SP-ALS and FP-ALS patients (Criteria 3).

3.1.4.Discussion

Progressive alterations in FC of motor and extra-motor brain regions were observed in patients experiencing both early and advanced disease. FC of brain regions subserving motor encoding were observed to be altered throughout the disease course. Specifically, FC impairments were

observed in brain regions subserving motor imagery in early disease and those subserving action observation in advanced disease.

3.2. Introduction

Amyotrophic lateral sclerosis (ALS) is a neurodegenerative disorder which affects motor neurons in the brain and spinal cord, typically presenting with an inability to perform activities of daily living such as walking, eating, dressing, and ultimately respiration. Such inability could be a consequence of the impairment of upper motor neurons (MNs) in the brain and lower MNs in the brainstem and spinal cord. The recognition of cognitive, behavioural, sensory, emotional, and visual impairments, in addition to motor impairments, within the clinical syndrome of ALS (R. Chipika et al. 2022; R. H. Chipika et al. 2022a; Strong et al. 2017) suggests a multisystem involvement of the disease and the occurrence of dysfunction in the network of neuronal populations that subserve these functions. The focality (or conversely, generalizability) of neuronal degeneration, and the relatively distinct progression patterns in individual neuronal pools, could contribute to the uniqueness of disease phenotype at the level of an individual patient. It is important to recognize the core unifying disease features across different ALS phenotypes towards achieving a confirmed diagnosis. Early detection of these features could help provide recommendations for disease management, including the development of general and individualized therapeutics for the improvement of patient outcomes such as slowing disease progression and extending patient survival (Genge and Chio 2023).

Disease staging systems (Chiò et al. 2013; Roche et al. 2012) in ALS characterize early disease based on observed clinical features and have been employed in neuroimaging studies to identify the correlates of disease stage-relevant structural and functional alterations in neuronal populations (Consonni et al. 2020; Floeter et al. 2018; S. Liu et al. 2021). However, these staging systems are based on the assumption that disease progression occurs by the incidence of disability in additional body regions (Roche et al. 2012) or functional domains (Chiò et al. 2013), thus overlooking the

accrual of disability in the already impaired body regions or functional domains. In continuation with this idea, disease can appear to be advanced in patients presenting at initial assessment based on the number of affected body regions/functional domains.

The limitations of these disease staging systems suggest the use of alternative methods to characterize early disease. Patient clinical features have also been used in landmark clinical drug trials (Abe et al. 2017; Sanofi-Aventis 2010) to define inclusion criteria that would allow for the study of drug effects and track disease outcomes. Two drugs – Riluzole and Edaravone – approved for the treatment of ALS in Canada have used such inclusion criteria for patient stratification. Administration of these drugs has been reported to extend patient survival and reduce oxidative stress. However, disease monitoring in ALS clinical trials is achieved using measures that are more sensitive to lower MN function. This can limit the understanding of disease mechanisms and drug effects at the level of upper MNs. A direct measurement of pathology and drug effects at a single neuron might be ideal in understanding the core cellular mechanisms of disease and effectiveness of therapeutics. However, in contrast to lower MNs, direct assessment of upper MNs is technologically more challenging to accomplish in a clinical setting. Additionally, due to the multisystem nature of ALS, it might be more beneficial to assess the functional properties of a network of specialized neurons.

Maximum drug effectiveness has been shown to be achieved in patients receiving therapeutic intervention in early disease identified by clinically-defined stratification criteria (T. Fang et al. 2018). Therefore, eligibility criteria for patient enrollment in drug trials are poised to identify treatment responders early, suggesting that the disease is different in patients not meeting enrollment criteria. However, it is possible that patients who are deemed ineligible for inclusion in these trials might respond to these treatments. Prior to the evaluation of drug effects, it is necessary to characterize cerebral networks in both sets of patients as it would provide a reference against which drug effectiveness can be tested. The study hypothesized that patterns of cerebral network function are distinct for patients subgrouped using clinically-defined stratification criteria. The

study aimed to examine longitudinal properties of cerebral networks in – a) the complete study ALS cohort and b) in patients experiencing early and advanced disease.

3.3. Methods

3.3.1.Study description

The study used data from multiple university centers across Canada and the United States constituting the Canadian ALS Neuroimaging Consortium (CALSNIC). The participating centers were in Edmonton (University of Alberta), Calgary (University of Calgary), Montreal (McGill University), Toronto (University of Toronto), Vancouver (University of British Columbia), Quebec City (Universite Laval) and Miami (University of Miami). The study was approved by the respective research ethics review boards at all participating centers.

3.3.2.Participants

The current study included 174 clinically diagnosed ALS patients and 165 healthy controls (HCs) recruited at baseline as part of CALSNIC by October 2022. All patients met diagnostic criteria for clinically possible, probable lab-supported, probable, or definite ALS according to the revised El Escorial criteria (Brooks et al. 2000). Participants were included if they had completed at least one study visit. Patients were not included in the study if they had a disease duration of more than five years at baseline, did not complete rs-fMRI scans, or presented with co-morbid frontotemporal dementia (FTD) or other neurological conditions. HCs were excluded from the study if they had previously received a diagnosis of any neurological or psychiatric conditions. See table 1 for details on demographics and clinical characteristics of our sample.

3.3.3.Magnetic resonance imaging

3.3.3.1. Scanner information

All imaging data in this study was acquired on MRI scanners with a field strength of 3T. In CALSNIC 1, Siemens systems were used in Edmonton (Prisma) and Montreal (Tim Trio), General Electric (Discovery MR 750) systems were used in Calgary and Toronto, and a Philips (Intera) system was used in Vancouver. In CALSNIC 2, Siemens (Prisma) systems were used in Edmonton, Montreal, and Toronto, a Siemens (Tim Trio) system was used in Miami, a General Electric (Discovery MR 750) system was used in Calgary, and a Philips (Achieva TX) system was used in Quebec City.

3.3.3.2. Magnetic resonance imaging protocol

A multicenter harmonized scanning protocol was employed to acquire T1-weighted (T1w) anatomical MRI and rs-fMRI from all participants in this study across all study visits. Participants were instructed to lie still with their eyes closed and to not think of anything in particular for the duration of the rs-fMRI scan. A brief description of the protocol for the Siemens (Prisma) scanner in both studies is provided in the following sections. A description of the complete protocol for other scanners can be found in our CALSNIC overview paper (Kalra, Khan, et al. 2020).

CALSNIC 1

A magnetization-prepared rapid gradient-echo imaging (MPRAGE sequence; Repetition time, TR= 2300 ms; Echo time, TE= 3.43 ms; Inversion time, TI= 900 ms; flip angle= 9°; FOV= 256 mm x 256 mm) was used to acquire T1w data with an isotropic resolution of 1 × 1 × 1 mm3. Whole-brain 3D T2*-weighted rs-fMRI data was acquired using an echo-planar imaging (EPI) pulse sequence with an isotropic voxel resolution of 3.5 × 3.5 × 3.5 mm3 and the following

specifications: TR = 2,200 ms; TE = 30 ms; field of view = 224 × 224 × 64 matrix; 40 slices, 192 trains; acquisition time = ~7 minutes.

CALSNIC 2

A magnetization-prepared rapid gradient-echo imaging (MPRAGE sequence; TR= 1700 ms; TE= 2.21 ms; TI= 880 ms; flip angle= 10°; FOV= 232 mm x 256 mm) was used to acquire T1w data with an isotropic resolution of 1 × 1 × 1 mm3. Whole-brain 3D T2*-weighted rs-fMRI data was acquired using an echo-planar imaging (EPI) pulse sequence with an isotropic voxel resolution of 3.5 × 3.5 × 3.5 mm3 and the following specifications: TR = 2,200 ms; TE = 30 ms; field of view = 224 × 224 × 64 matrix; 40 slices, 250 trains; acquisition time = 9 minutes 10 seconds.

3.3.3.3. Magnetic resonance image processing

3.3.3.3.1. T1-weighted MRI

T1w images across visits for participants completing more than one study visit were realigned and coregistered to each other to ensure voxel-matching using the available routines in the Statistical Parametric Mapping (SPM) software (version 12). Following realignment and coregistration, the "AverageImages" module within the Advanced Normalization Tools (ANTs) software was used across the T1w images on an individual level to generate an average T1w image in the native space of each participant. This average T1w image was used in the coregistration step of the rs-fMRI processing pipeline.

3.3.3.3.2. Resting-state fMRI

The rs-fMRI images were preprocessed using the longitudinal processing pipeline of the functional connectivity toolbox (CONN) based on SPM. The first four volumes were removed for every

participant to allow for steady state magnetization. The time series data for each participant were corrected for differences in image slice acquisition times, followed by realignment for head motion within and across imaging sessions using a six-parameter rigid body transformation algorithm. The mean multi-slice rs-fMRI data (temporally averaged across the time series) was co-registered to the average T1w image, and the resulting transformation matrices were applied to all volumes of the rs-fMRI data for longitudinal time points. The resultant co-registered functional images underwent spatial normalization to the Montreal Neurological Institute (MNI) template (Collins et al. 1992) space and smoothing with a Gaussian smoothing kernel of 8 mm full width at half-maximum.

3.3.3.3.3. Resting-state functional MRI analysis: Template Based Rotation

This technique of estimation of resting-state network (RSN) components (or, template maps) at the individual level utilizes the application of an *a priori*, out-of-sample network template for individual RSNs. This technique predicts RSN template maps, at an individual participant level, as a linear combination of time courses that correspond to spatial patterns in a reference template set, thereby removing the spatial and temporal orthogonality assumptions of distributed functional networks (at a group level). Refer to (Schultz et al. 2014) for a complete overview of this technique. RSN maps for each participant were generated for every longitudinal time point using the TBR code (Schultz et al. 2014). Ten target components (cerebellar gray, default mode, dorsal attention, frontal, left and right control, motor, precuneus, subcortical, and temporal language networks) were estimated for each participant by the TBR technique and were preselected based on correspondence to gray matter functional connectivity (FC) or disease relevance. The gray matter TBR components were identified as RSNs-of-interest in the current study. Individual subject resting-state functional connectivity (rsFC) maps underwent transformation from correlation (r)-maps to Fisher (z)-maps to allow for variance normalization. These z-maps were used in further statistical analyses.

3.3.4.Statistical analysis

3.3.4.1. Longitudinal ComBat Harmonization: Removing *study x scanner* interaction effects from voxel-wise FC

ComBat is a tool based on an Empirical Bayesian algorithm and is used to eliminate unwanted technical variability from biological data (Fortin et al. 2017). This technical variability can arise because of differences in scanner hardware, software, or imaging acquisition protocols (Fortin et al. 2017). ComBat can help dissect and remove this technical variability from biological variability by correcting for the additive and multiplicative scanner effects as well as small sample sizes at an individual scanner. This can help combine datasets with different acquisition protocols employed to acquire images with different scanner hardware and software specifications. In the CALSNIC studies, technical variability can occur only due to the additive and multiplicative effects from scanner hardware and software. There is no technical variability contributed by imaging acquisition protocols as these parameters were harmonized across scanners and across both CALSNIC studies. In the current study, the longitudinal ComBat harmonization method was applied using the 'longCombat' package on R statistical software (https://www.r-project.org/) to estimate and correct for additive and multiplicative scanner effects on RSN functional connectivity as well as to account for subject-specific effects (e.g., age, subject consistency) inherent to longitudinal studies (Beer et al. 2020). 3D functional connectivity maps across visits and across participants were combined using the 'fslmerge' routine on FSL to generate a 4D image. This was performed for individual RSNs. Of the 11 RSN components, 10 successfully underwent longitudinal harmonization. The motor RSN component was not subjected to the longitudinal combat harmonization pipeline as the data had a singular fit indicating that the model was optimally fit to the demographic variables, and performing harmonization by forcing the model would result in overfitting.

3.3.4.2. Group differences in resting-state functional connectivity

A sandwich estimator model (SwE, http://www.nisox.org/Software/SwE/) was used to assess differences in rsFC. Differences in rsFC were assessed between the HCs and the entire ALS group, as well as individual ALS subtypes (defined in the next section). A non-parametric restricted wild bootstrapping approach (number of bootstraps = 5000) was employed for small sample adjustments (type C2). In addition, an SwE implementation of the threshold free cluster enhancement technique (Smith and Nichols 2009) (TFCE) was employed to identify clusters that showed significantly different rsFC between ALS patients and HCs, as well as between different ALS subtypes. An explicit gray matter mask in the MNI space was applied to restrict all analyses of rsFC to gray matter voxels within the brain. Statistical significance for all group comparisons using SwE models was set at a family-wise error (FWE) corrected p-value less than 0.05.

3.3.5.Subgrouping

Patients in the current study were subgrouped into early and advanced disease stages based on criteria defined on measures recorded during routine clinical examinations. The clinical criteria used to stratify patients into early and advanced disease were extrapolated from the clinical drug trial criteria of Health Canada approved treatments for ALS (Abe et al. 2017; Sanofi-Aventis 2010) and included measures of forced vital lung capacity (%), duration from first symptom onset, and total score on the revised ALS functional rating scale (ALSFRSr) questionnaire. Another criteria was defined based on the median disease progression rate of the patient sample. The disease progression rate or rate of functional decline for an individual patient was calculated from the ALSFRSr using the formula: *Disease progression rate = (48 – ALSFRSr at baseline)/symptom duration in months*. The median disease progression rate of the ALS sample in the study was 0.44. For details see Chapter 2.

3.3.6. Identification of cerebral functional patterns across clinical subgroups

Longitudinal changes in RSN functional connectivity were assessed in patient subgroups identified at the baseline assessment using these subgrouping criteria. A SwE statistical model (as outlined in section 3.3.5.2.) was used to identify longitudinal patterns of disease stage-based network pathology by comparing RSN connectivities between HCs and individual patient subgroups. Analyses of RSN FC alterations between patient subgroups were also performed. Statistical significance was set at TFCE FWE-corrected p-value of less than 0.05.

3.4. Results

3.4.1. Demographic and clinical characteristics of the study sample

Participants included in the study were not matched for age and sex at the first study visit. The second follow-up visit (V2) had a drop out rate of 53.5% for patients (retained n = 81) and 39.4% for HCs (retained n = 100). The third follow-up visit (V3) had a drop out rate of 38.3% for patients (retained n = 50) and 23% for HCs (retained n = 77). One hundred and seventeen participants (nALS = 45, nHC = 72) completed rsfMRI scans for all three longitudinal visits. See table 1 for the baseline characteristics of the study population.

Table 1. Baseline demographic and clinical characteristics of the study population. Single asterisk (*) denotes $p < 0.05$ and double asterisk (**) denotes $p < 0.001$.

Characteristic	HC	ALS	Sig.
Number of participants	165	174	-
Age (years)	55.4 (10.1)	59.9 (10.5)	**
Sex: M/F	74/91	108/66	*

Education level (years)	16.5 (3.0)	15.2 (3.5)	**
Symptom duration (years)	-	1.7 (1.1)	-
Functional status (ALSFRS-R total)	-	37.9 (6.2)	-
Disease progression rate	-	0.7 (0.6)	-
Forced vital capacity (%)	-	89.0 (19.8)	-
Left UMN exam score	-	2.5 (1.5)	-
Right UMN exam score	-	2.4 (1.6)	-
Left LMN exam score	-	2.4 (1.2)	-
Right LMN exam score	-	2.5 (1.3)	-
Left finger tapping score	53 (13)	38 (16)	**
Right finger tapping score	59 (14)	43 (17)	**
Left foot tapping score	40 (10)	23 (15)	**
Right foot tapping score	43 (10)	25 (15)	**
ECAS total (/136)	114 (8)	103 (21)	**

3.4.2.ALS vs HC

FC of the motor network is observed to be progressively increased with the premotor and supplementary motor areas (premotor/SMA), anterior cerebellum, visual association and Broca's areas and reduced with the posterior cerebellum, FC of the temporal language network is observed to be reduced with the secondary visual cortex, and FC of the cerebellar gray network is reduced with the visuomotor area and the premotor/SMA (table 2, figure 1).

Table 2. Voxel-wise alterations in longitudinal FC between ALS and HC. RSN = resting-state network, MNI = Montreal Neurological Institute, ALS = amyotrophic lateral sclerosis, HC = healthy controls, BA = Brodmann area, R = right, L = left, B = bilateral

RSN	Contrast	Brain region	Cluster size	MNI coordinates			Z-value
				x	y	z	
Motor	ALS > HC	L premotor + supplementary motor areas (BA 6)	173	-54	3	27	3.97
		B anterior cerebellum	10	6	-42	-18	3.49
		L visual association area (BA 19)	11	-21	-45	-6	3.34
		L pars opercularis (Broca's area; BA 44)	6	-36	15	18	3.14
	ALS < HC	R posterior cerebellum	2	30	-66	-30	4.25
Temporal Language	ALS < HC	L secondary visual cortex (BA 18)	12	-24	-90	9	4.13
Cerebellar Gray	ALS < HC	L visuomotor area (BA 7)	76	-12	-54	57	4.43
		R premotor + supplementary motor areas (BA 6)	79	45	-6	27	4.27

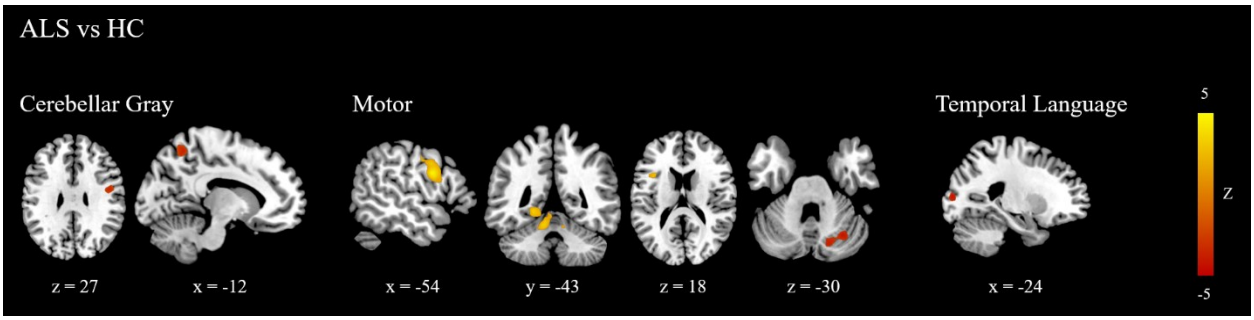

Figure 1. Voxel-wise differences in longitudinal FC between ALS and HCs.

3.4.3.Group comparisons of longitudinal FC across clinical subgroups

3.4.3.1. Criteria 1 patient subgroups

The left control network has increased FC with the agranular retro limbic cortex and the temporal language network has reduced FC with the visual association cortex in E-ALS compared to A-ALS (table 3, figure 2).

3.4.3.2. Criteria 2 patient subgroups

The motor network has increased FC with the left visual association cortex and reduced FC with the sensory association cortex in E-ALS compared to A-ALS (table 3, figure 2).

3.4.3.3. Criteria 3 patient subgroups

No differences in voxel-wise longitudinal FC were observed.

Table 3. Voxel-wise alterations in longitudinal FC between E-ALS and A-ALS. RSN = resting-state network, MNI = Montreal Neurological Institute, ALS = amyotrophic lateral sclerosis, HC = healthy controls, BA = Brodmann area, R = right, L = left

RSN	Contrast	Brain region	Cluster size	MNI coordinates			Z-value
				x	y	z	
Criteria 1							
Left Control	E-ALS > A-ALS	R agranular retrolimbic cortex (BA 30)	5	3	-42	9	3.82
Temporal Language	E-ALS < A-ALS	R visual association area (BA 19)	27	51	-63	15	3.41
Criteria 2							
Motor	E-ALS > A-ALS	L visual association area (BA 19)	4	-33	-93	21	4.55
	E-ALS < A-ALS	R sensory association area (BA 5)	21	12	-33	54	3.68
Criteria 3							
No suprathreshold clusters							

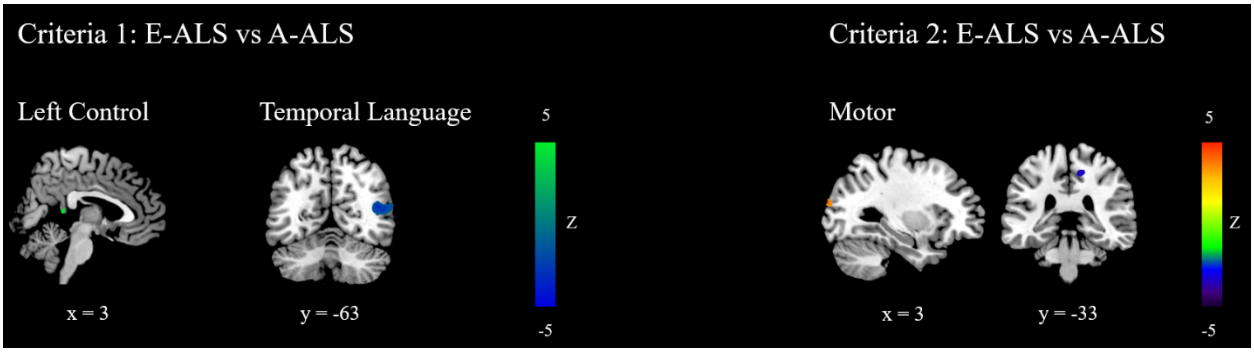

Figure 2. Voxel-wise differences in longitudinal FC between E-ALS and A-ALS.

3.4.4.Identification of longitudinal cerebral FC patterns of clinical subgroups

3.4.4.1. Criteria 1 patient subgroups vs HC

Longitudinal FC of the cerebellar gray network is reduced with the precentral gyrus and that of the motor network is increased with the visual association area in E-ALS when compared to HCs. Longitudinal FC of the frontal network is reduced with the middle temporal gyrus and that of the salience network is reduced with the caudate in A-ALS when compared to HCs (Table 4, Figure 3).

3.4.4.2. Criteria 2 patient subgroups vs HC

Longitudinal FC of the temporal language network is increased with the posterior cerebellum in A-ALS compared to HCs (Table 4, Figure 3).

3.4.4.3. Criteria 3 patient subgroups vs HC

In SP-ALS, longitudinal FC was reduced between the dorsal attention network and the primary visual cortex, the frontal network and the angular gyrus, the salience network and the caudate, and the cerebellar gray network and the visuomotor area, premotor/SMA, and the ventral posterior cingulate cortex when compared to HCs. In FP-ALS, longitudinal FC was reduced between the left control network and the premotor/SMA and increased between the motor network and secondary visual cortex as well as between the subcortical network and the posterior cerebellum when compared to HCs (Table 4, Figure 3).

Table 4. Voxel-wise alterations in longitudinal FC between ALS subgroups (E-ALS and A-ALS) and HCs. RSN = resting-state network, MNI = Montreal Neurological Institute, ALS = amyotrophic lateral sclerosis, HC = healthy controls, BA = Brodmann area, R = right, L = left, B = bilateral

Brain network	Contrast	Brain region	Brodmann area	Cluster size	MNI coordinates			Z
					x	y	z	
Criteria 1								
Cerebellar Gray	E-ALS < HC	R precentral gyrus	BA 4	4	36	-18	54	3.62
Frontal	A-ALS < HC	R middle temporal gyrus	BA 39	10	36	-72	18	3.54
Motor	E-ALS > HC	L visual association area	BA 19	112	-21	-48	-6	4.01
Salience	A-ALS < HC	R caudate	-	7	9	0	18	3.15
Criteria 2								
Temporal Language	A-ALS > HC	R posterior cerebellum	-	11	24	-66	-27	3.85
Criteria 3								
Cerebellar Gray	SP-ALS < HC	L visuomotor area	BA 7	450	-12	-57	54	3.99

		R premotor + supplementary motor areas	BA 6	16	45	-12	27	3.30
		R ventral posterior cingulate cortex	BA 23	8	12	-45	33	2.93
Dorsal Attention	SP-ALS < HC	L primary visual cortex	BA 17	66	-3	-87	9	3.50
Frontal	SP-ALS < HC	R angular gyrus	BA 39	79	36	-81	27	3.64
Left Control	FP-ALS < HC	R premotor + supplementary motor areas	BA 6	11	33	-12	33	3.92
		R caudate	-	1	21	-9	30	3.44
Motor	FP-ALS > HC	B secondary visual cortex	BA 18	174	3	-90	21	3.73
Salience	SP-ALS < HC	R caudate	-	33	15	-3	24	3.63
Subcortical	FP-ALS > HC	L posterior cerebellum	-	94	-9	-75	-24	4.01

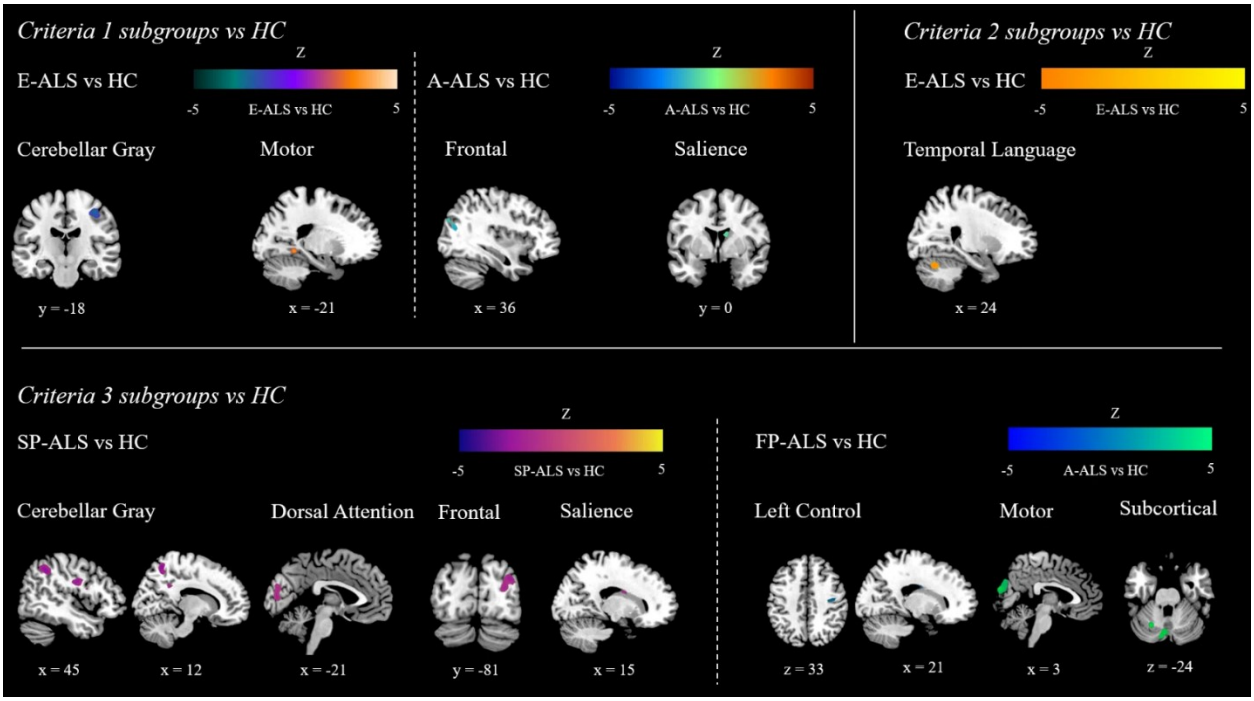

Figure 3. Voxel-wise differences in longitudinal FC between ALS subgroups (E-ALS and A-ALS) and HCs.

3.5. Discussion

The aim of the current study was to examine longitudinal alterations in resting-state FC in ALS patients and subgroups defined using clinically-defined stratification criteria. The main study findings included longitudinal FC alterations in both motor and extra-motor networks across the complete ALS cohort, and the abilities of criteria 1 and 2 (extrapolated from enrollment criteria for drugs Riluzole and Edaravone) but not criteria 3 (defined based on the median disease progression rate of the study cohort) to define patient subgroups with distinct longitudinal patterns of FC alterations in extra-motor and motor networks respectively. Longitudinal assessment of network properties in ALS suggests an impairment in the functioning of neuronal systems that underlie the encoding of voluntary motor function.

3.5.1. Impairment of brain networks underlying motor encoding

Motor encoding refers to the planning of an executable sequence of voluntary motor movements in response to internal stimuli. The network of regions participating in the processes (imagery, planning, and execution) underlying motor encoding are sequentially linked. Motor *imagery* entails the imagination, but not actual execution, of movement based on internalized recall of previously learned motor tasks from long-term to working memory (Munzert and Zentgraf 2009), motor *planning* entails the determination of the precise sequence of appropriate motor responses, and motor *execution* occurs by encoding the speed, direction, extent, and force of execution of the planned motor response. Planning of motor function by the premotor/SMA depends on cortical (prefrontal and parietal cortices) and subcortical (basal ganglia and posterior cerebellar) inputs (Henschke and Pakan 2023). The cortical-premotor/SMA circuits influence goal-directed motor

activity and the subcortical-premotor/SMA circuits provide continuous adaptive feedback to the primary motor cortex (PMC) for the generation of precise movements (Henschke and Pakan 2023).

Hypothesis-driven paradigm-based studies (Malek Abidi et al. 2021, 2022; Fiori et al. 2013; Hosni et al. 2019; Jelsone-Swain et al. 2015; Y. H. Liu, Huang, and Huang 2017; Lulé et al. 2007; Stanton et al. 2007) in ALS have assessed motor planning in goal-directed activity, primarily probing the cortical circuits that encode motor imagery. In the current study, without the need to plan an anticipated motor function (i.e., at rest), ALS patients experiencing early disease (as per Criteria 1) exhibit FC alterations in brain regions constituting the motor imagery network whereas patients experiencing advanced disease exhibit FC alterations in brain regions constituting the action observation network (Jelsone-Swain et al. 2015) – a network that functions in parallel to the motor imagery network and processes information from the external environment (for example, in visualizing motor tasks performed by someone else) to prepare for the execution of motor function. Brain regions involved in the processing of external (visuospatial) stimuli are reported to be affected in ALS (R. H. Chipika et al. 2022a) and demonstrate longitudinal FC alterations with cortical motor regions in the current study. This suggests that motor task internalization is impaired earlier on in the disease process and undergoes deterioration as the disease evolves. The premotor/SMA and the inferior parietal lobule, brain regions that constitute common anatomical links between action observation and motor imagery networks (Jelsone-Swain et al. 2015), were observed to have altered longitudinal FC in the current study. This is suggestive of their role in task switching during motor encoding and of a potential explanation that altered FC of these cortical regions might be associated with progressive motor execution impairments in ALS. As disease progresses, clinical motor ability worsens due to accumulation of pathological features and the action observation network – a component of the mirror neuron system – starts to become dysfunctional. Impairment of the mirror neuron system has been previously suggested in ALS (Eisen et al. 2015), especially in the early stages of disease (Wittstock et al. 2011). Contrasting observations in the current study and the previous study (Wittstock et al. 2011) suggests that a dysfunction of the mirror neuron system might occur early on in the disease process but likely assumes prominence in the advanced disease stages. In addition, the two studies used different

imaging techniques (transcranial magnetic stimulation vs rs-fMRI) and measures to assess neuronal function – alluding to the relative differences in sensitivities of the imaging techniques to the identification of neuronal functional impairments.

Although a commonly used method for patient subgrouping, Criteria 3 is able to identify FC alterations in brain regions underlying only the motor imagery network in both slow and fast progressing ALS patients. In patients experiencing advanced disease (as per Criteria 2), weakened functional linkage was observed between the temporal language network and the cerebellum – therefore being unable to pinpoint the specific neural system/s affected. In sum, the study findings reveal that Criteria 1 is most sensitive to disease stage-specific FC alterations in motor circuits, a characterization which is not possible when directly comparing all ALS patients to HCs or by the use of subgrouping criteria 2 and 3.

3.5.2. Links between longitudinal impairments of motor encoding and working memory in ALS

Processing of imagined movement in working memory is key to the planning and execution of motor function. In the planning phase, the determination of a motor response depends on salient elements of the imagined movement such as their speed or kinetics and the maintenance of motor images in the working memory (Munzert and Zentgraf 2009). Paradigm-based fMRI (Kobeleva et al. 2021; Vellage et al. 2016), EEG (Hammer et al. 2011; Zaehle et al. 2013), and cortical thickness (Libon et al. 2012) assessments have revealed impairments in brain networks subserving working memory operations in ALS. In early compared to advanced disease (Criteria 1), the left control network had increased longitudinal FC with the agranular retro limbic cortex, a constituent brain region within the posterior cingulate cortex (PCC). Slow progressing ALS patients (Criteria 3) demonstrated increased longitudinal FC of the ventral PCC with the cerebellar gray network when compared to HCs. The PCC is a cortical functional hub that is heavily connected to other cortical hubs and is implicated in cognition, visuospatial processing, and decision-making – functional

domains (Foster et al. 2023) that are affected in ALS (Consonni et al. 2021). The left control network constitutes, in part, the frontoparietal network system and is therefore important to mental processes that involve the utilization of working memory as well as decision-making in the context of goal-directed behaviour (Vincent et al. 2008). Clinically, the cerebellum is considered to play an integral role in the mediation of cognitive and behavioural processes, and its dysfunction has been shown in neurodegenerative conditions (for example, FTD) to be associated with impairments in the working memory, attention, visuospatial processing, and language domains (R. Chipika et al. 2022). Therefore, later on in the disease course, impairments of motor imagery are indicative of cognitive impairment that is known to occur in approximately 50% of patients presenting to a clinic with an El Escorial diagnosis of suspected ALS (Strong et al. 2017).

3.5.3. Interpreting longitudinal FC increase between the PMC and premotor/SMA

A hypothesis-driven approach in paradigm-based fMRI studies has been successful in characterizing the FC between the PMC and premotor/SMA in ALS. In the absence of pathology, activity of the healthy premotor/SMA increases during the ongoing learning of skilled movement and is reduced after the motor skill is learned (Berlot, Popp, and Diedrichsen 2020). While evidence of PMC activation during motor learning in healthy individuals is heterogeneous (Berlot, Popp, and Diedrichsen 2020), the PMC in ALS exhibits increased activity during imagined motor function (Jelsone-Swain et al. 2015; Lulé et al. 2007). In a neurodegenerative process such as ALS, increased premotor/SMA activation (Malek Abidi et al. 2021, 2022; Jelsone-Swain et al. 2015; Lulé et al. 2007) is suggestive of a compensatory response to counteract the reduced ability of the PMC to execute a learned motor task (Jelsone-Swain et al. 2015). While paradigm-based studies can successfully characterize activation profiles and effective connectivity between discrete motor regions, such characterizations are biased towards the specific study paradigm. Therefore, it is important to employ an unbiased approach towards uncovering the biological basis of these alterations. This can be achieved by studying the FC of the motor regions when not involved in the performance of an explicit task. In a baseline paradigm-free evaluation (Chapter 2) of the

cohort in the current study, the motor network (PMC) had increased intrinsic activation, reduced FC with the anterior cerebellum, and increased FC with the PCC and visuomotor areas. In another study, reduced FC between the PMC and the premotor/SMA was associated with reduced PMC concentrations of the neurochemical N-acetyl aspartate at baseline (Dey et al. 2022). Previous fMRI studies in ALS have not been successful in demonstrating FC alterations between the PMC and premotor/SMA at baseline (Zhou et al. 2013) or longitudinally (Castelnovo et al. 2020; R. A.L. Menke et al. 2018a; Trojsi et al. 2021) at rest. A previous EEG study has reported an association between structural degeneration and reduced activity in the motor areas (Nasseroleslami et al. 2019). It is postulated that, given the coherence between structural and functional connectivities, a highly connected brain region is unable to obtain high activity during a metabolically intense task and therefore delegates neural functioning to regions that are less connected (Zarei et al. 2022). The lack of physical constraints in less connected regions allows them to be highly activated, therefore compensating for the inability of the highly connected region to achieve the required activation amplitude to meet the task demands (Zarei et al. 2022). In the current study, the motor network (PMC) underwent progressive decline in functional activation (supplementary) and progressive FC increases with adjacent motor regions (premotor/SMA, Table 2). These observations in the absence of a motor encoding task suggest that additional pathological processes exist in ALS that could result in functional impairments of the motor networks even at rest. For example, progressive glutamatergic excitotoxicity (Blasco et al. 2014; Bradley R. Foerster et al. 2013; Pradhan and Bellingham 2021), which manifests in early stages of ALS as cortical hyperexcitability (Bakulin et al. 2016) and intensifies with increasing disease severity (Menon et al. 2020), might accentuate the already existing high metabolic demand on the PMC, causing it to be increasingly reliant on the premotor/SMA for the execution of motor tasks. FC impairment of the PMC might be a correlate of glutamate excitotoxicity-mediated degeneration (Van Den Bos et al. 2019) or clinically-relevant neuroanatomical deficits (Dey et al. 2022) in PMC neurons. As the premotor/SMA now assumes the functions of the PMC, in addition to intrinsic motor imagery and planning tasks, the metabolic demand on this region progressively increases. High metabolic demand is postulated to drive increased oxidative stress, and consequently increase the vulnerability of the neuronal pools (Strong and Swash 2022) to the degenerative process (Zarei et al. 2022). It is likely that processes such as the degeneration of PMC MNs and premotor/SMA

adaptation to maintain normal motor function start to occur during the long preclinical phase (Benatar et al. 2022) and before the first occurrence of symptoms of ALS. Because of diagnostic delays (Richards, Morren, and Pioro 2020), the disease is quite advanced by the time a patient participates in observational (e.g., neuroimaging) studies. Therefore, if a parallel was sought between the current study findings and a model of corticofugal axonal spread of TDP-43 proteinopathy (Braak et al. 2013) (occurring in ~90% of ALS patients), longitudinal FC alterations occurred in neuronal pools wherein TDP-43 accumulation occurred in Stages 1-3 of the axonal spread model. Keeping in mind the changes occurring in cortical motor regions during the preclinical phase, one can theorize that the accumulation of misfolded TDP-43 first occurs in PMC neurons and then in the premotor/SMA neurons – thereby helping understand disease mechanisms further by providing more granularity to the spread of disease pathology.

3.5.4. Contrasting directionality of FC alterations of the motor network at baseline and longitudinally

The PMC, anterior cerebellum, and premotor/SMA constitute important network nodes in motor processing. In a baseline evaluation of the ALS cohort in the current study (Chapter 2), the motor network had reduced FC with the anterior cerebellum, and increased FC with the PCC and visuomotor areas. Longitudinal FC increases of the PMC with the anterior cerebellum and premotor/SMA observed in the current study might suggest the occurrence of adaptive processes to counteract the baseline reduction in PMC FC and maintain network homeostasis. In the context of motor function, increased corticocerebellar FC is suggested to represent the occurrence of a compensatory reorganization to counteract the degeneration of the motor cortex (R. Chipika et al. 2022). Given the multiplicative effects of factors including but not limited to age, genetic predisposition, length of prodrome (Benatar et al. 2022), region of disease onset, disease severity, disease stage, and properties of RSNs on the pathophysiology of ALS, it might be challenging to make inferences regarding the directionality of FC alterations with disease evolution. However, pathology-dependent correlates of FC alterations in other study populations can provide some clues. For example, in a cohort of cognitively healthy individuals, an inverse association was

observed between levels of accumulated tau in the neocortex and FC of the DMN and salience RSNs (Schultz et al. 2017). In Parkinson's disease (PD), the DMN maintained normal functioning in earlier disease stages and underwent functional decline in later unmedicated stages; normal functioning of the DMN was partially restored on treatment with levodopa, indicating that the motor symptoms of PD occurred as a result of the neurochemical dysfunction of the dopaminergic mesolimbic system (Spetsieris et al. 2015). Such observations suggest that FC alteration patterns are specific to the underlying neurodegenerative process across different neurological disorders and are suggestive of functional segregation and the selective vulnerabilities of different neuronal pools to the disease process (Strong and Swash 2022).

3.5.5.Advantages of the current study

This is the first study in ALS that has utilized a number of new techniques to improve the sensitivity of resting-state fMRI in the detection of longitudinal network alterations. These techniques include the template-based rotation method to examine network properties in ALS, longitudinal ComBat harmonization to remove longitudinal effects of scanner and site, a sandwich estimator statistical model to account for missing data or participant dropouts thus allowing for the inclusion of all scans from all participants enrolled in the study, and a TFCE technique to improve the interpretability and sensitivity of the observed clusters of significant FC differences.

3.5.6.Limitations

The current study did not characterize the effects of therapeutic interventions on network FC in patients. Riluzole and Edaravone have respectively been shown to improve survival and reduce progression. However, the data on therapeutic intervention at the three visits was variable as some patients stopped taking medication due to drug side effects, and sometimes data collection across study centers was incomplete. In addition, treatment-based subgrouping within the disease stage-based patient subgroups would yield very small sample sizes. This suggests the need to conduct a

prospective study as part of a clinical drug trial that would use neuroimaging measures to assess drug effectiveness on cerebral function.

3.6. Conclusions and future directions

Deficits in neuronal processes underlying motor encoding, specifically in the motor imagery and action observation domains, occur in ALS and attain prominence with disease progression. Specifically, the study criteria 1, extrapolated from the inclusion criteria for the Riluzole study, was able to identify longitudinal FC impairments of cerebral networks subserving functioning of both motor processes in disease stage-based patient subgroups. These deficits in motor processing were interpreted based on the assumption that patients in early disease will eventually progress to an advanced disease stage based on the progressive changes in their clinical features. However, as this assumption does not account for disease features at the cerebral level, future studies could examine the properties of cerebral networks that stratify patients into early and advanced disease stages based on disease pathophysiology. This examination of cerebral network properties could also be extended in future studies to include measurements from other neuroimaging techniques such as transcranial magnetic stimulation and positron emission tomography, in addition to functional MRI.

Disease progression can be clinically defined based on two factors – the duration of symptoms and the degree of disability. In observational studies, it is challenging to independently model the effects of both factors on outcome measures. Clinical trials tend to enroll patients presenting to the clinic earlier, therefore focusing on identifying disease in patients early based on the duration from the onset of symptoms and not on their extent of disability. Patient subgrouping based on the median disease progression rate factors in both symptom duration and the extent of disability. However, as the measure of disability used in this method is more sensitive to lower MN function, it fails to characterize the complete extent of disease pathology in ALS. This is suggestive of the need to define subgrouping criteria which stratifies patients based on an upper MN-sensitive

disease measure. This could then be extended to develop a composite measure that would incorporate both upper and lower MN measures of disease pathology in ALS. This measure could be used to understand disease mechanisms and undergo evaluations regarding its potential as a primary endpoint or in the definition of drug targets in clinical trials.

3.7. Supplementary

Visit-wise functional activations of distinct resting-state networks

RSN	Visit 1			Visit 2			Visit 3		
	ALS	HC	p-value	ALS	HC	p-value	ALS	HC	p-value
Cerebellar Gray	0.26 (0.08)	0.43 (0.08)	<0.001*	0.27 (0.07)	0.39 (0.08)	<0.001*	0.27 (0.06)	0.43 (0.06)	<0.001*
DMN	0.32 (0.06)	0.23 (0.05)	<0.001*	0.26 (0.06)	0.26 (0.05)	n.s.	0.23 (0.05)	0.27 (0.05)	<0.001*
DAN	0.31 (0.05)	0.25 (0.05)	<0.001*	0.27 (0.05)	0.32 (0.05)	<0.001*	0.22 (0.05)	0.29 (0.04)	<0.001*
Frontal	0.42 (0.08)	0.50 (0.08)	<0.001*	0.49 (0.08)	0.57 (0.08)	<0.001*	0.33 (0.08)	0.51 (0.06)	<0.001*
Left Control	0.29 (0.06)	0.30 (0.05)	n.s.	0.29 (0.05)	0.28 (0.05)	n.s.	0.24 (0.05)	0.32 (0.05)	<0.001*
Motor	0.32 (0.05)	0.32 (0.05)	n.s.	0.27 (0.05)	0.32 (0.05)	<0.001*	0.23 (0.04)	0.35 (0.05)	<0.001*
Primary Visual	0.25 (0.18)	0.33 (0.05)	<0.001*	0.34 (0.07)	0.42 (0.06)	<0.001*	0.27 (0.07)	0.42 (0.06)	<0.001*
Right Control	0.25 (0.05)	0.31 (0.04)	<0.001*	0.28 (0.05)	0.27 (0.05)	n.s.	0.24 (0.04)	0.31 (0.05)	<0.001*
Salience	0.27 (0.04)	0.28 (0.04)	n.s.	0.29 (0.05)	0.29 (0.05)	n.s.	0.30 (0.04)	0.27 (0.04)	<0.001*

Subcortical	0.26 (0.05)	0.33 (0.06)	<0.001*	0.30 (0.05)	0.41 (0.05)	<0.001*	0.25 (0.05)	0.37 (0.06)	<0.001*
Temporal Language	0.39 (0.06)	0.38 (0.06)	n.s.	0.39 (0.06)	0.37 (0.06)	n.s.	0.28 (0.05)	0.38 (0.07)	<0.001*

Chapter 4: Characterization of distinct patterns of disease evolution in imaging-derived subgroups of amyotrophic lateral sclerosis

4.1. Abstract

4.1.1. Introduction

ALS is a neurodegenerative disorder with a unique complex clinical presentation across patients. This makes it challenging to identify the exact neuronal populations that are affected by the underlying pathophysiological disease mechanisms. Data-driven methods that utilize measures of brain structure and function have previously been successful in the identification of patient subgroups with distinct patterns of disease. However, owing to the differences in clustering algorithms and neuroimaging features used, there is no consensus in observations across studies. In addition, there is no clear understanding from these studies – conducted at baseline – of the patterns of disease evolution in the respective patient subgroups. Therefore, this study

hypothesized that disease evolution patterns were distinct in imaging-derived patient subgroups, and that the observed patterns were similar to those estimated at baseline.

4.1.2.Methods

174 ALS patients and 165 healthy controls (HCs) participated in the prospective, longitudinal, multicentre CALSNIC study. Each of these participants underwent a resting-state functional MRI (rs-fMRI) and was assigned to a patient subgroup based on a characterization of their disease features using clinically stratification criteria. A template-based rotation analysis method was utilized to obtain maps of functional connectivity (FC) from the rs-fMRI data. The longitudinal ComBat harmonization pipeline was utilized to remove variance effects of multicenter data. Measures of functional activations of discrete resting-state networks were utilized as inputs in a hierarchical clustering algorithm to identify imaging-derived patient subgroups. Clinical and network function measures were assessed across longitudinal time points to identify the patterns of disease evolution within each subgroup.

4.1.3.Results

Two patient subgroups (Subgroup 1 – S1, Subgroup 2 – S2) were identified based on their baseline measures of resting-state network function. In terms of clinical function, right foot tapping scores were higher in S2 compared to S1 patients at visit 1 and ECAS total scores were higher in S1 compared to S2 patients at visit 3 ($p < 0.05$). For S1 patients and S2 patients, there was a decline in bilateral foot tapping scores from visit 1 to 3 ($p < 0.05$). S1 patients also experienced a significant increase in bilateral upper motor neuron burden from visit 1 to 3 ($p < 0.05$). No alterations in upper or lower motor neuron burden scores were observed in S2 patients. In terms of functional activation of resting-state cerebral networks, a general reduction was observed in S1 patients, and a general increase was observed in S2 patients at visit 1 when compared pairwise with HCs ($p < 0.001$). By visit 3, functional activations of these networks were not significantly different from HCs for S1 and showed increases for S2 ($p < 0.001$). Network functional connectivities were significantly increased for both patient subgroups as well as for HCs ($p_{FWE} < 0.05$), therefore providing non-

specific information regarding behaviour of cerebral networks in the context of a pathological process. However, the spatial extent of connectivity alterations for S2 patients were lower than S1 patients.

4.1.4.Discussion

A characterization of longitudinal alterations in clinical function, neurological examination findings, and network function were able to independently point to distinct features of the disease process in both patient subgroups. However, the discordance in findings across the various examined features were unable to resolve the lack of coherence between biological and phenotypic features of the pathophysiological disease process.

4.2. Introduction

ALS is a neurodegenerative disorder wherein motor neurons in the central nervous system are impaired as a result of pathophysiological disease processes. This results in the emergence of clinically observable symptoms such as muscle weakness, spasticity, hyperreflexia, fasciculations, and atrophy. Depending on the motor neuron populations that are affected by the disease process, the relative presentations of these symptoms can be used to localize the focal point of the disease process. However, the complex nature of manifestation of disease pathological features, a long clinical prodrome (Benatar et al. 2022), as well as a long diagnostic delay in ALS (Richards, Morren, and Pioro 2020) can pose a challenge towards pinpointing the exact motor neurons that are affected by the disease process. This, in turn, can delay the indication of therapeutics which can target the affected motor neurons.

These gaps in literature can be addressed by the use of data-driven methods to identify patterns of neuronal impairment that are common across patient populations, thereby enabling the identification of the neuronal impairment patterns that contribute to specific clinical presentations.

This can help improve the coherence between biological and phenotypic characterization of ALS patients. Thus far, in the literature, clustering algorithms have been employed to group patients into distinct phenotypic subtypes based on neuroimaging features of brain structure (Bede et al. 2022b; Tan et al. 2022) and function (Chapter 2). In addition to the lack of sufficient literature on the use of neuroimaging features in the identification of phenotypic ALS subgroups, there currently exists no consensus on the core biological features that result in the various clinical presentations of ALS. For example, the use of structural measures of whole-brain cortical thickness and white matter fractional anisotropy classified the patients into three subgroups with pure motor, frontotemporal, and cingulate-parietal-temporal disease patterns (Tan et al. 2022). Another study utilized cortical thickness, volumetric, and white matter microstructural measures from 15 preselected brain regions and was able to identify two patient clusters, the larger of which had a frontotemporal disease pattern and the smaller cluster had a diffuse extra-motor disease pattern (Bede et al. 2022a). In Chapter 2, intrinsic activation values of discrete resting-state networks subgrouped the patients into early and advanced pathophysiological disease clusters which were in accordance with their corresponding clinical characteristics of disease severity. While existing disease staging systems classify patients based on the observable clinical features, they have been unsuccessful in characterizing distinct pathophysiological features of their disease processes. Despite the heterogeneity in patient classification, the recency of implementation of, and the differences in goals/hypotheses in each of these data-driven methods of patient classification, such approaches might be successful in segregating the contributions of the functional and neuroanatomical features to the disease process. Such methods might also be able to predict the patterns of disease evolution in patient subgroups at baseline, an assessment that is currently lacking in the literature.

In the current study, previously identified imaging-derived patient subgroups (Chapter 2) are assessed in the context of their longitudinal clinical and resting-brain functional characteristics. The study had two hypotheses: a) the patterns of cerebral function at rest are distinct in imaging-derived patient subgroups, and b) longitudinal disease characteristics of imaging-derived subgroups are similar to their baseline disease characteristics.

4.3. Methods

4.3.1.Participants

174 ALS patients and 165 healthy controls (HCs) were recruited from multiple university centers across Canada and the United States as part of CALSNIC by October 2022. The participating centers were in Edmonton (University of Alberta), Calgary (University of Calgary), Montreal (McGill University), Toronto (University of Toronto), Vancouver (University of British Columbia), Quebec City (Universite Laval) and Miami (University of Miami). The study was approved by the respective research ethics review boards at all participating centers.

All patients met diagnostic criteria for clinically possible, probable lab-supported, probable, or definite ALS according to the El Escorial criteria (Brooks 1994; Brooks et al. 2000). Participants were included into the study if they had completed at least one longitudinal study visit. Patients were excluded from the study if their symptom duration exceeded 5 years at baseline, or they did not complete rs-fMRI scans, or if they presented with co-morbid frontotemporal dementia (FTD) or other neurological conditions. HCs were excluded from the study if they had previously received a clinical diagnosis of any neurological or psychiatric disorders. See table 1 for details on demographics and clinical characteristics of our sample.

4.3.2.Image Acquisition

A multicenter harmonized scanning protocol, preadjusted for scanner variances, was used to acquire T1-weighted (T1w) structural MRI and T2*-weighted resting-state functional MRI (rs-fMRI) data from all participants in the study across all study visits. Participants were instructed to lie still with their eyes closed and to not think of anything in particular for the duration of the rs-fMRI scan. A brief description of the protocol for the Siemens (Prisma) scanner for CALSNIC 1

is provided in the following section. A description of the complete protocol for other scanners and CALSNIC 2 can be found in our CALSNIC overview paper (Kalra, Khan, et al. 2020).

A magnetization-prepared rapid gradient-echo imaging (MPRAGE sequence; Repetition time, TR= 2300 ms; Echo time, TE= 3.43 ms; Inversion time, TI= 900 ms; flip angle= 9°; FOV= 256 mm x 256 mm) was used to acquire T1w data with an isotropic resolution of 1 × 1 × 1 mm3. Whole-brain 3D T2*-weighted rs-fMRI data was acquired using an echo-planar imaging (EPI) pulse sequence with an isotropic voxel resolution of 3.5 × 3.5 × 3.5 mm3 and the following specifications: TR = 2,200 ms; TE = 30 ms; field of view = 224 × 224 × 64 matrix; 40 slices, 192 trains; acquisition time = ~7 minutes.

4.3.3.Image processing

4.3.3.1. T1-weighted MRI

All T1w images for participants completing at least two study visits were realigned and coregistered to each other to ensure voxel-matching using Statistical Parametric Mapping (SPM) software (version 12). Following realignment and coregistration, the "AverageImages" module within the Advanced Normalization Tools (ANTs) software was used to generate an average T1w image in the native space of each participant. This average T1w image was used in the coregistration step of the rs-fMRI processing pipeline.

4.3.3.2. Resting-state fMRI

The baseline and longitudinal preprocessing pipelines of the CONN toolbox (https://web.conn-toolbox.org/) were used to preprocess the rs-fMRI images. The first four volumes were removed for every participant to allow for steady state magnetization. The time series data for each participant were corrected for differences in image slice acquisition times, followed by realignment for head motion within and across imaging sessions using a six-parameter rigid body

transformation algorithm. The mean multi-slice rs-fMRI data (temporally averaged across the time series) was co-registered to the average T1w image, and the resulting transformation matrices were applied to all volumes of the rs-fMRI data for longitudinal time points. The resultant co-registered functional images underwent spatial normalization to the Montreal Neurological Institute (MNI) template (Collins et al. 1992) space and smoothing with a Gaussian smoothing kernel of 8 mm full width at half-maximum. The white matter and cerebrospinal fluid signals as well as motion estimates were removed from the data and further denoising was performed using a bandpass filter of 0.008-0.09 Hz. The filtered and denoised images were used in further analyses of resting-state functional connectivity (FC) using the template-based rotation (TBR) method.

4.3.3.3. Resting-state functional MRI analysis: Template Based Rotation

This technique of estimation of resting-state network (RSN) components (or, template maps) at the individual level utilizes the application of an *a priori*, out-of-sample network template for individual RSNs. This technique predicts RSN template maps, at an individual participant level, as a linear combination of time courses that correspond to spatial patterns in a reference template set, thereby removing the spatial and temporal orthogonality assumptions of distributed functional networks (at a group level). Refer to (Schultz et al. 2014) for a complete overview of this technique. RSN maps for each participant were generated for every longitudinal time point using the TBR code (Schultz et al. 2014). Eleven target components (cerebellar gray, default mode, dorsal attention, frontal, left and right control, motor, primary visual, salience, subcortical, and temporal language networks) were estimated for each participant by the TBR technique and preselected based on correspondence to gray matter functional connectivity (FC) or disease relevance. The gray matter TBR components were identified as RSNs-of-interest in the current study. Individual subject resting-state functional connectivity (rsFC) maps underwent transformation from correlation (r)-maps to Fisher (z)-maps to allow for variance normalization. These z-maps were used in further statistical analyses.

4.3.3.4. Subgrouping: Hierarchical clustering of patients based on resting-brain function

The method for patient subgrouping based on imaging-derived measures of functional connectivity of resting-state cerebral networks (or, resting-state networks – RSNs) is outlined in Chapter 2. Briefly, the TBR templates for individual RSNs were used as regions-of-interest to calculate RSN FC values from TBR maps for individual subject at a voxel-level. The voxel-wise FC values were averaged to obtain a single measure of intra-network connectivity for each RSN. These FC averages underwent adjustments for demographic variables (age, sex, and education level) using a multiple regression model. Adjusted FCs for the ALS group were transformed into z-scores based on the HC average. These z-transformed time courses for the ALS group were used as inputs in a hierarchical clustering analysis to identify patient subgroups with distinct biological characteristics. Eleven continuous variables (z-scored FC for 11 RSNs) were entered into the clustering model as inputs, the Ward's method was used for estimating the clusters, and a squared-Euclidean distance function was used as a measure of dissimilarity to identify patient subgroups. The number of solutions were not defined *a priori*. Two patient subgroups were identified and are referred to as S1 and S2 in the current study. These subgroups were identified in chapter 2 as experiencing early (S2) and advanced (S1) disease based on a combination of clinical and imaging features.

4.3.4. Statistical analysis

4.3.4.1. Longitudinal

A sandwich estimator model (SwE, http://www.nisox.org/Software/SwE/) was used to assess differences in rsFC. Differences in rsFC were assessed between the HCs and two imaging-derived ALS subgroups. A non-parametric restricted wild bootstrapping approach (number of bootstraps = 5000) was employed for small sample adjustments (type C2). In addition, an SwE implementation of the threshold free cluster enhancement technique (Smith and Nichols 2009) (TFCE) was employed to identify clusters that showed significantly different rsFC between ALS subgroups and

HCs. An explicit gray matter mask in the MNI space was applied to restrict all analyses of rsFC to gray matter voxels within the brain. Statistical significance for all group comparisons using SwE models was set at a family-wise error (FWE) corrected p-value less than 0.05.

4.3.4.2. ComBat Harmonization: Removing *study x scanner* interaction effects from voxel-wise rsFC

ComBat is a tool based on an Empirical Bayesian algorithm and is used to eliminate unwanted technical variability from biological data (Fortin et al. 2017). This technical variability can arise because of differences in scanner hardware, software, or imaging acquisition protocols (Fortin et al. 2017). ComBat can help dissect and remove this technical variability from biological variability by correcting for the additive and multiplicative scanner effects as well as small sample sizes at an individual scanner. This can help combine datasets with different acquisition protocols employed to acquire images with different scanner hardware and software specifications. In the CALSNIC studies, technical variability can occur only due to the additive and multiplicative effects from scanner hardware and software. There is no technical variability contributed by imaging acquisition protocols as these parameters were harmonized across scanners and across both CALSNIC studies. In the current study, the longitudinal ComBat harmonization method was applied using the 'longCombat' package on R statistical software (https://www.r-project.org/) to estimate and correct for additive and multiplicative scanner effects on RSN functional connectivity as well as to account for subject-specific effects (e.g., age, subject consistency) inherent to longitudinal studies (Beer et al. 2020). 3D functional connectivity maps across visits and across participants were combined using the 'fslmerge' routine on FSL to generate a 4D image. This was performed for individual RSNs. Of the 11 RSN components, 10 successfully underwent longitudinal harmonization. The motor RSN component was not subjected to the longitudinal combat harmonization pipeline as the data had a singular fit indicating that the model was optimally fit to the demographic variables, and performing harmonization by forcing the model would result in overfitting.

4.4. Results

4.4.1. Demographic and clinical characteristics of the study cohort

Table 1 shows the baseline and longitudinal demographic and clinical characteristics of the study cohort.

Table 1. Baseline and longitudinal demographic and clinical characteristics of the study cohort. Means (SD) are displayed for the assessed characteristics. Single asterisk (*) denotes $p < 0.05$ and double asterisk (**) denotes $p < 0.001$. n.s. denotes no significant differences.

Characteristic	Baseline (Visit 1)			Visit 2			Visit 3		
	HC	S1	S2	HC	S1	S2	HC	S1	S2
Number of participants	165	109	62	100	45	34	77	25	24
Age (years)	55.4 (10.1)	60.1 (10.6)**	59.8 (9.8)*	57.1 (9.4)	60.9 (10.7)*	61.8 (8.2)*	57.7 (9.7)	61.3 (11.4)	62.6 (2.2)*
Sex: M/F	74/91	66/43	41/21	43/57	24/21	25/9	37/40	13/12	16/8
Symptom duration (years)	-	1.6 (0.9)	1.9 (1.2)	-			-		
Functional status (ALSFRS-R total)	-	38 (6)	39 (6)	-	36 (6)	38 (5)	-	35 (7)	36 (5)
Left finger tapping score	53 (13)	38 (16)**	38 (16)**	54 (11)	39 (14)**	37 (14)**	56 (12)	32 (20)**	36 (16)**
Right finger tapping score	59 (14)	43 (17)**	42 (18)**	58 (12)	45 (17)**	42 (15)**	60 (13)	40 (16)**	41 (15)**
Left foot tapping score	40 (10)	22 (15)**	26 (15)**	42 (10)	23 (16)**	23 (16)**	44 (10)	21 (15)**	19 (17)**
Right foot tapping score	43 (10)	23 (15)**	29 (15)**	44 (10)	24 (16)**	27 (15)**	46 (10)	23 (15)**	22 (16)**

L UMN Burden score (/7)	-	2.6 (1.5)	2.4 (1.5)	-	2.8 (1.5)	2.3 (1.4)	-	2.4 (1.9)	2.1 (1.4)
R UMN Burden score (/7)	-	2.5 (1.6)	2.4 (1.5)	-	2.9 (1.7)	2.2 (1.4)	-	2.9 (1.9)	2.3 (1.4)
L LMN Burden score (/6)	-	2.6 (1.2)	2.3 (1.4)	-	2.8 (1.2)	2.5 (1.5)	-	3.0 (1.2)	2.4 (1.7)
R LMN Burden score (/6)	-	2.6 (1.2)	2.3 (1.3)	-	2.6 (1.2)	2.4 (1.5)	-	3.2 (0.8)	2.2 (1.6)
ECAS total (/136)	110 (14)	106 (20)**	107 (19)	116 (8)	112 (10)	112 (10)	114 (8)	115 (8)	105 (12)

4.4.2. Longitudinal RSN activations of the study groups

Table 2. Longitudinal evolution of RSN activation values of the study groups

Resting-state network	Baseline (Visit 1)			Visit 2			Visit 3		
	HC	S1	S2	HC	S1	S2	HC	S1	S2
Cerebellar Gray	0.30 (0.07)	0.28 (0.07)	0.30 (0.06)	0.35 (0.08)	0.33 (0.07)	0.33 (0.07)	0.34 (0.06)	0.33 (0.06)	0.34 (0.08)
Default Mode	0.25 (0.05)	0.22 (0.04) **	0.29 (0.04) **	0.23 (0.05)	0.19 (0.05) **	0.24 (0.04)	0.25 (0.05)	0.24 (0.04)	0.28 (0.05) *
Dorsal Attention	0.25 (0.04)	0.23 (0.04) *	0.28 (0.04) **	0.28 (0.04)	0.27 (0.05)	0.30 (0.04) *	0.26 (0.04)	0.24 (0.05)	0.28 (0.05) *
Frontal	0.42 (0.08)	0.41 (0.09)	0.44 (0.07) *	0.51 (0.08)	0.51 (0.08)	0.53 (0.07)	0.43 (0.04)	0.43 (0.07)	0.45 (0.09)
Left Control	0.27 (0.05)	0.24 (0.04) **	0.31 (0.04) **	0.28 (0.05)	0.24 (0.05) **	0.29 (0.04)	0.29 (0.05)	0.27 (0.05)	0.32 (0.05) *
Motor	0.28 (0.05)	0.26 (0.04) **	0.31 (0.04) **	0.27 (0.05)	0.25 (0.05) *	0.28 (0.04)	0.31 (0.05)	0.30 (0.04)	0.32 (0.04)

Primary Visual	0.36 (0.06)	0.34 (0.05) *	0.35 (0.05)	0.36 (0.05)	0.36 (0.06)	0.37 (0.06)	0.36 (0.06)	0.36 (0.07)	0.37 (0.08)
Right Control	0.26 (0.05)	0.23 (0.03) **	0.29 (0.04) **	0.28 (0.05)	0.25 (0.05) **	0.29 (0.04)	0.28 (0.05)	0.26 (0.04)	0.30 (0.04)
Salience	0.27 (0.05)	0.25 (0.04) **	0.30 (0.03) **	0.27 (0.04)	0.24 (0.05) *	0.27 (0.04)	0.27 (0.04)	0.26 (0.03)	0.29 (0.04) *
Subcortical	0.32 (0.05)	0.31 (0.05)	0.32 (0.04)	0.34 (0.05)	0.33 (0.05)	0.33 (0.05)	0.33 (0.06)	0.34 (0.05)	0.33 (0.06)
Temporal Language	0.29 (0.06)	0.27 (0.05) *	0.33 (0.05) **	0.34 (0.05)	0.33 (0.06)	0.35 (0.05)	0.35 (0.07)	0.32 (0.05)	0.36 (0.07)

4.4.3. Longitudinal alterations in RSN voxel-wise FC

Longitudinal FC reductions were observed for the cerebellar gray, default mode, frontal, left control, and salience networks for S1 patients and longitudinal FC increases were observed for the default mode and motor networks for S2 patients (Table 3, Figure 1).

Table 3. Voxel-wise differences in longitudinal functional connectivity between ALS subgroups (S1 and S2) and HCs. RSN = resting-state network, MNI = Montreal Neurological Institute, BA = Brodmann area, R = right, L = left, B = bilateral

RSN	Contrast	Brain region	Cluster size	MNI coordinates			Z-value
				x	y	z	
Cerebellar Gray	S1 < HC	L visuomotor area (BA 7)	17	-12	-54	57	3.95
Default Mode	S1 < HC	R Broca's area (pars opercularis) (BA 44)	273	39	12	33	3.51
		R premotor + supplementary motor areas (BA 6)	35	42	-9	57	3.35
		R primary motor cortex (BA 4)	10	33	-27	66	3.13

		R primary sensory cortex (BA 1)	10	48	-24	54	3.02
	S2 > HC	L anterior prefrontal cortex (BA 10)	10	-18	60	-9	3.33
		L medial temporal gyrus (BA 21)	8	-57	-18	-6	3.32
Frontal	S1 < HC	L lateral dorsolateral prefrontal cortex (BA 46)	15	-42	27	15	3.61
		R Broca's area (pars triangularis) (BA 45)	5	39	33	6	3.44
Left Control	S1 < HC	B caudate	726	15	24	12	3.88
		L posterior cingulate cortex (BA 31)	257	-24	-24	36	3.71
		L premotor + supplementary motor areas (BA 6)	13	-36	-3	45	2.71
Motor	S2 > HC	L supramarginal gyrus (BA 40)	2799	-42	-39	42	3.53
		R premotor + supplementary motor areas (BA 6)	223	33	-6	69	3.39
Salience	S1 < HC	R thalamus	15	3	-15	21	3.65

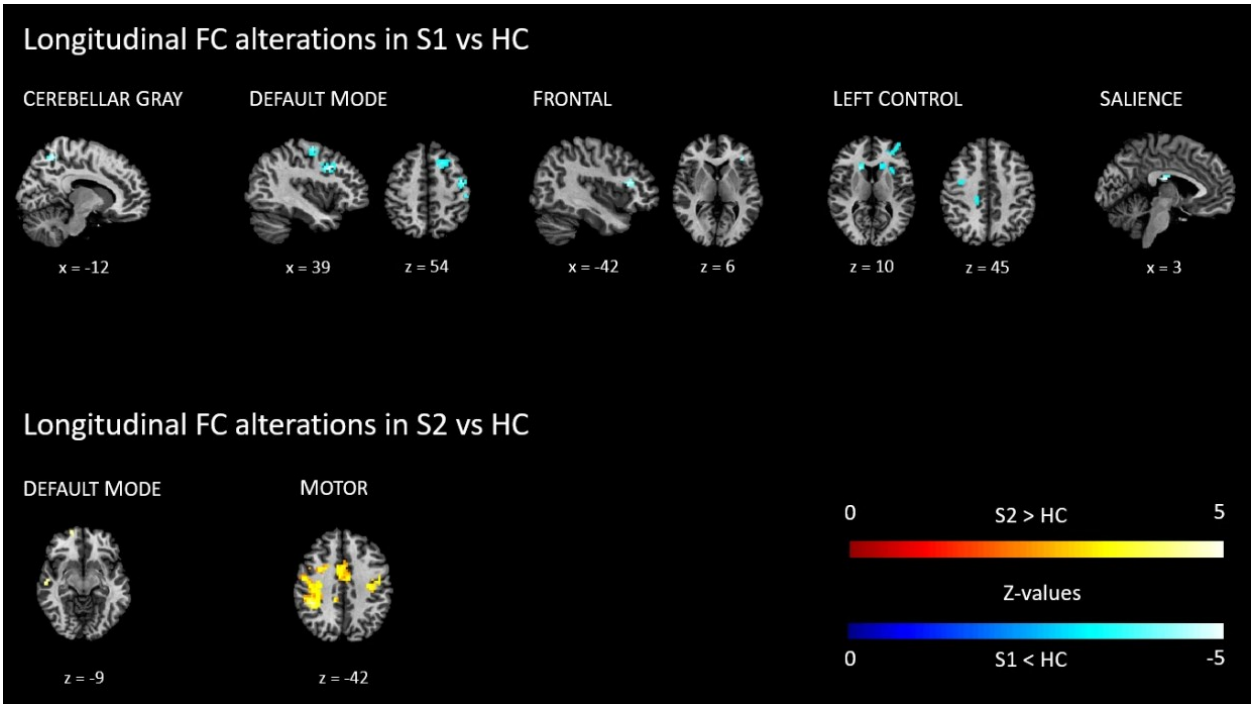

Figure 1. Voxel-wise alterations in longitudinal FC in imaging-derived patient subgroups compared to healthy controls

4.5. Discussion

The current study aimed to identify differences in function of resting-state networks in patient subgroups identified using imaging-based measures of RSN activations as well as examine the coherence between observed disease evolution patterns and those postulated at baseline (Chapter 2). Distinct patterns of RSN activations and functional connectivity patterns were observed in the identified patient subgroups. An assessment of clinical and imaging characteristics of disease evolution over a one-year observation period revealed a coherence between postulated disease evolution patterns at baseline assessment and actually observed disease evolution. Interpretations of findings corresponding to the aims are discussed in the next sections.

4.5.1. Distinctness of longitudinal evolution patterns of resting-state functional networks in imaging-derived patient subgroups

In terms of network activation values, at visit 1, S1 patients had reduced activations in the default mode, dorsal attention, motor, bilateral control, primary visual, salience, and temporal language networks whereas S2 patients had increased activations in the default mode, dorsal attention, frontal, motor, bilateral control, salience, and temporal language networks. At visit 2, S1 patients had reduced activations of the default mode, motor, bilateral control, and salience networks and S2 patients had increased activation in the dorsal attention network. At visit 3, while network activations of S1 patients were comparable to HCs, S2 patients had increased activations of the default mode, dorsal attention, left control, and salience networks. Overall, S1 and S2 patients had reduced and increased network activations respectively across visits. In accordance with the Scaffolding Theory of Aging and Cognition (STAC) (D. C. Park and Reuter-Lorenz 2009; Reuter-Lorenz and Park 2014), the effects of neurodegenerative processes in a brain region or a network of brain regions are compensated by the involvement of additional brain regions – resulting in an increase in activity in the recruited brain regions. However, with progression of the pathological process, a critical point is reached in the disease process after which there is a decline in

compensation (reduction in activation). The functional activation profiles of the RSNs across the timeline for the observation of disease evolution suggest that the disease might be more severe in S1 patients, and therefore this subgroup of patients might be experiencing more advanced disease than S2 patients.

In terms of longitudinal FC, network alterations of the S2 subgroup were less generalized than those of the S1 subgroup. S1 patients had longitudinal FC alterations in the cerebellar gray, default mode, frontal, left control, and salience networks and S2 patients had longitudinal FC alterations in the default mode and motor networks. The brain regions exhibiting altered longitudinal FC in S1 patients constitute in part the motor circuits that are involved in motor encoding and execution. As the disease evolves, the connectivity of these RSNs with motor regions progressively reduces, suggesting the occurrence of progressive impairment in brain regions subserving motor functions. Specifically, the cerebellar gray RSN has reduced FC with the visuomotor area, suggesting an impairment in motor coordination based on stimuli from the external environment. The default mode network has reduced FC with components of the sensorimotor network (primary sensory cortex, primary motor cortex, and the premotor/SMA regions) as well as the Broca's area, a brain region that participates in various aspects of motor encoding and execution (Papitto, Friederici, and Zaccarella 2020). The frontal network also has reduced FC with the Broca's area. The left control network has reduced FC with the caudate, posterior cingulate cortex, and the premotor/SMA. The caudate and premotor/SMA contribute to planning the execution of a motor function and the posterior cingulate cortex is a heavily connected brain region within the default mode network which helps in coordinating the functioning of multiple distinct cerebral networks in response to a task (Leech and Sharp 2014). The salience network has reduced FC with the thalamus, a brain region that acts as a center for the relay of top-down and bottom-up motor information. This suggests that multiple routes of information processing relating to motor execution are progressively impaired in S1 patients.

The motor network in S2 patients shows an increase in reliance on the premotor/SMA as well as the supramarginal gyrus – brain regions that are involved in motor planning. The default mode network also has increased FC with brain regions in the frontal and temporal cortices, suggesting that S2 patients have a frontotemporal pattern of disease in addition to a motor phenotype.

In sum, based on RSN activation patterns and FC alterations longitudinally, it seems apparent that impairments in brain regions subserving motor encoding occur in all ALS patients. Specifically, the findings of the current study suggest that S1 patients have a more severe disease with a predominant motor phenotype and S2 patients have a less severe disease with a motor-frontotemporal phenotype. This alludes to a distinct pattern of disease evolution in patient subgroups identified using imaging-derived measures, as well as to a coherence between disease evolution patterns postulated using only baseline data (Chapter 2) and actual longitudinal patterns of disease evolution.

4.5.2. Longitudinal clinical characterization of patient subgroups

At baseline evaluation, patients in the S2 subgroup had a longer symptom duration, a slower disease progression rate, and higher right foot tapping scores compared to S1 patients (Chapter 2 and current study). Based on these clinical observations, it seemed apparent that S2 patients underwent clinical decline slower than S1 patients which corroborated with observations of RSN function (Chapter 2). While voluntary motor function (foot tapping) is significantly different between subgroups at baseline, this significance is lost later in the disease course (visit 3). On the contrary, while cognitive function is not significantly different at baseline, differences between subgroups become apparent by the third longitudinal visit. S2 has lower cognitive scores than S1, therefore providing further evidence of a frontotemporal disease phenotype in S2 patients. It has been previously shown that cognitive decline occurs more frequently in the advanced as opposed to the early stages of disease (Chiò et al. 2019a). However, disease stages in this study were defined based on two disease staging systems (King's college staging and MiToS staging) which use

clinical measures to stage patients. S1 patients, but not S2 patients, had reduced ECAS total scores when compared to HCs at baseline but these differences were not observed at later visits. These observations are in line with findings from previous studies in ALS literature that suggest a strong coherence between motor and cognitive decline (Elamin et al. 2013; Oh et al. 2014; Phukan et al. 2012). However, it is challenging to monitor progression of cognitive decline in patients presenting with cognitive decline at baseline due to high rates of dropout in patients with cognitive decline (Chiò et al. 2019a).

In comparison to S1 patients, the emergence of cognitive decline in S2 patients at visit 3 suggests a delayed manifestation in cognitive impairment. Coupled with a greater spatial extent of network connectivity alterations, but not activation alterations of the motor network, this suggests a slower rate of the incidence of disease characteristics in S2 patients. This is indicative of differences in the timeline of clinical manifestation of the pathophysiological disease process in the two patient subgroups. However, these interpretations are unable to identify whether the pathophysiological disease process is distinct in the two subgroups.

4.5.3. Longitudinal change in clinical and functional connectivity measures

4.5.3.1. Clinical measures

Unique patterns of clinical change were observed between the baseline and third longitudinal study visits for the two patient subgroups. While foot tapping scores were significantly reduced for both subgroups S1 and S2 bilaterally, only subgroup S1 had significantly increased upper and lower motor neuron burden scores on the right side. While upper and lower motor neuron burden scores were elevated for S1 on the left side and for S2 bilaterally, they did not attain significance. This significant increase in burden at the level of both the upper and lower motor neurons during the same observation time frame suggests that the disease is more severe in S1 patients. In addition, the significant reduction in foot tapping scores in both subgroups suggests that the motor neurons constituting the foot region of the motor homunculus might have specific neuroanatomical

characteristics (relating to their microstructure and neurochemical profiles) that might suggest the potential role of this region in disease monitoring. A recent study (Chapter 5) has reported that concentrations of the neurochemical N-acetyl aspartate within the foot region of the motor homunculus of the primary motor cortex are associated with foot tapping scores, and reductions in these concentrations are associated with reduced functional connectivity of the primary motor cortex at baseline in ALS. In conjunction with the findings of the current study, one might postulate that a progressive decline in foot tapping scores might be suggestive of a progressive degenerative process within primary motor cortical neurons that could cause a decline in their functional and neuroanatomical properties.

4.5.3.2. Cerebral function measures

In terms of cerebral function, contrary to expectations, the decline in functional activation patterns from baseline to the third longitudinal visit were directionally similar for the S1 patients and HCs. In both groups, increases in resting-state functional activations were observed in the cerebellar gray, motor, bilateral control, subcortical, and temporal language networks. However, as expected, fewer functional activation alterations were observed for patients in the S2 subgroup compared to the S1 subgroup. Patients in the S2 subgroup experienced functional activation alterations for the cerebellar gray, right control, and temporal language networks but not for the motor, left control, and subcortical networks.

In S1 patients, while functional activations of the cerebellar gray and left control networks were increased, FCs of these networks were reduced with other regions, from V1 to V3. This suggests that these networks increase their functional activations as a compensatory response to a progressive neurodegenerative process, and progressively become self-reliant by reducing FC with other regions. In S2 patients, while the motor network had no increases in activation, it had increased FC with other brain regions. This follows the reasoning that in the presence of a metabolically-intense task, brain regions that are highly connected to other brain regions are unable

to obtain high activation and therefore delegate their functions to other brain regions that are less connected (Zarei et al. 2022). While no changes in activation were observed for the default mode network for either patient subgroup, the longitudinal FC of this network was reduced in S1 patients and increased in S2 patients. This is suggestive of a divergence of default mode network behaviour in response to the ALS disease process across both patient subgroups.

4.6. Discussion

In sum, a characterization of longitudinal alterations in clinical function, neurological examination findings, and network function were able to individually characterize the pathophysiological mechanisms underlying the disease process in distinct ALS patient subgroups. However, these measures put together are unable to distinguish between the pathophysiological disease mechanisms. Distinct features of disease were observable when a comparison of neurological examination findings was performed across subgroups. Clinical function was able to point towards a relative difference in the rate at which different features of the disease manifest so as to attain clinical significance. These patterns of clinical function changes were consistent with change in functional activation patterns of the cerebral resting-state networks in terms of the respective rates at which disease manifests in individual patient subgroups. However, network functional activations for all study populations (HCs and both patient subgroups) had similar directionality of alterations across visits, adding to the uncertainty of estimation of actual disease-related change versus measurement errors. Longitudinal changes in resting-state FC of the cerebral networks were indicative of lesser spatial extents of change in S2 patients compared to S1 patients. Additionally, differences in topographical network changes revealed a more motor phenotype for S1 patients and an additional frontotemporal phenotype in S2 patients. However, this might be possible because of selective dropouts of cognitively-impaired patients from the study.

4.7. Conclusions

When alterations in clinical and neuroimaging features from baseline to the last observational study visit were assessed, clinical measures were observed to be more likely to distinctly characterize the disease process as opposed to neuroimaging measures. This was contrary to expectations that cerebral network function would be more indicative of disease mechanisms in comparison to clinical measures as the patient subgroups were defined at baseline using activation patterns of cerebral RSNs. This lends additional evidence to the lack of coherence between biological and phenotypic characterizations of the ALS disease process, thereby presenting the possibility that patients might be subgrouped differently when considering only baseline features compared to the consideration of longitudinal patterns of functional activation in the clustering algorithm.

4.8. Limitations of the current study

In a longitudinal study, sources of noisy data include measurement errors and dropout or attrition rate. As such, it might be prudent to acquire multiple measurements of the same feature in order to monitor change. In the current study, multiple measurements of individual clinical or neuroimaging features could not be made owing to disease-related limitations faced by ALS patients, especially later on in their disease course. This partially explains any observed increases or decreases in clinical and neuroimaging measurements at visit 2 when such patterns of change were not expected. However, such change patterns could also be a characteristic of the disease process. Thus, it is important to be able to dissect actual disease-related change from measurement errors – an approach that was not taken in the current study.

4.9. Future directions

A future direction of the current study could be to estimate patient subgroups based on longitudinal patterns of change in their neuroimaging features, followed by an assessment of its ability to

identify distinct patterns of disease pathophysiology in the resultant patient subgroups. Another future direction could be to perform an assessment of measurement errors by acquiring the same set of measures more than once in a same day visit and again by repeating such measurements at longitudinal visits. This could help distinguish between disease-related changes and measurement errors.

4.10. Supplementary

S1. Patterns of longitudinal change from visit 1 to visit 3 in clinical measures

Clinical characteristic	S1	S2	HC
ALSFRS-R total	n.s.	n.s.	n.s.
R Finger Tapping	n.s.	n.s.	n.s.
L Finger Tapping	n.s.	n.s.	n.s.
R Foot Tapping	* ∧	* ∨	n.s.
L Foot Tapping	* ∧	* ∨	n.s.
R UMNB	* ∧	n.s.	n.s.
L UMNB	n.s.	n.s.	n.s.
R LMNB	* ∧	n.s.	n.s.
L LMNB	n.s.	n.s.	n.s.
ECAS total	n.s.	n.s.	n.s.

S2. Patterns of longitudinal change from visit 1 to visit 3 in functional activation measures

Network	S1	S2	HC
Cerebellar Gray	* ∧	* ∧	* ∧
Default Mode	n.s.	n.s.	n.s.
Dorsal Attention	n.s.	n.s.	n.s.
Frontal	n.s.	n.s.	n.s.
Left Control	* ∧	n.s.	* ∧
Motor	* ∧	n.s.	* ∧
Primary Visual	n.s.	n.s.	n.s.
Right Control	* ∧	* ∧	* ∧
Salience	n.s.	n.s.	n.s.
Subcortical	* ∧	n.s.	* ∧
Temporal Language	* ∧	* ∧	* ∧

* represents significant change from visit 1 to visit 3, n.s. represents no significant changes

∧ and ∨ represent the directionality of change from visit 1 to visit 3

Chapter 5: Motor cortex functional connectivity is associated with underlying neurochemistry in ALS

Avyarthana Dey[1, *], Collin C. Luk[1], Abdullah Ishaque[1], Daniel Ta[1], Ojas Srivastava[1], Dennell Krebs[1], Peter Seres[1], Chris Hanstock[1], Christian Beaulieu[1], Lawrence Korngut[2], Richard Frayne[2], Lorne Zinman[3], Simon Graham[3], Angela Genge[4], Hannah Briemberg[5], and Sanjay Kalra[1] for the Canadian ALS Neuroimaging Consortium (CALSNIC)

Author Affiliations:

1. University of Alberta, Edmonton, Alberta, Canada
2. University of Calgary, Calgary, Alberta, Canada
3. Sunnybrook Health Sciences Centre, Toronto, Ontario, Canada
4. McGill University, Montreal, Quebec, Canada
5. University of British Columbia, Vancouver, British Columbia, Canada

Corresponding author:

Dr. Sanjay Kalra

Address: 7-132F Clinical Sciences Building, 11350 83 Avenue NW, Edmonton, Alberta T6G 2G3

Email: kalra@ualberta.ca

Keywords: Amyotrophic lateral sclerosis, functional magnetic resonance imaging, diffusion tensor imaging, magnetic resonance spectroscopy, upper motor neuron disability

5.1. Abstract

5.1.1.Introduction

To identify structural and neurochemical properties that underlie functional connectivity impairments of the primary motor cortex and how these relate to clinical findings in amyotrophic lateral sclerosis (ALS).

5.1.2.Methods

52 ALS patients and 52 healthy controls, matched for age and sex, were enrolled from 5 centers across Canada for the Canadian ALS Neuroimaging Consortium study. Resting-state functional magnetic resonance imaging, diffusion tensor imaging, and magnetic resonance spectroscopy data were acquired. Functional connectivity maps, diffusion metrics, and neurometabolite ratios were obtained from the analyses of the acquired multimodal data. A clinical assessment of foot tapping (frequency) was performed to examine upper motor neuron function in all participants.

5.1.3.Results

Compared to healthy controls, the primary motor cortex in ALS showed reduced functional connectivity with sensory (T=5.21), frontal (T=3.70), temporal (T=3.80), putaminal (T=4.03), and adjacent motor (T=4.60) regions. In the primary motor cortex, N-acetyl aspartate (NAA, a neuronal marker) ratios and diffusion metrics (mean, axial, and radial diffusivity, fractional anisotropy) were altered. Within the ALS cohort, foot tapping frequency correlated with NAA ($r = 0.347$) and white matter fractional anisotropy ($r = 0.537$). NAA levels showed associations with disturbed FC of the motor cortex.

5.1.4.Conclusion

In vivo neurochemistry may represent an effective imaging marker of impaired motor cortex functional connectivity in ALS.

5.2. Key messages of this study

5.2.1.What is already known on this topic

The resting brain shows impaired functional connectivity in ALS. This can occur in conjunction with alterations in brain structure.

5.2.2.What this study adds

Compared to alterations in brain structure, alterations in neurochemical levels in the primary motor cortex may occur earlier and may be more sensitive to resting brain function in ALS.

5.2.3.How this study might affect research, practice, or policy

Clinical investigations could include assessments of primary motor cortical neurochemistry as an effective surrogate imaging marker of functional alterations in ALS. This might help provide an earlier diagnosis of ALS

5.3. Introduction

Amyotrophic lateral sclerosis (ALS) is an adult-onset neurodegenerative disorder. ALS manifests with an impaired ability to perform motor tasks (for example, walking, eating, or breathing) due to the degeneration of upper motor neurons (UMNs) in the primary motor cortex (PMC) and lower motor neurons in the brainstem and spinal cord. Clinical signs of ALS include muscular atrophy, fasciculations, hyperreflexia, weakness, and spasticity (Swinnen and Robberecht 2014). Of these, hyperreflexia, weakness, and spasticity are signs of UMN impairment. Task and resting-state functional magnetic resonance imaging (fMRI) (M Abidi et al. 2019; Bueno et al. 2019; Chenji et al. 2016; Mohammadi et al. 2015; Zhou et al. 2014) studies have shown impairments in synchronous activity (i.e., functional connectivity (FC)) occurring within and between motor and extra-motor brain regions. Studies using diffusion tensor imaging (DTI) and voxel-based morphometry have respectively shown evidence of altered microstructure of the corticospinal tract (F. Zhang et al. 2018) and atrophy in the precentral gyrus(Z. Chen and Ma 2010). Magnetic resonance spectroscopy (MRS) studies have shown alterations in neurochemical levels in the PMC in ALS patients when compared to healthy controls (Kalra 2019). These independent observations of UMN impairment, assessed in conjunction, could potentially provide deeper insights into ALS pathophysiology. Previous analyses of multiple MRI techniques have revealed associations between impaired cortical structure and function (Cheng et al. 2021; Douaud et al. 2011; Bradley R. Foerster et al. 2014; R. A.L. Menke et al. 2018b; Ratai et al. 2018). However, there is no adequate understanding of the association between the functional and anatomical (structure and neurochemistry) properties of affected UMNs inherent to the PMC in ALS.

To address this gap in literature, a multimodal approach was employed. fMRI, MRS, and DTI data were analyzed to assess FC, neurochemical, and microstructural properties of the PMC. It was hypothesized that, in ALS 1) there is altered FC of the PMC with the rest of the brain, 2) these FC alterations relate to underlying structural and/or neurochemical deficits, and 3) these FC alterations are associated with clinical measures of UMN impairment. An extensive investigational approach was thus applied to evaluate FC of the PMC across different brain regions, and to evaluate the relationship between FC and altered structural, neurochemical, and clinical measures.

5.4. Methods

5.4.1. Study design and participants

A prospective, multicenter magnetic resonance imaging (MRI) study was conducted at academic hospitals affiliated with universities at five centers located in Edmonton (University of Alberta), Calgary (University of Calgary), Montreal (McGill University), Toronto (Sunnybrook Health Sciences Centre), and Vancouver (University of British Columbia), as part of the Canadian ALS Neuroimaging Consortium (CALSNIC) (Kalra, Khan, et al. 2020). The study was approved by research ethics review boards at all participating centers.

Participant demographics and clinical characteristics are shown in Table 1 (and detailed in the Results section). Fifty-two patients with ALS were recruited from multidisciplinary ALS clinics at all centers. All patients met diagnostic criteria for clinically possible, probable-lab supported, probable, or definite ALS according to El Escorial criteria (Brooks et al. 2000). Patients were not included in the study if they had a symptom duration more than five years, did not complete imaging acquisition for either of the MRI sequences in this study, or presented with co-morbid frontotemporal dementia (FTD) or other neurological conditions. Fifty-two healthy controls matched for age, sex, and number of years of education, without a history of neurological or psychiatric conditions were also recruited into the study. See supplementary section 1 for a breakdown of participant numbers by site. Foot tapping frequencies (number of taps per 10 seconds) were recorded for all participants bilaterally and averaged. This clinical variable was selected based on the midline localization of the MRS region of interest, encompassing the foot region of the motor homunculus bilaterally. Therefore, the right/left foot tapping frequencies were averaged to obtain a single representative measure of UMN function.

Table 1. Participant demographics and clinical characteristics

Participant characteristics		ALS patients	Healthy controls	p-value
Number of participants		52	52	
Sex (n): Male / Female		34 / 18	25 / 27	n.s.
Age (years)				
	Mean ± SD	58.4 ± 10.0	54.9 ± 9.8	n.s.
	Median (Range)	57.5 (33.0 – 78.0)	56.0 (29.0 – 69.0)	
Education (number of years)				
	Mean ± SD	15.4 ± 4.0	16.6 ± 3.2	n.s.
	Median (Range)	15 (4 – 28)	16.25 (11 – 28)	
Onset (n)				
	Limb / Bulbar	42 / 10	-	
El Escorial clinical diagnosis category (n)				
	Definite ALS	11	-	
	Probable ALS	19	-	
	Probable ALS-lab supported	9	-	
	Possible ALS	12	-	
ALSFRS-R score (/48)				
	Mean ± SD	38.8 ± 5.2	-	
	Median (Range)	40 (22 – 47)	-	
Symptom duration (months)				
	Mean ± SD	26.7 ± 14.6	-	
	Median (Range)	21.5 (7.8 – 57.4)	-	
Foot tapping frequencies (taps/10s)				
	Mean ± SD	24 ± 15	40 ± 8	< 0.001
	Median (Range)	23 (0 – 64)	40 (24 – 62)	
ECAS Total (/136)				
	Mean ± SD	102.8 ± 17.7	113.3 ± 10.8	< 0.001
	Median (Range)	106 (53 – 127)	114 (62 – 134)	

5.4.2.Image acquisition

Imaging data were acquired on 3T Siemens scanners at Edmonton (Prisma) and Montreal (Tim Trio) using 20- and 32-channel receiving head coils, respectively; on 3T General Electric Healthcare (Discovery MR750) scanners at Calgary and Toronto using 12- and 8-channel receiving head coils, respectively; and on 3T Philips Achieva scanner at Vancouver using an 8-channel head coil receiver.

A multicenter harmonized scanning protocol, adjusted for scanner variances, was employed to acquire T1-weighted anatomical MRI, resting-state fMRI (rs-fMRI) of neuronal activity (measured indirectly by the blood oxygenation level-dependent effect), DTI, and single-voxel MRS data. For anatomical localization and normalization, a high-resolution *3D T1-weighted* (T1w) scan of the whole brain was acquired. A magnetization-prepared rapid gradient-echo imaging (MPRAGE sequence; Repetition time, TR= 2300 ms; Echo time, TE= 3.43 ms; Inversion time, TI= 900 ms; flip angle= 9°; field of view, FOV= 256 mm x 256 mm) was used to acquire T1w data with an isotropic resolution of 1 mm cubic. *Magnetic resonance spectroscopy* (MRS) data were acquired using a single voxel data acquisition protocol. As described previously (Srivastava et al. 2019), anatomical landmarks were used to place the MRS voxel in the left/right foot region of the PMC, centered symmetrically along the midline. A stimulated echo acquisition mode (STEAM) sequence was performed to acquire water suppressed spectra from the PMC with the following specifications: TR = 3,000 ms; TE = 160 ms; mixing time, TM = 40 ms; two acquisitions of 32 signal averages each. Whole-brain *3D T2*-weighted rs-fMRI* data was acquired using an echo-planar imaging (EPI) pulse sequence with an isotropic resolution of 3.5 mm cubic and the following specifications: TR = 2,200 ms; FOV = 224 × 224 × 64 matrix; 40 slices, 192 trains; acquisition time = ~7 minutes. Participants were instructed to lie still with their eyes closed during the rs-fMRI scan. A *2D spin-echo, single-shot, EPI pulse sequence* was used for the acquisition of diffusion-weighted images axially with the following specifications: TR = 10,000 ms; TE = 90 ms; flip angle = 90°; 70 slices; b0 images = 5; diffusion gradient directions = 30; steady magnetization, b0 = 1,000 s/mm^2; voxel size = 2 mm cubic. The parameters mentioned above are for the Siemens systems. MRI data acquired on the General Electric and Philips systems were harmonized to the

Siemens data with slight differences specific to the scanner manufacturer (Kalra, Khan, et al. 2020). Harmonization of MRI parameters was further ensured by scanning a set of participants twice at each scanner to ascertain test-retest and multicenter reliability (Ta et al. 2021).

5.4.3.Image processing

See figure 1 for an overview of the processing pipeline used in this study. The details of data processing for the different MRI modalities are discussed in the following sections.

5.4.3.1. Magnetic resonance spectroscopy

Magnetic resonance spectroscopy is an imaging technique that has been important to the study of neurological disorders. Metabolites such as N-acetyl aspartate (NAA) and NAA glutamate (NAAG), collectively referred to as total NAA (tNAA) moieties, provide an important marker of neuronal integrity (Kalra 2019). Ratios of tNAA to creatine (Cr), choline (Cho), or a combination (Cr+Cho) have been consistently shown to be reduced in the PMC and corticospinal tract regions, as well as in other extra-motor brain regions (Kalra 2019). Based on the consistency of observations of PMC tNAA neurochemistry in the literature, the neurometabolite ratios of interest in this study were tNAA/Cr and tNAA/Cho. As described in a previous study (Srivastava et al. 2019), the proton MRS spectra from the PMC underwent fitting using LCModel (version 6.1). Spectra were excluded from further analysis if visual inspection showed data corruption or if a standard deviation greater than 15% was obtained from the spectral fit. The peak areas for the NAA and NAAG metabolites were summed from the combined gray and white matter tissue classes within the MRS voxel to quantify the total amount of N-acetyl aspartyl moieties (tNAA) and expressed as ratios to creatine (Cr) and choline (Cho) for statistical analyses.

5.4.3.2. Generation of gray and white matter segments within the MRS region of interest

The whole-brain T1-weighted anatomical image underwent segmentation into the gray matter (GM), white matter (WM), and cerebrospinal fluid tissue classes using a standard voxel-based morphometry pipeline (http://dbm.neuro.uni-jena.de/vbm8/). The obtained whole-brain segments for the GM and WM tissue classes underwent voxel-wise matrix multiplication with the MRS voxel to generate GM and WM segments for the PMC region of interest, which were used in further analyses in the study (Figure 1). Prior to this multiplication, the T1-weighted and MRS voxel images of all included participants were inspected manually to ascertain accuracy in voxel-matching and to ensure that the subsequent FC and DTI analyses were performed in the exact anatomical region from which the MRS spectra were obtained.

5.4.3.3. Diffusion tensor imaging

As described in a previous study (Ishaque et al. 2019), the DTI data were processed using ExploreDTI (version 4.8.6). First, a visual quality check was performed to assess for scan quality, head motion, signal artifacts. Preprocessing steps included corrections for temporal signal drift using quadratic model, Gibbs ringing artifacts (5 non-diffusion-weighted images, lambda = 100, iterations = 100, step size = 0.01), head motion, and eddy current-induced geometric distortions. In particular, a non-rigid registration of the DTI data to the respective T1-weighted MRI data was performed for each participant to correct for EPI distortions. Following this, voxel-wise maps were calculated for four diffusion metrics: fractional anisotropy (FA), mean diffusivity (MD), radial diffusivity (RD), and axial diffusivity (AD). Subsequently, average values for these diffusion measures were estimated for the WM tissue classes within the PMC using the ‘fslmeants’ function in FSL (https://fsl.fmrib.ox.ac.uk/fsl).

5.4.3.4. Functional connectivity analysis for rs-fMRI

The rs-fMRI images were preprocessed using the functional connectivity toolbox (CONN) based on the Statistical Parametric Mapping (SPM) software (version 12, www.fil.ion.ucl.ac.uk/spm). The first four points in the time series of collected images were removed for every participant to account for the approach to steady state magnetization. The time series data for each participant were corrected for differences in image slice acquisition times, followed by realignment for head motion within each imaging session and across imaging sessions using a six-parameter rigid body transformation algorithm. The mean of the multi-slice rs-fMRI data (temporally averaged across the time series) was co-registered to the T1-weighted anatomical MRI data, and the resulting transformation matrix was applied to all time points of the rs-fMRI data within each session. Maps of FC were calculated in the 'native' anatomical space prior to transformation. Temporal correlations were performed voxel-wise between the rs-fMRI signal time-course of the PMC and other GM brain voxels to generate FC maps, using the PMC as a seed. A binary cutoff threshold was set at a Pearson correlation coefficient $r \geq 0.25$ (Buckner et al. 2009) to identify strongly correlated voxel pairs, as a proxy to brain regions depicting high levels of functional integration. The FC maps generated in the individual native space underwent normalization to the Montreal Neurological Institute (MNI) template (Collins et al. 1992) space and smoothing with a Gaussian smoothing kernel of 8 mm full width at half-maximum.

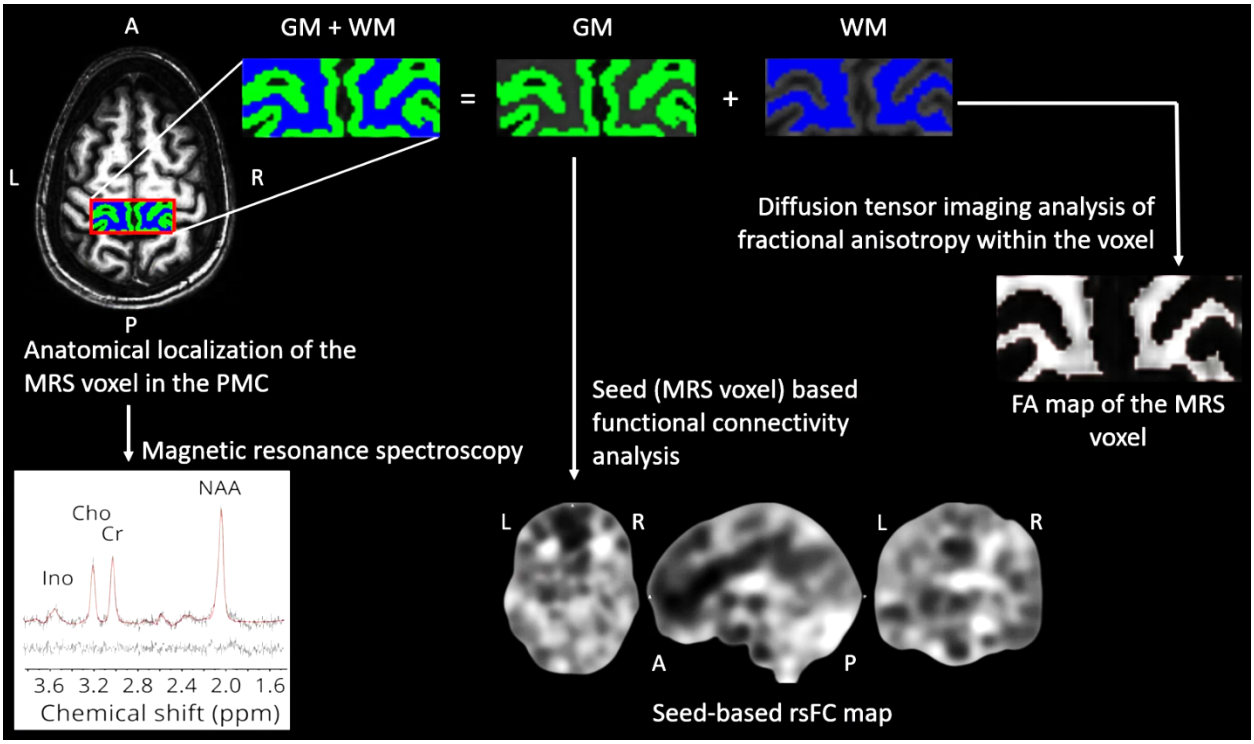

Figure 1. Overview of the processing pipeline. Spectral signatures of neurometabolites of interest were obtained from the PMC (MRS) voxel. The MRS voxel underwent segmentation into gray and white matter tissue classes, which respectively underwent analyses of functional connectivity and diffusion tensor imaging.

5.4.4.Rs-fMRI, MRS, and DTI statistical analyses

Statistical plan: All generalized linear models (GLM) utilized the available software routines in SPM12 and included CALSNIC center of data acquisition as a 'factor' in the statistical model. Significance for all analyses in SPM12 was set at a cluster threshold of k = 25 voxels (obtained after performing Monte-Carlo simulations for 5000 iterations and $p_{local} = 0.001$, $p_{global} = 0.05$ using a code developed in-house (Chenji et al. 2016). Significance for all analyses in SPSS was set at $p < 0.05$.

The following sections describe the statistical analyses performed in this study:

a) Group differences in resting-state FC: A univariate full factorial GLM was used in SPM12 to examine group differences in FC of the PMC with other brain regions. Diagnosis was included as a factor in the GLM in addition to the CALSNIC center of data acquisition. Age, sex, and number of years of education had no influence on FC differences, so these variables were removed from the model to allow for an increase in the degrees of freedom.
b) Group differences in diffusion and neurochemical measures: A univariate analysis of variance full factorial model was used in SPSS to examine group differences in the average GM and WM diffusion metrics (FA, MD, RD, AD) and neurochemical levels (tNAA/Cr, tNAA/Cho) within the PMC across the two groups. Site-wise scatterplots of the data were generated to test for any outliers in the data to be eliminated in further statistical analyses.
c) Relationship between diffusion and neurochemical measures & UMN dysfunction: The structural and neurochemical measures which revealed significant between-group differences underwent bivariate Pearson's correlational analyses with UMN measures in SPSS for the patient group. This was performed to identify the structural and neurochemical measures that were related to clinical UMN dysfunction. The imaging measures showing correlations with clinical variables were used in further analyses (see the next section).
d) Relationship between structural and neurochemical measures and FC differences in ALS: The structural and neurochemical measures showing significant correlations with UMN dysfunction were modelled as independent variables in a univariate full factorial GLM including CALSNIC center of data acquisition as a factor. Subsequent bivariate correlational analyses were performed in SPM12 to examine the associations between these imaging measures and FC differences.
e) Relationship between UMN dysfunction and FC differences in ALS: Foot tapping was modelled as an independent variable in the univariate full factorial model in SPM12 (from statistical analyses section 1) and correlational analyses were performed to examine the relationship with FC differences.
f) Relationship between structural, neurochemical, and functional characteristics and the rate of functional decline: The revised ALS Functional Rating Scale (ALSFRS-R), a 12-question self-administered questionnaire (maximum score = 48), was used to calculate the rate of functional

decline in ALS patients using the formula (48-ALSFRS-R score)/symptom duration. To ascertain the relationship between the rate of functional decline and MRI measures in the PMC, two sets of correlations were performed:

i. Bivariate Pearson's correlational analyses between spectroscopy, diffusion measures and disease progression rate (SPSS)
ii. Group-wise FC and disease progression rate (SPM12)

5.5. Results

5.5.1. Demographic and clinical characteristics of the sample

All patients in our study had a confirmed diagnosis of ALS and were matched with healthy controls on the basis of age and sex. Patients had an average symptom duration of 26.7 months and a mean ALSFRS-R score of 38.8/48, with forty-two patients having limb-onset ALS. Foot tapping frequencies were significantly reduced in ALS (Mean ± S.D. = 24 ± 15) compared to healthy controls (Mean ± S.D. = 40 ± 8). The score obtained on the Edinburgh Cognitive and Behavioral ALS Screen (ECAS) Total domain were significantly reduced in patients (Mean ± S.D. = 103 ± 18) compared to healthy controls (Mean ± S.D. = 113 ± 11) (Table 1). In terms of UMN involvement at the level of the lower limbs, as assessed on neurological examination, hyperreflexia was observed in 48/52 patients, spasticity was observed in 21/52 patients, and the Babinski sign was observed in 15/52 patients at the time of data acquisition.

5.5.2. Group differences in resting state FC

The PMC of ALS patients showed reduced FC with regions in adjacent bilateral premotor cortices and supplementary motor areas (cluster extent, k = 48, T = 4.50), bilateral primary sensory cortices (k = 95, T = 5.21), right putamen (k = 34, T = 4.03), right temporal pole (k = 38, T = 3.80), and right inferior frontal gyrus (k = 34, T = 3.70) (Figure 2, Table 2).

Table 2. Differences in resting-state FC. T-values and coordinates in MNI standard space are reported (T; x,y,z). R = right, B = bilateral, BA = Brodmann area, MNI = Montreal Neurological Institute.

Brain region	Brodmann area	Number of voxels in the cluster	Peak MNI coordinates			T-value
			x	y	z	
Reduced FC in ALS (contrast ALS < HC)						
B primary sensory cortex	BA 1	95	-12	-40	77	5.21
B premotor + supplementary motor area	BA 6	48	36	-4	59	4.60
R putamen	-	34	30	5	2	4.03
R temporal pole	BA 38	38	45	8	-25	3.80
R inferior frontal gyrus	BA 47	34	18	20	-28	3.70
Increased FC in ALS (contrast ALS > HC)						
- No suprathreshold clusters -						

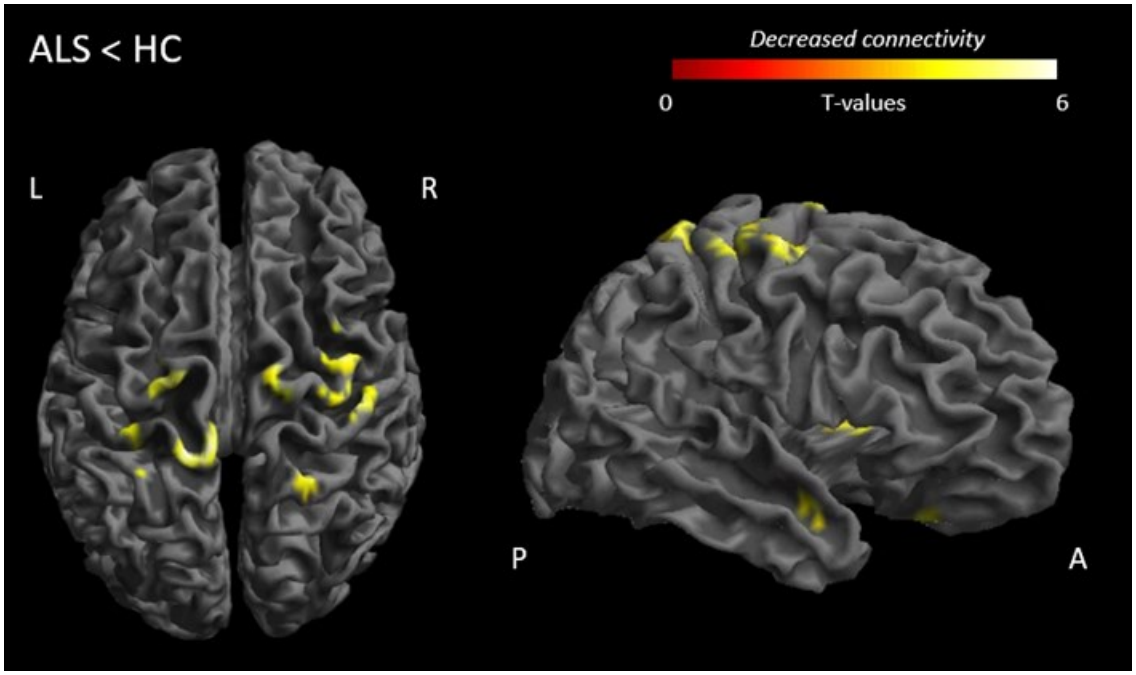

Figure 2. Functional connectivity of the primary motor cortex is reduced in ALS. L = left, R = right, A = anterior, P = posterior.

5.5.3. Group differences in diffusion and neurochemical measures in the primary motor cortex

Neurochemical ratios in the PMC were reduced for tNAA/Cr ($p < 0.001$) and tNAA/Cho ($p = 0.017$) in ALS when compared to HCs. For the DTI measures, FA ($p < 0.001$), MD ($p < 0.001$), and WM ($p = 0.022$) values were increased in the WM (Table 3).

Table 3. Summary of structural and neurochemical measures in the PMC. FA = fractional anisotropy, MD = mean diffusivity, RD = radial diffusivity, AD = axial diffusivity, tNAA = total NAA moieties, Cr = creatine, Cho = choline, SE = standard error. MD, RD, AD are x 10^{-3} mm^2/s

Imaging metric	Mean ± SE		p-value
	ALS	HC	
Neurochemical ratios			
tNAA/Cr	1.88 ± 0.03	2.05 ± 0.03	< 0.001
tNAA/Cho	2.44 ± 0.14	2.94 ± 0.14	0.017
Diffusion in PMC WM			
FA	0.38 ± 0.00	0.41 ± 0.00	< 0.001
MD	(0.80 ± 0.01)	(0.77 ± 0.01)	< 0.001
RD	(0.64 ± 0.01)	(0.6 ± 0.01)	0.022
AD	(1.12 ± 0.01)	(1.12 ± 0.01)	n.s.

5.5.4. Relationship of diffusion and neurochemical measurements with UMN function in ALS

Foot tapping frequencies showed positive significant correlations with FA values in the WM (Figure 3(a), r = 0.537, p < 0.001) and tNAA/Cr levels (Figure 3(b), r = 0.347, p = 0.023) in the PMC of the ALS cohort.

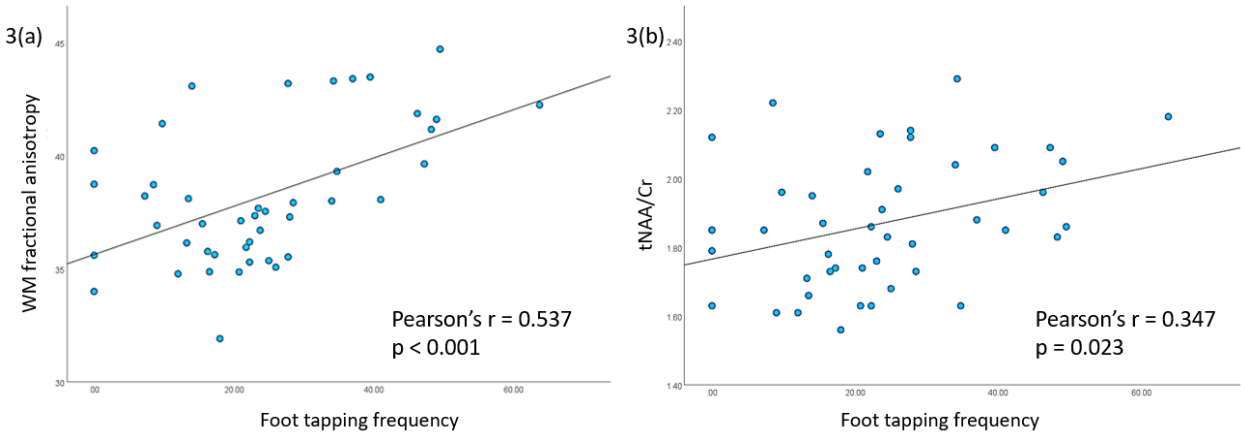

Figure 3. Correlations between foot tapping frequency and a) white matter fractional anisotropy and b) tNAA/Cr metabolite ratios.

5.5.5. Relationship between diffusion and neurochemical measures & FC differences

Despite WM FA showing stronger associations with clinical UMN impairment compared to tNAA/Cr, significant positive and negative associations of FC alterations were observed with tNAA/Cr and not WM FA values (Figure 4, Table 4).

Table 4. Regional associations of reduced functional connectivity with PMC neurochemistry and FA. T-values and coordinates in MNI standard space are reported (T; x, y, z). L = left, R = right, B = bilateral.

Group comparison	Brain region (Brodmann area)	Brodmann area	Type of association	T-value
Associations between reduced FC and tNAA/Cr ratios				
ALS < HC	L primary sensory cortex	BA 1	Positive	5.09
	R primary motor cortex	BA 4		4.55
	B premotor + supplementary motor area	BA 6		4.44
	R putamen	-		4.10
	R temporal pole	-		3.82
ALS < HC	R inferior frontal gyrus	BA 47	Negative	-4.12
Associations between reduced FC and WM FA - No suprathreshold clusters				

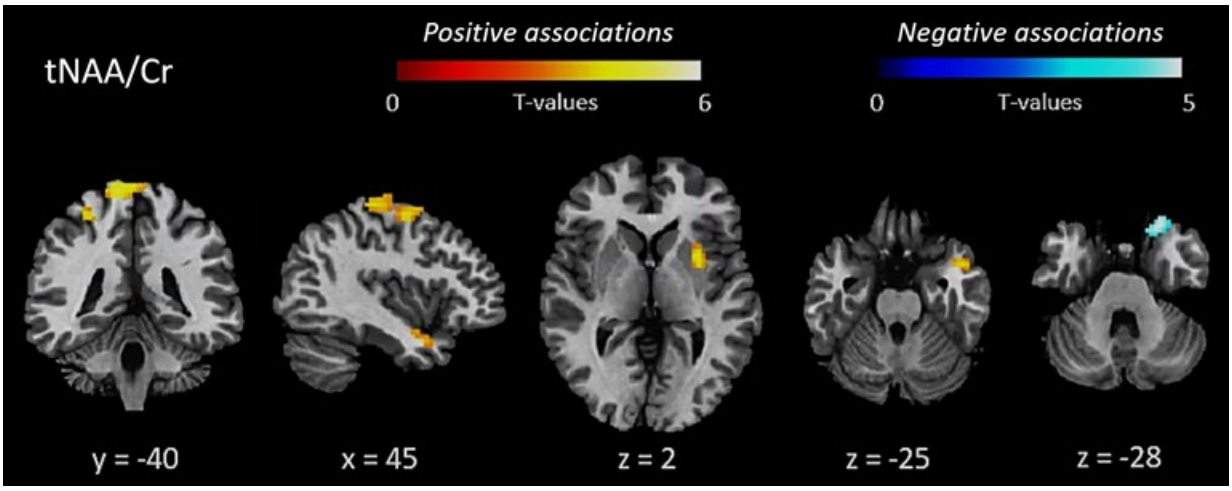

Figure 4. Regional associations of reduced functional connectivity with PMC neurochemistry. L = left, R = right, A = anterior, P = posterior.

5.5.6.Relationship between UMN function and FC reductions

There were no associations between foot tapping frequencies and FC alterations.

5.5.7.Relationship between structural, neurochemical, and functional connectivity measures and the rate of functional decline in ALS

There were no associations between rate of functional decline and structural or neurochemical measures of the PMC. A positive association was observed between the rate of functional decline and FC of the PMC with the right dorsal anterior cingulate cortex (BA 32; k = 343; T = 4.49) and the left thalamus (k = 51; T = 4.40). A negative association was observed between the rate of functional decline and FC of the PMC with the right ventral anterior cingulate cortex (BA 24; k = 244; T = 4.95), left dorsolateral prefrontal cortex (BA 9; k = 28; T = 3.92), and right ventral

posterior cingulate cortex (BA 23; k = 25; T = 3.62). When comparing ALS and HC cohorts, neither of these brain regions showed alterations in FC with the PMC.

5.6. Discussion

The present study sought to identify the effects of underlying diffusion and neurochemical deficits on PMC FC, and how these effects relate to clinical impairment in ALS. The main findings of the study are that FC of the PMC is reduced with multiple regions of the brain, the structural and neurochemical deficits in the PMC are associated with UMN dysfunction, and impaired PMC FC is related to altered neurochemistry but not white matter microstructure.

The majority of studies on resting-state fMRI in ALS have reported heterogeneous findings of altered FC within and between different resting-state networks, specifically the default mode and sensorimotor networks (Agosta et al. 2013a; Chenji et al. 2016; X. Fang et al. 2016; Mohammadi et al. 2009). In whole-brain resting-state fMRI studies that assessed other measures of resting brain function (e.g., regional homogeneity, fractional amplitude of low frequency fluctuations, etc.), altered function was identified in the motor and extra-motor brain regions (Bueno et al. 2019; Zhou et al. 2014). In region-of-interest-based studies on resting-state FC, reduced FC between the right and left motor cortices (Verstraete et al. 2010), altered FC of the motor cortex with other motor regions (superior parietal lobule, thalamus, basal ganglia, cerebellum) (Zhou et al. 2013), and altered FC of the motor cortex with extra-motor regions (superior frontal and temporal cortices) (Cheng et al. 2021) have been reported. The findings from the current study (Table 2) are congruent with these findings in ALS literature.

Multimodal MRI has been previously used to identify the neurobiological changes underlying impaired cerebral function. Such studies have revealed structural-functional congruence in impairment between motor connectivity and WM structure (Qiu et al. 2019; Schmidt et al. 2014;

J. Zhang et al. 2017) that relates to clinical measures (Douaud et al. 2011; Verstraete et al. 2010) (e.g., ALSFRS-R scores, disease progression rates). These studies assessed the co-occurrence of functional and structural but not neurochemical alterations – an investigation that has been conducted for the first time in the present study. Additionally, none of the aforementioned studies considered the somatotopic organization of the PMC in their interpretation of FC alterations in terms of clinical outcome measures. In the current study, the seed region was strategically defined in the foot region of the motor homunculus. The subsequent finding of the association between FC alterations and neurochemical concentrations in the PMC (Table 4) is important for enhanced understanding of the diverse nature of ALS disease pathology.

Previously, structural-functional decoupling and the heterogeneity of its occurrence has been postulated in multiple disease pathologies. Decoupling, in the context of cerebral connectivity, refers to the dissociation between functional and structural connectivity abnormalities in a disease-specific state (Skudlarski et al. 2010; Z. Zhang et al. 2011). In other words, decoupling simply refers to the co-occurring and/or sequential alterations in brain function and structure. For example, brain structural alterations preceding functional changes have been implicated cross-sectionally in major depressive disorder (Yao et al. 2019), in Parkinson's disease with no cognitive impairment (Rektor et al. 2018), and longitudinally in multiple sclerosis (Koubiyr et al. 2019). In contrast, functional alterations have been shown to precede structural changes in Alzheimer's disease (Lu et al. 2019). In patients with idiopathic Parkinson's disease, differential atrophy patterns in hippocampal subfields have been reported to precede their phenotypic diagnostic conversion to Parkinson's disease dementia (Low et al. 2019), suggesting that structural changes occur before impairment of clinically-defined cognitive functioning. In this study, no such evidence of sequential structure-function decoupling was observed.

Instead, we observed neurochemical-functional decoupling in relation to UMN impairment. To our best knowledge, there is no functional MRI evidence of neurochemical-functional decoupling in neurodegenerative disorders in humans. Of the three imaging measures investigated (FC, FA, and

tNAA/Cr), FA and tNAA/Cr levels were found to correlate strongly with clinical UMN impairment, but not FC. Furthermore, the relationship between FC reductions and tNAA/Cr concentrations, but not of FC reductions and WM FA, could suggest that in terms of imaging identifiers of clinical impairment, alterations in neurochemical properties of the PMC might be an earlier occurrence in ALS pathophysiology and be more sensitive towards probing the functional underpinnings of ALS. The present work also observed changes in the underlying brain tissue microstructure which correlated with clinical impairment. However, the lack of associations between these microstructural changes and FC alterations suggests that neurochemical changes might even precede structural changes and translate to alterations in brain function and clinical outcomes. However, such chronology of cerebral changes cannot be confidently inferred through a cross-sectional study, presenting the need to perform a longitudinal characterization of cerebral changes.

The present study benefits from a harmonized and multimodal MRI acquisition protocol across different ALS populations in Canada. This enables us to study different patient cohorts with varying clinical phenotypes of disease pathology across a multicenter cohort. This can provide a better understanding of the core neuronal processes that underlie cortical dysfunction in ALS. Additionally, harmonized imaging protocols can help reduce MRI system-related variance and increase statistical power (George et al. 2020). Another advantage of the present study is a localized, hypothesis-driven approach to uncover the diffusion and neurochemical signatures of altered function. This lowers the possibility of interpreting ALS disease pathology incorrectly by eliminating erroneous observations.

Heterogeneity of ALS, in terms of its clinical presentation and the underlying neurobiology, poses a challenge for scientific study of this complex disorder. Different genetic variants correlate with different clinical presentations of ALS (Brown and Al-Chalabi 2017). A limitation of the current study is that genetic information was not available for all patients. However, the present study controlled for heterogeneity to some extent by including patients who had a symptom duration of

no more than 5 years (Brown and Al-Chalabi 2017) and who did not previously receive a diagnosis of other neurological conditions such as FTD. Approximately 50% of patients presenting to a clinic with an El Escorial designation of suspected ALS can present with varying cognitive and behavioural impairments (Strong et al. 2017). Notably, there was no control for cognitive impairment as, even in patients presenting primarily with motor symptoms, brain regions outside the motor network could be affected (Christidi et al. 2018). Another limitation of this study could be the lack of control for the potential pharmacodynamic impact of Riluzole therapy, a glutamate agonist, on *in vivo* imaging features. Previously, Riluzole therapy has been shown to prolong survival (Bensimon, Lacomblez, and Meininger 1994) and in a small cohort to improve the concentrations of NAA after approximately 3 weeks of treatment (Kalra et al. 1998); however, the long term effects on NAA are unknown.

In conclusion, this study has shown that reduced functional connectivity of the motor cortex in ALS is linked to the local concentrations of N-acetyl aspartate. This highlights the importance of assessment of *in vivo* neurochemistry as an early pathophysiological marker of PMC functional changes in the characterization of ALS disease pathology. Based on the findings from this study, it could be helpful to include MRS of N-acetyl aspartate moieties within the PMC in relevant research protocols and in the investigation of patients with suspected ALS. However, we recognize that MRS can be more logistically challenging in a clinical setting because of the technical expertise required by the MRI system operator to accurately prescribe the MRS voxel. Future research studies could explore the functional, neurochemical, and structural dynamics of the PMC, longitudinally and also in relation to Riluzole therapy. Such studies could aim to explore in greater depth neurochemical contributions to functional impairment and cortical excitability, for example, with the use of MRS to quantify levels of excitatory and inhibitory neurotransmitters, as well as techniques such as transcranial magnetic stimulation and positron emission tomography to quantify cortical motor neuron excitation and glucose metabolism respectively.

5.7. Supplementary

A subgrouping analysis was performed in ALS patients with regions of onset in the bulbar and limb regions (Bulbar-onset ALS, Limb-onset ALS). Diffusion and spectroscopy measures were characterized for the two groups separately, and no differences in measurements were observed across the two patient cohorts. When comparing FC of the PMC between Bulbar- and Limb-onset ALS, no differences in FC were observed. We then investigated whether there were any differences in FC when each group was compared to HCs, and if these differences were congruent with group-level differences observed when comparing ALS to HCs (Table 2).

5.7.1.Bulbar-onset ALS vs HC

S1. Demographic and clinical characteristics

Participant characteristics		Bulbar-onset ALS	Healthy controls	p-value
Number of participants		10	52	
Sex (n): Male / Female		7 / 3	25 / 27	n.s.
Age (years)				
	Mean ± SD	56.3 ± 10.3	54.9 ± 9.8	n.s.
	Median (Range)	(41.0 – 72.0)	56.0 (29.0 – 69.0)	
Education (number of years)				
	Mean ± SD	16.8 ± 4.5	16.6 ± 3.2	n.s.
	Median (Range)	(12 – 25)	16.25 (11 – 28)	
ALSFRS-R score (/48)				
	Mean ± SD	38.3 ± 6.1	-	
	Median (Range)	(25 – 45)	-	
Symptom duration (months)				
	Mean ± SD	21.3 ± 12.1	-	
	Median (Range)	(9 – 43)	-	
Foot tapping frequencies (taps/10s)				
	Mean ± SD	31 ± 21	40 ± 8	0.047
	Median (Range)	(0 – 64)	40 (24 – 62)	
ECAS ALS Specific (/100)				
	Mean ± SD	79.0 ± 14.1	84.9 ± 9.0	n.s.

	Median (Range)	(46 – 95)	87 (40 – 98)	
ECAS Total (/136)				
	Mean ± SD	109 ± 15	113.3 ± 10.8	n.s.
	Median (Range)	(78 – 127)	114 (62 – 134)	

S2. Differences in resting state FC between Bulbar-onset ALS and HC

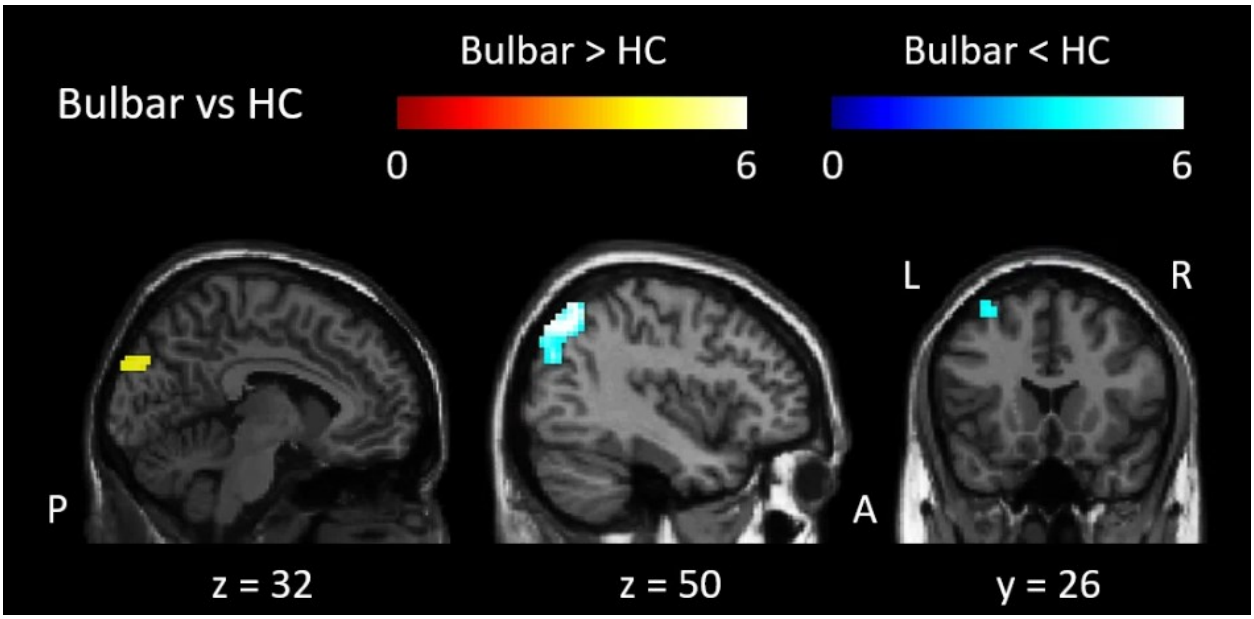

Figure S1. FC of the PMC in Bulbar-onset ALS. The colour bars represent the SPM(T) statistic for increased and reduced FC. Colour bars represent the SPM(T) statistic for each map across the whole brain ranging from lowest (blue) to the highest (red). See Table S2 for details on the cluster extents and locations. L = left, R = right, A = anterior, P = posterior.

Table S2. Differences in resting-state FC between Bulbar-onset ALS and HC. T-values and coordinates in MNI standard space are reported (T; x,y,z). R = right, L = left, BA = Brodmann area, MNI = Montreal Neurological Institute.

Brain region	Brodmann area	Number of voxels in the cluster	Peak MNI coordinates			T-value
			x	y	z	

Increased FC in Bulbar-onset ALS (contrast Bulbar-onset ALS > HC)						
L visual association cortex	BA 19	59	-6	-88	32	4.70
R secondary visual cortex	BA 18	45	27	-94	17	4.23
Reduced FC in Bulbar-onset ALS (contrast Bulbar-onset ALS < HC)						
L superior parietal lobule	BA 7	261	-33	-76	50	-4.86
L frontal eye fields	BA 8	31	-30	26	59	-4.90
R angular gyrus	BA 39	27	36	-73	44	-4.38

S3. Group differences in diffusion and neurochemical measures in the primary motor cortex in Bulbar-onset ALS

Imaging metric	Mean ± SE		p-value
	Bulbar-onset ALS	HC	
Neurochemical ratios			
tNAA/Cr	1.9 ± 0.08	2.05 ± 0.02	0.003
tNAA/Cho	2.34 ± 0.16	2.91 ± 0.21	n.s.
Diffusion in PMC WM			
FA	0.37 ± 0	0.41 ± 0	0.003
MD	(0.79 ± 0)	(0.76 ± 0)	0.006
RD	(0.64 ± 0)	(0.62 ± 0)	n.s.
AD	(1.11 ± 0)	(1.1 ± 0)	n.s.

S4. Relationship of diffusion and neurochemical measurements with UMN function in Bulbar-onset ALS

Variable	Foot tapping frequencies	
	Pearson's r	p
Neurochemical ratios		
tNAA/Cr	0.717	**0.045**
tNAA/Cho	0.601	n.s.
Diffusion in PMC WM		
FA	0.710	**0.049**
MD	-0.141	n.s.

RD	-0.315	n.s.
AD	0.266	n.s.

S5. Relationship between diffusion and neurochemical measures & FC differences in Bulbar-onset ALS

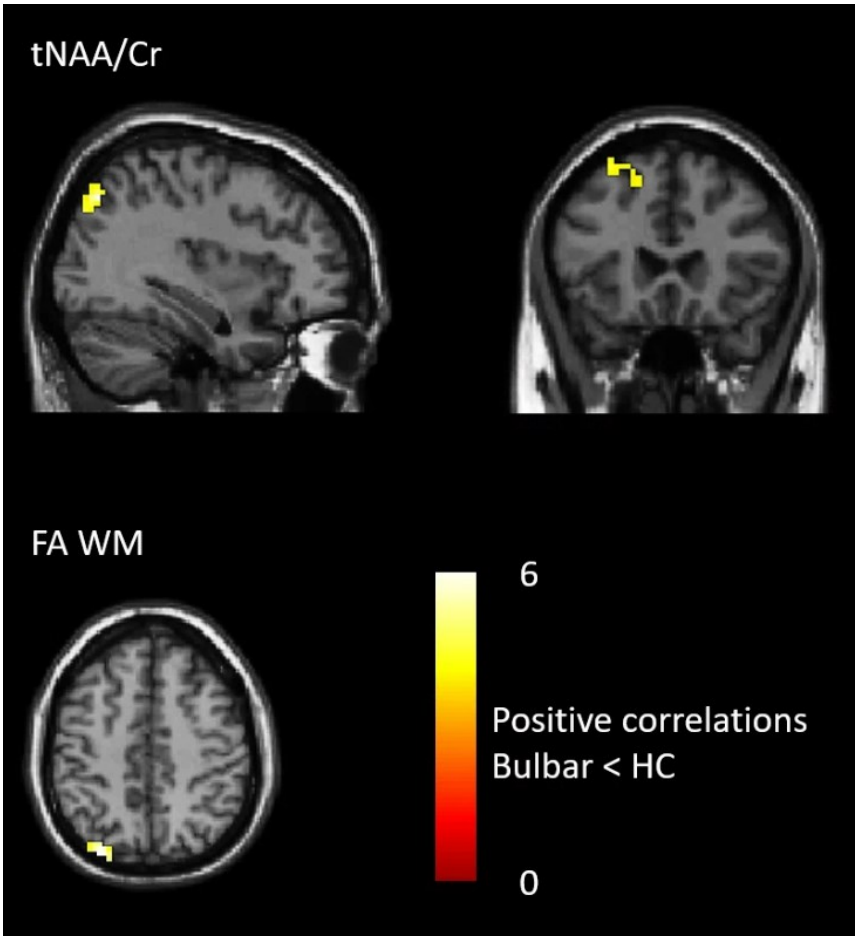

Figure S2. Positive regional associations of reduced functional connectivity with PMC neurochemistry and WM diffusion. Colour bars represent the positive SPM(T) statistic for each map (red to yellow). See Table S5 for details on the cluster extents and locations.

Table S5. Regional associations of reduced functional connectivity with PMC neurochemistry in Bulbar-onset ALS compared to HC. T-values and coordinates in MNI standard space are reported (T; x, y, z). L = left, R = right.

Group comparison	Brain region (Brodmann area)	Brodmann area	Type of association	T-value
Associations between reduced FC and tNAA/Cr ratios				
Bulbar-onset ALS < HC	R angular gyrus	BA 39	Positive	4.78
	L frontal eye fields	BA 8		4.09
Associations between reduced FC and FA WM values				
Bulbar-onset ALS < HC	L superior parietal lobule	BA 7	Positive	4.29

5.7.2.Limb-onset ALS vs HC

S6. Demographics and clinical characteristics

Participant characteristics		Limb-onset ALS	Healthy controls	p-value
Number of participants		42	52	
Sex (n): Male / Female		27 / 15	25 / 27	n.s.
Age (years)				
	Mean ± SD	58.9 ± 10.0	54.9 ± 9.8	n.s.
	Median (Range)	(33.0 – 78.0)	56.0 (29.0 – 69.0)	
Education (number of years)				
	Mean ± SD	15.0 ± 3.8	16.6 ± 3.2	0.033
	Median (Range)	(4 – 28)	16.25 (11 – 28)	
ALSFRS-R score (/48)				
	Mean ± SD	39.0 ± 5.0	-	
	Median (Range)	(22 – 47)	-	
Symptom duration (months)				
	Mean ± SD	27.9 ± 15.0	-	
	Median (Range)	(8 – 57)	-	
Foot tapping frequencies (taps/10s)				

	Mean ± SD	23 ± 13	40 ± 8	< 0.001
	Median (Range)	(0 – 50)	40 (24 – 62)	
ECAS ALS Specific (/100)				
	Mean ± SD	74.0 ± 16.0	84.9 ± 9.0	< 0.001
	Median (Range)	(29 – 95)	87 (40 – 98)	
ECAS Total (/136)				
	Mean ± SD	102 ± 18	113.3 ± 10.8	< 0.001
	Median (Range)	(53 – 127)	114 (62 – 134)	

S7. Differences in resting state FC between Limb-onset ALS and HC

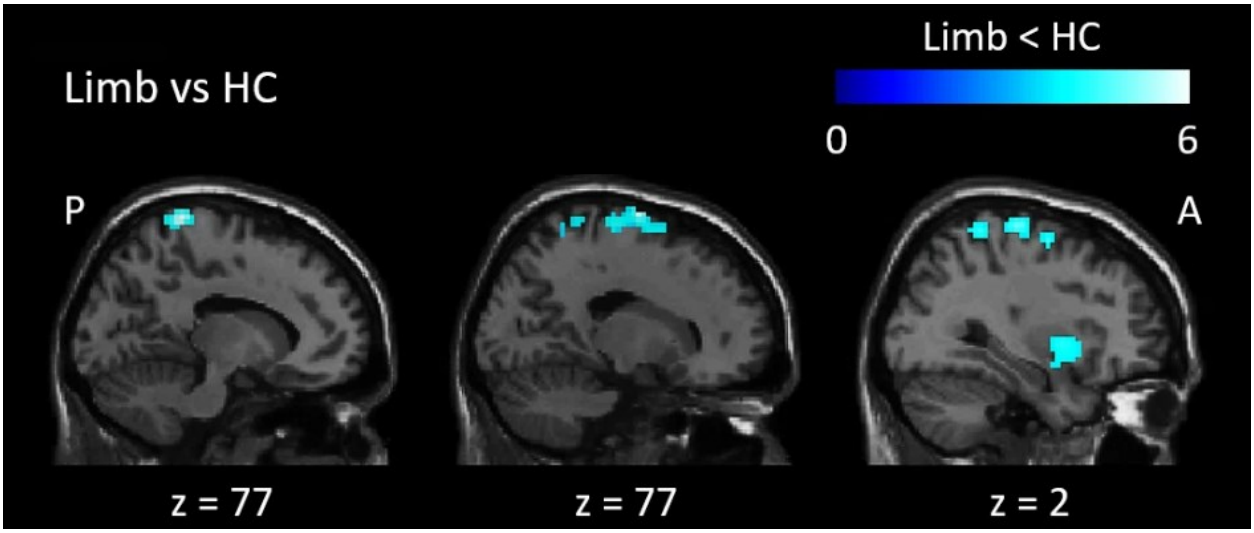

Figure S3. FC of the PMC in Limb-onset ALS. The colour bar represents the SPM(T) statistic for reduced FC. Colour bars represent the SPM(T) statistic for each map across the whole brain ranging from lowest (blue). See Table S7 for details on the cluster extents and locations. L = left, R = right, A = anterior, P = posterior.

Table S7. Differences in resting-state FC between Limb-onset ALS and HC. T-values and coordinates in MNI standard space are reported (T; x,y,z). R = right, L = left, BA = Brodmann area, MNI = Montreal Neurological Institute.

Brain region	Brodmann area	Number of voxels in the cluster	Peak MNI coordinates			T-value
			x	y	z	
Reduced FC in Limb-onset ALS (contrast Limb-onset ALS < HC)						
L primary sensory cortex	BA 1	448	-12	-40	77	5.81
R superior frontal gyrus	BA 6	329	18	-7	77	5.67
R putamen	-	133	30	5	2	4.40

S8. Group differences in diffusion and neurochemical measures in the primary motor cortex in Limb-onset ALS

Imaging metric	Mean ± SE		p-value
	Limb-onset ALS	HC	
Neurochemical ratios			
tNAA/Cr	1.91 ± 0.04	2.05 ± 0.02	< 0.001
tNAA/Cho	2.51 ± 0.08	2.91 ± 0.21	n.s.
Diffusion in PMC WM			
FA	0.38 ± 0	0.41 ± 0	< 0.001
MD	(0.79 ± 0)	(0.76 ± 0)	< 0.001
RD	(0.6 ± 0)	(0.6 ± 0)	0.046
AD	(1.1 ± 0)	(1.1 ± 0)	n.s.

S9. Relationship of diffusion and neurochemical measurements with UMN function in Limb-onset ALS

Variable	Foot tapping frequencies	
	Pearson's r	p
Neurochemical ratios		
tNAA/Cr	0.261	n.s.
tNAA/Cho	0.252	n.s.
Diffusion in PMC WM		
FA	0.492	**0.002**
MD	-0.269	n.s.
RD	-0.227	n.s.
AD	0.028	n.s.

S10. Relationship between diffusion and neurochemical measures & FC differences in Limb-onset ALS

There were no regional associations of FC reductions with PMC neurochemical and WM diffusion measures in limb-onset ALS.

S11. Assessment of whether correlations in Table 4 in the main document are driven by either ALS subgroup (Limb-onset ALS or Bulbar-onset ALS)

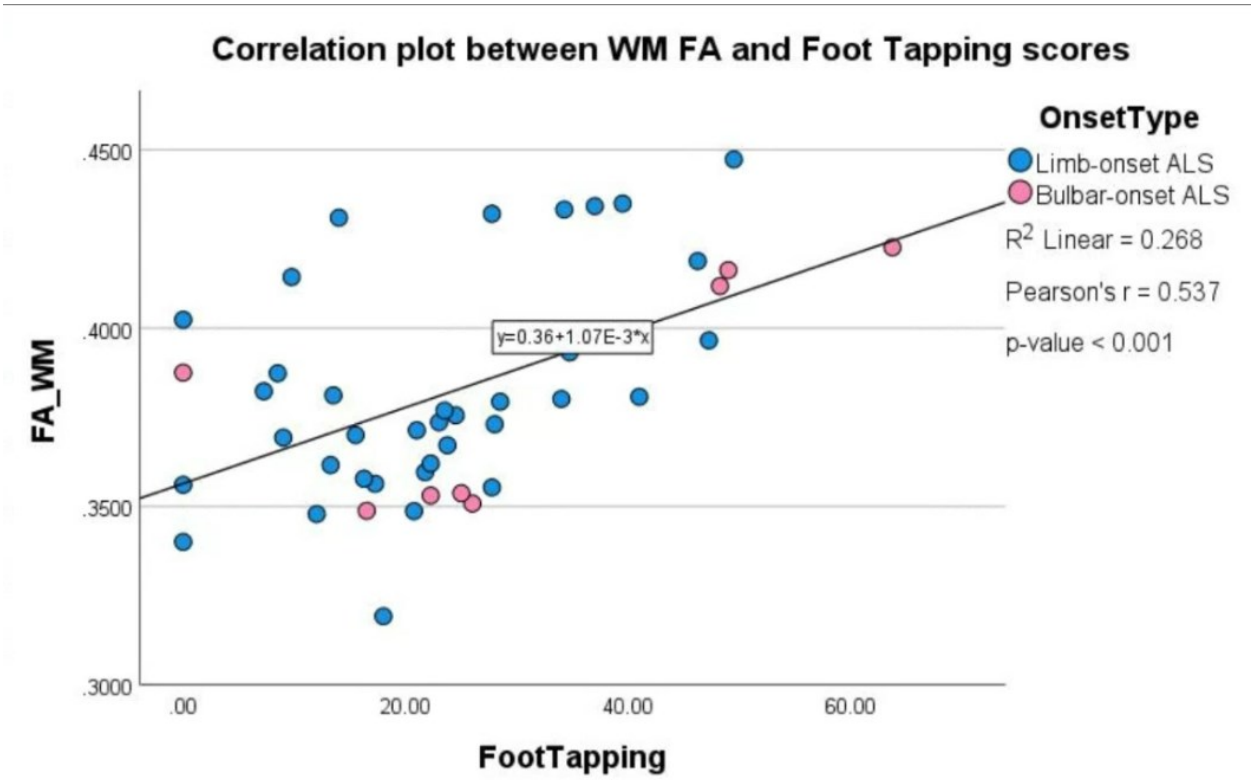

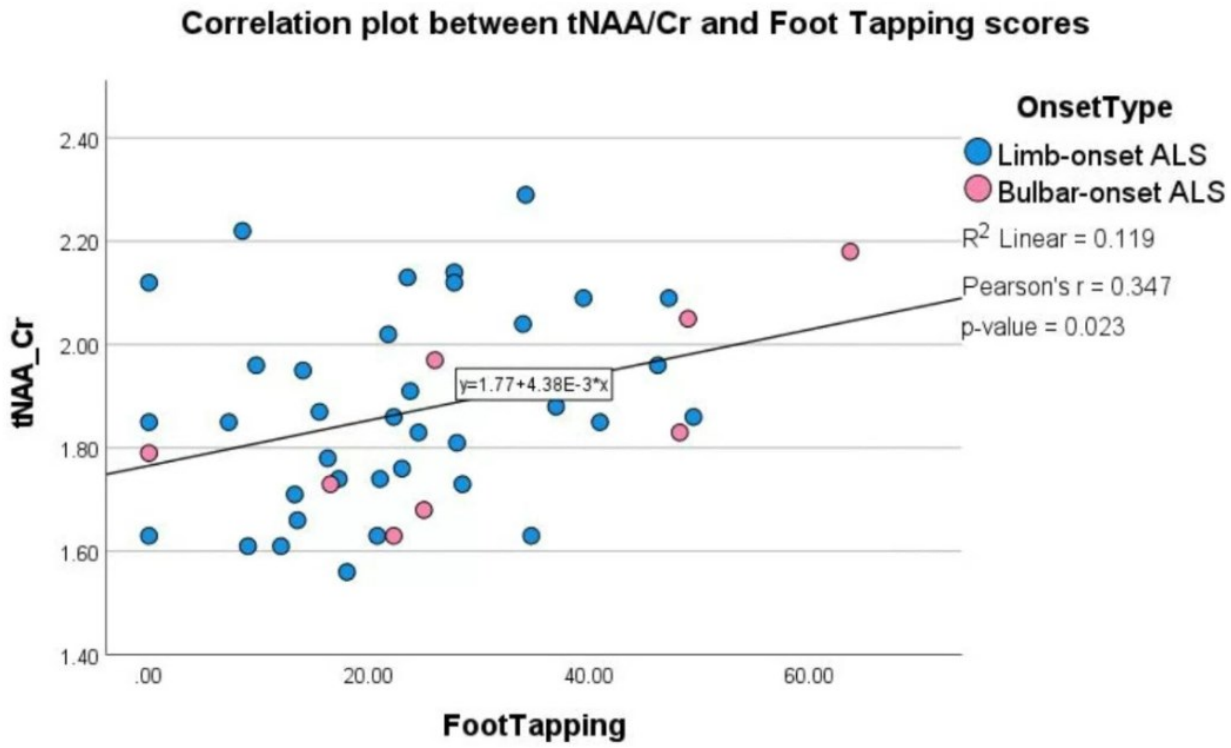

5.7.3.Conclusion

Due to the low sample size of ALS patients with bulbar-onset disease and no correlations between diffusion & neurochemical measures with FC differences in ALS patients with limb-onset disease, it is difficult to reliably interpret the findings in terms of the disease pathology. To ascertain whether the findings in the main study were driven by bulbar-onset ALS patients, we looked at the correlation plots between foot tapping frequencies and WM FA, tNAA/Cr. We did not observe any such evidence.

5.8. Author contributorship statement

AD analyzed and interpreted data and drafted the manuscript for intellectual content. CL acquired data and revised the manuscript for intellectual content. AI, DT, and OS analyzed data and revised

the manuscript for intellectual content. DK acquired data and revised the manuscript for intellectual content. PS contributed to MRI acquisition and revised the manuscript for intellectual content. CH contributed to the design of the MRS protocol, analyzed data, and revised the manuscript for intellectual content. CB contributed to the study design and revised the manuscript for intellectual content. LK, RF, LZ, SG, AG, and HB acquired data and revised the manuscript for intellectual content. SK contributed to the design and conceptualization of the study, acquired, analyzed and interpreted the data, and revised the manuscript for intellectual content.

5.9. Competing interest statement

The authors have no competing interests.

5.10. Ethics approvals

This study involves human participants and was approved by the Health Research Ethics Board, University of Alberta (reference number: Pro00036028), the Conjoint Health Research Ethics Board, University of Calgary (reference number: REB13-0651), the Research Ethics Office, Sunnybrook Health Sciences Centre (reference number: 445-2013), the Ethics Board, The Neuro, McGill University (reference number: NEU-13-016), and the Office of Research Ethics, University of British Columbia (reference number: H16-00528). Participants gave informed consent to participate in the study before taking part.

5.11. Funding information

The CALSNIC study was funded by the Canadian Institutes of Health Research fund (grant/award number: 123534), the ALS Society of Canada, Brain Canada, and the Shelly Mrkonjic Research Fund.

Chapter 6: General discussion

The objective of this thesis was to characterize markers of cerebral impairments in early pathophysiological disease in ALS. This could provide a better understanding of the distinctiveness of disease mechanisms in early and advanced disease and provide a step towards bridging the gap in understanding of the coherence between biological and clinical characterizations of the ALS disease process. This could allow physicians to accurately diagnose and stage ALS patients, making it possible for them to follow a personalized treatment strategy. Such personalized treatments could improve clinical function for patients as well as improve quality-of-life for patients and their caregivers. However, as such characterization of early disease markers is hindered by an inadequate understanding of disease mechanisms as well as the use of clinical function measures to assess disease severity, this thesis aimed to undertake an assessment of clinical and biological characteristics of the ALS disease process in patients experiencing different extents of disease severity. Patients were subgrouped based on two major classes of stratification criteria: imaging-derived (data-driven) and clinically-defined criteria. An assessment of the clinical and neuroimaging (resting-state functional activation and connectivity) features for these

patients was performed at baseline and longitudinal evaluations, following which an assessment of the cerebral neuroanatomical features (structure and chemical concentrations) was performed to identify the biology underlying functional impairment of cerebral resting-state networks.

In chapter 2, two distinct patient subgroups were identified using imaging-derived subgrouping. These patient subgroups were distinct in terms of their clinical and resting-state network characteristics. The spatial extents of alterations in network connectivity between imaging-derived patient subgroups were greater than that between patients identified using clinically-defined subgrouping criteria. These findings would suggest that imaging-derived measures were more sensitive to interindividual similarities in cerebral disease pathophysiology across patients as compared to clinically-defined measures, and therefore can be considered as a viable method for patient stratification in clinical drug trials. Additionally, this chapter utilized a template-based rotation (Schultz et al. 2014) analysis method to obtain maps of functional connectivity. An advantage of this method is that it is able to use external templates that are derived from a larger healthy population than that in the current study to estimate functional connectivity, as opposed to other existing methods. This helps in the removal of sample size requirements (to generate group-specific templates) and makes it possible to process single-subject data (due to the inversion of directionality when predicting functional connectivity maps at an individual level) while also maintaining spatial and temporal coherence between components. This is the first time in ALS literature that the template-based rotation method has been utilized for the estimation of distinct resting-state networks of the human connectome.

Chapter 3 aimed to evaluate disease evolution patterns at the level of cerebral networks in clinically-defined patient subgroups (identified in Chapter 2). Specifically, the aim was to examine whether clinically-defined patient subgrouping criteria were sensitive to the identification of longitudinal alterations in functional connectivity despite their non-sensitivity to the identification of functional connectivity alterations at baseline (as outlined in Chapter 2). Of the three applied clinically-defined criteria , Criteria 1 (devised on the clinical trial criteria for Riluzole) was able to

identify longitudinal functional connectivity impairments across patient subgroups in brain regions underlying motor encoding (action observation and motor imagery) and working memory. While Criteria 3 (based on the median disease progression rate of the complete ALS cohort) was able to identify functional connectivity alterations in brain regions subserving motor imagery, Criteria 2 (devised on clinical trial criteria for Edaravone) was unable to identify any differences in functional connectivity across subgroups. Therefore, Criteria 1 seemed to show the greatest sensitivity in the identification of longitudinal functional connectivity alterations across multiple networks. This study also further dissected the progressive dependence of the primary motor cortical regions on the premotor and supplementary motor areas as an adaptive response to the impairment of motor cortical function, potentially adding more granularity to the understanding of disease spreading mechanisms in ALS.

Chapter 4 aimed to evaluate disease evolution patterns at the level of cerebral networks in imaging-derived patient subgroups (identified in Chapter 2). Specifically, the aims were to assess whether disease evolved differently in the two patient subgroups and whether the postulated disease evolution patterns at baseline were in accordance with actual patterns of disease evolution. The study observed patients in Subtype 1 to have a more severe disease compared to patients in Subtype 2 based on longitudinal disease evolution, similar to the observations at baseline. While Subtype 1 patients were observed to have a predominantly motor phenotype of longitudinal change, Subtype 2 patients had an additional frontotemporal pattern of change. As patients with early manifestation of cognitive decline tend to drop out of longitudinal studies as shown in ALS (Chiò et al. 2019b), it might be possible that the longitudinal patterns of alterations and their corresponding clinical manifestations follow the same trajectory in both groups of patients, albeit with differences in the rates of the incidence of progressive changes. Due to the established correspondence in the literature between motor and cognitive impairments, and evidence from the current study, it seems apparent that monitoring the neuroanatomical health of neurons constituting the motor network might be beneficial towards providing insights into the disease process and in the potential development of a biomarker.

Chapter 5 aimed to uncover the neuroanatomical features that were associated with functional connectivity impairments of the primary motor cortex in ALS. Of the two neuroanatomical measures assessed (i.e., neurochemical concentrations and diffusion properties), both were correlated with clinical measures of upper motor neuron function, while only neurochemical concentrations were associated with functional connectivity alterations of the primary motor cortex. The findings of this study suggest that it is important to identify methods to improve the concentrations of N-acetyl aspartate (NAA) in the primary motor cortex early in the disease process, as this neurochemical seems to have a direct correlation with functional connectivity impairments of the primary motor cortical network. Potentially, based on the findings of this study, for motor network connectivity to undergo a smaller spatial extent of functional connectivity impairments, the concentrations of this neurochemical would need to be higher – perhaps alluding to the neuroprotective effects of NAA. Previously in the literature, increased spatial extent of activation was observed outside the primary motor cortical regions during the execution of a motor task (Mohammadi et al. 2011). Given the coherence in findings of the current thesis and previous studies in the literature, it might be prudent to extend the improvement of NAA using targeted drug therapies to people who are at risk of developing ALS. This could include first-degree relatives of patients with ALS, and potentially other related neurodegenerative conditions such as patients with diagnoses belonging in the frontotemporal dementia spectrum.

There is evidence of various modes of therapeutic interventions leading to improvement of motor function at the level of the upper motor neurons. For example, administration of noradrenergic enhancing drugs has been shown to improve motor performance, reduce the intrinsic activation of the motor network and the degree of functional connectivity alterations of the motor network (L. E. Wang et al. 2011). In patients with moderate-to-severe upper limb impairments, motor imagery training has been shown to reduce compensatory reorganization of the motor network and protect against ipsilateral alterations in motor functional connectivity resulting in improved motor outcomes (H. Wang et al. 2023). The utilization of brain-computer interfaces for 12 weeks has been shown to result in a decrease in motor network hyperactivation and the spatial extent of motor functional connectivity impairments (Humphries et al. 2022). Different modes of therapeutic

interventions previously published or based on the findings of Chapter 5 in this thesis, included as part of the standard-of-care of patients with ALS, might be helpful in improving clinical and neurological functional outcomes and potentially help improve patient survival while maintaining a better quality of life.

Despite the findings presented in this thesis, there are some limitations, in the current thesis and the literature in general, that need to be addressed. The first is the non-comparability of baseline and longitudinal functional MRI processing pipelines in terms of data handling. The additive effects of the use of baseline and longitudinal ComBat harmonization algorithms can result in differences in estimating functional activations within resting-state network. These limitations can be mitigated by conducting a step-wise study of these effects on resting-brain function (and potentially extended to other modalities) on brains that are scanned more than once. This would allow for rigorous quality control at baseline and longitudinally. Although the preprocessing and harmonization algorithms would be expected to minimize data manipulation to accurately provide relevant information without introducing more noise, there is a possibility that the differences in the methods of handling data by these algorithms could lead to more noisy data. Secondly, despite the use of patient subgrouping criteria devised on clinical trial-based patient stratification, an investigation of the effects of drug therapies on cerebral function were not conducted in this thesis. One major impediment to such investigation is that the mechanism of action of drugs such as Riluzole and Edaravone are not completely understood. Therefore, without a hypothesis-driven approach to identifying specific effects of these drugs, it would be challenging to examine the pharmacodynamic impact of these drugs on cerebral function. Another impediment to such investigation is the lack of a prospective, randomized, and controlled evaluation of drug effects on cerebral function. Thirdly, due to the lack of an effective clinical or neuroimaging-based biomarker of ALS, patients may present with multiple co-occurring pathologies that mimic the symptoms of ALS but may not be relevant to ALS. Disorders such as primary lateral sclerosis and progressive muscular atrophy are considered to be subtypes of ALS as there is impairment of upper motor neurons and lower motor neurons respectively in these conditions. However, co-occurring pathologies that mimic the clinical signs of ALS can not be identified until a postmortem

evaluation of brain and spinal cord tissue can be conducted. A patient mimicking the clinical signs of ALS was identified at the ALS Clinic in Edmonton (case report (Dey et al. 2021)).

In conclusion, the findings of this thesis strongly suggest that patient stratification efforts need to conduct objective evaluations of both upper and lower motor neuron function using multimodal clinical and imaging approaches, where applicable, in order to stratify their patients. The findings of this thesis also suggest the inclusion of imaging-based upper motor neuron measures as tools for disease tracking and monitoring in addition to lower motor neuron-driven clinical measures in clinical trials.

References

A, Al-Chalabi et al. 2010. “An Estimate of Amyotrophic Lateral Sclerosis Heritability Using Twin Data.” *Journal of neurology, neurosurgery, and psychiatry* 81(12): 1324–26. https://pubmed.ncbi.nlm.nih.gov/20861059/ (October 22, 2021).

Abe, Koji et al. 2017. “Safety and Efficacy of Edaravone in Well Defined Patients with Amyotrophic Lateral Sclerosis: A Randomised, Double-Blind, Placebo-Controlled Trial.” *The Lancet Neurology* 16(7): 505–12.

Abidi, M et al. 2019. “Adaptive Functional Reorganization in Amyotrophic Lateral Sclerosis: Coexisting Degenerative and Compensatory Changes.” *European Journal of Neurology* 0: 1–8. https://onlinelibrary.wiley.com/doi/pdf/10.1111/ene.14042 (August 14, 2019).

Abidi, Malek et al. 2021. “Neural Correlates of Motor Imagery of Gait in Amyotrophic Lateral Sclerosis.” *Journal of Magnetic Resonance Imaging* 53(1): 223–33. https://onlinelibrary-wiley-com.login.ezproxy.library.ualberta.ca/doi/full/10.1002/jmri.27335 (September 1, 2023).

———. 2022. “Motor Imagery in Amyotrophic Lateral Sclerosis: An FMRI Study of Postural Control.” *NeuroImage. Clinical* 35. https://pubmed.ncbi.nlm.nih.gov/35598461/ (September 1, 2023).

Agosta, Federica et al. 2013a. “Divergent Brain Network Connectivity in Amyotrophic Lateral Sclerosis.” *Neurobiology of Aging* 34(2): 419–27.

———. 2013b. “Divergent Brain Network Connectivity in Amyotrophic Lateral Sclerosis.” *Neurobiology of Aging* 34(2): 419–27.

———. 2014. “Intrahemispheric and Interhemispheric Structural Network Abnormalities in PLS and ALS.” *Human Brain Mapping* 35(4): 1710–22.

Agosta, Federica, Edoardo Gioele Spinelli, and Massimo Filippi. 2018. “Neuroimaging in Amyotrophic Lateral Sclerosis: Current and Emerging Uses.” *Expert Review of*

Neurotherapeutics 18(5): 395–406. https://doi.org/10.1080/14737175.2018.1463160.

Amunts, Katrin, Hartmut Mohlberg, Sebastian Bludau, and Karl Zilles. 2020. "Julich-Brain: A 3D Probabilistic Atlas of the Human Brain's Cytoarchitecture." *Science* 369(6506): 988–92. https://ebrains.eu (November 21, 2023).

Arsenault, Theodore et al. 2021. "Evaluation of Eddy Current Distortion and Field Inhomogeneity Distortion Corrections in MR Diffusion Imaging Using Log-Demons DIR Method." *Physics in Medicine and Biology* 66(3).

Ayala, Youhna M. et al. 2008. "Structural Determinants of the Cellular Localization and Shuttling of TDP-43." *Journal of Cell Science* 121(22): 3778–85. http://jcs.biologists.org/cgi/content/full/121/22/3778/DC1 (November 20, 2021).

Azhar, Syifa, and Le Roy Chong. 2023. "Clinician's Guide to the Basic Principles of MRI." *Postgraduate Medical Journal* 99: 894–903. https://doi.org/10.1136/pmj-2022-141998 (November 20, 2023).

Bakulin, Ilya S. et al. 2016. "Motor Cortex Hyperexcitability, Neuroplasticity, and Degeneration in Amyotrophic Lateral Sclerosis." *Update on Amyotrophic Lateral Sclerosis*. https://www.intechopen.com/chapters/50745 (September 5, 2023).

Barker, Peter B. et al. 2010. "Introduction to MR Spectroscopy in Vivo." *Clinical MR Spectroscopy* (1965): 1–18.

Barré-Sinoussi, Françoise, and Xavier Montagutelli. 2015. "Animal Models Are Essential to Biological Research: Issues and Perspectives." *Future Science OA* 1(4). /pmc/articles/PMC5137861/ (November 24, 2021).

Bear, Mark. 2016. 122 Anesthesia and Analgesia *Textbook of Neuroscience*.

Bede, Peter et al. 2022a. "Clusters of Anatomical Disease-Burden Patterns in ALS: A Data-Driven Approach Confirms Radiological Subtypes." *Journal of Neurology* 269(8): 4404. /pmc/articles/PMC9294023/ (January 9, 2023).

———. 2022b. “Clusters of Anatomical Disease-Burden Patterns in ALS: A Data-Driven Approach Confirms Radiological Subtypes.” *Journal of Neurology* 269(8): 4404–13. https://doi.org/10.1007/s00415-022-11081-3.

Beer, Joanne C. et al. 2020. “Longitudinal ComBat: A Method for Harmonizing Longitudinal Multi-Scanner Imaging Data.” *NeuroImage* 220: 117129.

Benatar, Michael et al. 2018. “Neurofilament Light: A Candidate Biomarker of Presymptomatic Amyotrophic Lateral Sclerosis and Phenoconversion.” *Annals of Neurology* 84(1): 130–39. https://onlinelibrary.wiley.com/doi/10.1002/ana.25276 (November 6, 2023).

———. 2022. “Mild Motor Impairment as Prodromal State in Amyotrophic Lateral Sclerosis: A New Diagnostic Entity.” *Brain* 145(10): 3500–3508. https://dx.doi.org/10.1093/brain/awac185 (September 5, 2023).

Benatar, Michael, Martin R. Turner, and Joanne Wuu. 2019. “Defining Pre-Symptomatic Amyotrophic Lateral Sclerosis.” *Amyotrophic lateral sclerosis & frontotemporal degeneration* 20(5–6): 303. /pmc/articles/PMC6613999/ (September 5, 2023).

Bensimon, G., L. Lacomblez, and V. Meininger. 1994. “A Controlled Trial of Riluzole in Amyotrophic Lateral Sclerosis.” *New England Journal of Medicine* 330(9): 585–91. http://www.nejm.org/doi/abs/10.1056/NEJM199403033300901 (December 7, 2019).

Berlot, Eva, Nicola J. Popp, and Jörn Diedrichsen. 2020. “A Critical Re-Evaluation of Fmri Signatures of Motor Sequence Learning.” *eLife* 9: 1–24.

Bharti, Komal et al. 2020. “Involvement of the Dentate Nucleus in the Pathophysiology of Amyotrophic Lateral Sclerosis: A Multi-Center and Multi-Modal Neuroimaging Study.” *NeuroImage : Clinical* 28. /pmc/articles/PMC7476068/ (June 23, 2023).

———. 2022. “Functional Alterations in Large-Scale Resting-State Networks of Amyotrophic Lateral Sclerosis: A Multi-Site Study across Canada and the United States.” *PLoS ONE* 17(6 June). https://pubmed.ncbi.nlm.nih.gov/35709100/ (September 20, 2022).

Biswal, Bharat, F. Zerrin Yetkin, Victor M. Haughton, and James S. Hyde. 1995. "Functional Connectivity in the Motor Cortex of Resting Human Brain Using Echo-Planar Mri." *Magnetic Resonance in Medicine* 34(4): 537–41. http://doi.wiley.com/10.1002/mrm.1910340409 (June 24, 2020).

Blasco, H., S. Mavel, P. Corcia, and P.H. Gordon. 2014. "The Glutamate Hypothesis in ALS: Pathophysiology and Drug Development." *Current Medicinal Chemistry* 21(31): 3551–75.

Bohannon, R. W., and M. B. Smith. 1987. "Interrater Reliability of a Modified Ashworth Scale of Muscle Spasticity." *Physical Therapy* 67(2): 206–7. https://academic.oup.com/ptj/article/67/2/206/2728158 (November 25, 2021).

Van Den Bos, Mehdi A J et al. 2019. "Molecular Sciences Pathophysiology and Diagnosis of ALS: Insights from Advances in Neurophysiological Techniques." www.mdpi.com/journal/ijms (October 20, 2021).

Van Den Bosch, L., P. Van Damme, E. Bogaert, and W. Robberecht. 2006. "The Role of Excitotoxicity in the Pathogenesis of Amyotrophic Lateral Sclerosis." *Biochimica et Biophysica Acta - Molecular Basis of Disease* 1762(11–12): 1068–82.

Boylan, Kevin. 2015. "Familial Amyotrophic Lateral Sclerosis." *Neurologic Clinics* 33(4): 807–30. http://dx.doi.org/10.1016/j.ncl.2015.07.001.

Braak, Heiko et al. 2013. "Amyotrophic Lateral Sclerosis - A Model of Corticofugal Axonal Spread." *Nature Reviews Neurology* 9(12): 708–14. https://www.nature.com/articles/nrneurol.2013.221 (October 23, 2021).

Brooks, Benjamin Rix. 1994. "El Escorial World Federation of Neurology Criteria for the Diagnosis of Amyotrophic Lateral Sclerosis." *Journal of the Neurological Sciences* 124(SUPPL.): 96–107.

Brooks, Benjamin Rix, Robert G. Miller, Michael Swash, and Theodore L. Munsat. 2000. "El Escorial Revisited: Revised Criteria for the Diagnosis of Amyotrophic Lateral Sclerosis." *Amyotrophic Lateral Sclerosis* 1(5): 293–99.

Brown, Robert H., and Ammar Al-Chalabi. 2017. “Amyotrophic Lateral Sclerosis” ed. Dan L. Longo. *New England Journal of Medicine* 377: 162–72. http://www.nejm.org/doi/10.1056/NEJMra1603471 (April 9, 2021).

Buckner, Randy L. et al. 2009. “Cortical Hubs Revealed by Intrinsic Functional Connectivity: Mapping, Assessment of Stability, and Relation to Alzheimer’s Disease.” *Journal of Neuroscience* 29(6): 1860–73.

Bueno, Ana Paula Arantes et al. 2019. “Regional Dynamics of the Resting Brain in Amyotrophic Lateral Sclerosis Using Fractional Amplitude of Low-Frequency Fluctuations and Regional Homogeneity Analyses.” *Brain Connectivity* 9(4): 356–64. www.liebertpub.com (August 15, 2019).

Buonocore, Michael H., and Richard J. Maddock. 2015. “Magnetic Resonance Spectroscopy of the Brain: A Review of Physical Principles and Technical Methods.” *Reviews in the Neurosciences* 26(6): 609–32.

Calhoun, Vince D, and Tülay Adali. 2006. “Unmixing FMRI with Independent Component Analysis - Using ICA to Characterize High-Dimensional FMRI Data in a Concise Manner.” *Ieee Engineering in Medicine and Biology Magazine* 25(2): 79–90.

de Carvalho, Mamede et al. 2008. “Electrodiagnostic Criteria for Diagnosis of ALS.” *Clinical Neurophysiology* 119(3): 497–503.

Castelnovo, Veronica et al. 2020. “Progression of Brain Functional Connectivity and Frontal Cognitive Dysfunction in ALS.” *NeuroImage: Clinical* 28: 102509.

Chen, Sheng, Pavani Sayana, Xiaojie Zhang, and Weidong Le. 2013. “Genetics of Amyotrophic Lateral Sclerosis: An Update.” *Molecular Neurodegeneration* 8(1): 28. /pmc/articles/PMC3766231/ (October 22, 2021).

Chen, Xueping, Chunyan Guo, and Jiming Kong. 2012. “Oxidative Stress in Neurodegenerative Diseases.” *Neural Regeneration Research* 7(5): 376. /pmc/articles/PMC4350122/ (October 23, 2021).

Chen, Zhiye, and Lin Ma. 2010. “Grey Matter Volume Changes over the Whole Brain in Amyotrophic Lateral Sclerosis: A Voxel-Wise Meta-Analysis of Voxel Based Morphometry Studies.” *Amyotrophic Lateral Sclerosis* 11(6): 549–54. https://www.tandfonline.com/doi/abs/10.3109/17482968.2010.516265 (February 8, 2021).

Cheng, Luqi et al. 2021. “Structural and Functional Underpinnings of Precentral Abnormalities in Amyotrophic Lateral Sclerosis.” *European Journal of Neurology* (January): 1–9.

Chenji, Sneha et al. 2016. “Investigating Default Mode and Sensorimotor Network Connectivity in Amyotrophic Lateral Sclerosis” ed. Cristina Cereda. *PLoS ONE* 11(6): e0157443. https://dx.plos.org/10.1371/journal.pone.0157443 (December 7, 2019).

Chinnery, Patrick F et al. 2012. “Epigenetics, Epidemiology and Mitochondrial DNA Diseases.” *International Journal of Epidemiology* 41(1): 177–87. https://academic.oup.com/ije/article/41/1/177/649968 (October 22, 2021).

Chiò, Adriano et al. 2013. “Development and Evaluation of a Clinical Staging System for Amyotrophic Lateral Sclerosis.” http://jnnp.bmj.com/ (September 10, 2023).

———. 2015. “Development and Evaluation of a Clinical Staging System for Amyotrophic Lateral Sclerosis.” *Journal of Neurology, Neurosurgery and Psychiatry* 86(1): 38–44.

———. 2019a. “Cognitive Impairment across ALS Clinical Stages in a Population-Based Cohort.” *Neurology* 93(10): E984–94. /pmc/articles/PMC6745732/ (November 30, 2023).

———. 2019b. “Cognitive Impairment across ALS Clinical Stages in a Population-Based Cohort.” *Neurology* 93(10): e984. /pmc/articles/PMC6745732/ (November 30, 2023).

Chipika, Rangariroyashe et al. 2022. “Cerebellar Pathology in Motor Neuron Disease: Neuroplasticity and Neurodegeneration.” *Neural Regeneration Research* 17(11): 2335–41. www.nrronline.org (January 17, 2023).

Chipika, Rangariroyashe H. et al. 2022a. “Alterations in Somatosensory, Visual and Auditory Pathways in Amyotrophic Lateral Sclerosis: An under-Recognised Facet of ALS.” *Journal*

of Integrative Neuroscience 21(3): 88. https://www.imrpress.com/journal/JIN/21/3/10.31083/j.jin2103088/htm (February 3, 2023).

Chipika, Rangariroyashe H et al. 2022b. "Alterations in Somatosensory, Visual and Auditory Pathways in Amyotrophic Lateral Sclerosis: An under-Recognised Facet of ALS." *Journal of Integrative Neuroscience* 21(3).

Christidi, Foteini et al. 2018. "Clinical and Radiological Markers of Extra-Motor Deficits in Amyotrophic Lateral Sclerosis." *Frontiers in Neurology* 9(NOV): 1005. /pmc/articles/PMC6262087/ (April 9, 2021).

Collins, D. Louis, Terence M. Peters, Weiqian Dai, and Alan C. Evans. 1992. "Model-Based Segmentation of Individual Brain Structures from MRI Data." *https://doi.org/10.1117/12.131063* 1808: 10–23. https://www.spiedigitallibrary.org/conference-proceedings-of-spie/1808/0000/Model-based-segmentation-of-individual-brain-structures-from-MRI-data/10.1117/12.131063.full (November 7, 2021).

Consonni, Monica et al. 2018. "Cortical Markers of Cognitive Syndromes in Amyotrophic Lateral Sclerosis." *NeuroImage: Clinical* 19(October 2017): 675–82. https://doi.org/10.1016/j.nicl.2018.05.020.

———. 2020. "Cortical Thinning Trajectories across Disease Stages and Cognitive Impairment in Amyotrophic Lateral Sclerosis." *Cortex; a journal devoted to the study of the nervous system and behavior* 131: 284–94. https://pubmed.ncbi.nlm.nih.gov/32811660/ (October 12, 2023).

Consonni, Monica, Eleonora Dalla Bella, Enrica Bersano, and Giuseppe Lauria. 2021. "Cognitive and Behavioural Impairment in Amyotrophic Lateral Sclerosis: A Landmark of the Disease? A Mini Review of Longitudinal Studies." *Neuroscience Letters* 754: 135898. https://doi.org/10.1016/j.neulet.2021.135898 (September 8, 2023).

Crockford, Christopher et al. 2018. "ALS-Specific Cognitive and Behavior Changes Associated

with Advancing Disease Stage in ALS." *Neurology* 91(15): E1370–80. http://dx.doi.org/10. (July 3, 2023).

D'Souza, Gary X. et al. 2021. "The Application of in Vitro-Derived Human Neurons in Neurodegenerative Disease Modeling." *Journal of Neuroscience Research* 99(1): 124–40.

Dawson, Ted M., Todd E. Golde, and Clotilde Lagier-Tourenne. 2018. "Animal Models of Neurodegenerative Diseases." *Nature Neuroscience 2018 21:10* 21(10): 1370–79. https://www.nature.com/articles/s41593-018-0236-8 (November 23, 2021).

Desikan, Rahul S. et al. 2006. "An Automated Labeling System for Subdividing the Human Cerebral Cortex on MRI Scans into Gyral Based Regions of Interest." *NeuroImage* 31(3): 968–80.

Dey, Avyarthana et al. 2021. "Mixed Pathologies Mimicking Motor Neuron Disease: A Case Report and Review of the Literature." *Folia Neuropathologica* 59(4): 403–8. https://doi.org/10.5114/fn.2021.111486 (November 21, 2023).

———. 2022. "Motor Cortex Functional Connectivity Is Associated with Underlying Neurochemistry in ALS." *Journal of neurology, neurosurgery, and psychiatry* 0: jnnp-2022-329993. https://jnnp.bmj.com/content/early/2022/11/15/jnnp-2022-329993 (December 15, 2022).

Douaud, Gwenaëlle et al. 2011. "Integration of Structural and Functional Magnetic Resonance Imaging in Amyotrophic Lateral Sclerosis." In *Brain*, , 3467–76. www.fmrib.ox.ac.uk/fsl (December 7, 2019).

Doucet, Gaëlle et al. 2011. "Brain Activity at Rest: A Multiscale Hierarchical Functional Organization." *Journal of Neurophysiology* 105(6): 2753–63.

van Eijk, Ruben P.A. et al. 2021. "Innovating Clinical Trials for Amyotrophic Lateral Sclerosis: Challenging the Established Order." *Neurology* 97(11): 528–36.

Eisen, Andrew et al. 2015. "Does Dysfunction of the Mirror Neuron System Contribute to

Symptoms in Amyotrophic Lateral Sclerosis?" http://dx.doi.org/10.1016/j.clinph.2015.02.003 (September 7, 2023).

Eisen, Andrew, Matthew Kiernan, Hiroshi Mitsumoto, and Michael Swash. 2014. "Amyotrophic Lateral Sclerosis: A Long Preclinical Period?" *Journal of Neurology, Neurosurgery and Psychiatry* 85(11): 1232–38.

Elamin, Marwa et al. 2013. "Cognitive Changes Predict Functional Decline in ALS: A Population-Based Longitudinal Study." *Neurology* 80(17): 1590–97. https://n.neurology.org/content/80/17/1590 (November 30, 2023).

Esposito, Sabrina et al. 2022. "Repetitive Transcranial Magnetic Stimulation (RTMS) of Dorsolateral Prefrontal Cortex May Influence Semantic Fluency and Functional Connectivity in Fronto-Parietal Network in Mild Cognitive Impairment (MCI)." *Biomedicines* 10(5).

Factor-Litvak, Pam et al. 2013. "Current Pathways for Epidemiological Research in Amyotrophic Lateral Sclerosis." *http://dx.doi.org/10.3109/21678421.2013.778565* 14(SUPPL1): 33–43. https://www.tandfonline.com/doi/abs/10.3109/21678421.2013.778565 (November 24, 2021).

Fang, Ton et al. 2018. "Stage at Which Riluzole Treatment Prolongs Survival in Patients with Amyotrophic Lateral Sclerosis: A Retrospective Analysis of Data from a Dose-Ranging Study." *The Lancet Neurology* 17(5): 416–22.

Fang, Xiaojing et al. 2016. "Disrupted Effective Connectivity of the Sensorimotor Network in Amyotrophic Lateral Sclerosis." *Journal of Neurology* 263(3): 508–16. https://pubmed.ncbi.nlm.nih.gov/26743627/ (April 9, 2021).

Fiori, F. et al. 2013. "Exploring Motor and Visual Imagery in Amyotrophic Lateral Sclerosis." *Experimental brain research* 226(4): 537–47. https://pubmed.ncbi.nlm.nih.gov/23503773/ (September 1, 2023).

Floeter, Mary Kay, Laura E. Danielian, Laura E. Braun, and Tianxia Wu. 2018. "Longitudinal

Diffusion Imaging across the C9orf72 Clinical Spectrum." *Journal of neurology, neurosurgery, and psychiatry* 89(1): 53–60. https://pubmed.ncbi.nlm.nih.gov/29054917/ (October 12, 2023).

Foerster, B. R. et al. 2012. "Decreased Motor Cortex γ-Aminobutyric Acid in Amyotrophic Lateral Sclerosis." *Neurology* 78(20): 1596–1600. /pmc/articles/PMC3348851/?report=abstract (November 4, 2020).

Foerster, Bradley R. et al. 2012. "Diagnostic Accuracy Using Diffusion Tensor Imaging in the Diagnosis of ALS. A Meta-Analysis." *Academic Radiology* 19(9): 1075–86. http://www.academicradiology.org/article/S1076633212002322/fulltext (February 8, 2021).

———. 2013. "An Imbalance between Excitatory and Inhibitory Neurotransmitters in Amyotrophic Lateral Sclerosis Revealed by Use of 3-t Proton Magnetic Resonance Spectroscopy." *JAMA Neurology* 70(8): 1009–16.

———. 2014. "Multimodal MRI as a Diagnostic Biomarker for Amyotrophic Lateral Sclerosis." *Annals of Clinical and Translational Neurology* 1(2): 107–14. http://doi.wiley.com/10.1002/acn3.30 (December 7, 2019).

Fornito, Alex, Andrew Zalesky, and Michael Breakspear. 2015. "The Connectomics of Brain Disorders." *Nature Reviews Neuroscience* 16(3): 159–72. http://dx.doi.org/10.1038/nrn3901.

Fortin, Jean Philippe et al. 2017. "Harmonization of Multi-Site Diffusion Tensor Imaging Data." *NeuroImage* 161(July): 149–70. https://doi.org/10.1016/j.neuroimage.2017.08.047.

Foster, Brett L et al. 2023. "A Tripartite View of the Posterior Cingulate Cortex." *Nature Reviews Neuroscience* 24(3): 173–89. https://doi.org/10.1038/s41583-022-00661-x (July 13, 2023).

Genge, Angela, and Adriano Chio. 2023. "The Future of ALS Diagnosis and Staging: Where Do We Go from Here?" *Amyotrophic Lateral Sclerosis and Frontotemporal Degeneration* 24(3–4): 165–74.

https://www.tandfonline.com/action/journalInformation?journalCode=iafd20 (September 10, 2023).

Genin, Emmanuelle C et al. 2016. “CHCHD10 Mutations Promote Loss of Mitochondrial Cristae Junctions with Impaired Mitochondrial Genome Maintenance and Inhibition of Apoptosis.” *EMBO Molecular Medicine* 8(1): 58. /pmc/articles/PMC4718158/ (October 22, 2021).

George, Allan, Ruben Kuzniecky, Henry Rusinek, and Heath R. Pardoe. 2020. “Standardized Brain MRI Acquisition Protocols Improve Statistical Power in Multicenter Quantitative Morphometry Studies.” *Journal of Neuroimaging* 30(1): 126–33. /pmc/articles/PMC7391934/ (April 9, 2021).

Gosselt, Isabel K., Tanja C.W. Nijboer, and Michael A. Van Es. 2020. “An Overview of Screening Instruments for Cognition and Behavior in Patients with ALS: Selecting the Appropriate Tool for Clinical Practice.” *Amyotrophic Lateral Sclerosis and Frontotemporal Degeneration* 21(5–6): 324–36. https://www.tandfonline.com/doi/abs/10.1080/21678421.2020.1732424 (November 26, 2021).

Goutman, Stephen A. 2017. “Diagnosis and Clinical Management of Amyotrophic Lateral Sclerosis and Other Motor Neuron Disorders.” *CONTINUUM Lifelong Learning in Neurology* 23(5, Peripheral Nerve and Motor Neuron Disorders): 1332–59.

Govaarts, Rosanne et al. 2022. “Cortical and Subcortical Changes in Resting-State Neuronal Activity and Connectivity in Early Symptomatic ALS and Advanced Frontotemporal Dementia.” *NeuroImage. Clinical* 34. https://pubmed.ncbi.nlm.nih.gov/35217500/ (September 20, 2022).

Gregory, Sarah et al. 2017. “Operationalizing Compensation over Time in Neurodegenerative Disease.” *Brain* 140(4): 1158–65.

Hal Blumenfeld. 2010. 148 *Neuroanatomy through Clinical Cases*.

Hammer, Anke et al. 2011. “A Neurophysiological Analysis of Working Memory in Amyotrophic Lateral Sclerosis.”

Hardiman, Orla et al. 2017. “Amyotrophic Lateral Sclerosis.” *Nature Reviews Disease Primers* 3: 17071. www.nature.com/nrdp (September 10, 2021).

Henschke, Julia U., and Janelle M.P. Pakan. 2023. “Engaging Distributed Cortical and Cerebellar Networks through Motor Execution, Observation, and Imagery.” *Frontiers in Systems Neuroscience* 17(April): 1–11.

van den Heuvel, Martijn P., and Olaf Sporns. 2011. “Rich-Club Organization of the Human Connectome.” *Journal of Neuroscience* 31(44): 15775–86.

Hosni, Sarah M. et al. 2019. “An Exploration of Neural Dynamics of Motor Imagery for People with Amyotrophic Lateral Sclerosis.” *Journal of neural engineering* 17(1). https://pubmed.ncbi.nlm.nih.gov/31597125/ (September 1, 2023).

Humphries, Joseph B. et al. 2022. “Motor Network Reorganization Induced in Chronic Stroke Patients with the Use of a Contralesionally-Controlled Brain Computer Interface.” *Brain-Computer Interfaces* 9(3): 179–92. https://doi.org/10.1080/2326263X.2022.2057757.

Ishaque, Abdullah et al. 2019. “Corticospinal Tract Degeneration in ALS Unmasked in T1-Weighted Images Using Texture Analysis.” *Human Brain Mapping* 40(4): 1174–83. https://onlinelibrary.wiley.com/doi/abs/10.1002/hbm.24437 (May 9, 2019).

Jelsone-Swain, Laura, Carol Persad, David Burkard, and Robert C. Welsh. 2015. “Action Processing and Mirror Neuron Function in Patients with Amyotrophic Lateral Sclerosis: An FMRI Study” ed. Marco Iacoboni. *PLoS ONE* 10(4): e0119862. https://dx.plos.org/10.1371/journal.pone.0119862 (August 15, 2019).

Juchem, Christoph, and Douglas L. Rothman. 2013. “Basis of Magnetic Resonance.” *Magnetic Resonance Spectroscopy: Tools for Neuroscience Research and Emerging Clinical Applications*: 3–14.

Kalra, Sanjay. 2019. “Magnetic Resonance Spectroscopy in ALS.” *Frontiers in Neurology* 10(MAY). https://www.frontiersin.org/article/10.3389/fneur.2019.00482/full (December 7, 2019).

Kalra, Sanjay, Hans Peter Müller, et al. 2020. “A Prospective Harmonized Multicenter DTI Study of Cerebral White Matter Degeneration in ALS.” *Neurology* 95(8): E943–52.

Kalra, Sanjay, Muhammad Umer Khan, et al. 2020. “The Canadian ALS Neuroimaging Consortium (CALSNIC) - A Multicentre Platform for Standardized Imaging and Clinical Studies in ALS.” *medRxiv*: 2020.07.10.20142679. https://doi.org/10.1101/2020.07.10.20142679 (November 8, 2020).

Kalra, Sanjay, Neil R. Cashman, Angela Genge, and Douglas L. Arnold. 1998. “Recovery of N-Acetylaspartate in Corticomotor Neurons of Patients with ALS after Riluzole Therapy.” *NeuroReport* 9(8): 1757–61.

Kalra, Sanjay, Peter Tai, Angela Genge, and Douglas L Arnold. 2006. “Introduction Rapid Improvement in Cortical Neuronal Integrity in Amyotrophic Lateral Sclerosis Detected by Proton Magnetic Resonance Spectroscopic Imaging.”

Kandel, Eric. 148 *Principles of Neural Science Fifth Edition*.

Karlsgodt, Katherine H. et al. 2008. “Developmental Disruptions in Neural Connectivity in the Pathophysiology of Schizophrenia.” *Development and Psychopathology* 20(4): 1297–1327.

Kashefi, Samira N., and Gavin P. Winston. 2020. “Diffusion Tensor Imaging.” *Neuroimaging Techniques in Clinical Practice: Physical Concepts and Clinical Applications*: 203–13.

Kobeleva, Xenia et al. 2021. “Brain Activity Is Contingent on Neuropsychological Function in a Functional Magnetic Resonance Imaging Study of Verbal Working Memory in Amyotrophic Lateral Sclerosis.” *European Journal of Neurology* 28(9): 3051–60.

Koubiyr, Ismail et al. 2019. “Dynamic Modular-Level Alterations of Structural-Functional Coupling in Clinically Isolated Syndrome.” *Brain* 142(11): 3428–39.

https://pubmed.ncbi.nlm.nih.gov/31504228/ (March 24, 2021).

Kraemer, Brian C. et al. 2010. “Loss of Murine TDP-43 Disrupts Motor Function and Plays an Essential Role in Embryogenesis.” *Acta Neuropathologica* 119(4): 409–19. https://link.springer.com/article/10.1007/s00401-010-0659-0 (November 20, 2021).

Leech, Robert, and David J. Sharp. 2014. “The Role of the Posterior Cingulate Cortex in Cognition and Disease.” *Brain* 137(1): 12–32.

Libon, David J. et al. 2012. “Deficits in Concept Formation in Amyotrophic Lateral Sclerosis.” *Neuropsychology* 26(4): 422. /pmc/articles/PMC3516292/ (September 8, 2023).

Liu, Shuangwu et al. 2021. “Hippocampal Subfield and Anterior-Posterior Segment Volumes in Patients with Sporadic Amyotrophic Lateral Sclerosis.” *NeuroImage. Clinical* 32. https://pubmed.ncbi.nlm.nih.gov/34655906/ (October 12, 2023).

Liu, Yi Hung, Shiuan Huang, and Yi De Huang. 2017. “Motor Imagery EEG Classification for Patients with Amyotrophic Lateral Sclerosis Using Fractal Dimension and Fisher’s Criterion-Based Channel Selection.” *Sensors (Basel, Switzerland)* 17(7). https://pubmed.ncbi.nlm.nih.gov/28671629/ (September 1, 2023).

Low, Audrey et al. 2019. “Hippocampal Subfield Atrophy of CA1 and Subicular Structures Predict Progression to Dementia in Idiopathic Parkinson’s Disease.” *Journal of Neurology, Neurosurgery and Psychiatry* 90(6): 681–87. https://pubmed.ncbi.nlm.nih.gov/30683708/ (March 24, 2021).

Lu, Jiaming et al. 2019. “Functional Connectivity between the Resting-State Olfactory Network and the Hippocampus in Alzheimer’s Disease.” *Brain Sciences* 9(12). https://pubmed.ncbi.nlm.nih.gov/31775369/ (March 24, 2021).

Lulé, Dorothée et al. 2007. “Cortical Plasticity in Amyotrophic Lateral Sclerosis: Motor Imagery and Function.” *Neurorehabilitation and Neural Repair* 21(6): 518–26.

Luo, Chun Yan et al. 2012. “Patterns of Spontaneous Brain Activity in Amyotrophic Lateral

Sclerosis: A Resting-State FMRI Study." *PLoS ONE* 7(9).

Mahmood, Faisal, and Rasmus Hvass Hansen. 2017. "Diffusion Weighted Magnetic Resonance Imaging for Detection of Tissue Electroporation In Vivo." *Handbook of Electroporation* 1–4: 723–43.

Mansfield, P. 1978. "Imaging by Nuclear Magnetic Resonance." 21: 18–30.

Marin, Benoît et al. 2017. "Variation in Worldwide Incidence of Amyotrophic Lateral Sclerosis: A Meta-Analysis." *International Journal of Epidemiology* 46(1): 57. /pmc/articles/PMC5407171/ (October 22, 2021).

McMillan, Corey T. et al. 2022. "Defining Cognitive Impairment in Amyotrophic Lateral Sclerosis: An Evaluation of Empirical Approaches." *Amyotrophic Lateral Sclerosis and Frontotemporal Degeneration*. https://www.informahealthcare.com/doi/abs/10.1080/21678421.2022.2039713 (December 14, 2022).

Mejzini, Rita et al. 2019. "ALS Genetics, Mechanisms, and Therapeutics: Where Are We Now?" *Frontiers in Neuroscience* 13(December): 1–27.

Menke, R. A.L., M. Proudfoot, K. Talbot, and M. R. Turner. 2018a. "The Two-Year Progression of Structural and Functional Cerebral MRI in Amyotrophic Lateral Sclerosis." *NeuroImage: Clinical* 17: 953–61.

———. 2018b. "The Two-Year Progression of Structural and Functional Cerebral MRI in Amyotrophic Lateral Sclerosis." *NeuroImage: Clinical* 17: 953–61. https://doi.org/10.1016/j.nicl.2017.12.025 (February 8, 2021).

Menke, Ricarda A. L. et al. 2014. "Widespread Grey Matter Pathology Dominates the Longitudinal Cerebral MRI and Clinical Landscape of Amyotrophic Lateral Sclerosis." *Brain* 137(9): 2546–55. https://academic.oup.com/brain/article-lookup/doi/10.1093/brain/awu162 (February 8, 2021).

Menke, Ricarda A.L. et al. 2012. “Fractional Anisotropy in the Posterior Limb of the Internal Capsule and Prognosis in Amyotrophic Lateral Sclerosis.” *Archives of Neurology* 69(11): 1493–99.

Menke, Ricarda A L et al. 2016. “Neuroimaging Endpoints in Amyotrophic Lateral Sclerosis.”

Menon, Parvathi et al. 2020. “Cortical Hyperexcitability Evolves with Disease Progression in ALS.” *Annals of Clinical and Translational Neurology* 7(5): 733–41.

Mohammadi, Bahram et al. 2009. “Changes of Resting State Brain Networks in Amyotrophic Lateral Sclerosis.” *Experimental Neurology* 217(1): 147–53.

———. 2011. “Functional Neuroimaging at Different Disease Stages Reveals Distinct Phases of Neuroplastic Changes in Amyotrophic Lateral Sclerosis.” *Human Brain Mapping* 32(5): 750–58. https://onlinelibrary.wiley.com/doi/full/10.1002/hbm.21064 (July 5, 2023).

———. 2015. “Amyotrophic Lateral Sclerosis Affects Cortical and Subcortical Activity Underlying Motor Inhibition and Action Monitoring.” *Human Brain Mapping* 36(8): 2878–89. http://doi.wiley.com/10.1002/hbm.22814 (August 15, 2019).

Monteverdi, Anita et al. 2022. “Subject-Specific Features of Excitation/Inhibition Profiles in Neurodegenerative Diseases.” *Frontiers in Aging Neuroscience* 14(August): 1–17.

Mukherjee, Pratik et al. 2008. “Diffusion Tensor MR Imaging and Fiber Tractography: Theoretic Underpinnings.” *American Journal of Neuroradiology* 29(4): 632–41.

Munzert, Jörn, and Karen Zentgraf. 2009. “Motor Imagery and Its Implications for Understanding the Motor System.” *Progress in Brain Research* 174: 219–29.

Nasseroleslami, Bahman et al. 2019. “Characteristic Increases in EEG Connectivity Correlate With Changes of Structural MRI in Amyotrophic Lateral Sclerosis.” *Cerebral Cortex* 29: 27–41. https://academic.oup.com/cercor/article/29/1/27/4608063 (September 9, 2023).

Ogura, Aya et al. 2019. “Semantic Deficits in ALS Related to Right Lingual/Fusiform Gyrus Network Involvement.” *EBioMedicine* 47: 506. /pmc/articles/PMC6796569/ (February 3,

2023).

Oh, Seong Il et al. 2014. “Spectrum of Cognitive Impairment in Korean ALS Patients without Known Genetic Mutations.” *PLoS ONE* 9(2). https://pubmed.ncbi.nlm.nih.gov/24498297/ (November 30, 2023).

Papitto, Giorgio, Angela D. Friederici, and Emiliano Zaccarella. 2020. “The Topographical Organization of Motor Processing: An ALE Meta-Analysis on Six Action Domains and the Relevance of Broca’s Region.” *NeuroImage* 206: 116321.

Park, Bo Yong, Kyoungseob Byeon, and Hyunjin Park. 2019. “FuNP (Fusion of Neuroimaging Preprocessing) Pipelines: A Fully Automated Preprocessing Software for Functional Magnetic Resonance Imaging.” *Frontiers in Neuroinformatics* 13: 5.

Park, Denise C., and Patricia Reuter-Lorenz. 2009. “The Adaptive Brain: Aging and Neurocognitive Scaffolding.” *Annual Review of Psychology* 60: 173–96. /pmc/articles/PMC3359129/ (August 17, 2023).

Phukan, Julie et al. 2012. “The Syndrome of Cognitive Impairment in Amyotrophic Lateral Sclerosis: A Population-Based Study.” *Journal of Neurology, Neurosurgery and Psychiatry* 83(1): 102–8. http://jnnp.bmj.com/ (November 30, 2023).

Pinto-Grau, Marta et al. 2021. “Patterns of Language Impairment in Early Amyotrophic Lateral Sclerosis.” *Neurology: Clinical Practice* 11(5): e634. /pmc/articles/PMC8610537/ (February 3, 2023).

Pizoli, Carolyn E. et al. 2011. “Resting-State Activity in Development and Maintenance of Normal Brain Function.” *Proceedings of the National Academy of Sciences of the United States of America* 108(28): 11638–43. https://www.pnas.org/doi/abs/10.1073/pnas.1109144108 (October 8, 2023).

Plewes, Donald B., and Walter Kucharczyk. 2012. “Physics of MRI: A Primer.” *Journal of Magnetic Resonance Imaging* 35(5): 1038–54.

Pradhan, Jonu, and Mark C. Bellingham. 2021. “Neurophysiological Mechanisms Underlying Cortical Hyper-Excitability in Amyotrophic Lateral Sclerosis: A Review.” *Brain Sciences* 11(5).

Proudfoot, Malcolm, Peter Bede, and Martin R. Turner. 2018. “Imaging Cerebral Activity in Amyotrophic Lateral Sclerosis.” *Frontiers in Neurology* 9(JAN): 1148. /pmc/articles/PMC6332509/ (June 29, 2023).

Qiu, Ting et al. 2019. “Precentral Degeneration and Cerebellar Compensation in Amyotrophic Lateral Sclerosis: A Multimodal MRI Analysis.” *Human Brain Mapping* 40(12): 3464–74. http://rfmri.org/DPARSF (August 14, 2019).

Raichle, Marcus E. 2015. “The Brain’s Default Mode Network.” *Annual Review of Neuroscience* 38(April): 433–47.

Ratai, Eva Maria et al. 2018. “Integrated Imaging of [11C]-PBR28 PET, MR Diffusion and Magnetic Resonance Spectroscopy 1H-MRS in Amyotrophic Lateral Sclerosis.” *NeuroImage: Clinical* 20: 357–64.

Reddy, P Hemachandra. 2008. “Mitochondrial Medicine for Aging and Neurodegenerative Diseases.”

Rektor, Ivan et al. 2018. “White Matter Alterations in Parkinson’s Disease with Normal Cognition Precede Grey Matter Atrophy.” *PLoS ONE* 13(1). https://pubmed.ncbi.nlm.nih.gov/29304183/ (March 24, 2021).

Renton, Alan E. et al. 2011. “A Hexanucleotide Repeat Expansion in C9ORF72 Is the Cause of Chromosome 9p21-Linked ALS-FTD.” *Neuron* 72(2): 257–68. https://reader.elsevier.com/reader/sd/pii/S0896627311007975?token=135223507361023BFEE27AA0E3F2C3421CA9626E3BFFC438818517E9C9F1AEB39EDA13F569FDFD67F706BBDE8E05101D&originRegion=us-east-1&originCreation=20211121032844 (November 20, 2021).

Reuter-Lorenz, Patricia A., and Denise C. Park. 2014. “How Does It STAC Up? Revisiting the

Scaffolding Theory of Aging and Cognition." *Neuropsychology Review* 24(3): 355–70. /pmc/articles/PMC4150993/ (August 17, 2023).

van Rheenen, Wouter et al. 2016. "Genome-Wide Association Analyses Identify New Risk Variants and the Genetic Architecture of Amyotrophic Lateral Sclerosis."

Richards, Danielle, John A. Morren, and Erik P. Pioro. 2020. "Time to Diagnosis and Factors Affecting Diagnostic Delay in Amyotrophic Lateral Sclerosis." *Journal of the Neurological Sciences* 417(March): 117054. https://doi.org/10.1016/j.jns.2020.117054.

Roche, Jose C et al. 2012. "A Proposed Staging System for Amyotrophic Lateral Sclerosis." *Brain* 135(3): 847–52.

Rosenthal, Zachary P. et al. 2020. "Local Perturbations of Cortical Excitability Propagate Differentially Through Large-Scale Functional Networks." *Cerebral Cortex* 30(5): 3352–69.

Sanjay Kalra, Neil R. Cashman, Angela Genge and Douglas L. Arnold. 1998. "Recovery of N-Acetylaspartate in Corticomotor Neurons of Patients with ALS after Riluzole Therapy." *NeuroReport* 9(8): 1757–61. https://www.tandfonline.com/doi/abs/10.1080/21678421.2016.1188961 (May 9, 2019).

Sanofi-Aventis. 2010. "Product Monograph Rilutek (Riluzole)." *Product Monograph* 3.0: 1–37. http://products.sanofi.ca/en/rilutek.pdf.

Schaper, Charles D. 2019. "Analytic Model of FMRI BOLD Signals for Separable Metrics of Neural and Metabolic Activity." *bioRxiv*: 573006. https://www.biorxiv.org/content/10.1101/573006v1.

Schmidt, Ruben et al. 2014. "Correlation between Structural and Functional Connectivity Impairment in Amyotrophic Lateral Sclerosis." *Human Brain Mapping* 35(9): 4386–95. https://pubmed.ncbi.nlm.nih.gov/24604691/ (April 9, 2021).

Schultz, Aaron P. et al. 2014. "Template Based Rotation: A Method for Functional Connectivity

Analysis with a Priori Templates." *NeuroImage* 102(P2): 620–36. http://dx.doi.org/10.1016/j.neuroimage.2014.08.022.

———. 2017. "Phases of Hyperconnectivity and Hypoconnectivity in the Default Mode and Salience Networks Track with Amyloid and Tau in Clinically Normal Individuals." *The Journal of Neuroscience* 37(16): 4323. /pmc/articles/PMC5413178/ (September 4, 2023).

Seitzman, Benjamin A., Abraham Z. Snyder, Eric C. Leuthardt, and Joshua S. Shimony. 2019. "The State of Resting State Networks." *Topics in Magnetic Resonance Imaging* 28(4): 189–96.

Shefner, Jeremy M et al. 2020. "A Proposal for New Diagnostic Criteria for ALS." *Clinical Neurophysiology* 131(8): 1975–78. https://doi.org/10.1016/j.clinph.2020.04.005 (November 26, 2021).

Shellikeri, Sanjana et al. 2019. "Speech Processing Network Regional Involvement in Bulbar ALS: A Multimodal Structural MRI Study." *Amyotrophic lateral sclerosis & frontotemporal degeneration* 20(5–6): 385. /pmc/articles/PMC6648678/ (January 24, 2023).

Skudlarski, Pawel et al. 2010. "Brain Connectivity Is Not Only Lower but Different in Schizophrenia: A Combined Anatomical and Functional Approach." *Biological Psychiatry* 68(1): 61–69.

Slanzi, Anna et al. 2020. "In Vitro Models of Neurodegenerative Diseases." *Frontiers in Cell and Developmental Biology* 8: 328.

Smith, Stephen M., and Thomas E. Nichols. 2009. "Threshold-Free Cluster Enhancement: Addressing Problems of Smoothing, Threshold Dependence and Localisation in Cluster Inference." *NeuroImage* 44(1): 83–98. http://dx.doi.org/10.1016/j.neuroimage.2008.03.061.

Soares, José M., Paulo Marques, Victor Alves, and Nuno Sousa. 2013. "A Hitchhiker's Guide to Diffusion Tensor Imaging." *Frontiers in Neuroscience* 7(7 MAR): 31.

Spetsieris, Phoebe G. et al. 2015. "Metabolic Resting-State Brain Networks in Health and

Disease." *Proceedings of the National Academy of Sciences of the United States of America* 112(8): 2563–68. https://www.pnas.org/doi/abs/10.1073/pnas.1411011112 (September 4, 2023).

Srivastava, Ojas et al. 2019. "Cerebral Degeneration in Amyotrophic Lateral Sclerosis: A Prospective Multicenter Magnetic Resonance Spectroscopy Study." *Neurology: Clinical Practice* 9(5): 400–407.

Stanton, Biba R. et al. 2007. "Cortical Activation during Motor Imagery Is Reduced in Amyotrophic Lateral Sclerosis." *Brain research* 1172(1): 145–51. https://pubmed.ncbi.nlm.nih.gov/17765211/ (September 1, 2023).

Strong, Michael J. et al. 2009. "Consensus Criteria for the Diagnosis of Frontotemporal Cognitive and Behavioural Syndromes in Amyotrophic Lateral Sclerosis." *Amyotrophic Lateral Sclerosis* 10(3): 131–46.

———. 2017. "Amyotrophic Lateral Sclerosis - Frontotemporal Spectrum Disorder (ALS-FTSD): Revised Diagnostic Criteria." *Amyotrophic Lateral Sclerosis and Frontotemporal Degeneration* 18(3–4): 153–74. http://dx.doi.org/10.1080/21678421.2016.1267768.

Strong, Michael J, and Michael Swash. 2022. "Finding Common Ground on the Site of Onset of Amyotrophic Lateral Sclerosis." *Neurology*: 10.1212/WNL.0000000000201387.

Swinnen, Bart, and Wim Robberecht. 2014. "The Phenotypic Variability of Amyotrophic Lateral Sclerosis." *Nature Reviews Neurology* 10(11): 661–70.

Ta, Daniel et al. 2021. "Progressive Neurochemical Abnormalities in Cognitive and Motor Subgroups of Amyotrophic Lateral Sclerosis." *Neurology* 97(8): e803–13.

Tae, Woo Suk et al. 2018. "Current Clinical Applications of Diffusion-Tensor Imaging in Neurological Disorders." *Journal of Clinical Neurology (Seoul, Korea)* 14(2): 129. /pmc/articles/PMC5897194/ (November 19, 2023).

Takeuchi, Ryoko et al. 2016. "Heterogeneity of Cerebral TDP-43 Pathology in Sporadic

Amyotrophic Lateral Sclerosis: Evidence for Clinico-Pathologic Subtypes." *Acta neuropathologica communications* 4(1): 61. https://actaneurocomms.biomedcentral.com/articles/10.1186/s40478-016-0335-2 (November 20, 2021).

Tan, Harold H.G. et al. 2022. "MRI Clustering Reveals Three ALS Subtypes With Unique Neurodegeneration Patterns." *Annals of Neurology*.

Taylor, J. Paul, Robert H. Brown, and Don W. Cleveland. 2016. "Decoding ALS: From Genes to Mechanism." *Nature* 539(7628): 197–206.

Tedeschi, Gioacchino et al. 2012. "Interaction between Aging and Neurodegeneration in Amyotrophic Lateral Sclerosis." *Neurobiology of Aging* 33(5): 886–98.

Thakore, Nimish J., Brittany R. Lapin, Hiroshi Mitsumoto, and R. Pooled. 2022. "Early Initiation of Riluzole May Improve Absolute Survival in Amyotrophic Lateral Sclerosis." *Muscle and Nerve* 66(6): 702–8.

Thome, Janine et al. 2022. "Classification of Amyotrophic Lateral Sclerosis by Brain Volume, Connectivity, and Network Dynamics." *Human Brain Mapping* 43(2): 681–99.

Tremolizzo, Lucio et al. 2014. "Primitive Reflexes in Amyotrophic Lateral Sclerosis: Prevalence and Correlates." *Journal of Neurology* 261(6): 1196–1202. https://link.springer.com/article/10.1007/s00415-014-7342-7 (November 25, 2021).

Trojsi, Francesca et al. 2021. "Frontotemporal Degeneration in Amyotrophic Lateral Sclerosis (ALS): A Longitudinal MRI One-Year Study." *CNS Spectrums* 26(3): 258–67.

Turner, Martin et al. 2020. "Primary Lateral Sclerosis: Consensus Diagnostic Criteria." *J Neurol Neurosurg Psychiatry* 91: 373–77. http://jnnp.bmj.com/ (November 26, 2021).

Turner, Martin R., and Matthew C. Kiernan. 2012. "Does Interneuronal Dysfunction Contribute to Neurodegeneration in Amyotrophic Lateral Sclerosis?" *Amyotrophic Lateral Sclerosis* 13(3): 245–50.

van Veenhuijzen, Kevin et al. 2022. “Longitudinal Effects of Asymptomatic C9orf72 Carriership on Brain Morphology.” *Annals of Neurology*.

Vellage, Anne Katrin et al. 2016. “Working Memory Network Changes in ALS: An FMRI Study.” *Frontiers in Neuroscience* 10(APR): 1–10.

Vernet, Marine et al. 2014. “Frontal Eye Field, Where Art Thou? Anatomy, Function, and Non-Invasive Manipulation of Frontal Regions Involved in Eye Movements and Associated Cognitive Operations.” *Frontiers in Integrative Neuroscience* 8(AUG): 1–24.

Verstraete, Esther et al. 2010. “Motor Network Degeneration in Amyotrophic Lateral Sclerosis: A Structural and Functional Connectivity Study.” *PLoS ONE* 5(10).

Vincent, Justin L. et al. 2008. “Evidence for a Frontoparietal Control System Revealed by Intrinsic Functional Connectivity.” *Journal of Neurophysiology* 100(6): 3328. /pmc/articles/PMC2604839/ (October 12, 2023).

Vucic, Steve et al. 2021. “Cortical Hyperexcitability: Diagnostic and Pathogenic Biomarker of ALS.” *Neuroscience Letters* 759. https://doi.org/10.1016/j.neulet.2021.136039 (September 6, 2021).

Wang, Hewei et al. 2023. “Motor Network Reorganization after Motor Imagery Training in Stroke Patients with Moderate to Severe Upper Limb Impairment.” *CNS neuroscience & therapeutics* 29(2). https://pubmed.ncbi.nlm.nih.gov/36575865/ (October 10, 2023).

Wang, Ling E. et al. 2011. “Noradrenergic Enhancement Improves Motor Network Connectivity in Stroke Patients.” *Annals of Neurology* 69(2): 375–88. https://onlinelibrary.wiley.com/doi/full/10.1002/ana.22237 (October 10, 2023).

Wang, Wenzhang et al. 2016. “The Inhibition of TDP-43 Mitochondrial Localization Blocks Its Neuronal Toxicity.” *Nature medicine* 22(8): 869. /pmc/articles/PMC4974139/ (October 22, 2021).

Wang, Zhi Li et al. 2019. “Split-Hand Syndrome in Amyotrophic Lateral Sclerosis: Differences

in Dysfunction of the Fdi and Adm Spinal Motoneurons." *Frontiers in Neuroscience* 13(MAY): 371.

Welsh, Robert C, Laura M Jelsone-Swain, and Bradley R Foerster. 2013. "The Utility of Independent Component Analysis and Machine Learning in the Identification of the Amyotrophic Lateral Sclerosis Diseased Brain." *Frontiers in Human Neuroscience* (MAY). www.frontiersin.org (January 16, 2023).

Witiuk, Kelsey et al. 2014. "Cognitive Deterioration and Functional Compensation in ALS Measured with FMRI Using an Inhibitory Task." *Journal of Neuroscience* 34(43): 14260–71.

Wittstock, Mathias et al. 2011. "Mirror Movements in Amyotrophic Lateral Sclerosis." *Amyotrophic Lateral Sclerosis* 12(6): 393–97. https://www.tandfonline.com/action/journalInformation?journalCode=iafd20 (September 7, 2023).

Woolley, Susan C., and S. Katz Jonathan. 2008. "Cognitive and Behavioral Impairment in Amyotrophic Lateral Sclerosis." *Physical Medicine and Rehabilitation Clinics of North America* 19(3): 607–17.

Xiao, Shangxi et al. 2015. "Isoform-Specific Antibodies Reveal Distinct Subcellular Localizations of C9orf72 in Amyotrophic Lateral Sclerosis." *Annals of Neurology* 78(4): 568–83. https://onlinelibrary.wiley.com/doi/full/10.1002/ana.24469 (November 20, 2021).

Yao, Zhijun et al. 2019. "Structural Alterations of the Brain Preceded Functional Alterations in Major Depressive Disorder Patients: Evidence from Multimodal Connectivity." *Journal of Affective Disorders* 253: 107–17. https://pubmed.ncbi.nlm.nih.gov/31035211/ (March 24, 2021).

Yunusova, Yana et al. 2019. "Frontal Anatomical Correlates of Cognitive and Speech Motor Deficits in Amyotrophic Lateral Sclerosis." *Behavioural Neurology* 2019.

Zaehle, T et al. 2013. "Working Memory in ALS Patients: Preserved Performance but Marked

Changes in Underlying Neuronal Networks." *PLoS ONE* 8(8): 71973. www.plosone.org (September 8, 2023).

Zarei, Mahdi et al. 2022. "High Activity and High Functional Connectivity Are Mutually Exclusive in Resting State Zebrafish and Human Brains." *BMC Biology* 20(1): 1–20. https://bmcbiol.biomedcentral.com/articles/10.1186/s12915-022-01286-3 (September 5, 2023).

Zhang, Feifei et al. 2018. "Altered White Matter Microarchitecture in Amyotrophic Lateral Sclerosis: A Voxel-Based Meta-Analysis of Diffusion Tensor Imaging." *NeuroImage: Clinical* 19: 122–29. /pmc/articles/PMC6051469/ (February 8, 2021).

Zhang, Jiuquan et al. 2017. "Aberrant Interhemispheric Homotopic Functional and Structural Connectivity in Amyotrophic Lateral Sclerosis." *Journal of Neurology, Neurosurgery and Psychiatry* 88(5): 374–80.

Zhang, Zhiqiang et al. 2011. "Altered Functional–Structural Coupling of Large-Scale Brain Networks in Idiopathic Generalized Epilepsy." *Brain* 134(10): 2912–28. https://academic.oup.com/brain/article/134/10/2912/322444 (August 24, 2022).

Zhou, Fuqing et al. 2013. "Altered Motor Network Functional Connectivity in Amyotrophic Lateral Sclerosis: A Resting-State Functional Magnetic Resonance Imaging Study." *NeuroReport* 24(12): 657–62.

———. 2014. "Alterations in Regional Functional Coherence within the Sensory-Motor Network in Amyotrophic Lateral Sclerosis." *Neuroscience Letters* 558: 192–96. https://www.sciencedirect.com/science/article/pii/S0304394013010227?via%3Dihub (August 15, 2019).

Zou, Zhang Yu et al. 2017. "Genetic Epidemiology of Amyotrophic Lateral Sclerosis: A Systematic Review and Meta-Analysis." *Journal of neurology, neurosurgery, and psychiatry* 88(7): 540–49. https://pubmed.ncbi.nlm.nih.gov/28057713/ (November 20, 2021).